Spring 2015

Studies of the interaction of biogenic volatile organic compounds and NOx in forest environments

Kevin M. McAvey
Purdue University

Graduate School Form 30
(Updated 11/20/2014)

PURDUE UNIVERSITY
GRADUATE SCHOOL
Thesis/Dissertation Acceptance

This is to certify that the thesis/dissertation prepared

By Kevin M. McAvey

Entitled STUDIES OF THE INTERACTION OF BIOGENIC VOLATILE ORGANIC COMPOUNDS AND NOX IN FOREST ENVIRONMENTS

For the degree of Doctor of Philosophy

Is approved by the final examining committee:

Paul B. Shepson

Mary J. Wirth

Garth J. Simpson

Peter T. Kissinger

To the best of my knowledge and as understood by the student in the Thesis/Dissertation Agreement, Publication Delay, and Certification/Disclaimer (Graduate School Form 32), this thesis/dissertation adheres to the provisions of Purdue University's "Policy on Integrity in Research" and the use of copyrighted material.

Paul B. Shepson

Approved by Major Professor(s): _____

_____

Approved by: R. E. Wild 04/13/2015

Head of the Department Graduate Program Date

STUDIES OF THE INTERACTION OF BIOGENIC VOLATILE ORGANIC COMPOUNDS AND NO_X IN FOREST ENVIRONMENTS

A Dissertation

Submitted to the Faculty

of

Purdue University

by

Kevin M. McAvey

In Partial Fulfillment of the

Requirements for the Degree

of

Doctor of Philosophy

May 2015

Purdue University

West Lafayette, Indiana

To my friends and family that I have lost, and to the ones still around and never let me give up.

ACKNOWLEDGMENTS

In the middle of difficulty lies opportunity.

- Albert Einstein

I would like to thank Dr. Paul Shepson and the entire Shepson lab for their constant help and guidance through my graduate career. I would also like to thank my GCxGC collaborators Timothy Starn, John Seeley, and Steve Bertman. I would like to thank James Zimmerman, Hartmut Hedderich, Mike Everly, and the rest of the Jonathan Amy Facility for Chemical Instrumentation for their support and expertise in helping rebuild TRENI and develop our GCxGC sampling system. I would like to also thank Daniel Lazzaro, Gregory Jarvis, Keith Steelman, Matthew Hostetler, and others who provided me with the knowledge and tools to be a slightly better organic chemist. I would also like to thank all the friends who listened to my constant grumblings and bickering over a few beers.

My career as a chemist so far has been enhanced by several people. The first is my high school chemistry teacher, Mr. Rudat, who showed me that chemistry was fascinating. The second is my undergraduate advisor, Dr. Richard Cole, who encouraged me to try to achieve greater things in life. I'd also like to thank President Obama. Most

importantly, I would like to thank my family for their continued support no matter what I do in life.

TABLE OF CONTENTS

Page

Page

LIST OF TABLES

LIST OF FIGURES

Figure Page

Figure Page

Figure Page

ABSTRACT

McAvey, Kevin Michael. PhD., Purdue University, May 2015. Studies of the Interaction of Biogenic Volatile Organic Compounds and NO_x in Forest Environments. Major Professor: Paul B. Shepson.

Ozone is a pollutant that causes crop damage, adverse health effects, and is a contributor to global climate change. Ozone concentrations are predicted to rise over the next half-century along with global temperature. Ozone production is controlled by the chemistry between biogenic volatile organic compounds and NO_x ($NO + NO_2$), and therefore, a greater understanding of NO_x + BVOC chemistry along with their sources and sinks is needed. One large uncertainty in understanding NO_x + BVOC chemistry is the production of organic nitrates ($RONO_2$), which act as a radical termination step in the production of O_3. In this work, we present two modified instruments built to better understand the sources of NO_x and BVOCs. The result of one field campaign to identify the source of early morning NO_x plumes is presented. The development of a novel sampling system for a GCxGC system is presented, along with data obtained by the instrument during a field campaign. Finally, a 0-D chemical model is used to identify the BVOC precursors most important to the formation of organic nitrates.

CHAPTER 1 INTRODUCTION

1.1 Tropospheric Chemistry

High ground level ozone (O_3) concentrations and photochemical oxidants have become a worldwide concern due to the impacts on human health, with thousands of studies showing impacts such as decreased vital capacity (Koren et al., 1989), enhanced response to inhaled allergen (Ball et al., 1999), inflammation (Nightingale et al., 1999), and irreversible changes in lung structure (Dockery et al., 1996; Gauderman et al., 2000; Raizenne et al., 1996). High ozone concentrations are also of concern due to their role in global climate change (IPCC, 2007) crop loss (Tang et al., 2013), and forest damage (de Vries et al., 2014). Measurements of O_3 during the nineteenth century suggest that pre-industrial ground level O_3 concentrations were less than 10 ppb (Volz and Kley, 1988). During the past century, background concentrations of ground level ozone have quadrupled, and O_3 could rise another 40-60% by 2100 if current emission trends continue (Isaksen et al., 2009; Meehl et al., 2007).

The troposphere is the lowest portion of the atmosphere and extends from the Earth's surface to a height of 7 to 20 km above sea level (Finlayson-Pitts and Pitts, 2000). The troposphere is oxidative due to the presence of OH radicals, O_3, and NO_3 radicals. Ozone controls the oxidizing capacity of the atmosphere through the formation of OH and NO_3 radicals (discussed below), which react rapidly with nearly all volatile organic

compounds (VOCs) and many inorganic compounds. They serve as the mechanism by which the atmosphere "cleans" itself. Through oxidation, O_3, OH radicals, and NO_3 radicals, are able to effectively remove VOCs from the atmosphere by oxidizing VOCs leading either to the production of carbon dioxide or products with lower vapor pressures and/or more highly water soluble species (Finlayson-Pitts and Pitts, 2000; Goldstein and Galbally, 2007). These lower vapor pressure- higher water solubility species are then removed from the atmosphere through dry deposition, wet deposition, or uptake into aerosol (Goldstein and Galbally, 2007). Aerosols are then removed from the atmosphere through dry or wet deposition.

Ozone is produced and controlled in the atmosphere by the chemistry that occurs between NO_x (NO_2 + NO) and VOCs. Through the chemistry occurring between NO_x, VOCs, and O_3, atmospheric smog that pollutes many urban regions is formed (Haagen-Smit, 1952). The following sections of this chapter will go into further depth on the sources, sinks, and chemistry of the key components that control the oxidative capacity of the troposphere.

Current research in the field of tropospheric chemistry has shown that a substantial fraction of VOCs have rarely been directly measured and that a review of the global budget for VOCs shows that we cannot account for the loss of approximately half of the non-methane VOCs entering the atmosphere (Goldstein and Galbally, 2007). Computer modeling, chamber experiments, and large scale field campaigns have been the general means of identifying and evaluating the knowledge of NO_x and VOC chemistry. There have been many advances in the past few years in the understanding of tropospheric chemistry, including better branching ratio predictions for important

reactions and the ability to quantify various VOCs. This review will attempt to explain the greater understanding of the fate of NO_x through interactions with the process of VOC oxidation, including which individual VOCs contribute most to ozone production and organic nitrate production, and what is currently unknown about NO_x chemistry and the effects of regulation on the concentration of oxidants and the changes in chemistry occurring in the troposphere.

1.2 Boundary Layer Meteorology and its Effect on NO_x Chemistry

A large factor in understanding NO_x-BVOC chemistry is understanding boundary layer dynamics. In a traditional laboratory, samples can be contained within glassware and have fixed volumes and mixing speeds. In the atmosphere, there are a multitude of factors affecting the mixing and associated concentration of species.

The atmosphere is separated into four distinct layers based on their temperature lapse rate; the troposphere, the stratosphere, the mesosphere, and the thermosphere. Figure 1.1 shows the location and approximate heights of each layer.

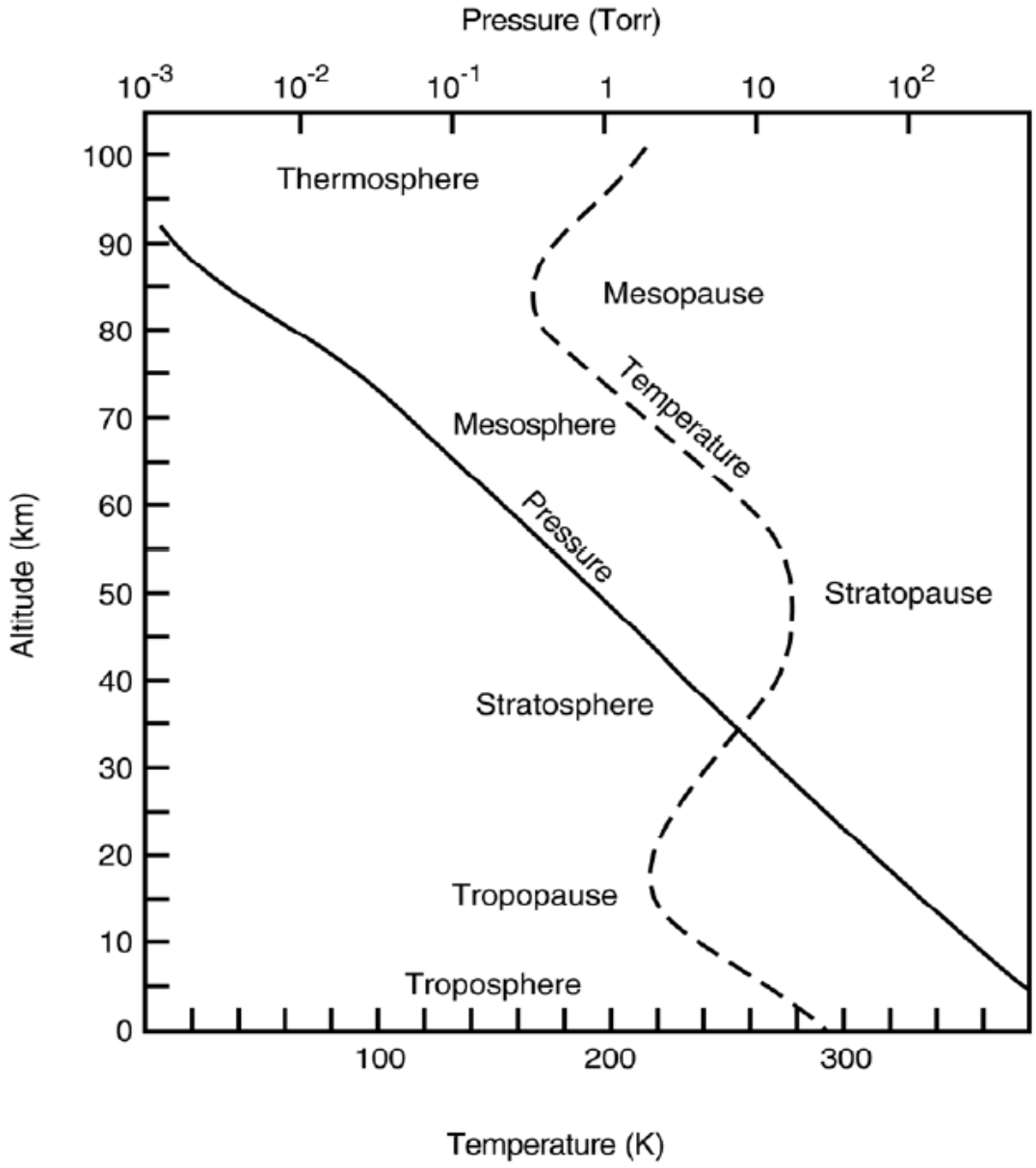

Figure 1.1 Structure of the atmosphere along with temperature and pressure profile. Finlayson-Pitts and Pitts, (2000).

Within the lowest layer, the troposphere, exists the boundary layer. The boundary layer is defined as the fraction of the Earth's atmosphere that is directly influenced by the presence of the Earth's surface, and responds to surface forcings with a timescale of

about an hour or less (Stull, 1988). BVOCs come from vegetation, and are therefore directly connected and influenced by the dynamics of the boundary layer (Guenther et al., 2000; Guenther et al., 1993). NO_x in the troposphere comes from surface emissions such as the burning of fossil fuels, biomass burning, and soil emissions, and the transport of these emissions are highly dependent on the structure and motion occurring within the boundary layer (Oliver et al., 1996).

Within the boundary layer, there exists turbulence, or gustiness superimposed on the mean wind, and is visualized as irregular swirls of motion called eddies (Stull, 1988). These eddies are generally created by surface forcings in the boundary layer. Examples of such forcings include solar heating and buoyancy, and wind shear. Solar heating occurs when solar radiation heats the ground faster than the air above it, causing buoyant warm air at the surface to rise, and the pressure difference from the warm air rising causes cool air from the top of the boundary layer to move towards the surface. Another forcing is wind shear. Wind shear is when two layers of air with different mean wind direction meet, and usually induce turbulence (Stull, 1988). These two forcings have an enormous impact on the mixing that occurs within the boundary layer, and therefore influence NO_x-BVOC chemistry.

The development of the boundary layer is shown in Figure 1.2.

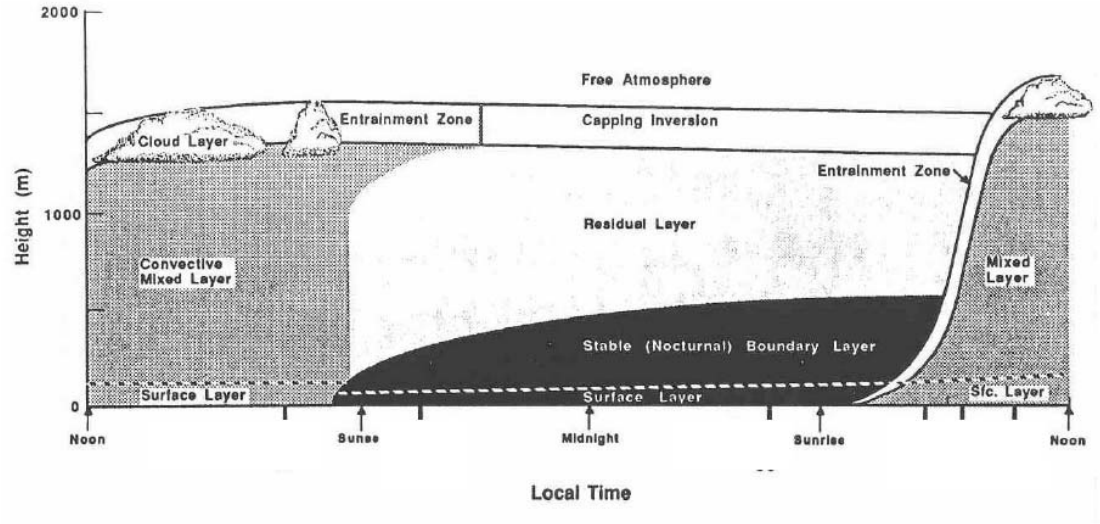

Figure 1.2. Idealized diurnal structure of the boundary layer (Stull, 1988).

There are four major areas to the development of the boundary layer. The first is the well mixed convective layer. The mixed convective layer begins in the morning at sun rise and continues as long as there is solar forcings. Due to solar forcings, the air in the mixed layer is very turbulent and well mixed. When the sunsets, the ground cools faster than the air above and it, ending the large turbulent mixing within the mixed layer, and creating a stable, poorly mixed surface layer. The cool air at the surface creates the second major component, the nocturnal boundary layer. This layer experiences only sporadic turbulence. When solar forcing stops, a residual layer is formed on top of the nocturnal boundary layer, and this layer contains the remaining emissions from the previous day in a layer that is less turbulent than the mixed layer. When the sun rises again in the morning, the solar forcing returns, and the daytime mixed nocturnal boundary layer begins to mix with the residual layer, creating the convective mixed layer. The fourth

area that effects the development of the boundary layer is the entrainment zone. Entrainment is when a turbulent flow mixes with a non-turbulent flow (Stull, 1988).

One of the main difficulties in understanding boundary layer dynamics is the understanding of turbulence. The scope and scale of describing the equations that represent turbulent flow is beyond this review. Detailed equations that represent turbulence can be found in Stull (1988). One of the largest problems with understanding turbulence is the closure problem. The closure problem is stated as the number of unknowns in the sets of equations that describe turbulent flow is larger than the number of equations, and therefore, the total statistical description of turbulence requires an infinite set of equations (Stull 1988). The most common way to solve this problem is to use K-theory, shown in equation 1.1 where K is referred to as the eddy diffusivity, u_j is the wind speed for j dimensions, ξ is any variable (momentum, heat, moisture, etc…), $\overline{u_j'\xi'}$ is the flux of ξ, and $\frac{\partial \xi}{\partial x_j}$ is the gradient of ξ.

$$\overline{u_j'\xi'} = -K\frac{\partial \xi}{\partial x_j} \qquad \text{Equation 1.1}$$

K-theory is a first order closure in which a scalar value of K (m^2s^{-1}) is used to approximate the second and further moments that describe turbulent flow (Stull, 1988). This theory is extensively used because it is computationally inexpensive (Forkel et al., 2006), but frequently fails when larger-size eddies are present (Stull, 1988), and when heterogeneous surfaces are present (Bryan et al., 2012). K-theory is very problematic for forest environments because the eddy diffusivity constant used for the mixed convective layer (e.g. at 500 m in daytime) is 2 orders of magnitude higher than at the forest canopy surface layer (Gao et al., 1993) and therefore when used near the canopy surface breaks

down completely due to frictional related changes due to the heterogeneous surfaces of the canopy (Raupach et al., 1996). Therefore, most models have large uncertainties in describing vertical mixing within and above the canopy and poorly describe atmosphere-forest exchanges of NO_x, BVOCs and oxidants (Ganzeveld et al., 2006; Saylor, 2013; Wolfe and Thornton, 2011).

1.3 NO_x

Emissions of NO_x have a wide range of atmospheric implications including stimulated forest growth (Costa et al., 2011), growth of secondary organic aerosol (Xu et al., 2014) and controlling ozone production in the troposphere (Ridley et al., 1992a). Since the first trace level measurements of NO by (Fontijn et al., 1970), measurements of NO_x have been a vital part of understanding the chemical processes that govern the composition and quality of tropospheric air. NO_x can directly and indirectly control the major oxidants in the atmosphere and controls VOC oxidation pathways (Lin et al., 1988; Thompson, 1992).

Nitrogen dioxide photo dissociates at wavelengths less than 420 nm to produce NO and a ground state triplet oxygen atom, which can then react with O_2 to form O_3 as shown in reaction 1.1, 1.2, and 1.3. This reaction is critical in atmospheric chemistry as NO_x emissions are the only significant anthropogenic source of O_3 in the troposphere (Finlayson-Pitts and Pitts, 2000). From reactions 1.1, 1.2, and 1.3, the overall net of these reactions is nothing and the only way O_3 is produced is by reactions which convert NO into NO_2 without destroying O_3 (discussed within) (Thornton et al. 2002).

$$NO + O_3 \longrightarrow NO_2 + O_2 \quad (1.1)$$

$$NO_2 + h\nu \longrightarrow NO + O(^3P) \quad (1.2)$$

$$O_2 + O(^3P) \longrightarrow O_3 \quad (1.3)$$

Over the contiguous United States the primary source of NO_x is fossil fuel burning (7.3 Tg N yr^{-1}), followed by soil emissions (0.5 Tg N yr^{-1}), lightning (0.4 Tg N yr^{-1}), and from incomplete combustion in biomass burning (0.3 Tg N yr^{-1}) (Oliver et al., 1996). There still remains a large uncertainty in the magnitude of emissions from various sources. From satellite measurements, estimated global soil NO_x emission measurements vary from 7 (Yan et al., 2005) to 21 Tg N yr^{-1} (Davidson and Kingerlee, 1997). There are limited measurements of soil fluxes, canopy fluxes, and lightning induced NO_x, due to the difficulty in obtaining these measurements (Geddes and Murphy, 2014). While there are a large number of experiments exploring the interactions between NO_x and BVOCs, there remains a large uncertainty in the formation of oxidized BVOCs and their role in the sequestration of NO_x, partly due to the vast number of BVOCs and partly due to the complexity of reaction products from these reactions. The role of NO_x in BVOC oxidation is discussed within.

1.4 Biogenic Volatile Organic Compounds

A wide variety of non-methane hydrocarbons are emitted into the atmosphere from either anthropogenic sources or biogenic sources, with emission inventories showing that biogenic volatile organic compounds (BVOCs) exceed anthropogenic emissions by an order of magnitude worldwide and by a factor of 1.5 for the United States (Guenther et al., 2000; Guenther et al., 1995). BVOCs are generally categorized as

isoprene (C_5H_8), monoterpenes ($C_{10}H_{16}$), sesquiterpenes ($C_{15}H_{24}$), diterpenes ($C_{20}H_{32}$), non-terpenoids (which include oxygenated terpenes such as 2-methyl-3-buten-2-ol (MBO)), other species (such as hexene derivatives), and short chain oxygenated hydrocarbons, such as methanol and acetone (Seco et al., 2007). Figure 1.3 shows the structure of some common BVOCs measured in the atmosphere.

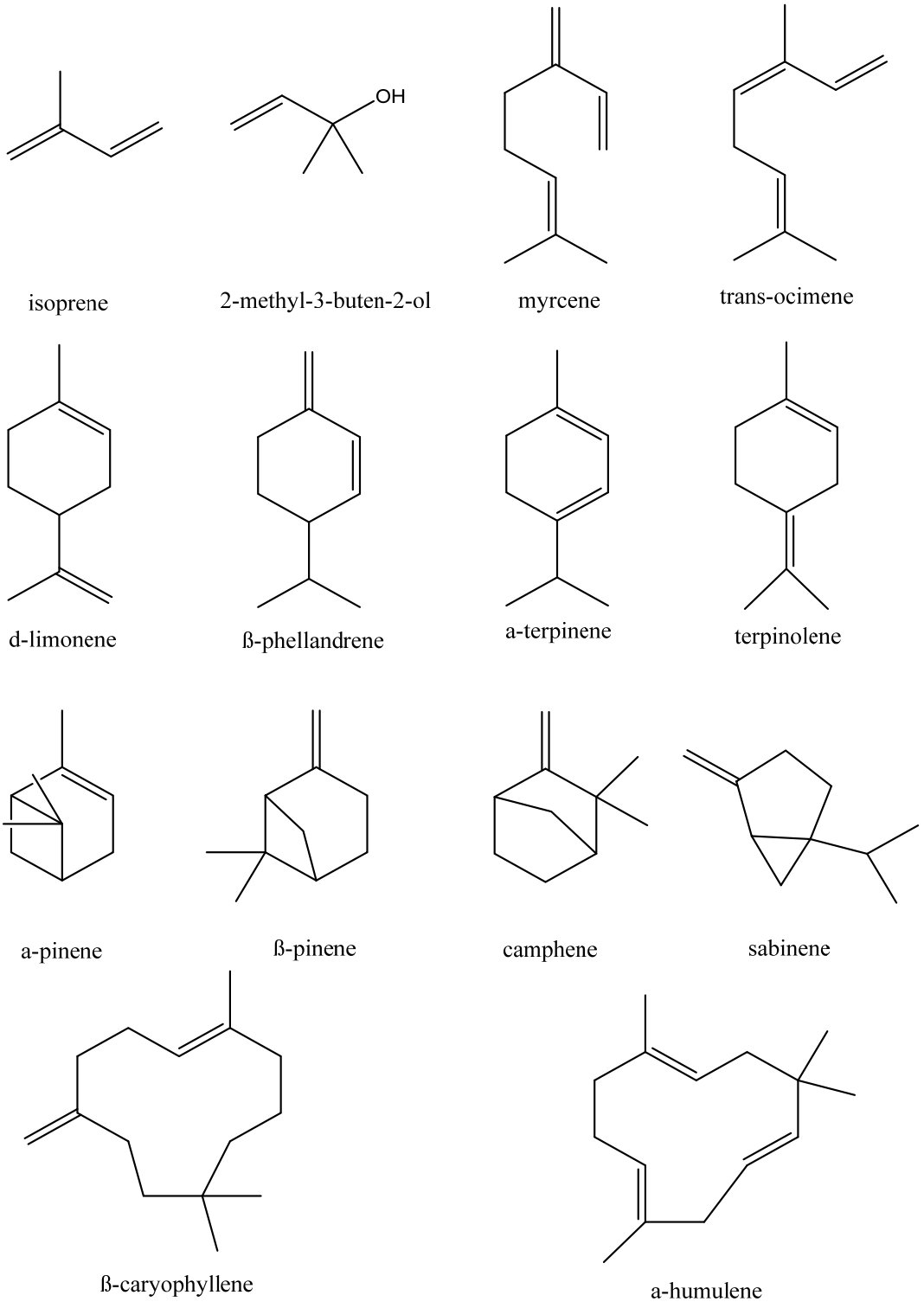

Figure 1.3 Commonly observed BVOCs and their structure.

Global BVOC emissions are estimated to be 1150 Tg C yr^{-1}, with isoprene being the dominant BVOC, with an estimated 500 Tg C yr^{-1} emitted each year. In the United States, BVOC emissions are estimated to be 84 Tg C yr^{-1}, of which 30% is isoprene, 25% are monoterpenes and sesquiterpenes, and 45% are non-terpenoid compounds (Guenther et al., 1995). Atmospheric samples can contain thousands, if not millions, of possible VOCs. Goldstein and Gallaby (2007) have estimated that there can be well over 1 million possible 10 carbon organic compounds, with 100 alkane isomers alone. When searching the Beilstein preparative organic chemistry database for compounds with boiling points below 300°C and less than 11 carbons, only 791 known compounds are found, showing the lack of understanding of the complexity of atmospheric samples (Goldstein and Galbally, 2007). The complexity of samples is also increased due to oxidation processes occurring in the atmosphere. The ozonolysis of a single BVOC, longifolene, was shown to create over 200 identifiable oxidation products by comprehensive two-dimensional gas chromatography (Isaacman et al., 2011), and that is a small fraction of the potential products generated by comprehensive models (Aumont et al., 2005).

BVOC emissions are generally temperature and radiation dependent (Guenther et al., 1993). The composition of the biosphere determines which BVOCs are emitted. The forests of northern Michigan and in the southeastern United States have been found to be largely isoprene emitters (Carroll et al., 2001). The ponderosa forests of the western United States are dominated by MBO and monoterpene emissions (Kim et al., 2010). The forests outside of Nashville, Tennessee have been shown to be large isoprene emitters (Starn et al., 1998). MacKenzie et al. (2011) found distinctive VOC footprints from a rainforest in Borneo and a nearby palm oil plantation. Measured isoprene concentrations

in the rainforest were ~4 times higher than at the nearby palm oil plantation. Measured monoterpene concentrations in the palm oil plantation were half of that measured in the rainforest. Even in highly urbanized areas such as Atlanta, Georgia, the emissions of isoprene have been estimated to be larger than anthropogenic hydrocarbons from industrial processes (Lindsay et al., 1989). BVOCs are generally more reactive to OH, NO_3, and O_3 than anthropogenic VOCs (Atkinson and Arey, 2003), and hence their local chemistry has a much more profound effect on local and global climate (Goldstein and Galbally, 2007). Therefore, for the rest of this chapter will only focus of BVOCs.

BVOCs are fundamental in the formation of secondary organic aerosol. Through the oxidation of BVOCs with OH, O_3, and NO_3, generally lower volatility products are formed (Hallquist et al., 2009; Kroll and Seinfeld, 2008). The reduction in vapor pressure from the oxidation of BVOCs can be seen in Table 1.1, which shows the general multiplicative factor in the change of vapor pressures of BVOCs.

Table 1.1 Change in vapor pressure due to the addition of functional groups. Table taken from Kroll and Seinfeld (2008).

Changes to vapor pressure of an organic compound upon addition of common functional groups, based upon group-contribution method predictions of Pankow and Asher (2007)

Functional group	Structure	Change in vapor pressure (298 K)[a]
Ketone	–C(O)–	0.10
Aldehyde	–C(O)H	0.085
Hydroxyl	–OH	5.7×10^{-3}
Hydroperoxyl	–OOH	2.5×10^{-3}
Nitrate	$-ONO_2$	6.8×10^{-3}
Carboxylic acid	–C(O)OH	3.1×10^{-4}
Peroxyacid	–C(O)OOH	3.2×10^{-3}
Acyl peroxynitrate	$-C(O)OONO_2$	2.7×10^{-3}
Extra carbon[b]	$-CH_2-$, etc.	0.35[b]

[a]Multiplicative factor.

[b]For comparison between changes in polarity (by addition of a functional group) and changes to size of the carbon skeleton. Vapor pressure also depends on carbon skeleton structure; see Pankow and Asher (2007).

These reduced vapor pressure products are more water soluble and can uptake into or onto aerosol or other surfaces. The mechanisms for the oxidation of BVOCs leading to different functional groups are discussed within this review.

The importance of speciating BVOCs is apparent when measuring the secondary organic aerosol (SOA) yield from BVOC oxidation reactions. SOA yield is the fraction of the total mass of the BVOC that ends up in the aerosol phase after oxidation. SOAs are aerosols formed when atmospheric oxidation products of VOCs undergo gas-particle transfer, and will be discussed below. Lee et al. (2006b) subjected eight monoterpenes to oxidation by OH, and found the SOA yield to vary from 58% for limonene to 25% for α-terpinene. Lee et al. (2006a) studied the oxidation of 6 monoterpenes by O_3 and found that the SOA yield varied from 54% for 3-carene to 11% for myrcene. Fry et al. (2014) studied the SOA yield from the reaction of 11 different BVOCs with the NO_3 and found that the SOA yield varied from 0 (α-pinene) to 86% (limonene). These SOA yields have been found to change with temperature, as lower temperatures generally result in higher SOA yields (Takekawa et al., 2003). These studies show that just isomers of $C_{10}H_{16}$ have vast differences not only in reactivity, but in product speciation. The oxidation pathways which lead to these different products are discussed below.

It has become increasingly necessary to separate BVOCs into their individual isomers due to the large differences in reactivity. Table 1.2 shows the lifetimes of BVOCs for each oxidant.

Table 1.2 Atmospheric lifetimes of selected BVOCs with respect to OH, O_3, and NO_3. Table is taken from Atkinson (2003).

Calculated atmospheric lifetimes of biogenic volatile organic compounds

Biogenic VOC	Lifetime[a] for reaction with		
	OH[b]	O_3[c]	NO_3[d]
Isoprene	1.4 h	1.3 day	1.6 h
Monoterpenes			
Camphene	2.6 h	18 day	1.7 h
2-Carene	1.7 h	1.7 h	4 min
3-Carene	1.6 h	11 h	7 min
Limonene	49 min	2.0 h	5 min
Myrcene	39 min	50 min	6 min
cis-/*trans*-Ocimene	33 min	44 min	3 min
α-Phellandrene	27 min	8 min	0.9 min
β-Phellandrene	50 min	8.4 h	8 min
α-Pinene	2.6 h	4.6 h	11 min
β-Pinene	1.8 h	1.1 day	27 min
Sabinene	1.2 h	4.8 h	7 min
α-Terpinene	23 min	1 min	0.5 min
γ-Terpinene	47 min	2.8 h	2 min
Terpinolene	37 min	13 min	0.7 min
Sesquiterpenes			
β-Caryophyllene	42 min	2 min	3 min
α-Cedrene	2.1 h	14 h	8 min
α-Copaene	1.5 h	2.5 h	4 min
α-Humulene	28 min	2 min	2 min
Longifolene	2.9 h	> 33 day	1.6 h
Oxygenates			
Acetone[e]	61 day[f]	> 4.5 year[g]	> 8 year[f]
Camphor	2.5 day[h]	> 235 day[h]	> 300 day[h]
1,8-Cineole	1.0 day[i]	> 110 day[j]	1.5 year[i]
cis-3-Hexen-1-ol	1.3 h[k]	6.2 h[k]	4.1 h[k]
cis-3-Hexenyl acetate	1.8 h[k]	7.3 h[k]	4.5 h[k]
Linalool	52 min[k]	55 min[k]	6 min[k]
Methanol	12 day[f]	> 4.5 year[g]	2.0 year[f]
2-Methyl-3-buten-2-ol	2.4 h[l]	1.7 day[m]	7.7 day[n]
6-Methyl-5-hepten-2-one	53 min[o]	1.0 h[o]	9 min[o]

These lifetimes, calculated as the inverse of the rate constant times the concentration of the oxidant, were calculated assuming $2x10^6$ molecules/cm^3 of OH, $7x10^{11}$ molecules/cm^3 of O_3, and $2.5x10^8$ molecules/cm^3 of NO_3. Therefore, an understanding not only of the BVOCs, but the oxidants is needed to understanding O_3 chemistry in the troposphere.

1.5 Oxidants

1.5.1 OH Radical

The hydroxyl radical is a highly reactive compound with an unpaired electron and is formed mainly by reactions 1.4 and 1.5.

$$O_3 + h\nu \longrightarrow O(^1D) + O_2 \quad (1.4)$$

$$O(^1D) + H_2O \longrightarrow 2OH \quad (1.5)$$

When O_3 is photolyzied ($\lambda < 310$ nm), a singlet state oxygen is formed. When there is water vapor present, the singlet state oxygen reacts with water vapor to form 2 OH radicals (Finlayson-Pitts and Pitts, 2000). Thus, the oxidizing potential of the troposphere is dependent on the availability of O_3, radiation, and absolute humidity. OH radicals can also be formed from the oxidation of BVOCs by O_3 (discussed within), which can be a substantial fraction (24-62%) of OH formed during the day (Elshorbany et al., 2009; Heard et al., 2004). OH radicals are considered to be the most important oxidant in the atmosphere due to their high reactivity and production rate (Fuchs et al., 2013).

Typical daytime values of OH concentrations found in the atmosphere are between 1-10 x 10^6 molecules/cm^3, with tropical regions experiencing much higher concentrations due to the increased sunlight and water vapor (Taraborrelli et al., 2012). However, there is debate on the accuracy of the measurements. Mao et al. (2012) reported that around 50% of the OH measured is the result of internally generated OH radicals, possibly from the oxidation of BVOCs and that OH measurements not using a chemical blank would result in OH concentrations that are artificially high.

Hydroxyl radicals initiate oxidation by adding across a carbon-carbon double bond, or by abstracting a hydrogen from BVOCs as shown in Figure 1.4.

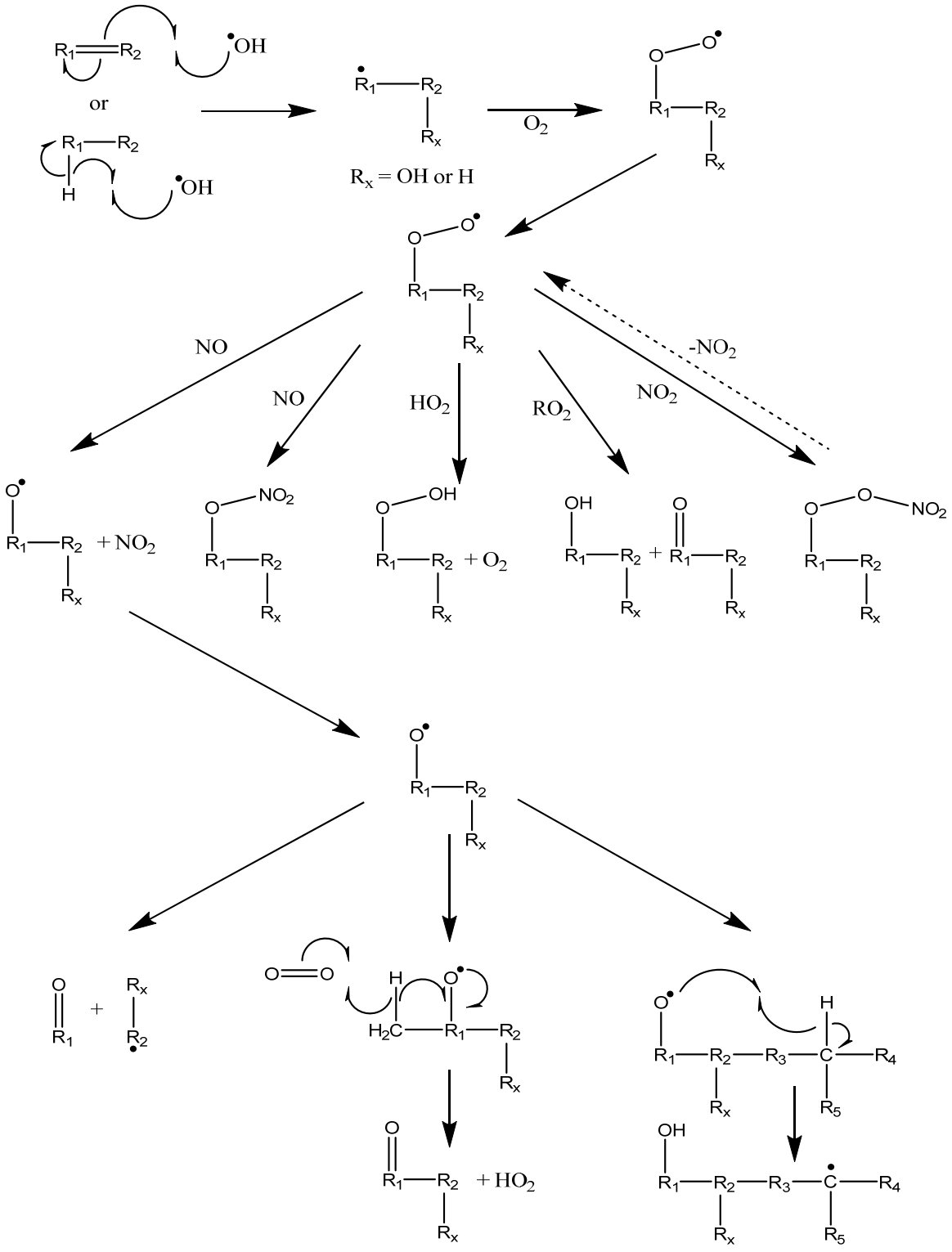

Figure 1.4 Oxidation pathway of BVOC and OH chemistry.

Models have predicted that the H-abstraction pathway isn't important in small simple alkenes such as ethene, but can be the initiation reaction for over 30% of larger BVOCs, such as monoterpenes and sesquiterpenes (Peeters et al., 2007; Peeters et al., 1999; Vereecken and Francisco, 2012). The alkyl radical formed from the initial OH addition or abstraction then reacts with O_2 to form a peroxyradical. The fate of the peroxyradical is determined by both the carbon backbone of the species and whether the reaction is occurring under high NO_x or low NO_x conditions. The boundary between high and low NO_x is generally accepted as around 150 ppt and is defined as the point at which a peroxy radical has an equal probability of reacting with NO or another RO_2 (Xie et al., 2013).

Under high NO_x conditions, NO_2 can add to the peroxy radical forming what is commonly referred to as a peroxy nitrate (RO_2NO_2). Peroxy nitrates are generally unstable at high temperatures and their stability is dependent on the carbon backbone of the BVOC. Peroxy nitrates are also generally light sensitive and can decompose back into peroxy radicals and NO_2 (Finlayson-Pitts and Pitts, 2000). Parrish et al. (1993) have shown that on average, peroxy nitrates were 12-25% of the total NO_y ($NOy=NO+NO_2+NO_3+HNO_3+N_2O_5+HONO$+all other oxidized nitrogen species) at six rural sites in North America, and therefore provide a temporary storage for NO_x that is capable of transporting NO_x to rural and remote locations.

In high NO_x conditions peroxy radicals can react with NO that can either add to the peroxy radical to form an organic nitrate or abstract an oxygen from the peroxy radical to form an alkoxy radical and NO_2. The branching ratio, or the fraction of the time that the organic nitrate is formed, is highly dependent on the structure of the BVOC, with larger species producing more organic nitrate (Arey et al., 2001). The alkoxy radical can

then undergo three different chain terminating steps shown in Figure 1.4. The alkoxy radical can undergo a hydrogen shift, forming an alcohol-alkyl radical. While this is a minor pathway observed in laboratory studies, it is highly important in SOA formation. (Ehn et al., 2014b) have shown that 1,5-hydrogen shifts can produce first generation extremely-low vapor pressure volatile organic compounds that are thought be essential in SOA formation. The second pathway is through the cleavage of the carbon-carbon bond adjacent to the alkoxy carbon forming a carbonyl and alkyl radical. The alkyl radical can then react with O_2 again repeating the peroxy radical cycle. Alkoxy radicals can also react with oxygen, which abstracts a hydrogen atom forming HO_2 and a carbonyl compound (Atkinson and Arey, 2003).

Under low NO_x conditions, the fate of the peroxy radical is much different. With very little NO or NO_2 available to abstract or add to the peroxy radical, the peroxy radical can react with other peroxy radicals as shown in Figure 1.4. Generally, in low NO_x conditions, RO_2 reacts primarily with HO_2 (Kroll et al., 2006; Presto et al., 2005). RO_2-HO_2 reactions can lead to either hydroperoxide, alcohols, and/or carbonyls. In some cases, RO_2-RO_2 reactions can lead to dimers. This reaction pathway is important in the formation of secondary organic aerosol, as RO_2 –HO_2 reactions tend to lead to products with much lower vapor pressures (Surratt et al., 2010).

1.5.2 O_3

Ozone is one of the central oxidants in the atmosphere due to its reactivity and abundance. The production of ozone in the troposphere is governed by the emission of

VOCs and their interaction with the NO_x cycle (reactions 1.1, 1.2, and 1.3), as shown in Figure 1.5.

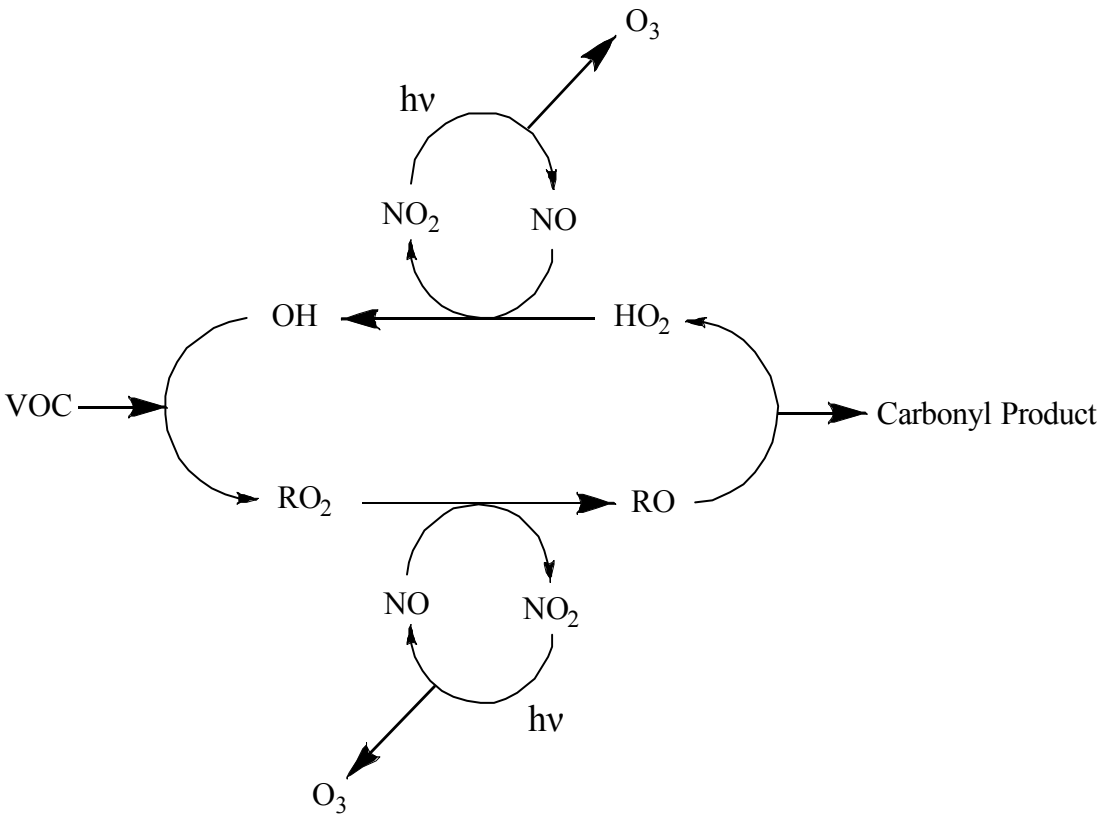

Figure 1.5 Overview of O_3 production from the oxidation of BVOCs

Ozone is produced by the conversion of NO into NO_2 through reactions with peroxy radicals in the troposphere. Due to the photolysis of NO_2 into NO, the NO_x cycle continues, but without the destruction of O_3, giving a net production of O_3. This process is described in greater detail below.

Due to the relatively long atmospheric lifetime of ozone (~10-14 days), there is net transport of O_3 by diffusion from the stratosphere into the troposphere (Atkinson and Arey, 2003). It should be noted the production of O_3 in the stratosphere, the layer of the atmosphere above the troposphere, is very different and will not be investigated in this chapter. These two sources of O_3 are balanced by losses including photolysis, reaction with BVOCs and deposition to surfaces. Ozone measured at remote sites is typically around 40 ppb, while some polluted urban regions have been shown to exhibit mixing ratios well above 100 ppb (Oltmans and Levy, 1994).

The oxidation of alkenes by ozone always begins with addition across a double bond to form a primary ozonide as shown in Figure 1.6.

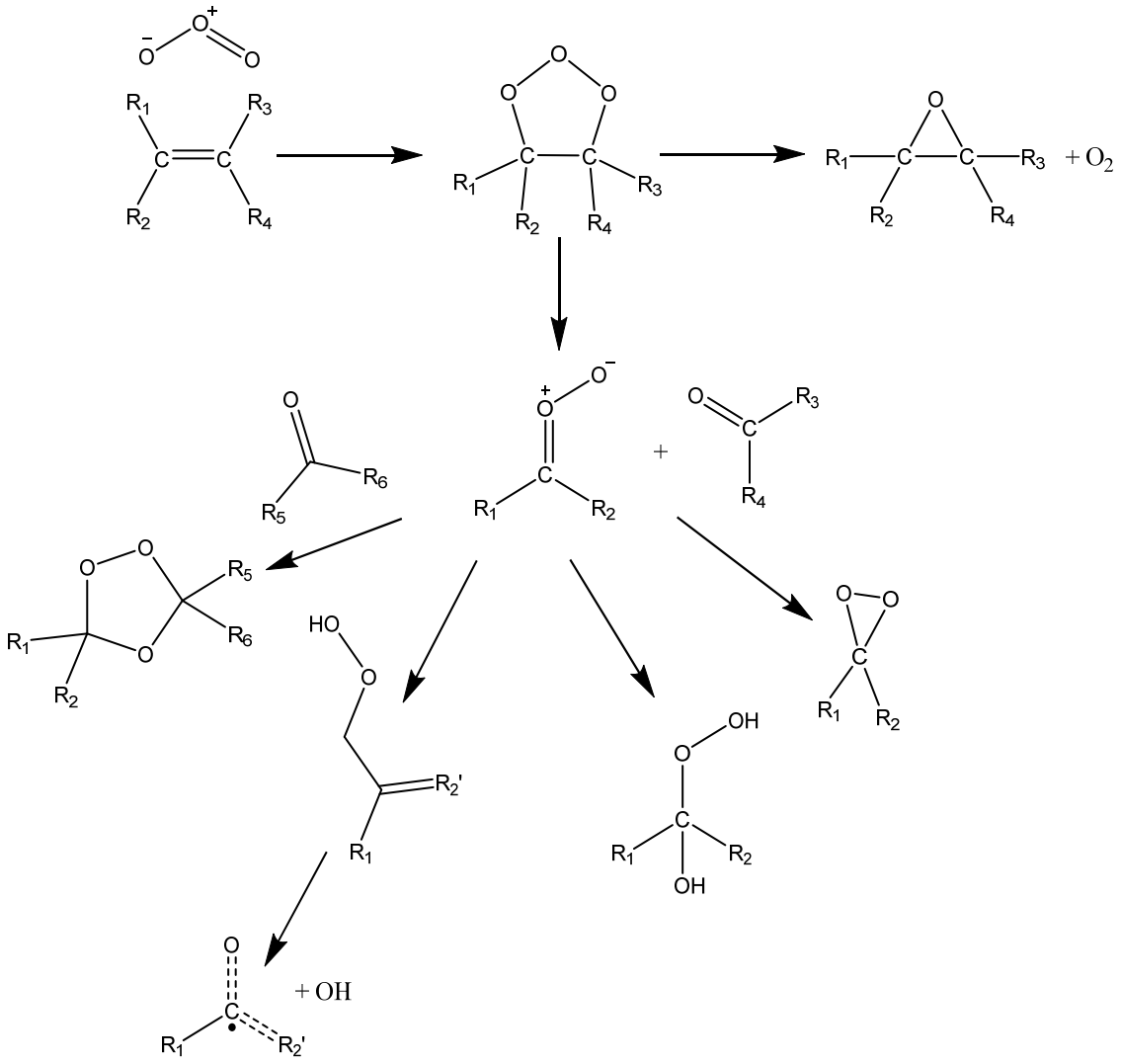

Figure 1.6 Oxidation pathway of O_3 and BVOCs.

There are two different paths upon which the primary ozonide can proceed, including rapidly decomposing to form a carbonyl product and a Criegee intermediate or by forming an epoxide. The formation of epoxides is a minor pathway (Atkinson, 2007). The formation of the Criegee intermediate from the primary ozonide leaves the intermediate with substantial internal energy that can either be stabilized by collisional energy transfer or dissociate into smaller species. Criegee intermediates can undergo *syn*-isomerization to

form a hydroperoxide, which can then dissociate into an OH radical and alkyl radical (Aschmann et al., 2002). Criegee intermediates can also undergo anti-isomerization to form a dioxirane functionality (Atkinson and Arey, 2003). The formation of dioxirane has been shown to lead to the formation of carboxylic acids, which have a profound effect on SOA formation and growth (O'Neal and Blumstein, 2004). Reactions of carbonyl compounds and water vapor with the Criegee intermediates lead to the formation of secondary ozonides and hydroperoxides, respectively (Atkinson and Arey, 2003). A key feature of the ozonolysis reaction is the cleavage of the carbon-carbon double bond, which can lead to products with decreased volatility (acyclic and exo-cyclic double bonds) or increased volatility (endo-cyclic double bonds). However the lower volatility of certain products can be offset by the addition of functional groups, therefore the vapor pressure change due to cleavage of the carbon-carbon double bond is highly dependent on the carbon backbone (Kroll and Seinfeld, 2008).

The fate of Criegee intermediates is highly uncertain. The nature of the Criegee intermediate, as either a bi-radical or zwitterion, was only recently determined. Model calculations (Nguyen et al., 2007) and laboratory studies of simple Criegee intermediates (Lee et al., 2012) have shown that most Criegee intermediates are most likely zwitterions. Chamber studies of ozonlysis reactions have shown that Criegee intermediates can react with water vapor to form hydroxyhydroperoxides, which could be stable or decompose to a carbonyl plus H_2O_2 or to a carboxylic acid plus H_2O. However, other studies have shown that the presence of water vapor has no effect on the production of OH from the ozonolysis of BVOCs, indicating that the chemistry of Criegee intermediates is not well understood (Taatjes et al., 2014).

There is very little research on the effect of NO_x during ozonalysis reactions (interaction with Criegee intermediates). This is because in any attempt to study O_3 and NO_x chemistry, NO_3 will be formed (discussed below), and distinguishing between O_3 and NO_3 oxidation becomes difficult to differentiate. Reactions to study the effect of NO_x on O_3 chemistry would require specially filtered light that could photolyize NO_2 into NO, NO_3 into NO_2, and prevent the photolysis of O_3 (so that the formation of the OH radical does not interfere). No known chamber currently has this capability.

1.5.3 The Nitrate Radical

The nitrate radical is formed by the reaction of O_3 with NO_2 and is in equilibrium with N_2O_5 in the troposphere as shown in reactions 1.6 and 1.7.

$$NO_2 + O_3 \longrightarrow NO_3 + O_2 \qquad (1.6)$$

$$NO_3 + NO_2 \rightleftharpoons N_2O_5 \qquad (1.7)$$

Due to the large absorption cross section of NO_3 in the UV (<640 nm) (Johnston et al., 1996), it rapidly decomposes during the day and was believed to only be important during the night and in highly polluted regions. However, NO_3 chemistry plays an important role in influencing daytime photochemistry (Brown and Stutz, 2012). Penkett et al. (1993) have shown that NO_3 more efficiently removes unsaturated hydrocarbons from the troposphere than OH on regional scales. NO_3 chemistry effects the NO_x cycle, as (Stutz et al., 2010) have shown that up to 50% of emitted NO_x throughout a 24 hour period in urban areas can be removed through nocturnal processing. Pratt et al. (2012) showed that a significant fraction (~10%) of isoprene nitrates formed during the daytime was a result of NO_3 chemistry. NO_3 dominates the oxidation of dimethyl sulfide in coastal

regions, affecting the sulfur cycle in marine areas, therefore having a large effect on SOA formation (Stark et al., 2007). Due to its high reactivity, NO_3 generally has a lifetime of under a minute, but has been measured in the hours range at desert sites downwind of a polluted urban environment (Platt et al., 1984). Typical NO_3 mole ratios for urban environments are between a 30 ppt maximum during the early evening hours and below the detection limit of 1 ppt for most of the day (Smith et al., 1995). For rural areas, such as central Alabama, NO_3 concentrations rarely exceeded the 1 ppt detection limit for a month long campaign (unpublished data).

The nitrate radical, similar to the OH radical, initiates the degradation of olefinic BVOCs by addition across a carbon-carbon double bond, followed by reaction with O_2, to form an nitrooxy-peroxy radical. It is possible for the nitrate radical to oxidize alkanes and saturated alcohols, ethers, esters, and ketones by H-atom abstraction, but the rates of this process is too slow to be considered atmospherically relevant (Perring et al., 2013). However, H-atom abstraction is important for aldehydes, due to the weak H-C bond of the aldehyde functionality (Atkinson and Arey, 2003). The addition of either OH or NO_3 across a double bond has about the same effect on the vapor pressure of the resulting products (Kroll and Seinfeld, 2008).

1.5.4 Cl Atom

Chlorine atom chemistry has traditionally only believed to be important in areas near oceans, where there is a large source of Cl from seawater (Behnke et al., 1997; Erickson et al., 1999; Spicer et al., 1998). Recent observations by (Thornton et al., 2010) and (Mielke et al., 2011) have shown concentrations of $ClNO_2$ of 400 ppt and 250 ppt,

respectively, at continental sites located over 1000 km from the nearest ocean, suggesting large continental sources of chlorine. Finlayson-Pitts (1989) and Behnke et al (1992) discovered that the heterogeneous chemistry of N_2O_5 leads to the formation of $ClNO_2$, a daytime chlorine radical precursor and species that serves as a temporary Cl and NO_x reservoir as shown in reactions 1.7, 1.8, and 1.9.

$$NO_2\,(g) + NO_3\,(g) \rightleftharpoons N_2O_5\,(g) \qquad (1.7)$$

$$N_2O_5\,(g) + Cl^-\,(aq) \longrightarrow ClNO_2(g) + NO_3^-(aq) \qquad (1.8)$$

$$N_2O_5\,(g) + H_2O\,(aq) \longrightarrow 2HNO_3\,(aq) \qquad (1.9)$$

$$ClNO_2\,(g) + h\nu \longrightarrow Cl\,(g) + NO_2\,(g) \qquad (1.10)$$

$ClNO_2$ is sufficiently long-lived to photodissocate into NO_2 and Cl, which can accelerate photochemical ozone production (Mielke et al., 2011).

Chlorine chemistry is difficult to observe due to the high reactivity and low chlorine concentrations of near $1x10^5$ molecules/cm^3 at maximum (Spicer et al., 1998). While Cl atom concentrations are found in lower mixing ratios then OH radicals, they are more reactive (Aschmann and Atkinson, 2013), in some cases rate constants for BVOC-Cl reactions are two orders of magnitude faster than OH (Aschmann and Atkinson, 2013; Spicer et al., 1998). This means that even though Cl atom concentrations are relatively low compared to other oxidizing species, they can significantly contribute to atmospheric chemistry and are significant oxidants near oceans, polluted sources, and in sea-ice covered regions (Liao et al., 2014). While the rates of reaction for Cl initiated oxidation are faster than OH initiated oxidation, Cl oxidation occurs mainly by abstraction of a H atom and the oxidation pathway proceeds similar to that found in Figure 1.4 (Faxon and Allen, 2013; Jobson et al., 1994).

1.6 Overview of Oxidation Pathways

From the previous section, the oxidation pathway of the atmosphere is simplified in Figure 1.7. Overall, oxidation of BVOCs leads to products with lower vapor pressures that can either be deposited onto surfaces or absorbed into aerosols or other liquids. If the first generation products are not of sufficient vapor pressure or solubility to partition into aerosols, the first generation products can be subjected to further oxidation by O_3, OH, NO_3, or Cl and so on. Hydrocarbons in the atmosphere can be oxidized, via OH radical chemistry in the presence of O_2, all the way to CO_2 and H_2O.

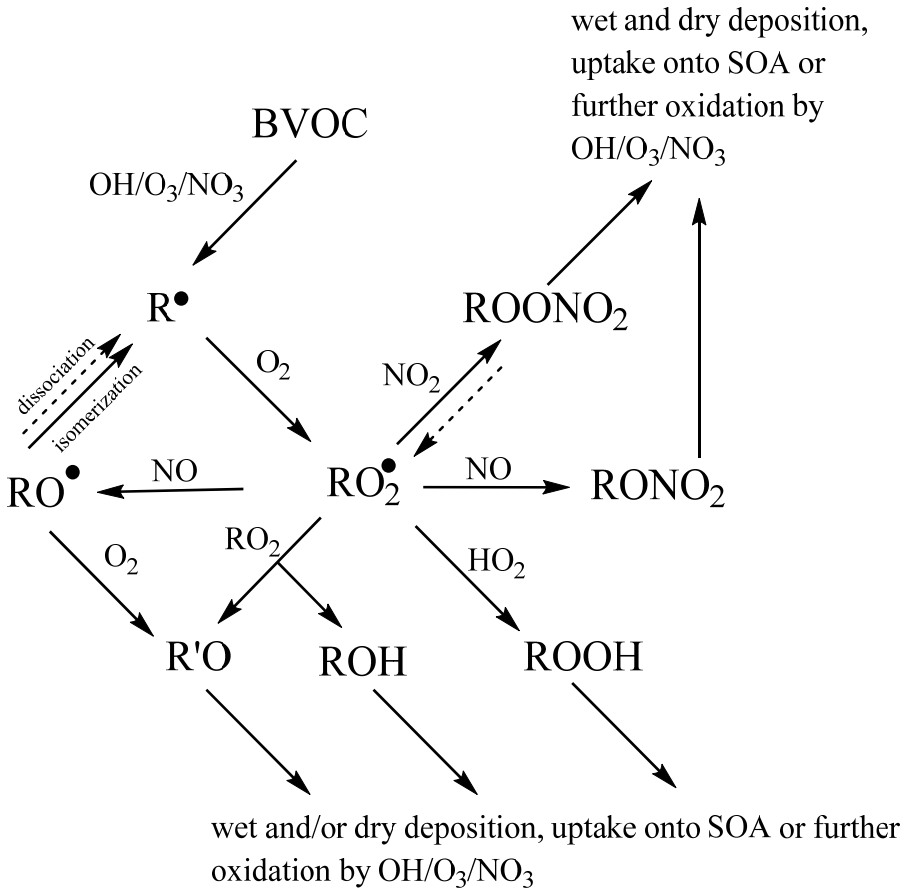

Figure 1.7 Simplified BVOC oxidation scheme.

It should be noted, that at sufficiently large NO concentrations (e.g. > 100 ppt) for nearly every BVOC oxidized, two NO molecules are converted into NO_2 (one from RO_2 + $NO \longrightarrow NO_2$ and one from $HO_2 + NO \longrightarrow NO_2$). From the current understanding of ozone production at steady state, O_3 production is then expressed quantitatively by Equation 1.2 (Thornton et al., 2002), for daytime sunlit conditions.

$$P_{O3} = k_{NO+HO2}[NO][HO_2] + k_{NO+RO2}[NO][RO_2] \qquad \text{Equation 1.2}$$

This production is not exactly two molecules of O_3 produced, because of chain terminating steps in the HO_x and NO_x cycle. The HO_x cycle is terminated when closed shell compounds are formed, including alcohols and dimers (Kroll and Seinfeld, 2008). RO_2 can react with other RO_2 to make an alcohol and carbonyl compound, but RO_2 primarily reacts with HO_2 (Presto et al., 2005). The NO_x cycle is terminated when OH reacts with NO_2 to form HNO_3, NO_2 reacts with RO_2 to form peroxy nitrate species, and when RO_2 reacts with NO to form $RONO_2$ (Thornton et al. 2002).

One of the most important factors in understanding the production of O_3 by the oxidation of BVOCs is O_3 production is not linearly dependent on NO_x concentrations. Reactions 1.11 through 1.17 show the OH-BVOC chemistry dependence on NO_x. Reactions 1.12 and 1.15 propagate the chain reaction and make O_3. At higher mixing ratios of NO_x, the reaction between NO_2 and OH forming HNO_3 (reaction 1.17) becomes prominent and sequesters the formation O_3 by limiting the amount of OH that reacts with BVOCs (Perring et al., 2013; Ridley et al., 1992a; Thornton et al., 2002). At low concentrations of NO_x, the chain is terminated by the formation of peroxides and alcohols (reaction 1.16).

$$R + OH \xrightarrow[O_2]{} ROO \quad (1.11)$$

$$ROO + NO \longrightarrow RO + NO_2 \quad (1.12)$$

$$ROO + NO \longrightarrow RONO_2 \quad (1.13)$$

$$RO \xrightarrow[O_2]{} \text{products} + HO_2 \quad (1.14)$$

$$HO_2 + NO \longrightarrow OH + NO_2 \quad (1.15)$$

$$RO_2 + HO_2 \longrightarrow \text{products} \quad (1.16)$$

$$OH + NO_2 \longrightarrow HNO_3 \quad (1.17)$$

A visual representation of this phenomena can be seen in Figure 1.8.

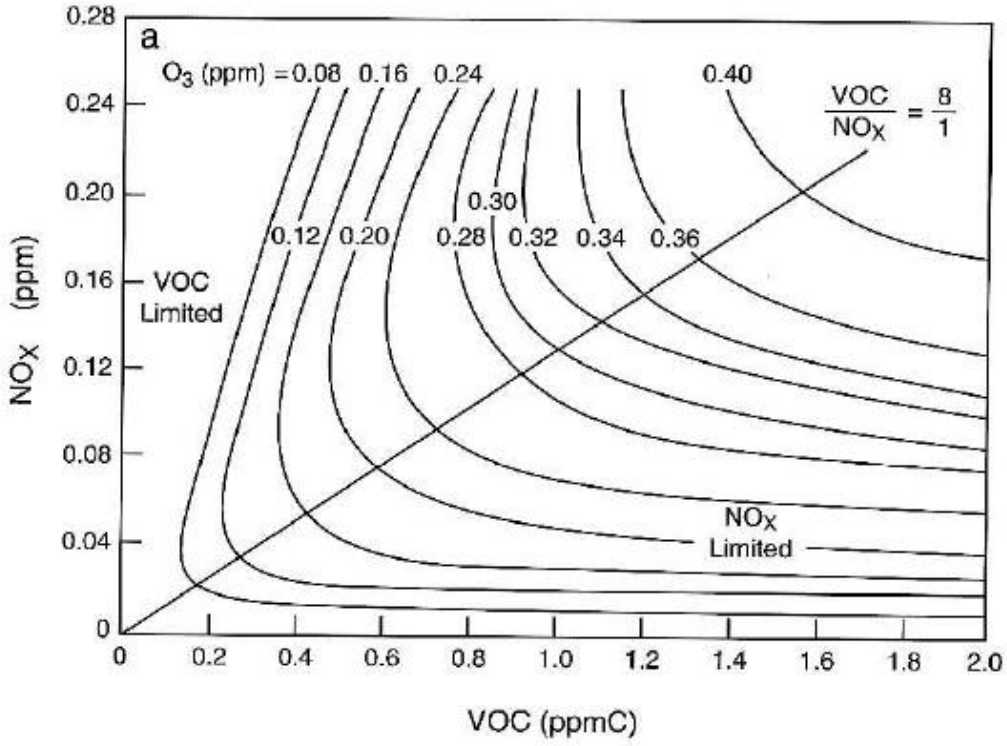

Figure 1.8 Isopleth showing the non-linear dependence of O_3 formation on NO_x and VOC emissions. Figure taken from Dodge (1977).

As shown in Figure 1.8, there are conditions that can lead to increase O_3 production by lowering NO_x concentrations. A key factor in understanding tropospheric chemistry is knowing the chain terminating steps in BVOC oxidation, including organic nitrate formation.

1.7 Organic Nitrate formation and Effects on Tropospheric Chemistry

Understanding the formation of organic nitrates ($RONO_2$) is critical to understanding tropospheric chemistry. Measurements of total $RONO_2$ have shown that $RONO_2$ is a large portion of NO_y in rural environments (Beaver et al., 2012; Murphy et al., 2006). However, the reactions and production of organic nitrates along with their effect on the composition of the atmosphere is poorly understood (Mao et al., 2013; Sommariva et al., 2011; Thornberry et al., 2001). One pressing question that is still unanswered is the long term fates of organic nitrates and whether they are a temporary storage of NO_x or if they release some fraction of NO_x during second or subsequent generation oxidation processes (Lockwood et al., 2010; Mao et al., 2013; Paulot et al., 2009).

Due to isoprene being the dominant BVOC emission, there has been much research in the area the effect of isoprene chemistry and the production of isoprene nitrates on local and regional tropospheric chemistry (Beaver et al., 2012; Ito et al., 2007; Mao et al., 2013; Paulot et al., 2012; von Kuhlmann et al., 2004; Weaver et al., 2009; Wu et al., 2007; Xie et al., 2013). By adjusting the yield of isoprene nitrates from 4% to 12%, Wu et al. (2007) modeled a 10% decrease in worldwide O_3 concentrations. There are large uncertainties in isoprene + NO_3 chemistry as isoprene is an important sink for NO_3

(Brown et al., 2009; Hurst et al., 2001; Starn et al., 1998). Studies have shown that NO_3 reaction only accounts for 6-7% of isoprene oxidation (Horowitz et al., 2007), but the reaction can contribute to 30-60% of the total isoprene nitrate mixing ratio in the eastern United States (Paulot et al., 2012; von Kuhlmann et al., 2004). Pratt et al. (2012) found that isoprene + NO_3 chemistry contributed to ~9% of isoprene nitrates during the day and ~42% at night in a mixed forest in northern Michigan. There is uncertainty regarding the fate of isoprene nitrates as Ito et al. (2007) and Perring et al. (2009a) estimated that the fate of isoprene nitrates is dominated by losses when oxidized by OH and O_3 while Giacopelli et al. (2005) and Horowitz et al. (2007) have concluded deposition is the primary sink. Ng et al. (2008) have shown that the NO_3 + isoprene reaction leads to di-nitrates and oligomers that could be important in SOA formation, and a significant pathway for the removal of NO_x from the troposphere.

While there has been considerable research into isoprene nitrates, there have been few studies on the production or impact of monoterpene nitrates and other BVOC nitrate species (Browne et al., 2014; Pratt et al., 2012; Rindelaub et al., 2015). There has also been very little insight into the specific reactions or pathways that lead to organic nitrate production (Paulot et al., 2009). Arey et al. (2001) have shown that in general, larger species have larger organic nitrate yields. Understanding these reactions is also critical in understanding secondary organic aerosol production, as organic nitrates are believed to be SOA precursors (Hallquist et al., 2009; Ng et al., 2008; Rindelaub et al., 2015) and therefore could have a significant effect on global climate change.

1.8 Importance of NO_x-BVOC Chemistry in Global Climate Change

Understanding BVOC oxidation is critical to understanding the future of global climate change. As previously described above, the oxidation of BVOCs generally leads to compounds with lower vapor pressures and are higher water solubility. These species are then able to form secondary organic aerosol (SOA). SOA accounts for a significant fraction of ambient tropospheric aerosol (Hallquist et al., 2009). SOA, like primary aerosols (aerosols directly emitted into the atmosphere, including wind-blown dust, particles from volcanic eruptions, particles from biomass burning, etc…), scatter and absorb radiation, participate in heterogeneous chemical reactions, influence cloud formation (Hallquist et al., 2009), and therefore have a central role in climate change (IPCC, 2007). As previously stated, BVOCs are temperature dependent (Guenther et al., 1993), and as global temperatures rise, so will BVOC emissions, along with SOA (Heald et al., 2008). Ambient aerosols have been shown to have damaging effects on respiratory and cardiovascular systems (Davidson et al., 2005; Harrison and Yin, 2000; Pope III and Dockery, 2006). The magnitude of these effects remains highly uncertain due to a lack of understanding of the sources, properties, mechanisms of formation, and composition of aerosols. There is also a significant gap in identifying the quantity of SOA in the atmosphere as bottom-up estimates of total biogenic SOA give fluxes of 12-70 Tg/yr while top-down estimates have the rate at 140-910 TgC/yr(Goldstein and Galbally, 2007).

1.8.1 Organic Nitrates and their Role in SOA Formation

While there has been considerable research leading to a better understanding of the processes that govern SOA formation, there is still not a quantitative and predicative understanding of SOA formation (Hallquist et al., 2009). There have been multiple studies showing the dependence of aerosol formation on NO_x and BVOC concentrations (Ng et al., 2007; Presto et al., 2005; Pye et al., 2010; Xu et al., 2014). Ng et al. (2007) have shown that under high-NO_x conditions, monoterpene and sesquiterpene SOA yields are higher and this is either a result of increased H-shift reactions described above, or due to higher organic nitrate yields found with bigger BVOC species (Arey et al., 2001). Ng et al. (2008) have found that in high NO_x conditions, isoprene nitrates could lead to di-nitrate and oligomer formation, and increase the isoprene SOA yield significantly. Pye et al. (2010) found that the fast reaction of monoterpenes with NO_3 is a major contributor to surface level aerosol concentrations in anthropogenically influenced areas. Organic nitrates have been observed in ambient aerosol, and the fraction of total organic nitrate in aerosol showed an equilibrium-like response to temperature cycles, suggesting some reversible absorptive partitioning (Fry et al., 2013).

1.9 Instrumentation for Atmospheric Chemistry Research

Current atmospheric chemistry research is focused on reactive trace gases and particles relevant to climate and air quality. One of the main challenges of studying atmospheric chemistry is developing instrumentation to observe reactions that occur on time scales of less than a second when the concentrations of trace species are generally in the ppb to ppt range (Farmer and Jimenez, 2010). To fully elucidate a clear understanding

of sources, sinks, mixing ratios, reaction rates, and products, appropriate instrumentation has to be developed. To make atmospherically relevant measurements, instrumentation has to meet certain criteria, including;

1. Rapid time resolution (greater than 1 Hz sampling frequency, (Nguyen et al., 2015))
2. Portability
3. Ease of Calibration
4. Stability with respect to pressure and temperature fluctuations
5. Minimal inlet design
6. Lack of interfering species and sampling artifacts
7. Limit of detection below atmospherically relevant concentrations

The current understanding of atmospheric chemistry is limited by the analytical techniques currently available and by a lack of certified standards of atmospherically relevant species (organic nitrates, organosulfates, radical species, etc.). While each of these techniques has its strong points, all of them suffer from limitations and therefore the need for overall improvement would help elucidate the role of NO_x in atmospheric chemistry.

1.9.1 O_3, NO_x, and NO_y

Ozone was first measured in the atmosphere by embedding a paper strip with KI and starch which when exposed to ozone changed violet and the intensity of the color change was used to determine O_3 concentrations (Schoenbein, 1840). O_3 has been measured by adding excess NO into a reaction chamber, and reacting ambient O_3 with the

NO to form excited state NO_2, which then returns to ground state, releasing a photons in the near infrared region which can be measured by a photomultiplier tube (Walega et al., 1991). Reactions 1.18 and 1.19 show the process.

$$O_3 + NO \longrightarrow NO_2^* + O_2 \quad (1.18)$$

$$NO_2^* \longrightarrow NO_2 + hv \quad (1.19)$$

The most common method for the detection of ozone is by ultra-violet absorption at 254 nm. In commercial instruments, O_3 is detected in a flow cell by measuring the absorption at 254 nm. In another similar cell, the sampled air is scrubbed of O_3 by Hopcalite, a mixture of copper and manganese oxides to give a blank signal. However this method is subject to interferences from compounds such as H_2O_2 and isobutyl nitrite, which also absorb at 254 nm and are scrubbed by Hopcalite. At ambient concentrations, this problem is ignored due to much higher concentrations of O_3 dwarfing any interference signals.

NO has been measured since the 1970s by the reaction of NO with O_3 to form excited state NO_2 as described above in reactions 1.18 and 1.19 (Fontijn et al., 1970). The first method to measure NO_x was made by measuring NO first, then passing the sample across a heated (~ 350°C) molybdenum converter to convert the NO_2 into NO, and the difference between the two signals was determined to be the signal from NO_2 (Joseph and Spicer, 1978). While this converter is able to effectively convert ~100% of NO_2 into NO, it is known to be subject to interferences (Navas et al., 1997). Compounds such as peroxy nitrates, organic nitrates, $ClNO_2$, and HNO_3 are known to convert into NO in this converter, giving artificially high NO_x concentrations (Grosjean and Harrison, 1985).

To solve the interference problem from commercial Mo converters, new methods were developed to accurately measure NO_x mixing ratios. The two most accurate ways

for measuring NO_x are through the use of blue-light light-emitting diodes (LEDs) as NO_2 converters and laser-induced fluorescent spectroscopy (LIF). Blue-light LEDs originally used light focused at 365 nm to photolytically convert NO_2 into NO followed by chemiluminescence detection via reaction with O_3, then the difference between NO and NO_2 divided by the converter efficiency would give the concentration of NO_2 in the sample (Buhr, 2007). Current blue-light LEDs utilize 395 nm to photolyize NO_2 into NO without converting HONO into NO and work done by Sadanaga et al. (2010) has shown the ability to convert nearly 90% of NO_2 into NO. In LIF, a sample is passed through an incident laser of 585 nm, and the intensity of the fluorescence at 750 nm is then used to determine the concentration of NO_2 in the sample (Thornton et al., 2000).

NO_y is measured though either passing the sample through a heated (300°C) gold tube converter with a dilution of gas of carbon monoxide to reduce all odd-nitrogen species to NO (Bollinger et al., 1983) or through thermal dissociation to NO_2 followed by measurement by laser-induced fluorescence (Day et al., 2002). To speciate organic nitrate, Day et al. (2002) used different temperature regions of 200°C, 350°C, and 600°C to thermally dissociate peroxy nitrates, alkyl and hydroxyalkyl nitrates, and HNO_3 into NO_2, which could then be measured by LIF. Reactions 1.20 through 1.22 show the process of thermal dissociation.

$$RO_2NO_2 \xrightarrow[200\ C]{} NO_2 + RO_2 \quad (1.20)$$

$$RONO_2 \xrightarrow[350\ C]{} NO_2 + RO \quad (1.21)$$

$$HNO_3 \xrightarrow[600\ C]{} NO_2 + OH \quad (1.22)$$

1.9.2 BVOCs

The greatest difficulty in quantifying BVOCs is the vast number of species present in the atmosphere and that many of the species in the atmosphere contain similar structural and physical properties. As previously stated, there are well over 200 observable oxidation products from the ozonolysis of a single sesquiterpene (Isaacman et al., 2011) and two-dimensional gas chromatography instruments are able to see over 500 compounds with a wide range of polarities and volatilities in urban air samples (Lewis et al., 2000). A large uncertainty in understanding the effect of BVOCs on the oxidizing capacity of the atmosphere is the inability to speciate all compounds that impact the oxidative capacity of the atmosphere. Figure 1.9 shows a graph from Hallquist et al. (2009) showing what is needed for an ideal instrument for the detection of BVOCs, that is the ability to detect all organic mass with molecular identification on a fast time scale.

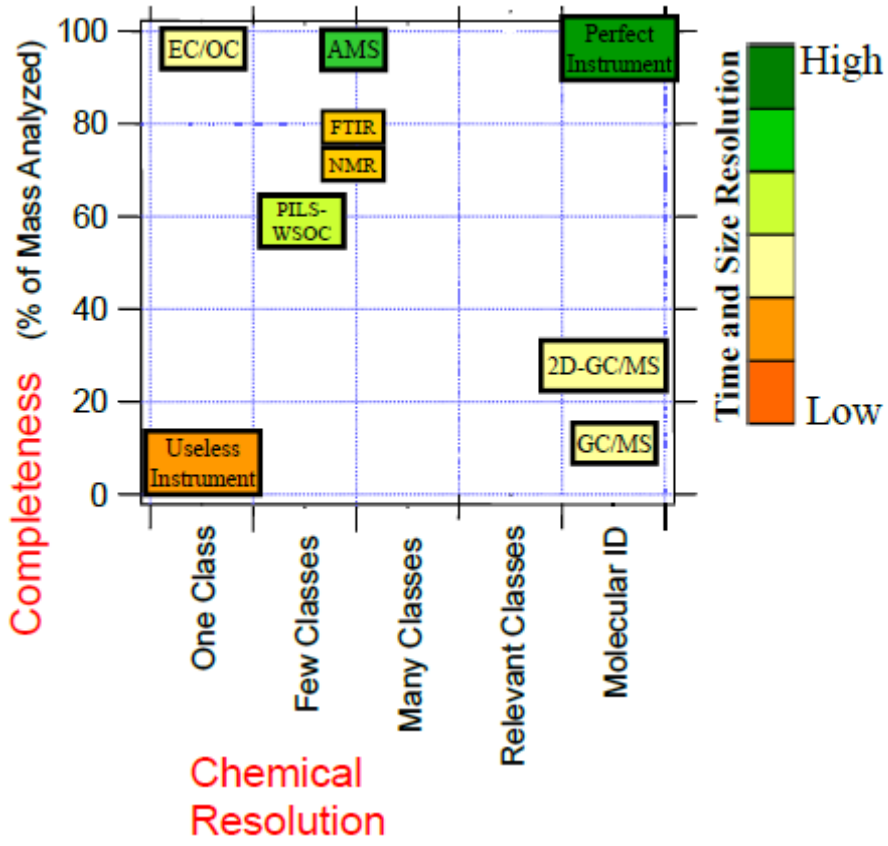

Figure 1.9 Graphical representation of current instruments with their advantages and limitations. Figure is taken from Hallquist et al. (2009)

Techniques such as Fourier transform spectroscopy (Rinsland et al., 1987), tunable diode laser spectroscopy (Anderson and Zahniser, 1991), gas chromatography coupled with a FID detector, and mass spectrometry have identified hundreds of different BVOCs in the troposphere (Isaacman et al., 2012). However, spectroscopic techniques lack the ability to speciate compounds and are only able to detect organic functional groups. Gas chromatography is the most common method for separation of BVOCs, but long narrow bore columns have limited resolving power (Hamilton, 2010a, b). Lee et al. (2005) showed that when using proton-transfer reaction mass spectrometry (PTR-MS),

the total observed monoterpene concentration was 30% higher than observed by pre-concentration followed by GC separation, showing that methods to speciate BVOCs are not observing some fraction of total BVOCs. PTR-MS is a commonly used MS method which utilizes H_3O^+ to ionize BVOCs (Lindinger and Jordan, 1998) and can identify a multitude of BVOCs, but lacks the ability to speciate isomers (Mielke et al. 2010).

Comprehensive two-dimensional gas chromatography (GCxGC) provides a vastly improved method for the separation of BVOCs. By coupling a secondary column to a primary column, through a modulator, GCxGCs have been able to obtain vastly improved peak capacities, with the total peak capacity equal to the arithmetic product of the two columns peak capacities (Liu and Phillips, 1991). Venkatramani and Phillips (1993) found that by using a two separation phases, peak capacity increased from 1000 to 50000. Lewis et al. (2000) first showed the resolving power of non-comprehensive (the entire sample was not separated on the second dimension) two dimensional GC (GC-GC) instruments for atmospheric samples by detecting over 100 new compounds. Lewis et al. (2000) showed that one-dimensional GC could possibly lead to underestimating the organic content of the atmosphere for urban samples, and up to two-thirds of the total carbon mass can be undetected. Due to the resolving power of 2D-GC systems, they are an optimal technique for the detection of BVOCs that can survive the columns and separation temperatures.

Detection of BVOCs is generally accomplished by flame-ionization detection, electron-capture detection, or mass spectrometry. In a flame-ionization detector, the analyte is burned in a small oxy-hydrogen flame producing CH^+ ions, which create a current that can be measured (McNair and Miller, 1998). Flame ionization detectors are

widely used due to their excellent limit-of-detection of near 10^{-11} g (~50 ppb), response to all hydrocarbons, excellent linearity over 6 orders of magnitude, excellent stability, and predictability of relative sensitivities. However, FIDs suffer from lack of structural information. Without an analytical standard, the identification of a peak in a FID chromatogram is impossible (McNair and Miller 1998).

Electron-capture detectors are selective detectors that have an excellent response to compounds with high electron affinities (Lovelock, 1961). In electron capture detectors, samples are detected by their ability to decrease the level of an ion current inside a detection cell due to lower mobility of the analyte ions in an electric field. Radioactive sources, such as ^{63}Ni emit beta particles, which collide with carrier gases to produce more electrons, which produces a current. When the analyte elutes from the column, it collects the electrons, and a decrease in the current is observed, which is proportional to the concentration of the analyte and its electron affinity. This technique has excellent limits-of-detection, linearity over 4 orders of magnitude, and fair stability (McNair and Miller, 1998). The main flaws in this detection method are that the detector does not provide a means to elucidate structural information of the analyte and the detector is only responsive to species that have high electron capture cross sections, such as organohalogens or organonitrates.

The most common method for the detection of BVOCs is mass spectrometry (MS). Mass spectrometry allows for the identification of analytes by ionizing the sample and separation of species by their mass-to-charge ratio. Structural information can be obtained from the fragmentation patterns during the ionization process or during tandem mass spectrometry, in which a parent ion is isolated, subjected to high energy collisions

that induce dissociation, and the subsequent fragments are separated by another mass analyzer and detected (McNair and Miller, 1998; Mielke et al., 2010).

To fully understand the effect of BVOC chemistry on the NO_x cycle, accurate, precise, and fast instrumentation is need to measure organic nitrate species and BVOCs. Peroxy acyl nitrates are generally measured by utilizing a cooled GC followed by electron capture detection(Bertman et al., 1993). The use of chemical-ionization mass spectrometry (CIMS), which utilizes ion-molecule reactions to selectively ionize target molecules has become the dominant method for the fast detection of nitrogen containing species (Farmer and Jimenez, 2010). Different ionization agents have been used for the detection of various NO_y components, including CF_3O^- (Crounse et al., 2006) and I^- (Lee et al., 2014a) to detect organic nitrates and SiF_5^- to detect HNO_3 (Huey, 2007). While this technique is ideal in that the soft-ionization does not fragment the analytes of interest, without a separation method, isomer identification is not yet possible.

1.10 Knowledge Gaps in our Understanding of BVOC/NOx Chemistry

While there has been dramatic improvement in the understanding of BVOC and NO_x chemistry and instrumentation over the past decade, there are still significant discrepancies between atmospheric models and measurements, indicating our lack of knowledge of tropospheric processes. The measured SOA concentrations found in the air are much higher than predicted by various models (Goldstein and Galbally, 2007). There are discrepancies in the global O_3 concentrations, with models showing global tropospheric ozone production can vary from 2300 to 5300 Tg yr^{-1} (Wu et al., 2007). Measurements of isoprene and OH radicals have shown an unknown source of OH

recycling in the atmosphere, which may explain deviations between modeled and measured OH mixing ratios (Fuchs et al., 2013). These problems will push the field of atmospheric chemistry to develop new instrumentation, determine new chemical pathways, and perform unique field measurements that will further our knowledge of the processes which dictate global air quality.

1.11 Thesis Overview

In this thesis, I will describe the modification of a NO_x chemiluminescence instrument to identify the source of NO_x that is commonly observed in the early morning hours. I will describe the development, testing, study of a new sampling system for a comprehensive flow-modulated two-dimensional gas chromatography instrument. I will show modeled organic nitrate production in the southeastern United States.

CHAPTER 2 NEW INSIGHTS INTO THE SOURCE OF THE EARLY MORNING NO_X PLUMES OBSERVED THROUGH MULITPLE HEIGHT AND FLUX MEASUREMENTS IN A NORTHERN UNITED STATES FOREST

2.1 Introduction

Emissions of NO_x ($NO + NO_2$) have a wide variety of environmental and health impacts including stimulation of forest growth (Costa et al., 2011; Lockwood et al., 2008; Magnani et al., 2007; Ollinger et al., 2002), an effect (indirectly and directly) on atmospheric aerosol concentrations and composition (Xu et al., 2014), and controlling tropospheric ozone production through reactions involving hydrocarbons and OH radicals (Ridley et al., 1992b). NO_x regulates photochemical production of tropospheric ozone, along with hydroxyl and peroxy radical concentrations directly and indirectly (Lin et al., 1988; Thompson, 1992). When nitric oxide (NO) is converted to nitrogen dioxide (NO_2) by oxidants other than ozone, such as hydroperoxyl radicals (HO_2) or organic peroxy radicals (RO_2), a net photochemical production of ozone results (Ridley et al. 1992). NO_x chemistry, in the presence of other species such as biogenic volatile organic compounds (BVOCs) (Rollins et al., 2010), NH_3 (Dentener and Crutzen, 1994), and humidity produces nitric acid and aerosol. Thus, through connection to ozone and aerosol production, and through impacts on the carbon cycle, nitrogen chemistry is linked to changes in the climate (Hallquist et al., 2009). Full details of NO_x chemistry can be found in Chapter 1.

Global emissions of NO_x were estimated to be 22.9 Tg N yr^{-1} in 2003 and 24.1 Tg N yr^{-1} in 2006 and global NO_x emissions over land increased 9.2% globally from 2003-2006 (Lamsal et al., 2011). Over the contiguous United States, fossil fuel burning emits 7.3 Tg N yr^{-1} into the atmosphere, while smaller contributions include biomass burning (0.3 Tg N yr^{-1}), soil emissions (0.5 Tg N yr^{-1}), and lightning (0.4 Tg N yr^{-1}) (Oliver et al., 1996; Zhang et al., 2003). While NO_x emissions have decreased over North America in the past decade, global NO_x emissions have increased due to increased fossil fuel usage in Asia (Lamsal et al., 2011). Understanding the sources and fate of NO_x and the distribution of odd nitrogen species is important for quantifying human impacts on both atmospheric composition and climate.

There is still a large uncertainty in the determination of the sources, sinks, and chemistry of NO_x due to the complex chemistry and dynamics of its sources and sinks. The role of forested environments is one of the largest uncertainties in understanding global NO_x emissions and fates (Fang and Mu, 2006; Min et al., 2014). Studies have shown that leaf surfaces can either act as a NO_x source or sink, depending on whether ambient concentrations of NO_x reach a compensation point (Conrad, 1996), which has been shown to range between 0.1-3 ppb (Breuninger et al., 2012; Chapparo-Suarez et al., 2011; Raivonen et al., 2009; Sparks et al., 2001). To account for the differences between observed NO_x and O_3 concentrations above and below forest canopies, many large scale models impose an ad-hoc canopy reduction factor (fraction of soil NO emissions that are converted to temporary or permanent reservoirs of NO_x, including peroxy acetyl nitrate, organic nitrates, and HNO_3 before they can escape out of the canopy) to force agreement between below and above canopy concentrations, which has been applied to many field

studies (Fang and Mu, 2006; Jacob and Wofsy, 1990; Min et al., 2014; Wang and Leuning, 1998; Yienger and Levy, 1995). Recent work by Min et al. (2014) has shown that there is a measureable significant chemical in-canopy reduction factor from NO_x emitted by microbes in the soil. There are significant gaps in the understanding of forest-atmosphere exchange of NO_x, mainly due to the lack of direct observations (Geddes and Murphy, 2014).

Due to the advances in satellite technology, there are a multitude of estimated global soil NO_x emission measurements, however they vary from 7 (Yan et al., 2005) to 21 Tg N yr^{-1} (Davidson and Kingerlee, 1997). The spread in these observations represents the spatial heterogeneity of emissions as well as the difficulty in interpreting and obtaining accurate emission data. Currently, there is limited understanding of the biogeochemical processes that produce or consume NO_x (Chapparo-Suarez et al. 2011). Much uncertainty remains in the chemical processing of NO_x, including the formation and fate of organic nitrates in the boundary layer (Lockwood et al., 2010; Paulot et al., 2009; Xie et al., 2013). To better understand the chemistry, biological, and meteorological phenomena controlling NO_x concentrations, methods such as measurements at multiple heights (discussed below), flux measurements of NO_y species ($NO + NO_x + HNO_3 + NO_3 + PAN + RONO_2$ + all other oxidized nitrogen species) (Min et al., 2012; Turnipseed et al., 2006; Wolfe et al., 2009), and the development and use of instrumentation for NO_x flux measurements (Farmer et al., 2006; Horii et al., 2004) have been recently developed.

One phenomenon of NO_x, addressed by Alaghmand et al. (2011), is the observation of high concentration of NO_x in the early morning above the canopy, the

source of which was difficult to elucidate. Figure 2.1 shows a typical rise in the concentration of NO_x on the morning of August 9th, 2012.

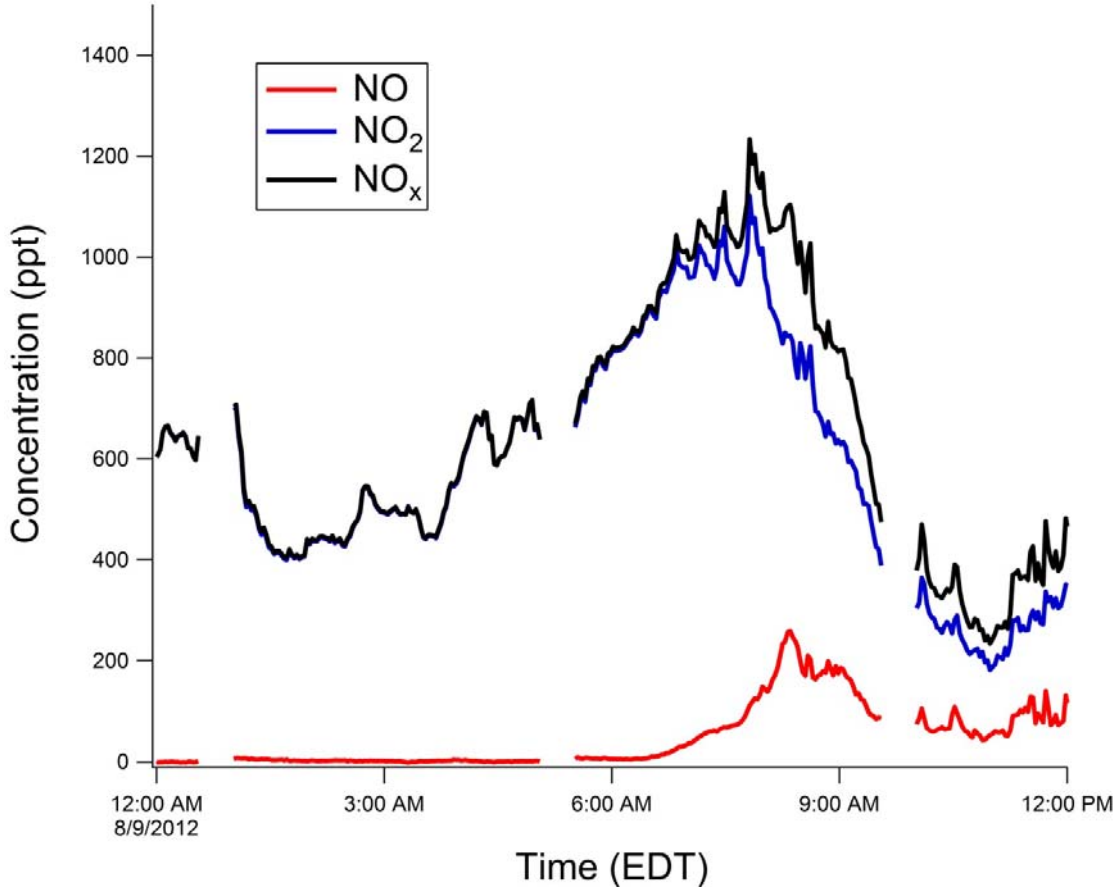

Figure 2.1 Typical rise in early morning NO_x mole ratios for the morning of August 9th, 2012.

These early morning plumes have since been reported by Seok et al. (2013) and (Wolfe et al., 2013), at the University of Michigan Biological Station (UMBS) and the Manitou Forest Observatory, respectively. Proposed sources of these early morning NO_x maxima include long-range transport of polluted air masses, downward mixing of polluted air masses during the break-up of the nocturnal boundary layer (NBL) (See Chapter 1.2), and

soil and/or foliar emissions. Alaghmand et al. (2011) hypothesized that these plumes are most likely the result of surface and combustion emissions accumulating in the NBL followed by transport to the sampling site. Seok et al. (2013) have shown that morning NO_x maxima occur after leaf fall (during the winter) and are therefore not of a foliar biogeochemical origin. At a rural forested site in northern Michigan, measured soil emissions have not been substantial enough to explain the morning NO_x plume, and the source of the morning plumes is unlikely to be local emissions due to the lack of any known local pollution sources at the remote measuring site (Alaghmand et al., 2011). To further understand the sources of early morning NO_x maxima, vertical profile and flux measurements were made at a remote forest site with high time resolution in order to help identify the major source of early morning NO_x maxima.

2.2 Experimental

A field study was conducted in the summer of 2012 at the Program for Research on Oxidants: Photochemistry, Emissions and Transport (PROPHET) measurement site at the University of Michigan Biological Station (UMBS). Figure 2.2 shows the location of UMBS.

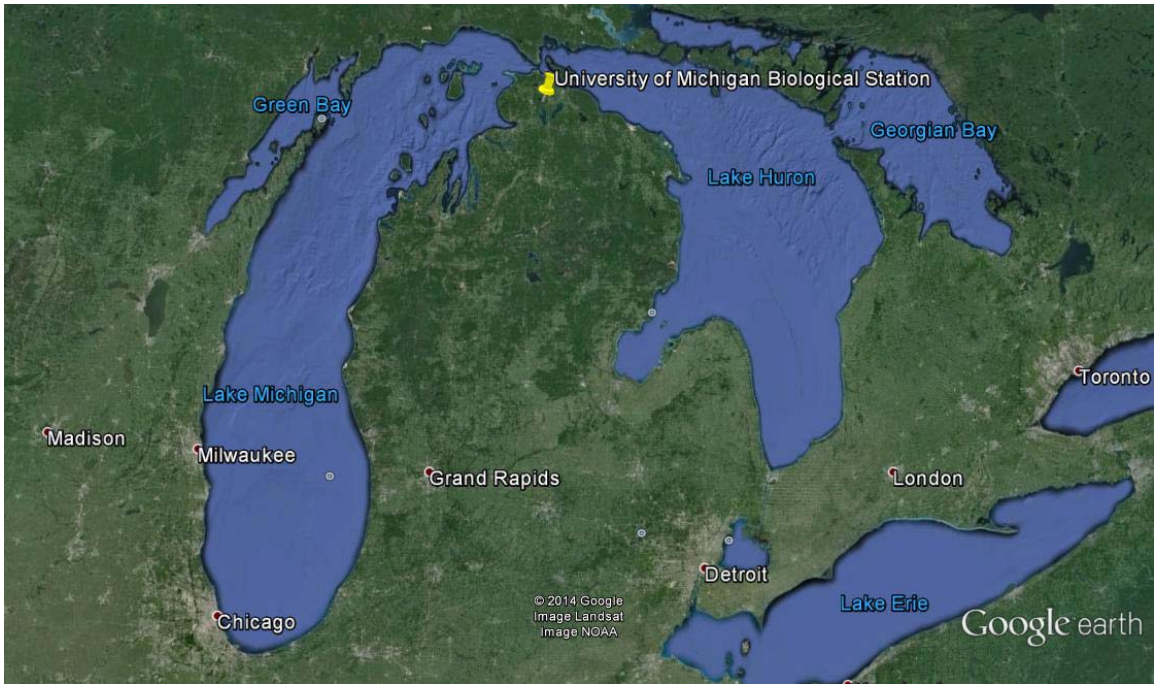

Figure 2.2 Location of the University of Michigan Biological Station.

Full details of the site can be found in Carroll et al. (2001). Briefly, the site consists of a 31.5 m tall scaffolding tower in a rural mixed deciduous/coniferous forest in northern Michigan. Figure 2.3 shows the tower located within the mixed forest.

Figure 2.3 Photo of the PROPHET tower located at UMBS. Photo courtesy of the Environmental Research Institute of Michigan.

The site has a temperate climate and is dominated by aspen trees with a mix of some maple, oak, birch, and beech (Gough et al., 2007). The understory at this site is from 0 to ~12 m and the crown layer (canopy layer that includes tree branches and leaves) is approximately 12 to 23 m (Schmid et al., 2003).

Measurements of NO_x were made at three heights during the campaign: 1.5 m, 18 m, and 31.5 m. NO_x mole ratios were concurrently measured using two instruments. First, flux measurements were conducted with a custom built two-channel chemiluminescent instrument (Air Quality Designs). This instrument measures the photons emitted when

ambient NO reacts with excess O_3 to produce excited state NO_2, which then transitions back to ground state, releasing a photon (λ = 600-3000 nm) as shown in reactions 2.1 and 2.2 (Fontijn et al., 1970; Minarro et al., 2011).

$$NO + O_3 \longrightarrow NO_2^* + O_2 \quad (2.1)$$

$$NO_2^* \longrightarrow NO_2 + hv \quad (2.2)$$

$$NO_2 + hv \longrightarrow NO + O(^3P) \quad (2.3)$$

This instrument was operated by Jeffery Geddes, a member of Jennifer Murphy's research group at the University of Toronto. NO_2 conversion into NO was achieved using a blue LED converter using 395 nm light as shown in reaction 2.3 (Buhr, 2007). This instrument contained the converter in a custom detachable inlet that was placed at the top of the tower. All NO_x flux measurements for this field campaign were made at the top of the tower with a sonic anemometer placed directly below the inlet. Details of the flux measurements can be found in Geddes and Murphy (2014).

Another custom built single channel chemiluminescent NO_x analyzer based on the design of Ridley and Grahek (1990) was used to measure NO_x mole ratios at multiple heights through the use of a 4 port valve (Hamilton MVP, Reno, NV). A design schematic of the sampling method is shown in Figure 2.4.

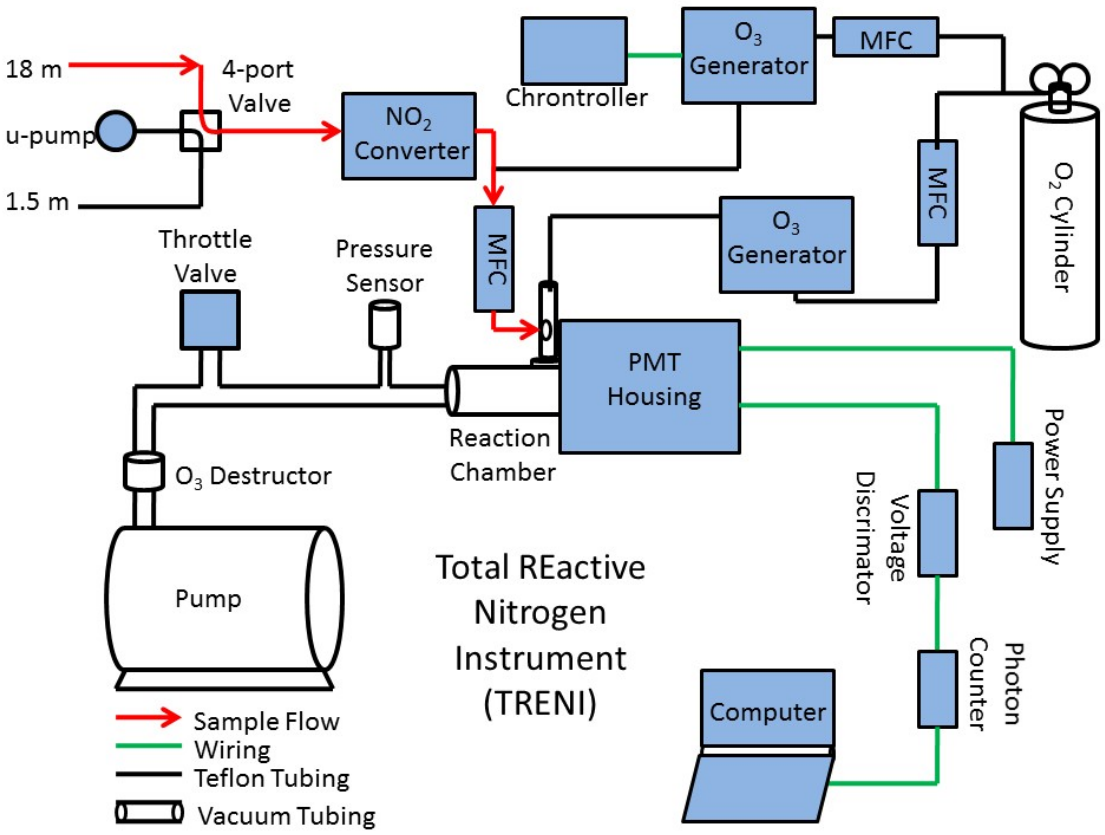

Figure 2.4 Flow Schematic of the instrument used to measure NO_x at multiple heights.

In this instrument, a four port valve was used to switch measurement heights (1.5 or 18 m). Ambient air was drawn through the instrument to a reaction chamber where it is reacted with a flow of ~1.3% O_3. Ambient NO in the reaction chamber was oxidized by O_3 to an excited state NO_2 which emitted a photon which was then measured with a photomultiplier (PMT) tube as shown in reactions 2.1 and 2.2. All flows in the instrument were controlled by mass flow controllers (MFCs) and the sampling flow rate was set at 1 liter per minute.

Similar to the flux instrument, a blue-light LED photolytic converter (Air Quality Design) was used to convert NO_2 into NO as shown in reaction 2.3. The converter was

tested before, during, and after the field campaign. The NO_2 conversion efficiency was measured using an external mixing bulb to react a standard gas of 5.17 ppm NO and a known flow rate of O_3 creating a known amount of NO_2. Figure 2.5a shows a schematic of this calibration method while 2.5b shows a visual representation of the NO_2 conversion efficiency calculation.

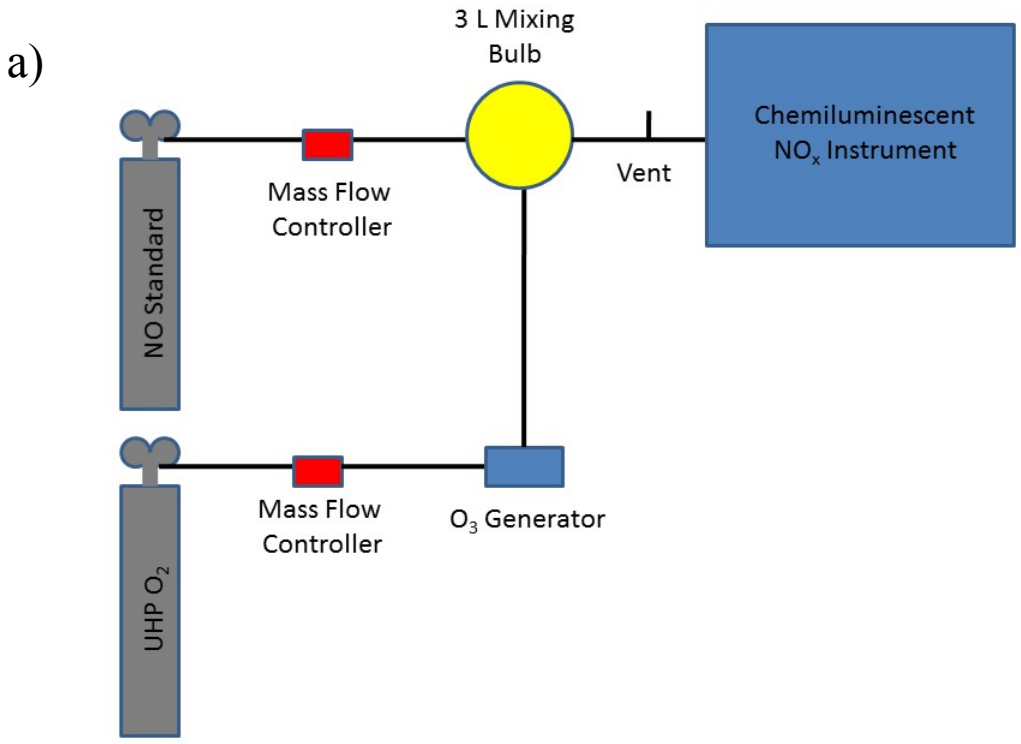

Figure 2.5 Schematic of NO_2 conversion efficiency test (2.5a) and visual representation of data from conversion test (2.5b).

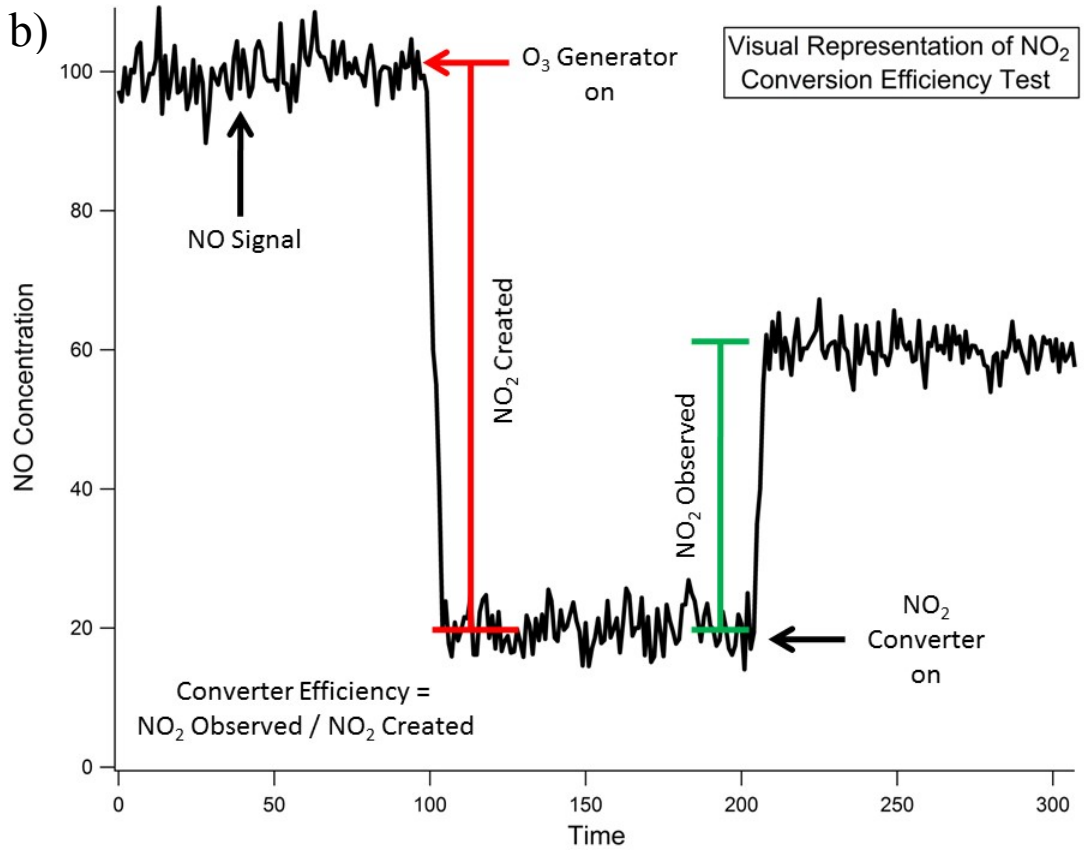

Figure 2.5 continued.

The NO_2 converter efficiency was also tested by the use of a standard tank of 4.83 ppm NO_2. The converter efficiency was calculated as 56 ± 6%, and there was no significant difference between using the mixing bulb method or the standard tank. Artifact and blank tests were performed every 30 minutes by adding an external flow of ozone upstream of the reaction chamber to titrate out any ambient NO and leaving any possible unknown contaminants that may produce photons in the chamber. Calibrations were performed daily for this instrument by mixing ultra-high purity air (Airgas) with a standard of 5.17 ppm NO (Praxair, Inc.), and the drift in sensitivity was found to be around 1% per day, as shown in Figure 2.6.

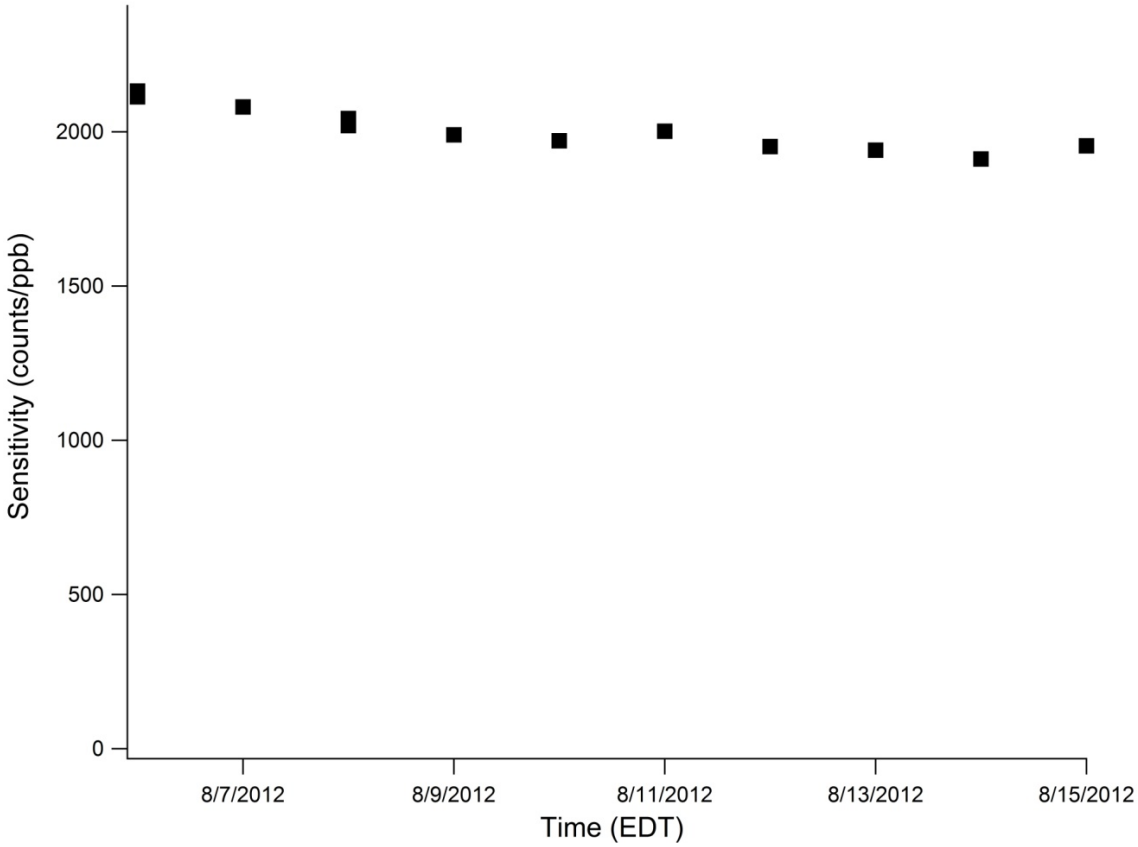

Figure 2.6 Sensitivity of the Purdue chemiluminescence instrument during the Summer of 2012.

For this instrument, two sampling lines, both 30 m long Teflon ¼ inch OD tubing, were connected to the instrument located at the base of the PROPHET tower and extended to locations outside of the laboratory. One inlet was placed within the canopy at 18.5 m while the other was fixed approximately 1.5 m from the forest floor. Teflon filter holders equipped with 1 μm Teflon filters were attached to the end of the sampling lines to prevent particles from entering the instrument. While one inlet was sampling, the other was being flushed with ambient air by the use of a KNF μpump (Trenton, NJ) at a flow rate of 1.5 L/min.

To compare the two instruments, both instruments sampled from the top of the PROPHET tower (31.5 m) for one day. Figure 2.7 shows the measured concentrations for the two instruments.

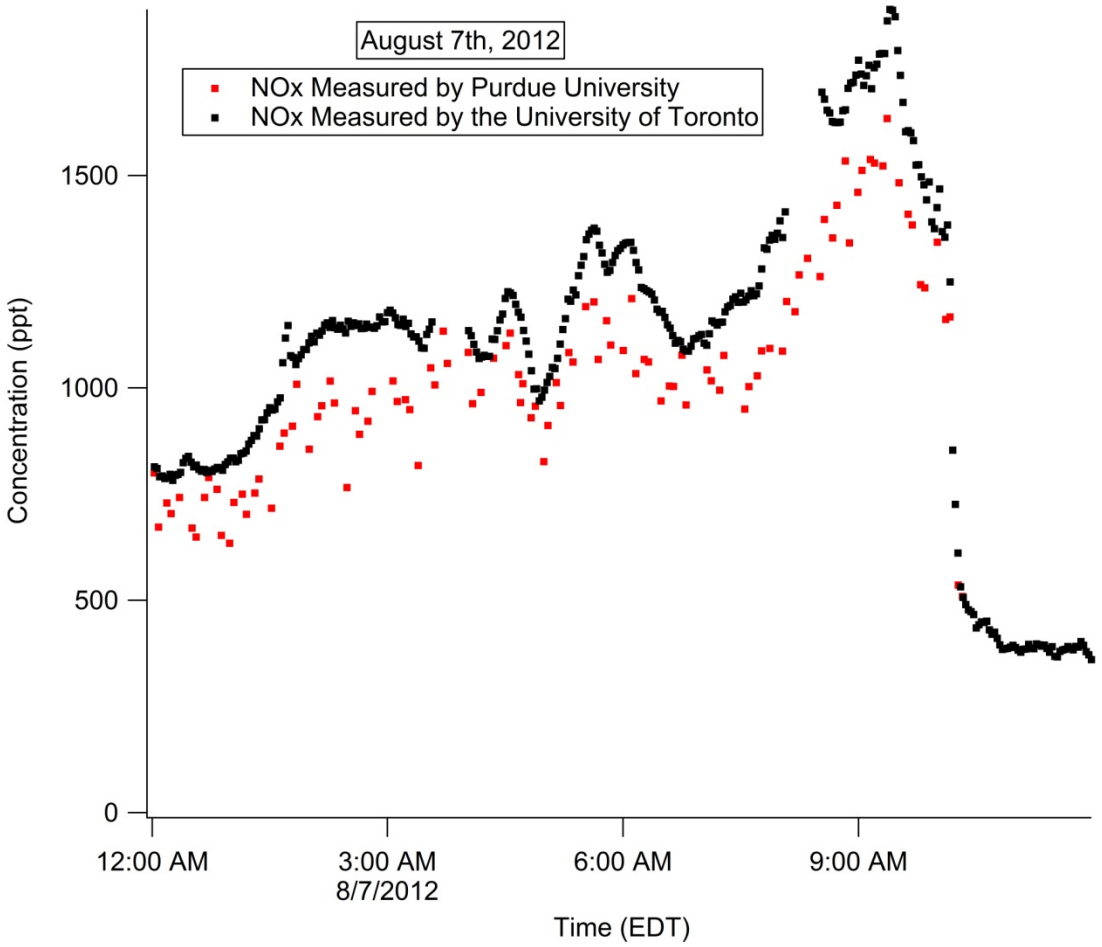

Figure 2.7 Inter-comparison of the two NO_x instruments.

The NO_x flux instrument from the University of Toronto measured concentrations that were consistently a factor of 1.1 higher than the two-inlet instrument from Purdue. As

both instruments used the same calibration standard, the source of error is most likely due to humidity corrections and another unknown source of error.

Water vapor has long been known to be a source of interference in NO_x chemiluminescence instruments as water vapor is known to absorb the photons emitted from excited state NO_2 (Gerboles et al., 2003). While water vapor in the air is generally measured as relative humidity, the absolute humidity is more important in affecting the chemiluminescent signal (Gerboles et al., 2003). When the Purdue instrument was calibrated with UHP air that was saturated (100% relative humidity) and dry (0% relative humidity), the sensitivity of the instrument changed by 6%. This is consistent with Gerboles et al. (2013), who found an increase of absolute humidity of 14 g m^{-3} (100% relative humidity during their experiment) resulted in a signal decrease of 7%. No corrections for the Purdue instrument were made because of the relatively small effect relative humidity had on the instrument.

Another known source of error in NO_x measurements is O_3 titration during sampling. Ozone titration occurs when ambient ozone reacts with NO in the dark sampling line, and due to the lack of a light source in the line, the NO steady state concentration is perturbed (Seok et al., 2013). The loss of light within the sampling line causes two shifts to occur with NO_x. The conversion of NO to NO_2 as shown in Reaction 2.4 and the conversion of NO_2 into NO_3 as shown in Reaction 2.5.

$$NO + O_3 \longrightarrow NO_2 + O_2 \qquad (2.4)$$

$$NO_2 + O_3 \longrightarrow NO_3 + O_2 \qquad (2.5)$$

To account for sampling line losses, O_3 concentrations is used to calculate the loss of NO within the sampling line given the residence time and the rate constant for reaction 2.4

(Minarro et al., 2011; Seok et al., 2013). Seok et al. (2013) found that if the ambient sample had a residence time of 15 seconds within the sampling line, up to 32% of ambient NO was converted into NO_2 by O_3, depending on air sample temperature, O_3 mixing ratio, and line pressure. Due to the long sampling lines (30 m), the residence time for the 2-channel instrument was 35 seconds. Assuming initial conditions of 30 ppb O_3, 1 ppb of NO_2, and 50 ppt of NO, 18 ppt (36%) of NO would be converted into NO_2 during the time the sample was in the sampling line and 0.9 ppt of NO_3 would be formed. No corrections were made for ozone titration in the two-inlet instrument because there were no O_3, pressure, or temperature measurements taken at the 1.5 m and 18 m sampling heights and therefore no accurate corrections could be made.

Ozone was measured with a Model 49C Thermal Environmental Instruments (Boston, MA) with a precision of ± 1 ppb and accuracy of ±1%. Ozone was sampled from the top of the tower near the flux instrument inlet. UV radiation was measured with a radiometer at 1 m, 7 m, 21 m, and 32 m above the ground.

2.3 Results and Discussion

2.3.1 Mole Ratios of NO_x and O_3

The mole ratios of NO, NO_2, NO_x, and O_3 as a function of time at 31.5 m for a representative 10 day period (August 4th to August 14th) during the campaign are shown in Figure 2.8.

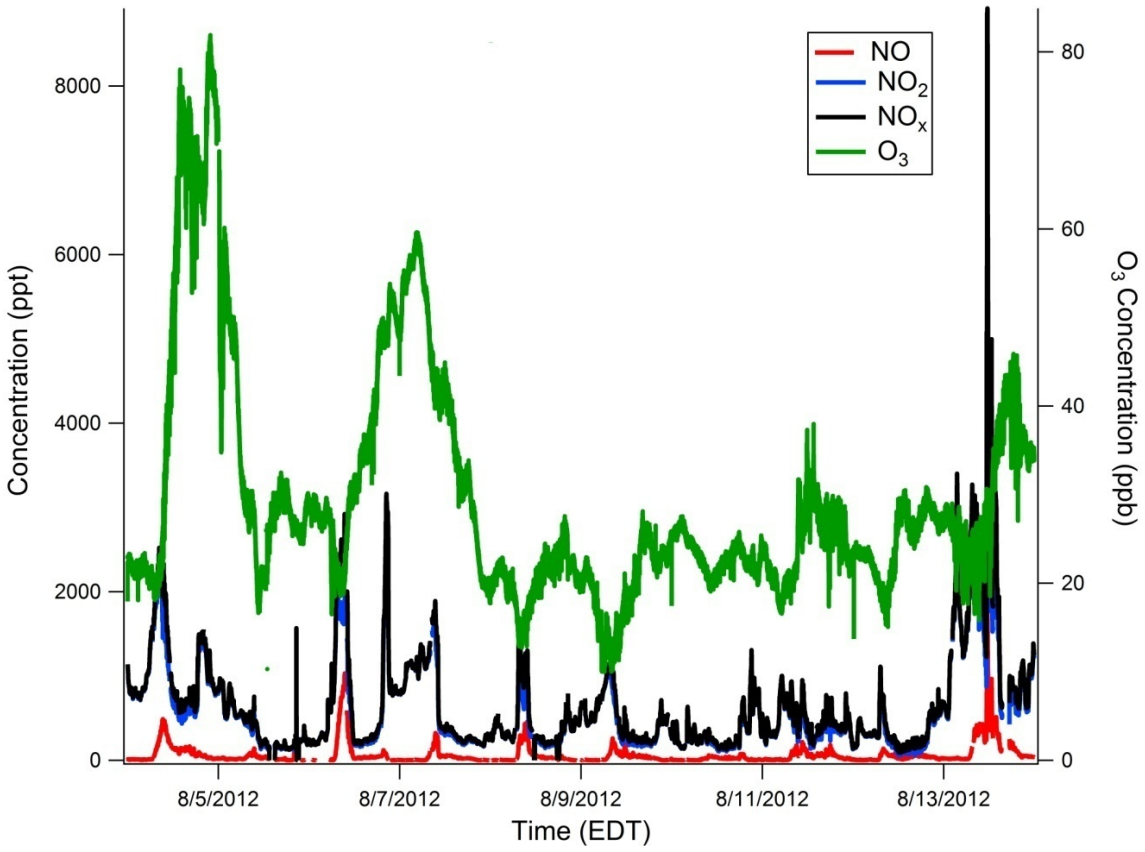

Figure 2.8 Diurnal pattern of NO, NO_2, NO_x, and O_3 observed at the PROPHET tower site in the summer of 2012.

NO_x mixing ratios exhibited a diurnal pattern driven by photochemistry. NO_2 had a median concentration of ~500 ppt, with spikes in the morning near 1000 ppt. Photolysis of NO_2 in the morning resulted in an increase in NO mixing ratios. The concentration of O_3 exhibited a similar pattern seen previously at this site (Thornberry et al., 2001), with increasing concentrations during the day, decreasing concentrations at night, and a dramatic drop in mixing ratios in the early morning coinciding with the increase in NO_x. See Chapter 1.2 for full details of the effect of the development of the boundary layer on NO_x-BVOC chemistry.

2.3.2 Long-term Trends in Morning NO_x

The first step in elucidating the source of the early morning NO_x is to determine if the source is from anthropogenic or biogenic sources. One way to determine this is to observe the long term trends of NO_x at the site. Due to increased regulation of atmospheric pollutants such as NO_x, anthropogenic emissions have been declining over North America (Lamsal et al., 2011; Russell et al., 2012). If the source of the early morning NO_x was from a purely anthropogenic source, there should be a decline in the magnitude of the spike, as satellite measurements of concentrations of NO_x have decreased over North America over the past decade by ~6% (Lamsal et al., 2011), with decreases of ~30% over cities and 26% over power plants (Russelll et al. 2012). Figure 9a, b, and c show the diurnal average of NO_x at UMBS for the summers of 2000, 2008, and 2012, respectively. NO_x was measured at UMBS from July 1st to August 12th for the summer of 2000, June 21st to July 24th for the summer of 2008, and August 4th to August 14th for the summer of 2012. The peak of the early morning rise in NO_x can be seen at ~0830 in 2000 and 2012, and around 0630 for 2008. The peak in the early morning NO_x can be seen at ~0830 for all three years.

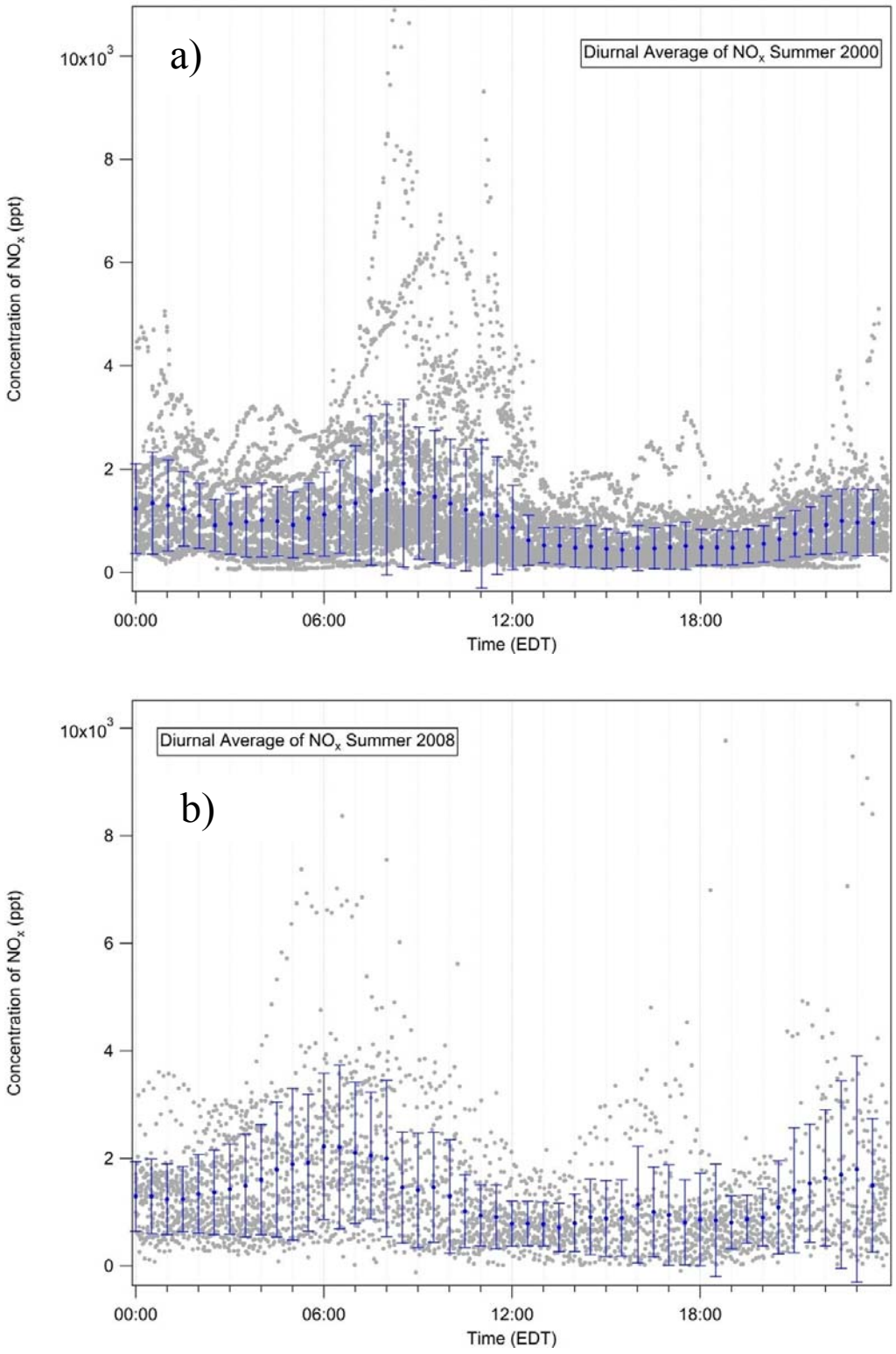

Figure 2.9 Observed concentrations of NO_x during the summers of 2000 (a), 2008 (b), and 2012 (c).

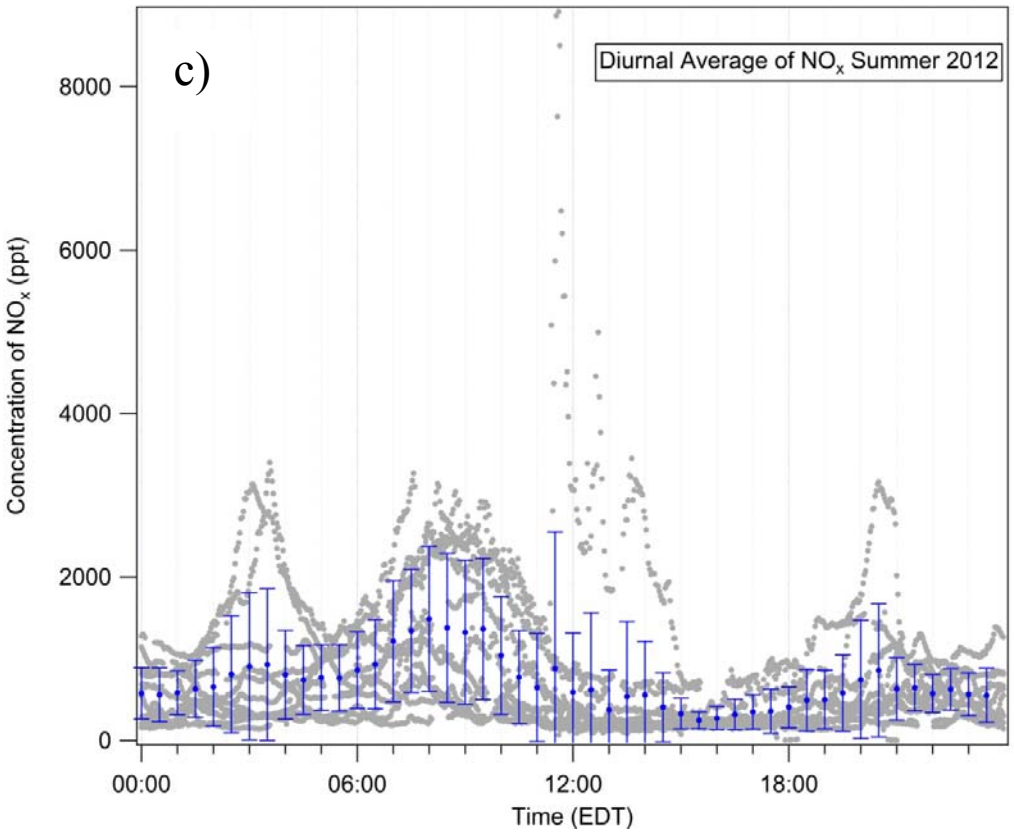

Figures 2.9 continued.

The diurnal averages show that the early morning NO_x mole ratio averages have remained relatively similar over the 12 years shown (and average of ~1 ppb increase during the morning spike for all three years); suggesting the source of the early morning NO_x is biogenic. This hypothesis is based on limited data and is refuted by Seok et al. (2013), who found that the rise in NO_x mole ratios in the morning above the canopy continued into winter months, suggesting an anthropogenic source. These observations show that the source of the early morning NO_x plume may not be due solely to an anthropogenic or a biogenic source.

2.3.3 Flux Measurements

Flux measurements of NO_x and NO_y were performed by Jeffrey Geddes. Full details of the flux measurements can be found in Geddes and Murphy (2014). Here, a brief explanation and summary of his measurements are described in reference to identifying the source of the increased mole ratios of NO_x in the morning.

Due to the limited precision of the flux instrument, the flux measurements of NO_x had uncertainties between 50-100%, and it was advised not to make any definitive conclusions based on the measurements. All measurements of early morning NO_x fluxes were not significantly different from zero. The error of the flux measurements was so high, that it could not be concluded if the flux was positive (moving up from the canopy) or negative (towards the canopy). Night time observations were near zero or within the estimated instrument random variability and therefore undetectable. Fluxes in NO and NO_2 were opposite in direction when they were able to be measured, an example of chemical flux divergence which is caused by vertical gradients in NO/NO_2 ratios (Gao et al., 1993; Horri et al., 2004). When fluxes of NO_x were observed, which occurred only during the middle of the day, they ranged from 150-450 nmoles/m^2 hr. This range of fluxes in NO_x could account for a ~0.6-2.4 ppb increase in NO_x, however, this did not occur in the morning. Therefore, there are no NO_x flux measurements that can conclusively help identify the source of the early morning NO_x plume.

Alaghmand et al. (2011) reported soil fluxes of NO at 180 nmoles/m^2 hr from measurements in the summer of 2003 and calculated that this flux could account for a possible 0.7 ppb increase in NO_x in the morning, assuming there was no chemistry occurring between the sampling inlet and ground, and that the NO_x emitted diffused into

a 40x1x1 m cube. This means that soil emissions could significantly contribute to the early morning NO_x plumes. However, chemistry can occur after emission in below-canopy environment that were not taken into account in the Alaghmand et al. (2011) calculation. As stated above, canopy reduction factors are large and have been measured to be nearly 25-80% (Fang and Mu, 2006; Jacob and Wofsy, 1990; Min et al., 2014; Wang and Leuning, 1998; Yienger and Levy, 1995). The in-canopy chemistry which produces organic nitrates and HNO_3 (Chapter 1.7) has not been measured at UMBS, and therefore, no accurate calculations can be made as the impact of soil emissions on the rise in the early morning NO_x above the canopy. These results indicate a need for higher precision instrumentation for sites that are nitrogen limited (Costa et al., 2011) and therefore have smaller NO, NO_2, and NO_x fluxes.

2.3.4 Wind Direction and Speed

To determine if the increase in early morning NO_x mole ratios comes from long range transport, the wind direction and back trajectories of 5 days that exhibited early morning NO_x plumes were examined. If the source of the NO_x was from a consistent distant anthropogenic or biogenic point source that traversed over long distances to the site, back trajectories should show the location or direction of the source. Figure 2.10 shows the wind rose plots taken with a sonic anemometer located at top of the PROPHET tower, indicating the direction, magnitude, and probability of direction and magnitude of the wind, for the 5 mornings examined in which early morning NO_x plumes were observed. The wind direction was from the north to northwest on the mornings of August 8th, 9th, and 12th, while winds were from the west to southwest for the mornings of August

13th and 14th. Wind speeds rarely reached over 5 m/s, and only after the sun had risen on the morning of August 9th.

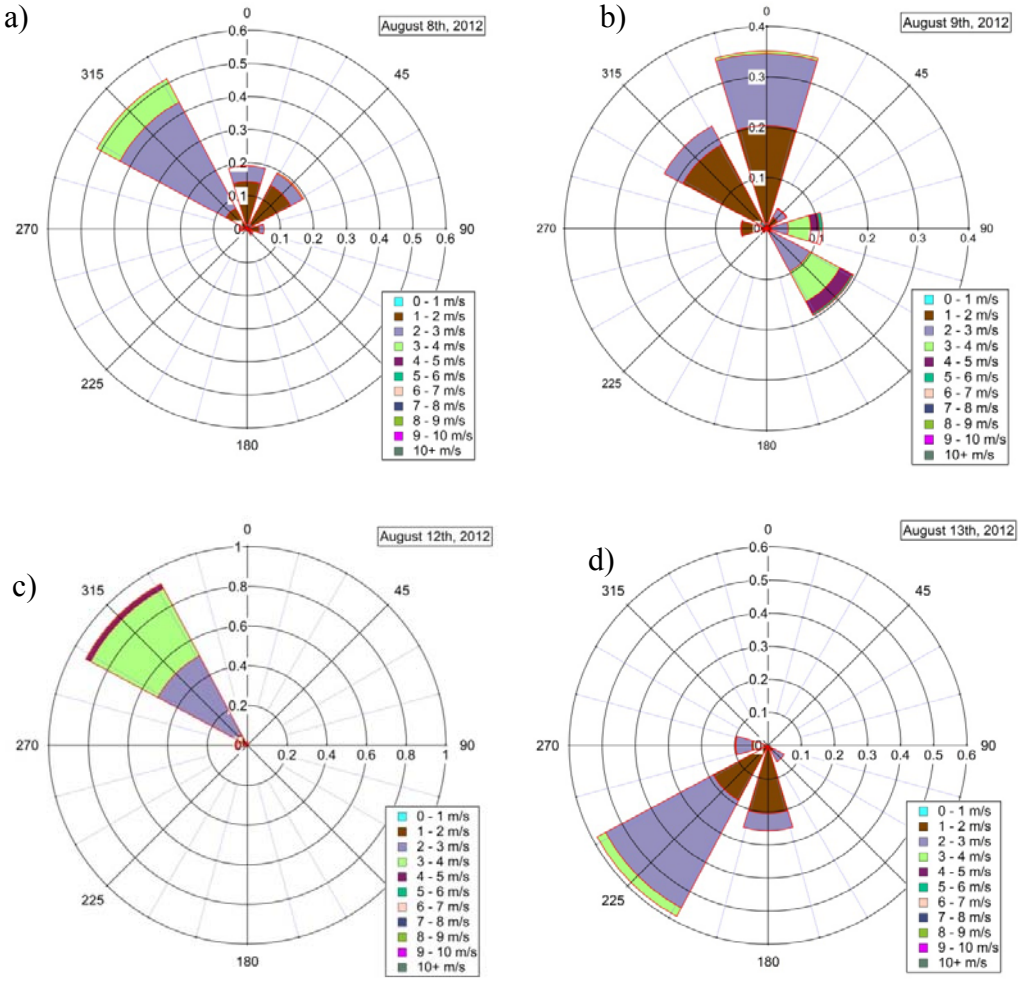

Figure 2.10 Wind rose plots for the 5 selected mornings. Winds are from 00:00 to 12:00 on each respective day. Wind speeds are in m/s. Figure 10a represents the morning hours for August 8th, 2012, while b, c, d, and e represent the 9th, 12th, 13th, and 14th, respectively.

e)

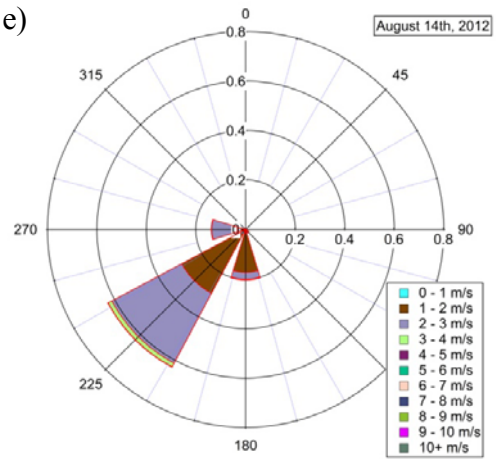

Figure 2.10 continued.

Figure 2.10 shows that wind direction and speed do not appear to make a difference in the source or intensity of the early morning NO_x peaks.

HYSPLIT back trajectories were calculated to show the origin of the air mass that traversed over the site previous to the morning NO_x plume. Twelve hour HYSPLIT back trajectories (Draxler and Rolph, 2014a; Rolph, 2014) for the representative days show that the air masses that arrived at UMBS on the representative mornings begin in southern Ontario, the middle of Lake Superior, just south of Green Bay, Wisconsin, and just north of Milwaukee, Wisconsin, shown in Figure 2.11.

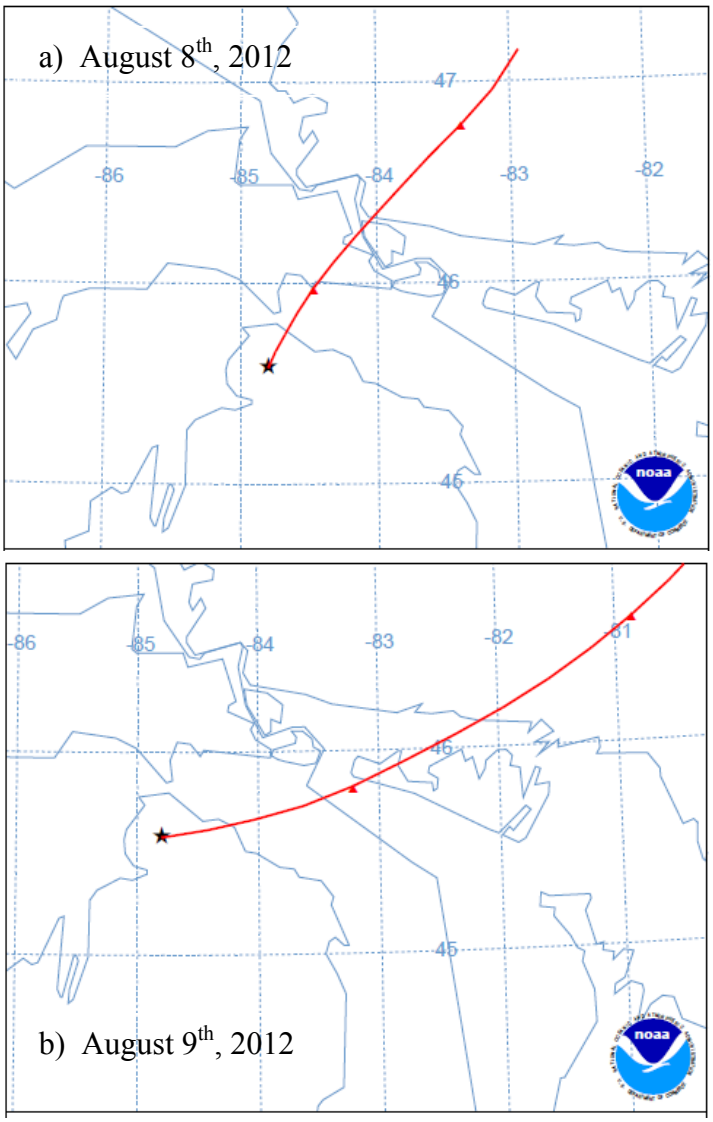

Figure 2.11 12 hour HYSPLIT back trajectories for August 8th (a), August 9th (b), August 12th (c), August 13th (d), and August 14th (e), 2012.

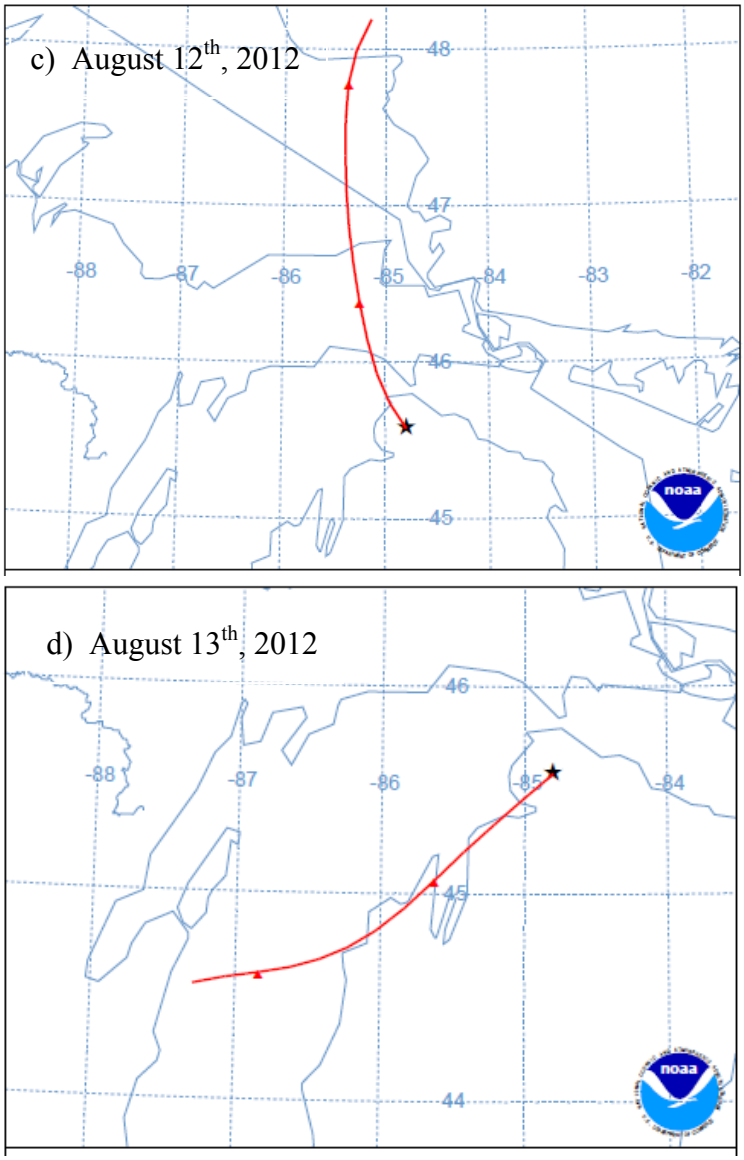

Figure 2.11 Continued.

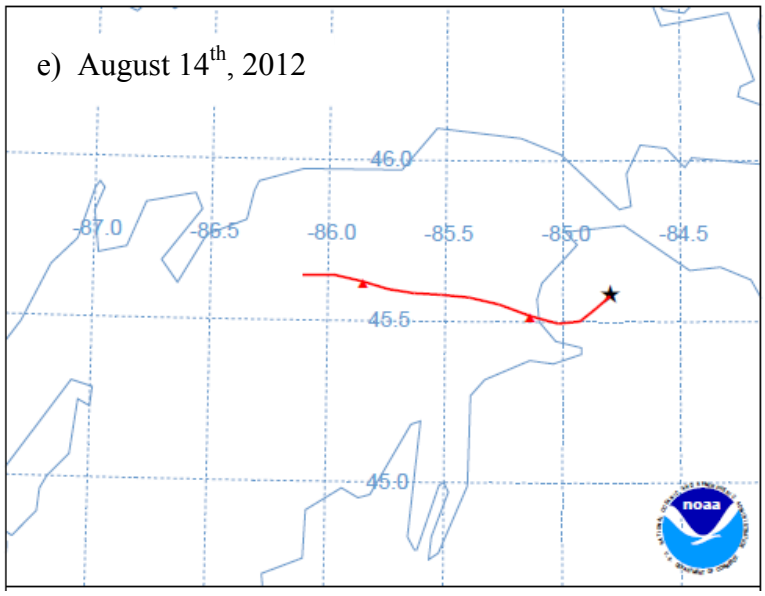

Figure 2.11 continued.

Twelve hour HYSPLIT trajectories were chosen because NO_x is generally converted into HNO_3 or organic nitrates within 3-10 hours (Min et al. 2014), and therefore represent a conservatively large area. While back trajectories indicating air masses that originated near Green Bay (Figure 2.11d) could be polluted, there are no potential high NO_x sources from Lake Michigan (August 14th, Figure 2.11e) or rural Canada (August 8th, August 9th, and August 12th, Figure 2.11a,b,and c, respectively). This, along with correlating pollution tracers and other HYSPLIT back trajectories described in Alaghmand et al. (2011), have shown that the source of the air mass or long range transport have very little effect on the early morning NO_x source, and therefore it seems more likely the source must be due to a relatively local scale process.

2.3.5 Concurrent Measurements at Various Heights

To better understand the source of the early morning NO_x plume, measurements of the vertical profile of NO_x concentration were made. If the source of the early morning plume is the result of downward mixing during the breakup of the NBL, the observed NO_x at the top of the tower should increase before measurements at lower heights. If soil or canopy emissions are responsible, the inlets at 1.5 m or 18 m should see the increased NO_x concentrations first. This experiment design was attempted by Seok et al. (2013), however, it had flaws. Seok et al. (2013) used a heated Mo catalyst to convert NO_2 into NO, which has been shown to convert other oxidized species into NO, including organic nitrates, PAN, and HNO_3, and therefore the data are difficult to interpret and draw conclusions from without knowing the exact distribution and mixing ratios of oxidized components of NO_y (Winer et al., 1974). Additionally, only one instrument was used to measure $NO_{x,MO}$ (NO_x measured using a MO converter to account for the artificially high concentrations) from 6 different heights at 5 minute sampling periods. This 30 minute vertical profile is longer than the timescale for canopy mixing/venting (~100 seconds) (Kim et al., 2013; Min et al., 2014), and Bryan et al. (2012) have shown that vertical mixing through the canopy at this site can be underestimated by 50-70% during the daytime and near an order of magnitude at night. That means when the NO_x source occurs in the morning, it takes less than 2 minutes for NO_x to be mixed within the sampling region (0-40 m). The long sampling period employed by Seok et al. (2013) could under sample plume mixing, resulting in the morning NO_x plume not being accurately identified.

By using two instruments, the sampling time at different altitudes are near simultaneous, with most (>95%) measurements above the canopy within one minute of the measurements in and below the canopy when both instruments were operational.

To better understand the evolution of the early morning NO_x mixing ratios, data for a representative day was plotted as a function of height in Figure 2.12.

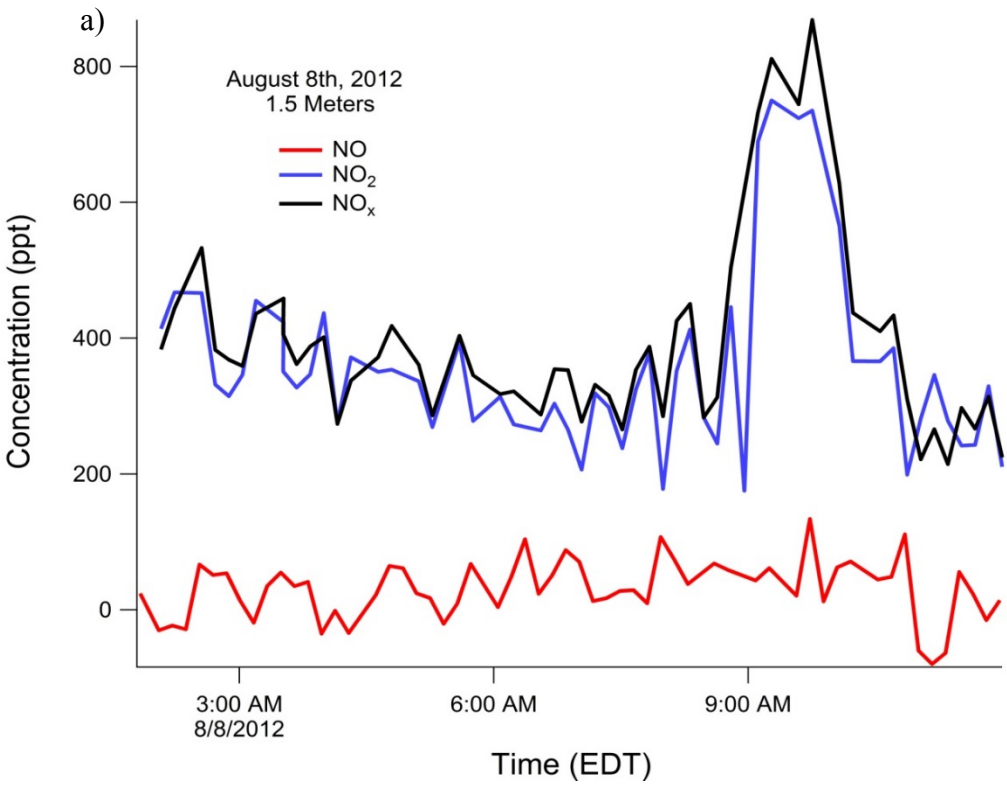

Figure 2.12. A typical vertical profile measurement showing the shape and concentrations observed on August 8th, 2012. Figure 12a shows the measured mole ratios at 1.5 meters while 12b and 12c show 18 and 31.5 m, respectively.

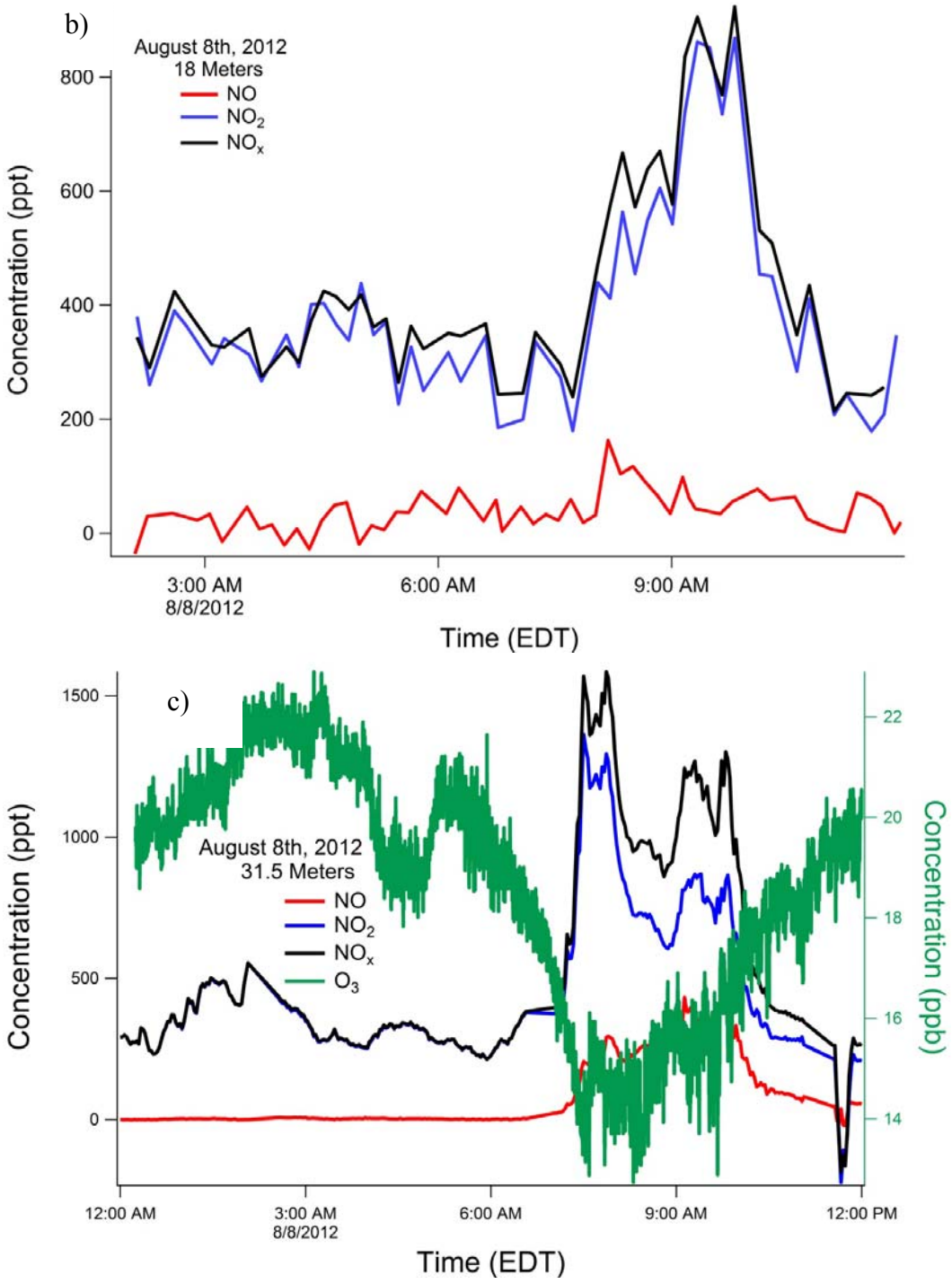

Figure 2.12 continued.

Figure 2.12 shows that the average concentration of NO_x during the night of August 8th was ~350 ppt. The mixing ratio of NO_x sharply increased at the 31.5 m inlet just after 0600, while the NO_x increase for 1.5 and 18 m didn't occur until just before 0900. When the NO_x concentration is plotted against time by itself, as shown in Figure 2.13 for the 5 representative days, the differences between the three heights becomes more distinct for all 5 days.

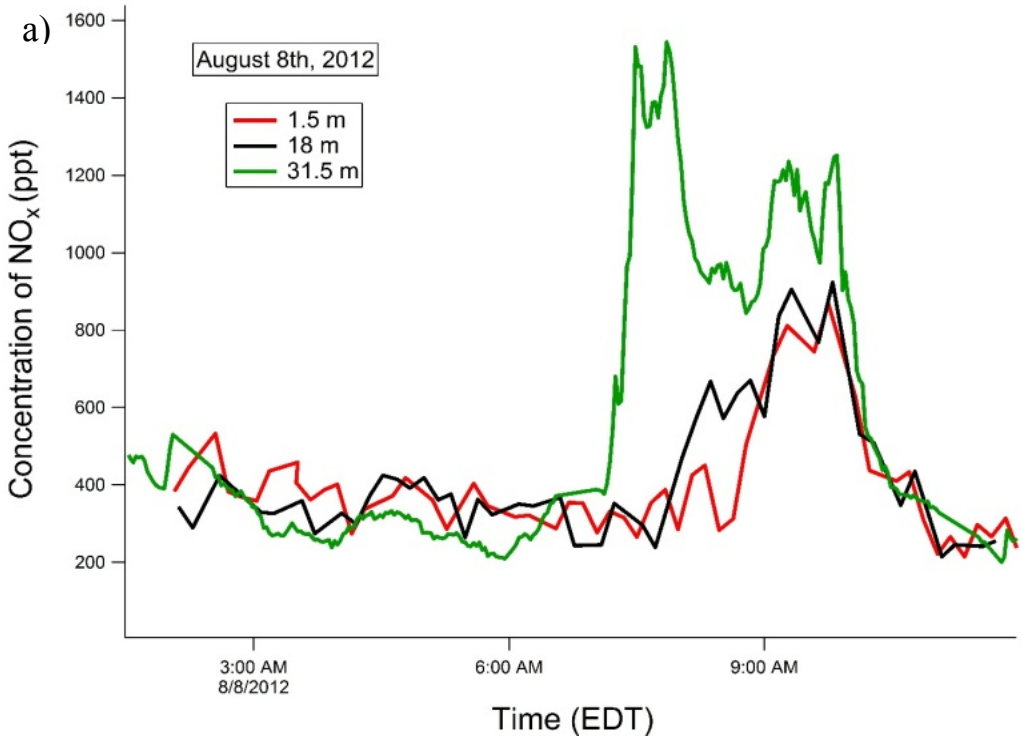

Figure 2.13 Evolution of NO_x mixing ratios at various heights during the 2012 campaign. Figure 2.13a represents the morning of August 8th, while b, c, d, and e represent the 9th, 12th, 13th, and 14th, respectively.

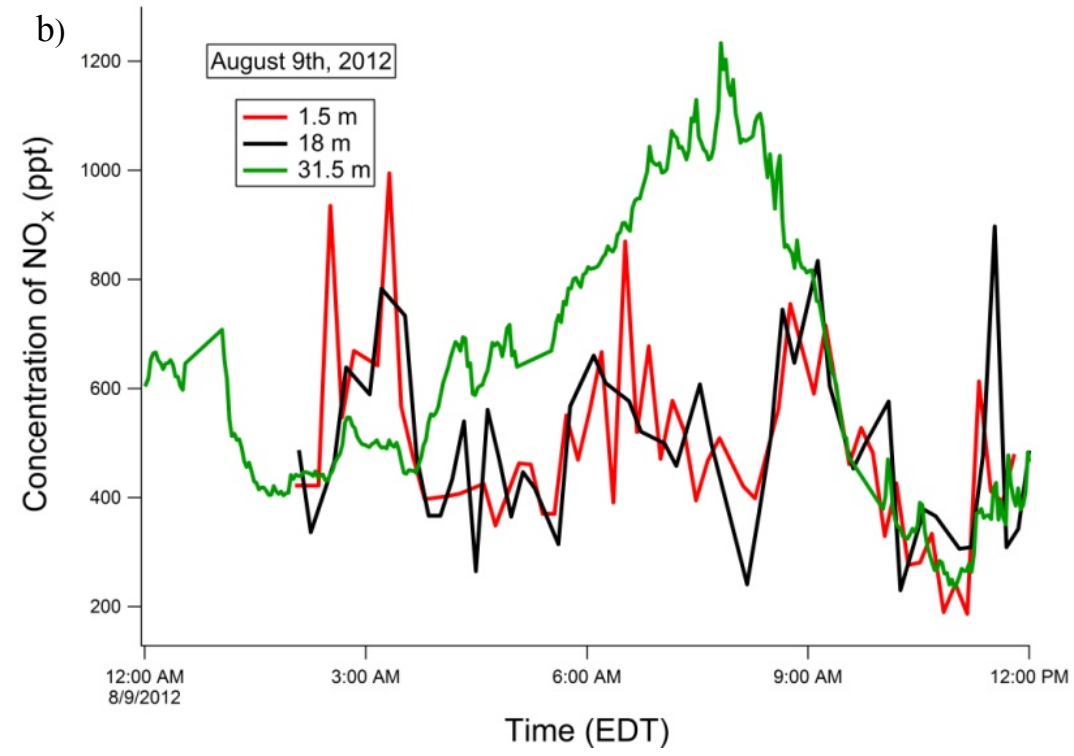

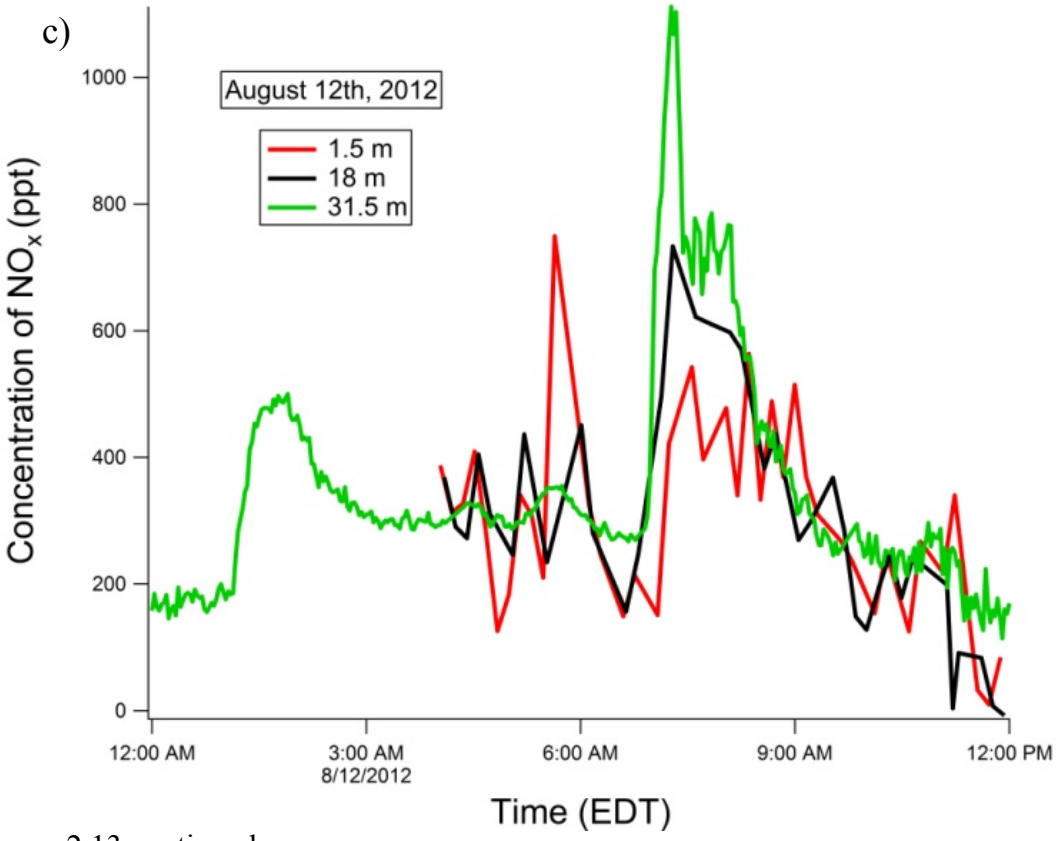

Figure 2.13 continued.

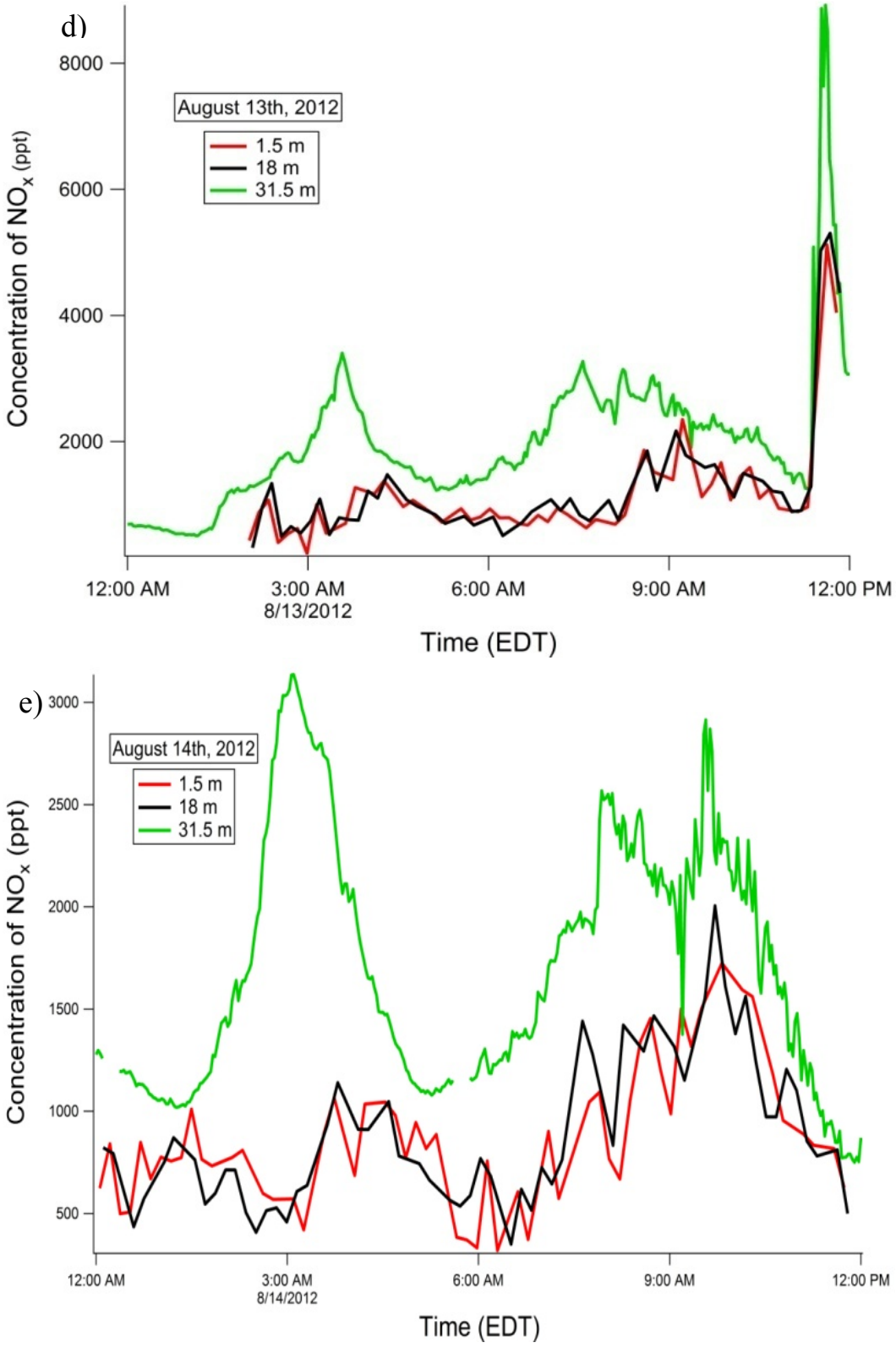

Figure 2.13 continued.

To illustrate the differences in the concentrations observed from within and below the canopy to above the canopy, the ratios of NO_x from above the canopy (31.5 m) to within the canopy (18 m) and to below the canopy (1.5 m) were plotted as a function of time, as shown in Figure 2.14.

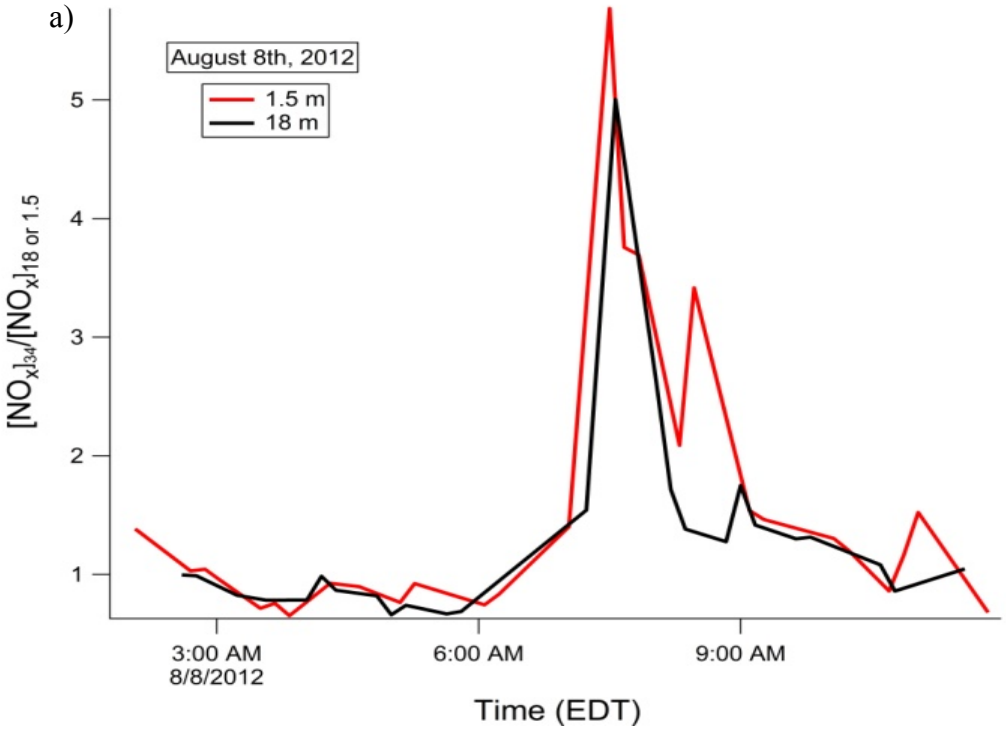

Figure 2.14. Ratio of [NO_x] at 31.5 m over [NO_x] at 18 m and 1.5 m for five mornings. Figure 2.14a represents the morning of August 8th, 2012, while b, c, d, and e represent the mornings of the 9th, 12th, 13th, and 14th, respectively.

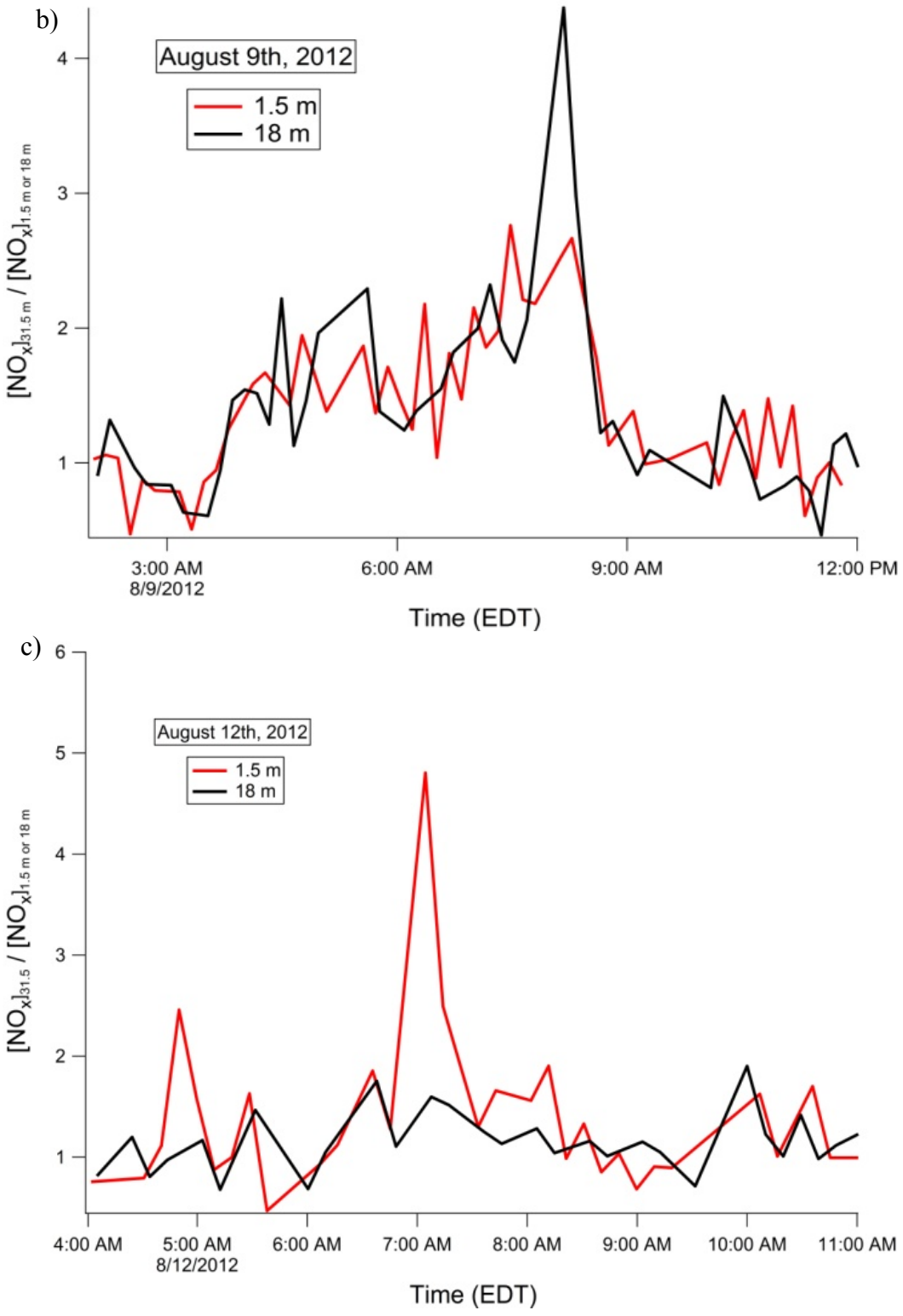

Figure 2.14 Continued.

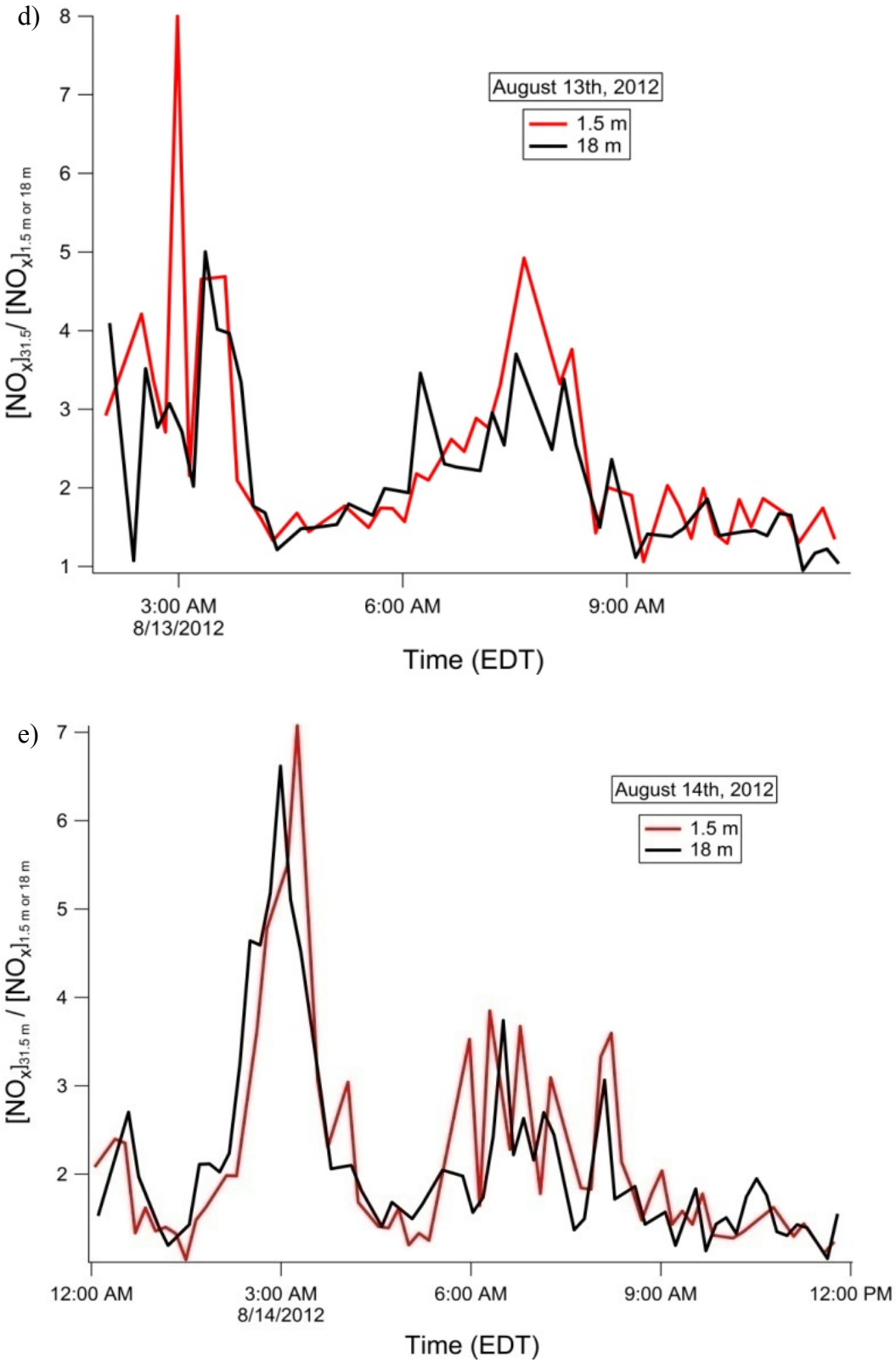

Figure 2.14 Continued.

While the mixing ratios measured by the flux instrument were consistently a factor of 1.1 higher during the comparison study as seen in Figure 2.7, the factor of 2-7 increase in mixing ratios above the canopy seen during the five representative days cannot be explained by instrument uncertainty or error alone. There is a clear increase in the NO_x mixing ratios above the forest canopy that is not seen below the canopy.

The evolution of NO_x mixing ratios on August 8th (Figure 2.13a) appears to be a clear indication of downward mixing of polluted air during the breakup of the NBL. Sunrise for this morning occurred at 0556, before the increase in NO_x mixing ratios began. From Figure 2.13a, it is apparent that the concentration of NO_x increased at 31.5 m first, followed by 18 m, and then 1.5 m. This shows that air masses with higher concentrations of NO_x from the residual layer mixed downward towards the site on the morning, and caused the increase in the NO_x mixing ratios. This same pattern can be seen on the mornings of August 13th and August 14th in Figure 2.13d and Figure 2.13e, respectively. However, the evolution of the mixing ratios for August 9th and August 12th (Figures 13b and 13c) do not appear to be caused by the break-up of the NBL. August 9th has a clear increase of NO_x starting around 0300, which gradually increases throughout the rest of the early morning hours. August 12th didn't exhibit a slow gradual increase, but rather a dramatic increase shortly after sunrise. There were no known tracers of pollution, such as CO or toluene, measured during the summer of 2012, and therefore no conclusive identification of pollution can be determined.

2.3.6 In Canopy Chemistry and the Morning NO_x Maxima

As shown in Figure 2.14a, b, d, and e there is a clear difference between NO_x mixing ratios in the early morning hours above and below the canopy. Below canopy measurements in the past have indicated that the BVOCs identified in and below the canopy are different from the BVOCs observed in the well mixed layer above the canopy. This creates difficulties in identifying not only the source, but the magnitude of the rise in early morning NO_x mixing ratios. If the below canopy sink of NO_x is sufficiently great (through the production of organic nitrates), it could remove NO soil emissions, only to have the stored NO_x released at higher elevations. It could also mean that if the early morning air mass arrived at all 3 heights quickly, there would be a delay between NO_x concentrations observed above the canopy and below, since most of the highly reactive BVOC emissions would be located within the canopy (Wolfe et al., 2011).

Examples of fast reactions occurring below the canopy include Goldstein et al. (2004) who found that the fast ozone deposition numbers measured were due to chemical losses of O_3 within the canopy by reactions with a large source of reactive BVOCs, most likely monoterpenes or sesquiterpenes. Wolfe et al. (2013) observed a large source of unexplainable RO_2 production occurring below the canopy. Hu et al. (2013) measured terpene concentrations below and above the canopy, and observed that ~80% of the monoterpene limonene that is emitted from vegetation does not escape the canopy due to its fast oxidation by O_3, OH radicals, or NO_3 radicals. Min et al. (2014) attributed the difference in NO_x mixing ratios above and below the canopy to a large chemical sink of NO_x within the forest canopy. This is a likely cause of some of the differences in NO_x mixing ratios observed at multiple heights during this campaign. Without BVOC or

other oxidant measurements at multiple heights during this study, it is impossible to determine if BVOC/NO_x chemistry (See Chapter 1) is the reason for the mixing ratio differences at multiple heights during the night and early morning hours.

2.3.7 0300 Increase in NO_x

August 13th (Figure 2.13d) shows a large increase in NO_x that occurs in the middle of the night with the maximum concentration seen at 0300. A possible source of the 0300 peak on August 13th is likely a static parcel of air that accumulated NO_x during the formation of the NBL, and slowly drifted across the site above the canopy. August 14th (Figure 2.13e) also had a large concentration peak, with a near 2.5 ppb increase in NO_x at 3:00 am. This peak can also be seen slightly on August 12th (Figure 2.13c), but due to instrument maintenance, the two-inlet instrument was not operational. August 9th (Figure 2.13b) also shows a gradual increase of NO_x around 3:00 am, but rather than decay in magnitude after reaching some point, it grows throughout the night. A possible explanation for this observation is atmospheric stratification in the NBL, also called fanning (Gossard et al., 1985; Stull, 1988). If the NO_x was emitted into the NBL, it would spread out into horizontally thin layers, creating regions of higher and lower concentration, dependent on the level of O_3 and aerosol that accumulated into that layer. Gossard et al. (1985) observed fine-scale vertical structure in aerosols, temperature, humidity, and turbulence in the NBL. The air mass above the canopy could develop its own unique fine vertical structure, and the increase in NO_x mixing ratios observed near 0300 am above the canopy may be due to intermittent turbulent bursting, or sporadic

vertical mixing events, which could push air masses with higher NO_x from the residual layer, into the NBL.

2.3.8 Relationship between Vertical Mixing and NO_x Spikes

To determine if any of the early morning NO_x plumes were due to increased turbulence, and therefore increased mixing in the NBL, the friction velocity at the nearby Ameriflux tower was calculated. Friction velocity is the measure of total vertical flux of horizontal momentum near the surface of the Earth, or the turbulence created by wind shear (Stull 1988). Friction velocity (u_*) is generally measured as shown in Equation 2.1, where u' is the perturbation about the mean of the mean flow of wind, w' is the perturbation about the mean of vertical winds, and v' is the perturbation about the mean of the wind perpendicular to the mean flow.

$$u_*^2 = \left[\overline{u'w'}^2 + \overline{v'w'}^2\right]^{0.5} \qquad \text{Equation 2.1}$$

An observed increase in friction velocity would indicate increased turbulence, and could indicate vertical mixing between different layers in the NBL. Figure 2.15 shows the measured friction velocity at the Ameriflux tower and UV radiation measured at the PROPHET tower.

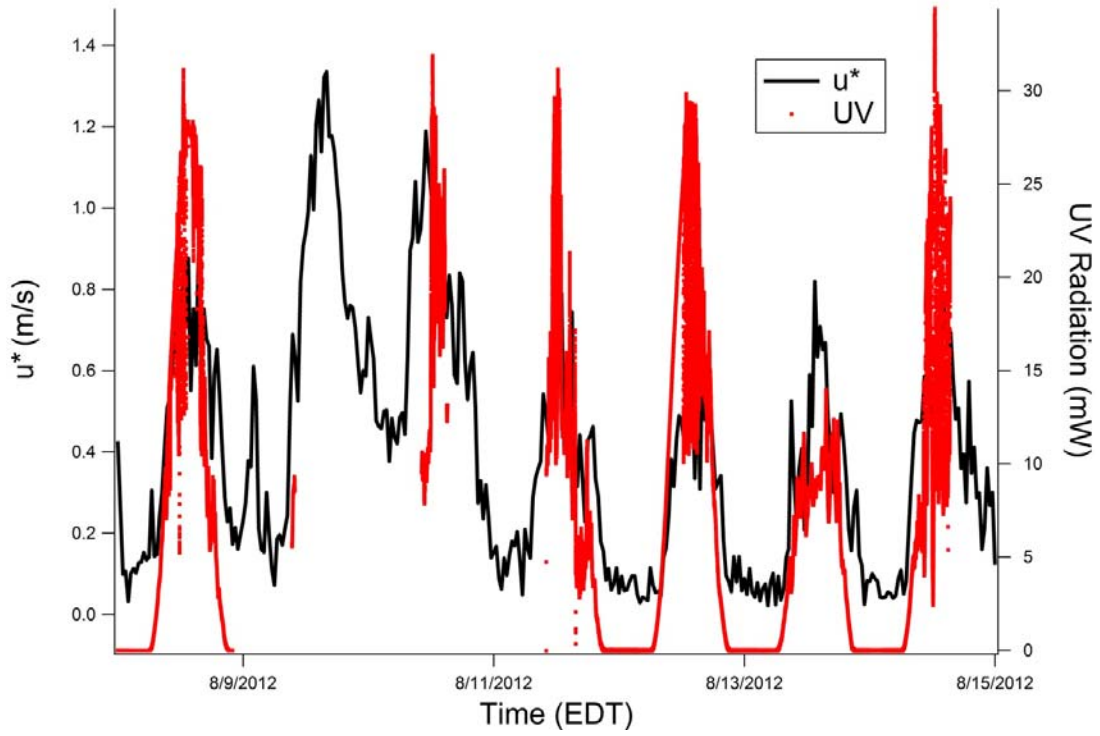

Figure 2.15 UV radiation (uv) and friction velocity (u_*) measured at UMBS during the summer of 2012.

UV data was missing from August 9th and most of August 10th. During the mornings of August 12th, 13th, and 14th, the increase in friction velocity (u_*) is clearly correlated with the increase in radiation and there is very little turbulence occurring at night. Calm conditions in this case were determined to be anything with a u* of less than 0.35, which is the point when turbulence is too weak to mix the below canopy air with the above canopy air (Barr et al., 2013). On August 9th there is a clear increase in the friction velocity observed at the Ameriflux tower, however, no increase of NO_x can be seen above the canopy. Instead it is one of the only times that NO_x mixing ratios below the canopy are higher than above the canopy. This provides more evidence that the mixing between the canopy boundary layer is not well understood, and may indicate that

turbulent motion during the night may induce downward mixing of polluted air from the residual layer into the canopy. The presence of the increased NO_x mixing ratio at 0300 during the summer of 2012 is still not well understood.

2.4 Conclusions

The early morning rise in the mixing ratio of NO_x at the surface does not have a definitive source currently. From the data presented, it appears plausible that there are unknown sources of pollution in northern Michigan which emit NO_x into a stratified NBL. Three out of five days studied suggest that the increase in NO_x mixing ratios at the canopy height in the morning are due to either polluted air from aloft traversing downwards or due to a large chemical sink occurring below and within the chemistry. The possibility of a large chemical sink of NO_x within and below the forest is plausible, but cannot be confirmed due to a lack of BVOC measurements below, within, and above the canopy. The presence of NO_x peaks occurring in the early morning hours (0300) indicates that the source of increased NO_x does not originate from photochemical sources. Flux measurements proved to be inconclusive, as the flux of NO_x at the site in the morning was too small to be measured even with a current state of the art instrument.

As stated in Wolfe et al. (2011) and Geddes and Murphy (2014), there are still significant uncertainties in the understanding of forest-atmosphere exchanges and interaction. Without flux measurements of BVOCs, NO_x, OH, and O_3, an understanding of nighttime NO_x chemistry and species fate will remain ambiguous. The greatest uncertainty in modeling these NO_x concentrations arises from the lack of a computationally efficient alternative to K-theory (see Chapter 1.2) when predicting inner

canopy turbulence, sweep-ejections, and similar events (Wolfe et al. 2011). It is also difficult to measure the effect of nocturnal wind structure and how it effects plume growth (Gupta et al., 1997). The presence of intermittent turbulence in the NBL makes it difficult to clarify the effect of chemistry occurring below the canopy and its effect on NO_x mixing ratios above the canopy. While models have attempted to describe the above canopy chemistry and transport, below the canopy differences exist in both BVOC and NO_x mixing ratios (Ganzeveld et al., 2002; Hu et al., 2013; Saylor, 2013; Wolfe and Thornton, 2011). Currently there are still large uncertainties in NO_x-biosphere interactions, and there is a need for greater understanding of canopy scale phenomena.

Future field campaigns are needed to further identify the cause of the early morning NO_x plumes observed above the canopy. This problem could and should be addressed by the use of concurrent multi-height measurements of wind speed, BVOCs, OH, NO_3, O_3, NO_x, and total NO_y measurements. Future field campaigns should also utilize aircraft based NO_x instrumentation to travel upwind of the PROPHET site to help identify any possible unknown anthropogenic pollution sources. Finally, sounding data should be used to identify the structure of the NBL, and whether stratified layers of polluted air are present and if the breakup of these layers leads to increases in NO_x mole ratios (Gossard et al., 1985).

CHAPTER 3 DEVELOPMENT OF AN AUTOMATED COMPREHENSIVE FLOW MODULATED TWO-DIMENSIONAL GAS CRHOMATOGRAPH (GCxGC) FOR THE QUANTIFICATION OF NON-METHANE HYDROCARBONS (NMHC)

3.1 Introduction

A wide variety of non-methane hydrocarbons (NMHCs) are emitted into the atmosphere where they can affect ozone production (Council, 1991; Starn et al., 1998; Williams et al., 1997), aerosol formation, and the biogeochemical cycling of carbon (Guenther, 2002). The most important NMHCs are biogenic volatile organic compounds (BVOCs), including isoprene (C_5H_8), monoterpenes ($C_{10}H_{16}$), and sesquiterpenes ($C_{15}H_{24}$) and a wide variety of oxygenated compounds. An estimated 1150 Tg C/ yr of BVOCs are emitted worldwide and these emissions are an order of magnitude greater than anthropogenic NMHCs (Fehsenfeld et al., 1992; Guenther et al., 1995). There is a large uncertainty about the rate of BVOC emissions (Hewitt and Street, 1992) and the fate of their oxidation products including organic nitrates (Goldstein and Galbally, 2007). The major pathway for removal of BVOCs is through the reaction with OH radicals, O_3, and NO_3 radicals (Atkinson, 2007).

A large uncertainty in understanding the effect of BVOCs on the oxidizing capacity of the atmosphere is the inability to observe and speciate all compounds. This complexity can be seen in identifying saturated alkanes, where alkanes with a carbon number of 10 have 75 different isomers and saturated alkanes with a carbon number of 20

have 4347 possible isomers (Adahchour et al., 2006). Lee et al. (2005) showed that when using proton-transfer reaction mass spectrometry, the total observed monoterpene concentration was 30% greater than observed by pre-concentration followed by GC separation, showing that methods to speciate BVOCs do not observe some fraction of total BVOCs. It has become increasingly necessary to speciate and quantify BVOCs due to the large differences in their reactivity and aerosol production potential of isomers (Atkinson, 2007; Lee et al., 2006a).

One of the greatest problems in quantifying BVOCs is the vast number of species present in the atmosphere and that many of the species in the atmosphere contain similar structural and physical properties. Techniques such as Fourier transform spectroscopy (Rinsland et al., 1987), tunable diode laser spectroscopy (Anderson and Zahniser, 1991), gas chromatography coupled with a flame-ionization detector, and mass spectrometry have identified hundreds of different BVOCs in the troposphere. However, spectroscopic techniques lack the ability to speciate compounds and are only able to detect organic functional groups. Gas chromatography is the most common method for separation and detection of BVOCs, but even long narrow bore columns have limited resolving power (Hamilton, 2010a). To perform long-term observations of BVOCs, an ideal instrument would be able to separate and resolve key BVOC isomers along with their reaction products, have high sensitivity towards BVOCs, high precision with stable detector response factors, and the ability to fractionate BVOCs and their oxidation products into classes based on size and functionality. This instrument would allow for the identification of compounds that are the most important in the formation of SOA and in controlling the O_3 and aerosol production potential.

Comprehensive two-dimensional gas chromatography (GCxGC) provides a vastly improved method for the separation of BVOCs. By coupling a secondary column to a primary column, through a modulator, GCxGCs have been able to obtain vastly improved peak capacities, with the total peak capacity equal to the arithmetic product of the two columns peak capacities (Liu and Phillips, 1991; Phillips and Beens, 1999). GCxGC instruments offer a much larger peak capacity than conventional GC methods. Peak capacity is used to measure the separation capability and is defined as the number of peaks that can be separated with a resolution of unity in a given time interval (Shen and Lee, 1998). Venkatramani and Phillips (1993) found that by using two separation phases, peak capacity increased from 1000 to 50000. The difference between comprehensive two-dimensional GC (GCxGC) and heart-cut GC (GC-GC) is that in GCxGC, the entire sample is transferred from the primary to secondary column, and therefore every analyte reaches the detector at the end of the secondary column. In GC-GC, only a fraction of the primary eluent is transferred to the secondary column (Adahchour et al., 2006). Lewis et al. (2000) first showed the resolving power of heart-cut two dimensional GC (GC-GC) instruments for atmospheric samples by detecting over 100 new compounds. Xu et al. (2003) were the first to use GCxGC on atmospheric samples and measured 650 different compounds (S/N>100) in a single chromatogram, but were only able to identify 235 of those peaks. It was shown that one-dimensional GC could possibly lead to underestimating the organic content of the atmosphere for urban samples and up to two-thirds of the carbon mass can be undetected. Due to the resolving power of GCxGC and GC-GC systems, they are an optimal technique for the detection of BVOCs that can survive the GC oven or ovens. Figure 3.1 shows an example of the complexity of an

atmospheric sample that was collected with a GCxGC instrument coupled to a time-of-flight mass spectrometer (TOF-MS) detector from an air mass above a black spruce fire (Hatch et al. 2013).

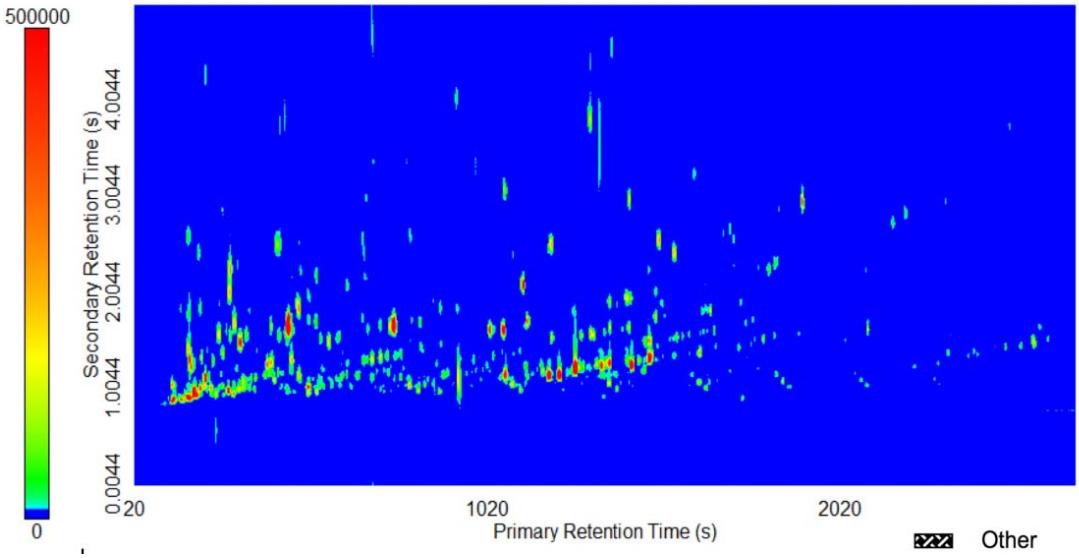

Figure 3.1 A GCxGC chromatogram of BVOCs emitted from a black spruce fire. The color scale is in arbitrary units, showing the intensity of the total ion chromatogram from the mass spectrometer.

Lewis et al. (1997) described a novel GC-GC for the separation of isoprene and dimethyl sulfide that implemented two separate, isothermal ovens. While their design cut total energy usage for aircraft measurements, they were only able to effectively separate high volatility compounds. Goldstein et al. (2007) built an in-situ thermal desorption instrument for the separation and identification of semi-volatile components in aerosols. Pankow et al. (2012), in an attempt to determine BVOC complexity and retention data, used a commercial GCxGC time-of-flight mass spectrometry system to effectively

separate hundreds of compounds from leaves of two tree species. Su et al. (2011) designed a novel heart-cut Dean's switch (a 3 port valve that directs the primary flow to either a waste column or onto the secondary column) that utilized back-flushing to detect C_3-C_{12} compounds. In this set up, the outflow of two secondary columns were combined before entering a mass spectrometer, and one of the secondary columns was back flushed to achieve delayed elution of heavier compounds. While a TOF-MS provides another dimension of separation and excellent mass accuracy, it must be tuned daily and experiences fluctuations in signal stability in field study environments and therefore requires frequent calibrations. Quadrupole and linear ion trap detectors also suffer from problems including the need for daily tuning, poor limit of detections (deGouw and Warneke, 2007), and inability to separate isomers (Mielke et al., 2010; Paulot et al., 2009). Mass spec techniques are also more expensive then flame-ionization detectors and electron-capture detectors.

Recent attempts at a more functional GCxGC instrument have been made using comprehensive flow-switching modulators, an ideal long term modulator due to the lack of cryogens needed. Tranchida et al. (2013) first attempted to create a GCxGC-qMS system, but found that nearly 80% of the primary flow needed to be diverted from the modulator and the sensitivity in the GCxGC system was 3-4 times lower than found in conventional GC-MS. Ghosh et al. (2013) attempted to use a traditional Dean's switch as part of the GC-GC-MS system, but found that the system suffered from a low duty cycle of 0.1. Edwards et al. (2013) made a miniaturized GCxGC system with a modified low-cost photo-ionization detector, but were only able to measure parts per billion level concentrations. In the work presented below, we attempt to develop an ideal instrument

(sub-ppt detection limits, detection of compounds from C_5 to C_{15}, and ability to separate and quantify compounds with nitrate ester bonds) for the separation and detection of the wide range of BVOCs found in chamber experiments and in ambient samples.

3.2 Experimental

3.2.1 Calibration System

To conduct quantitative measurements, a calibration system is necessary. For this, we developed a diffusion based calibration system shown in Figure 3.2. This system is based on the system described by Gautrois and Koppmann (1999), where seven compounds, i.e. isoprene, toluene, isobutyl nitrate, α-pinene, 2-ethyl-hexyl nitrate, decane, and trans-caryophyellene, were selected to represent a wide volatility range of BVOCs.

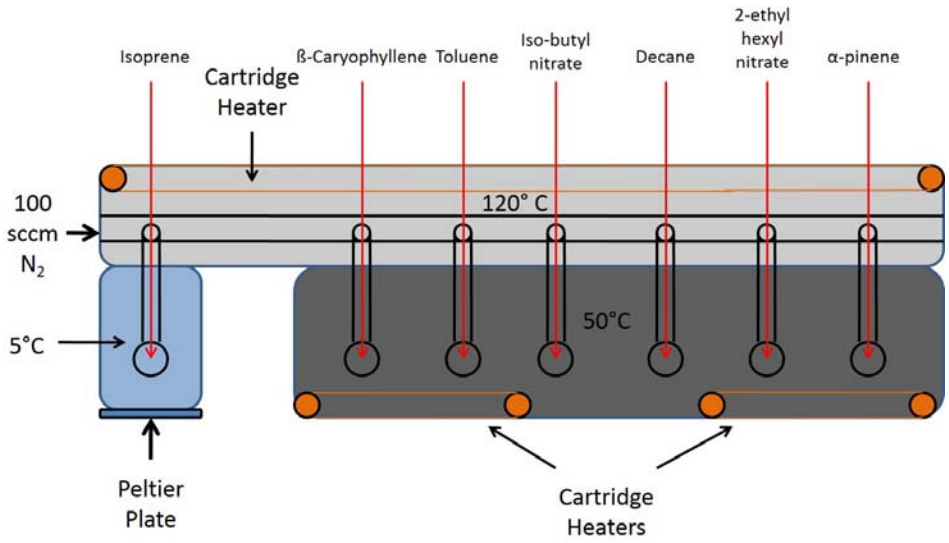

Figure 3.2 Schematic of the calibration system.

The diffusion rate for the standards was determined using Equation 3.1 (Altshuller and Cohen, 1960). Diffusion coefficients were determined from Equation 3.2 (Tucker and Nelken, 1990). Previously determined vapor pressures for isobutyl nitrate, 2-ethyl hexyl nitrate, and trans-caryophyellene were not available so they were calculated using Equation 3.3 (Grain, 1990). Heats of vaporization for isobutyl nitrate, 2-ethyl hexyl nitrate, and trans-caryophyllene were determined according to Equation 3.4 (Fishtine, 1963).

$$r = \frac{0.3328 M_r P A}{RTL} \log\left(\frac{P}{P-p}\right) \qquad \text{Equation 3.1}$$

$$D = 0.0017 T^{1.75} M_r^{0.5} \left(P\left(Va^{1/3} + Vb^{1/3}\right)^2\right) \qquad \text{Equation 3.2}$$

$$\frac{\Delta H_{vb}}{T_b} = \Delta S_{vb} = K_p(8.75 + R \ln T_b) \qquad \text{Equation 3.3}$$

$$\ln P_{vp} = \frac{\Delta H_{vb}(T_b - C_2)^2}{\Delta Z_b R T_b^2} * \left[\frac{1}{(T_b - C_2)} - \frac{1}{(T - C_2)}\right] \qquad \text{Equation 3.4}$$

$$C_2 = -18 + 0.19 T_b \qquad \text{Equation 3.5}$$

In Equations 3.1-3.5, r is the rate of diffusion (g/s), D is the diffusion coefficient (m^2/s), M_r is the reduced mass, P is atmospheric pressure (1 atm), p is the saturation vapor pressure (atm) in atmospheres at temperature T (K), L is the length of the diffusion tube (cm), T is 323 K for all compounds except isoprene, where T = 278 K, A is the area of the diffusion tube (cm^2), Va and Vb are molar volumes for the gas in question and nitrogen, ΔH is heat of vaporization, ΔZ is 0.97, C_2 is an estimated constant found using Equation 3.5, also known as Thompson's Rule (Thomson, 1959), T_b is the boiling point temperature (K) at STP, and R is the ideal gas constant.

The internal diameters of the diffusion capillaries were calculated so that each capillary had a diameter between 0.152 to ~2 mm and a length of 5 cm, not including the bulb diameter. Table 3.1 lists the calculated inner diameters needed to produce a 3.8×10^{-9} gram per second diffusion rate and the actual inner diameter used.

Table 3.1 Dimensions of diffusion tubes

Compound	Calculated I.D. (mm)	Actual I.D. (mm)	Bulb Diameter (mm)	Length (mm)
Isoprene	0.160	0.152	10.28	60.45
Trans-caryophyllene	4.340	5.00	10.17	59.20
toluene	0.230	0.229	10.29	60.04
Isobutyl nitrate	0.290	0.305	10.17	60.45
Decane	0.750	0.75-1.25	10.18	60.43
2-ethyl-hexyl nitrate	1.800	1.75-2.25	10.24	62.54
α-pinene	0.510	0.508	10.17	60.06

Actual inner diameters were chosen due to the limited availability of calculated inner diameter tubing. Outer diameters of the tubing ranged from 0.55 to 0.74 cm. The seven diffusion vials were created by blowing an approximately 1 mL bulb into the bottom a piece of defined ID tubing. For the vials in which needles were too large to inject a standard, a small Teflon cap with a reservoir was sealed to the top of the diffusion vial

with an o-ring and the bottom of the vial was submerged in liquid nitrogen. The temperature change created a relative vacuum which pulled the liquid standard into the diffusion vial.

Due to the high vapor pressure of isoprene, a special block with Peltier plates had to be made to cool the isoprene vial to 5° C. The other standards were heated to 50° C with cartridge heaters inserted into the block. The seven diffusion tubes were inserted to a silanized stainless steel block (Kreuger and McCloskey, 1969) so that the ends of the diffusion tubes were situated just inside the 9.525 mm diameter bore through the block. The diffusion vials were compressed between the stainless steel block and a steel plate, and sealed with Viton o-rings (McMaster Carr, Elmhurst, IL) to create an air-tight connection. The silanized stainless steel block was heated to 100°C. To minimize possible oxidation reactions with the trans-caryophyellene (Helmig et al., 2003) and to flush the components into dilution air, ultra-high purity nitrogen was constantly passed over the diffusion vials at a flow rate of 100 sccm. The system was leak checked daily to ensure minimal oxygen was present.

To determine the diffusion rate of the standards in the calibration system, the mass loss rates of the seven standards was determined by measuring the mass of the diffusion vials on a weekly or bi-weekly basis. The vials were filled and allowed to diffuse till empty or near empty three different times. Cleaning occurred in-between each filling by flushing the vials with acetone and nano-pure water. For the first fill, the diffusion vials were inserted into a Teflon block heated to 100° C. This differs from Figure 3.2, which shows 120° C. It was determined from blank and calibration samples that the Teflon block in which the heads of the diffusion vials were inserted was emitting

contaminants. The Teflon block also suffered from near severe deformation at 100° C. For the second and third configurations, the Teflon block was replaced with a stainless steel block that was heated to 120° C.

Attempts to create calibration curves from the direct mixing of the 100 sccm calibration diffusion source with a 1000 to 10000 sccm dilution flow of ultra-high purity air was unsuccessful. The 100 sccm flow from the calibration system could not thoroughly mix in small (100-1000 mL) mixing chambers that could fit inside the sampling system oven. To create calibration curves, ~100 L Teflon bags were connected to the sampling system for various time periods to create multi-point calibration curves. The bags were filled with ~80 L of air. All MFCs used were calibrated by bubble meters. Uncertainties from this calibration method are described within.

3.2.2 Sampler

To create a sampler for a comprehensive flow modulated GCxGC, certain criteria had to be achieved. The first was that the analytes from the air has to be pre-concentrated before entering the GCxGC. For this instrument, a FID was used to detect hydrocarbons. FIDs work by burning hydrocarbons to create ions, which are collected and form a small current that becomes the FID signal. FIDs typically are only able to measure 10^{-11}grams or around 50 ppb from a 10 mL sample volume without any sample pre-concentration techniques (McNair and Miller, 1998). Typical atmospheric concentrations of BVOCs are in the ppt range and therefore require some kind of pre-concentration technique (Fehsenfeld et al., 1992; Goldan et al., 1995). The second criterion that had to be met was that water had to be removed from the system. Water is found in much higher

concentrations in the atmosphere than BVOCs. Water can hydrolyze or bond to the stationary phase that coats the capillary column commonly used in GC analysis. When water competes for binding sites, it causes shifts in the retention time of analytes. Therefore, it is important to remove all water from the pre-concentrated sample. The third criterion that had to be met was that the sample has to be injected into the GCxGC system in a narrow plug or small volume of carrier gas to reduce band broadening and achieve the best resolution possible (McNair and Miller, 1998).

To evaluate the best method for sampling BVOCs, three configurations of the sampler were tested. In the first configuration, a two stage sorbent trap method was employed. In the second configuration, a single sorbent trap was employed, followed by a custom designed cryofocusing trap. In the third configuration, a single sorbent trap was used to concentrate BVOCs. The first configuration was tested because it theoretically offered a means to identify BVOCs with a volatility range including the highly volatile isoprene through semi-volatile substances, such as sesquiterpenes. The second configuration was tested because the two trap method did not effectively focus higher volatility analytes such as isoprene. The third configuration was tested because during a field campaign. It was determined that the cryogens needed to focus isoprene depleted at a much higher rate in the field than in a laboratory environment, and therefore, became too expensive. Details of these configurations are discussed below.

Figure 3.3 shows the flow path of the sample for the first configuration of the system.

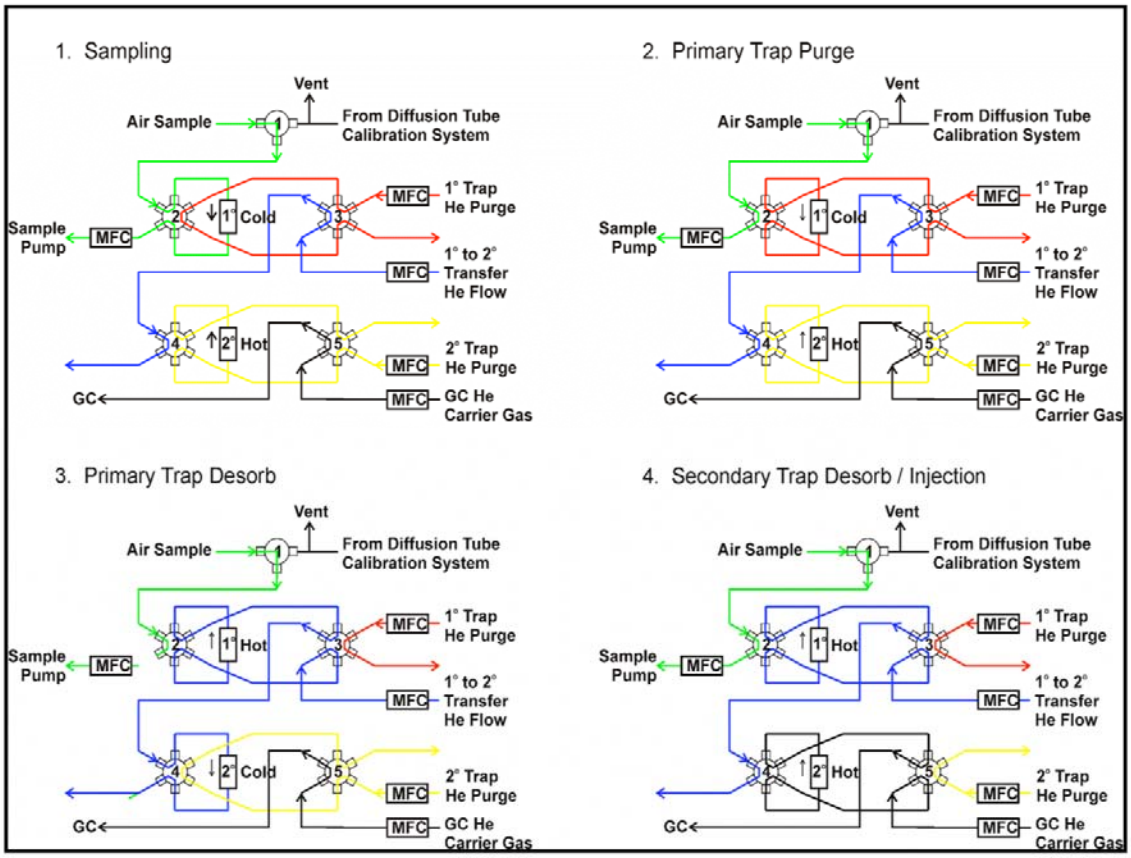

Figure 3.3 Sampling diagram of the first configuration sampling system.

Six Vici Valco 6 port valves (Houston, TX) were housed in a custom made oven, maintained at 100° C. All lines inside the oven were 1/8th inch OD Silcosteel with hydroguard stainless steel (Restek, Bellefonte, PA) and were housed inside the oven. The sample was first trapped in a 7 inch long, 3/8th inch OD trap cooled by Peltier plates to 10° C. The trap was filled with 50/50 (g/g) Tenax TA (60/80 mesh, Macheray & Nagel) and Carbopack B (20-40 mesh, Supelco). The structure of Tenax and Carbopack B are shown in Figure 3.4.

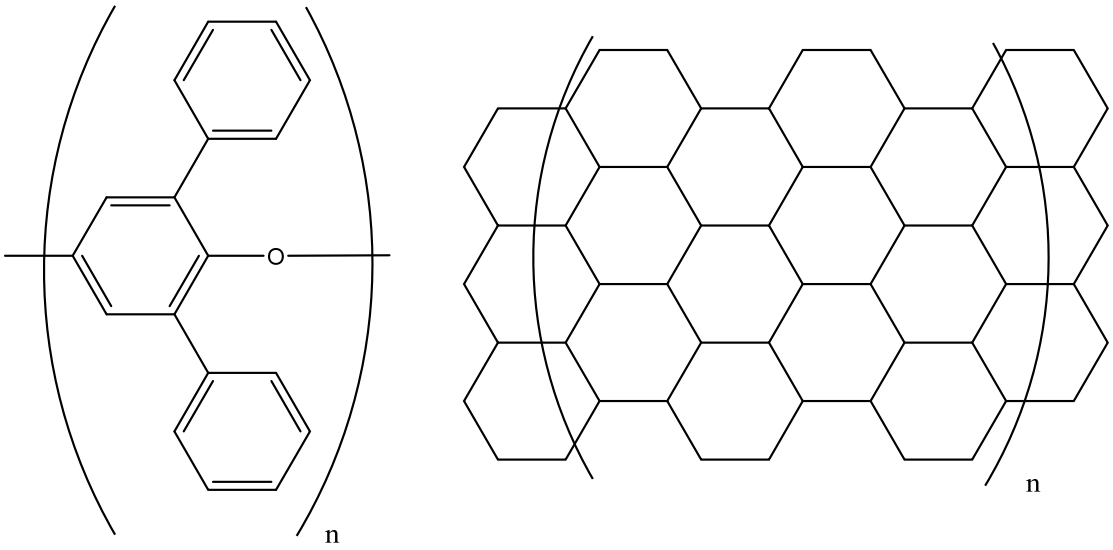

2,6-diphenylphenylene oxide
Tenax TA

Graphatized Black Carbon
Carbopack B

Figure 3.4 Structure of the sorbent materials used to trap BVOCs.

Tenax is a sorbent material that is comprised of poly-2,6-diphyenylphenylene oxide and is used to trap VOCs with carbon numbers from 7 to 26 (Arnts, 2010; Dettmer and Engewald, 2002). Carbopack B is a comprised of graphitized carbon black and provide a non-specific site for adsorption processes, meaning London dispersion forces are the driving force and are able to trap VOCs with carbon numbers from 4 to 12 (Bruner et al., 1990). The trap was preconditioned by flushing it with helium (99.995% purity) at 15 ml/min while being heated to 300° C for 12 h. This removed any volatile impurities that may have been in the sorbents, including monomers of the sorbents. The sampling method involves adsorbing analytes onto the sorbents, while the bulk components of air pass through the trap. The trap can be rapidly heated under carrier gas flow to desorb and inject the analyte into the column.

Sampling onto the first trap lasted 20 minutes and occurred at a flow rate of 50 ml/min. After sampling, the first sorbent trap was back-flushed at 10 ml/min for 10 min with ultra-high purity (UHP) helium to purge the trap of any O_2, H_2O, and other small non-BVOC components. The second trap was a 1/8th inch OD trap that was cooled to 10° C by Peltier plates. The smaller second trap was needed to focus the analytes before they were injected into the GC. Transfer from the first trap to the second trap was achieved by heating the first trap to 200° C with a set of cartridge heaters. A flow of 10 ml/min of UHP He was used to transfer the sample from the first trap to the cooled second trap. After 10 minutes of transferring to the second trap, the sample was then injected into the GCxGC system. The sample was transferred into the GC by heating the second sorbent trap to 200° C and passing 1 sccm of ultra-high purity He through the trap for 10 minutes. The final transfer temperatures were chosen in an attempt to trap, concentrate, and desorb organic nitrate species without thermally degrading them, which becomes significant at ~150° C (Hiskey et al., 1991) and all organic nitrates degrade at ~220° C (Day et al., 2002).

Figure 3.5 shows a chromatogram of a sample taken during a field campaign at the University of Michigan Biological Station (UMBS) in the summer of 2012.

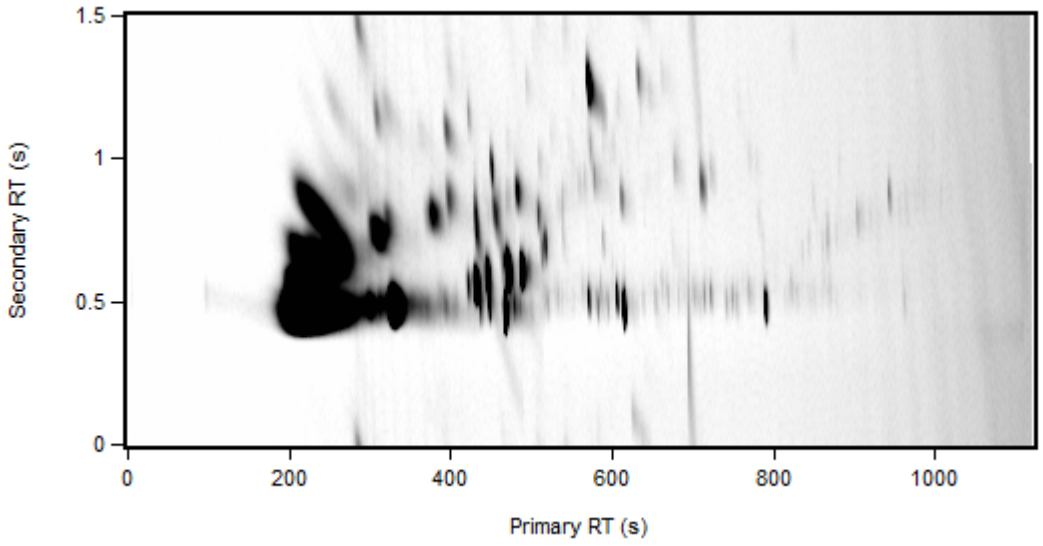

Figure 3.5 GCxGC chromatogram of ambient sample from UMBS using configuration 1.

From the figure, it can be seen that the compounds with lower volatilities (right side of chromatogram), such as monoterpenes and sesquiterpenes, were successfully concentrated and injected into the GCxGC system. However, higher volatility BVOCs (left side of chromatogram), such as isoprene, came out of the sampling system in a plug that was too broad. The GCxGC system was unable to resolve the very broad plug that precluded identification and quantification of the many coeluting species.

The second configuration of the sampler utilized a single 1/8th inch OD sorbent trap coupled to a liquid nitrogen cooled cryofocuser. A cryofocuser is a device that uses a cryogen to condense analytes into a small volume. Upon rapid heating, the analytes vaporize and can be injected into the GC in a narrow volume. Figure 3.6 shows the schematic of the second configuration.

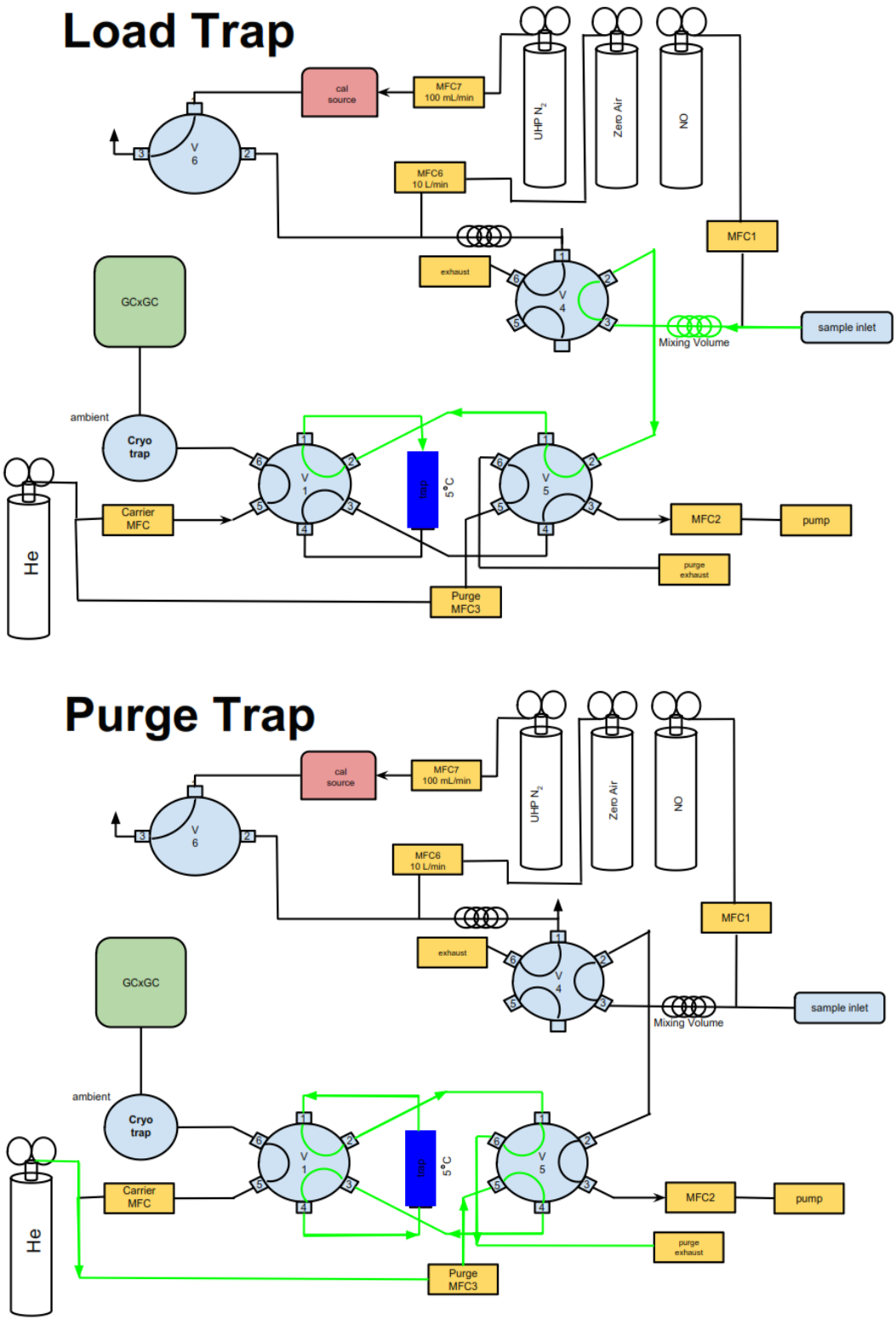

Figure 3.6 Flow schematic of the 2nd configuration of the sampling system.

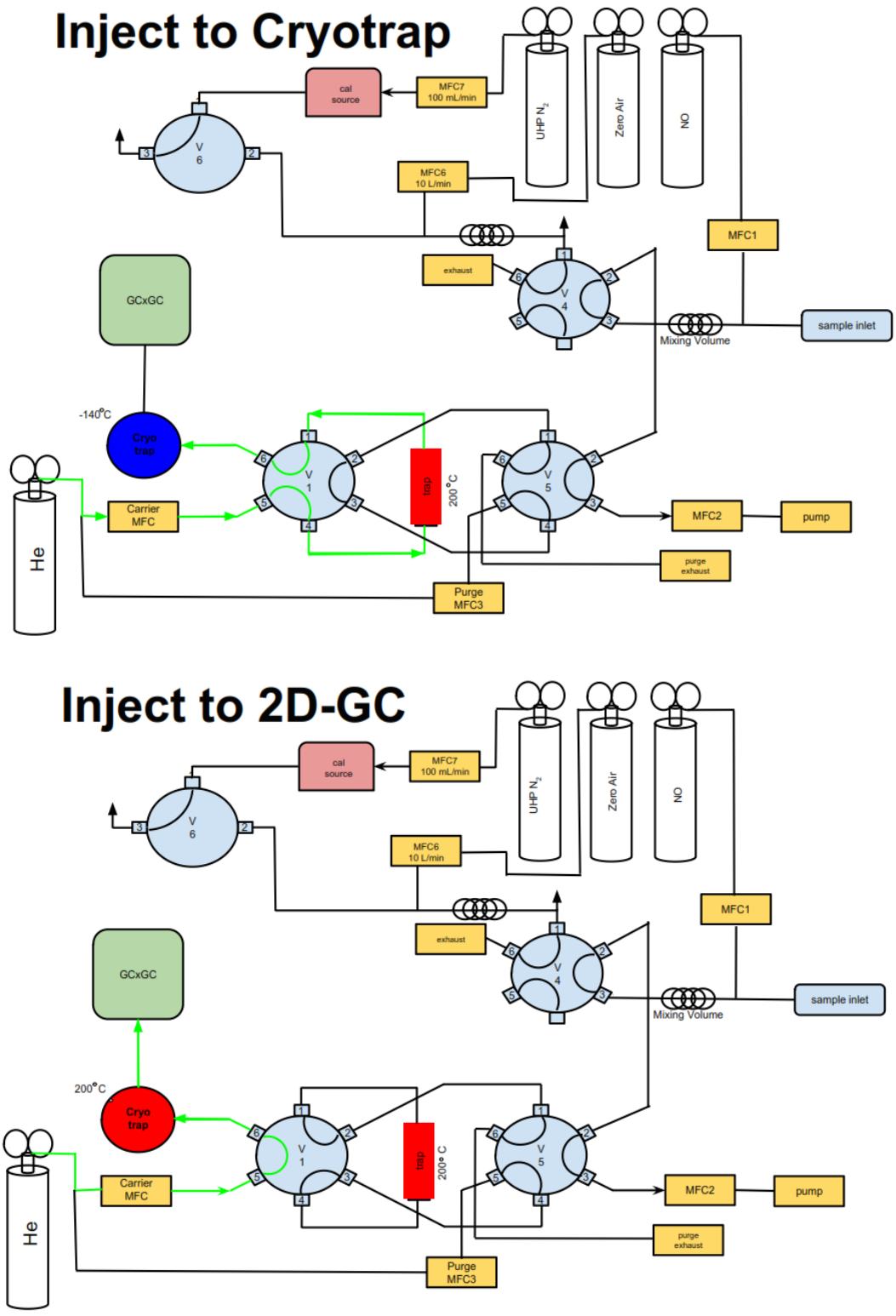

Figure 3.6 Continued.

In this configuration, the sample was mixed with 1 ml/min of 1044 ppm and mixed in a 0.5 m length of tubing to remove any O_3 which would oxidize alkenes adsorbed onto the trap (Helmig, 1997). Analytes were adsorbed to the sorbent trap which was cooled at 5° C by Peltier plates. The sorbent trap was then back flushed with UHP He at 10 mL/min for 5 min to remove water and other species not adsorbed to the trap. The cryofocuser was then cooled to -140° C by liquid nitrogen and the sorbent trap was then heated to 200° C by cartridge heaters and a flow of He was used to transfer the analytes from the sorbent trap to the cryofocuser. The cryofocuser was then heated to ~200° C and a 1.0 mL/min flow of UHP He was used to transfer the analytes in the cryofocuser into the GCxGC system.

Figure 3.7 shows the design of the cryofocuser. The cryofocuser consisted of a ceramic insert inside a stainless steel case with a Nichrome wire wound inside. A type K thermocouple was welded to the Nichrome wire to monitor the temperature of the system. Two ports on the stainless steel body were used to inject and vent liquid nitrogen to cool the system. After multiple tests, it was determined that -140° C was an ideal temperature to cool the cryotrap. This temperature was chosen because at this temperature, isoprene and other high volatility BVOCs were concentrated into a very small plug, using the least amount of liquid N_2.

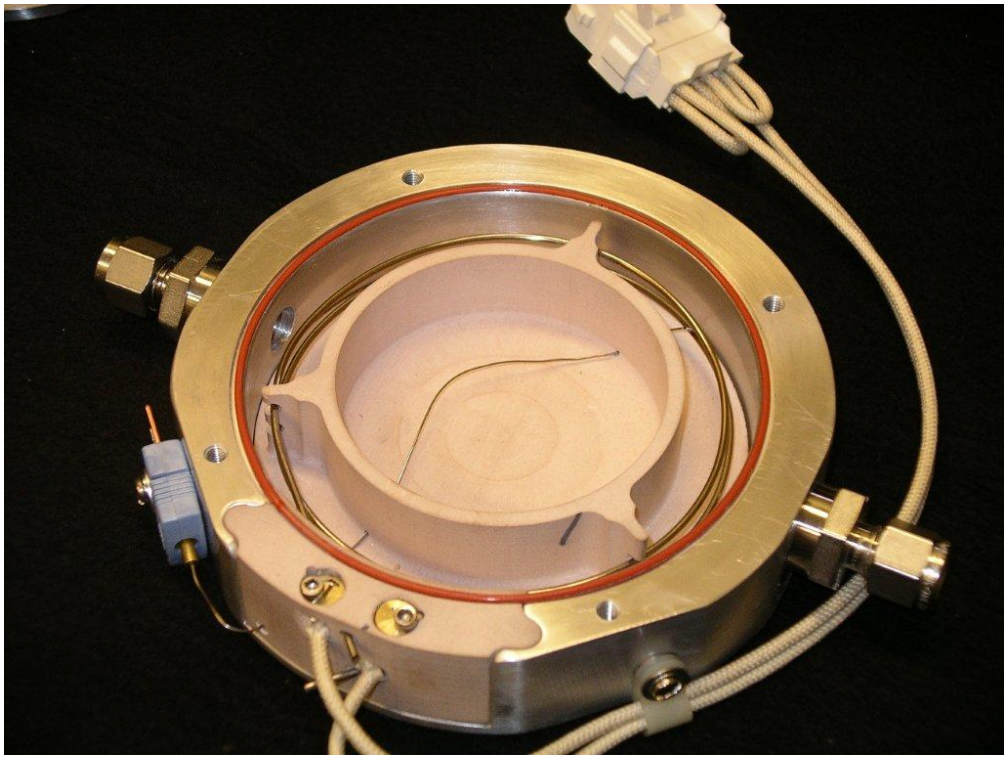

Figure 3.7 Design of the custom cryofocusing unit.

Two electrodes were placed on opposite ends of the Nichrome wire. A 12 V, 200 amp power supply was applied across the wire to heat the cryofocuser. Heating from -140° C to 200° C took place in ~3 seconds. The rapid temperature increase was faster than the ability of an Omega Micromega controller to read precisely, resulting in the final temperature to overshoot the 200° C setting to between 220° C to 240° C.

Figure 3.8 shows a typical chromatogram of an ambient sample and a standard of isoprene, methyl vinyl ketone, and methacrolein taken with configuration 2.

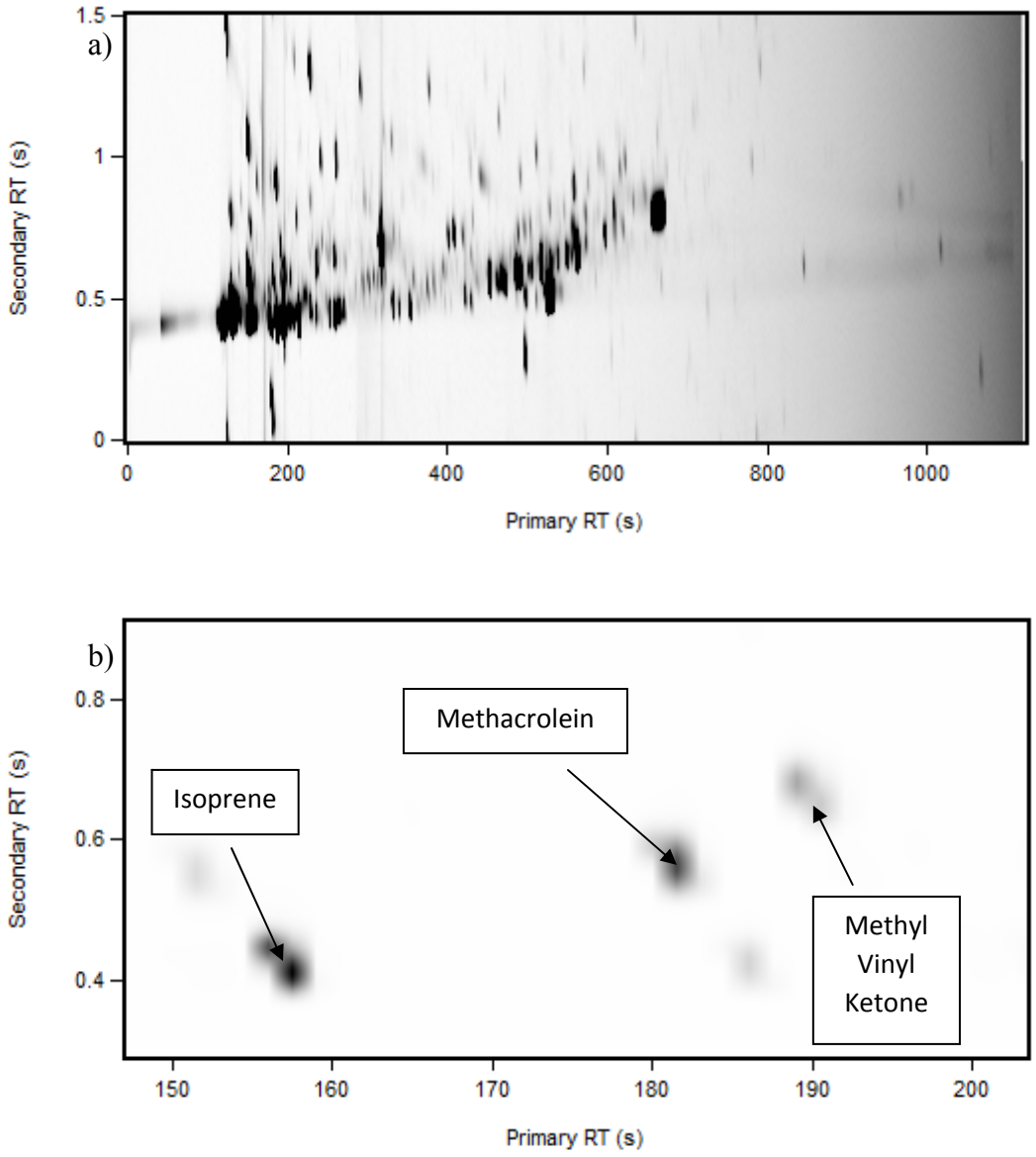

Figure 3.8 Chromatogram of ambient sample (a) and isoprene, methyl vinyl ketone, and methacrolein standard (b) taken during SOAS using configuration 2.

From Figure 3.8 it can be seen that the higher volatility analytes were injected into the GCxGC system and successfully separated. However, the cost and load of using liquid N_2 in a field application became too great. In laboratory studies, a tank of 180 L of liquid N_2 lasted ~1.5 weeks running continuously. During the Southern Oxidant and Aerosol Study

in rural Alabama, a tank of liquid N_2 lasted ~1 day. Another unknown problem that arose during the campaign was the unexpected failure of the heating element on the cryofocuser. On multiple occasions, the heating element failed to work and samples were never injected into the GCxGC. A third configuration was built in the field to deal with the unforeseen problems.

The third configuration of the sample relied solely on a single 1/8 inch OD hypodermic piece of stainless steel that was filled with 50/50 (mass/mass) tenax/carbopack B. A schematic of the configuration is shown in Figure 3.9. The temperature of the GC oven was maintained at 40° C in an attempt to focus the analytes on the head of the primary column.

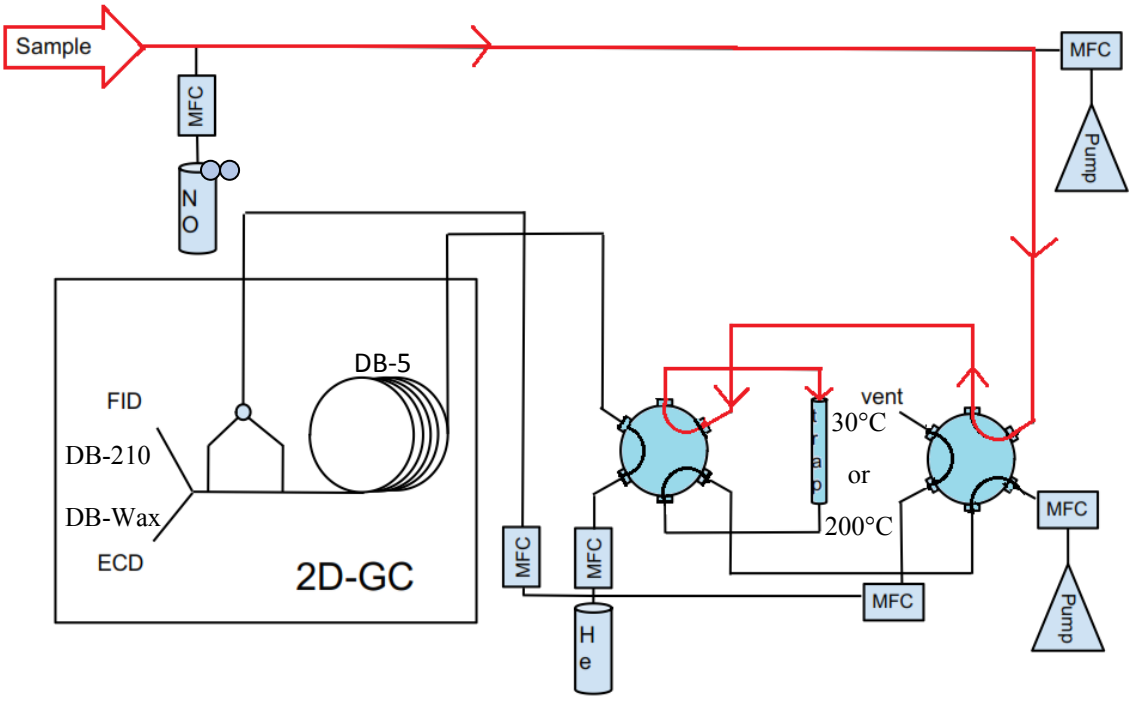

Figure 3.9 Schematic of configuration 3.

Figure 3.10 shows a typical chromatogram for an ambient sample taken with the sampling system using configuration 3 during the SOAS campaign.

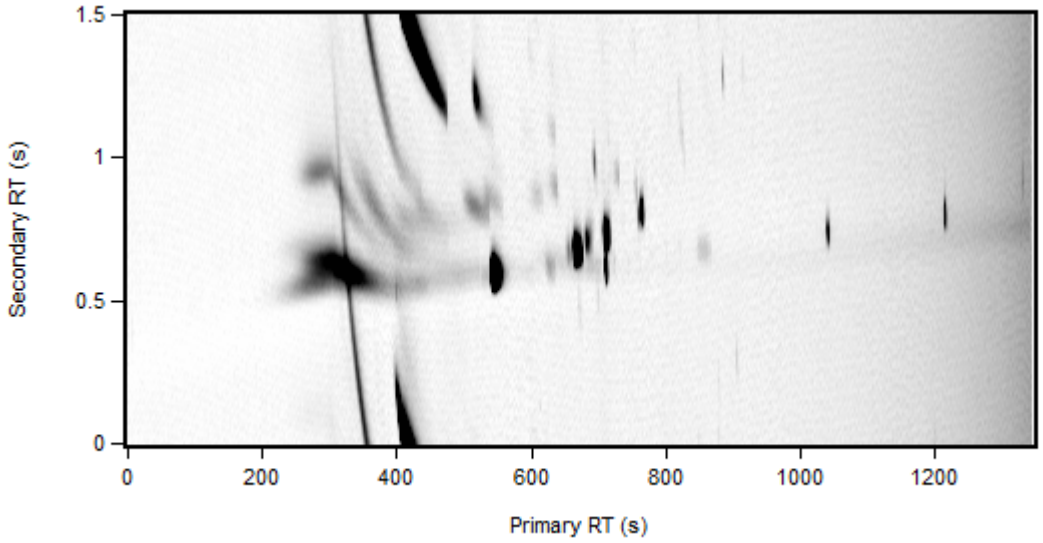

Figure 3.10 Chromatogram of ambient sample obtained during the SOAS campaign with configuration 3.

With this configuration, low volatility analytes such as monoterpenes were separated and detected, however, high volatility analytes such as isoprene were not injected in a suitably narrow plug to enable unambiguous separation and detection.

3.2.3 GCxGC

The GCxGC was a modified Agilent 7890. Differential flow modulation was used as the means of transferring the sample from the first to secondary columns (Bueno and Seeley, 2004). The concept of differential flow modulation can be seen in Figure 3.11.

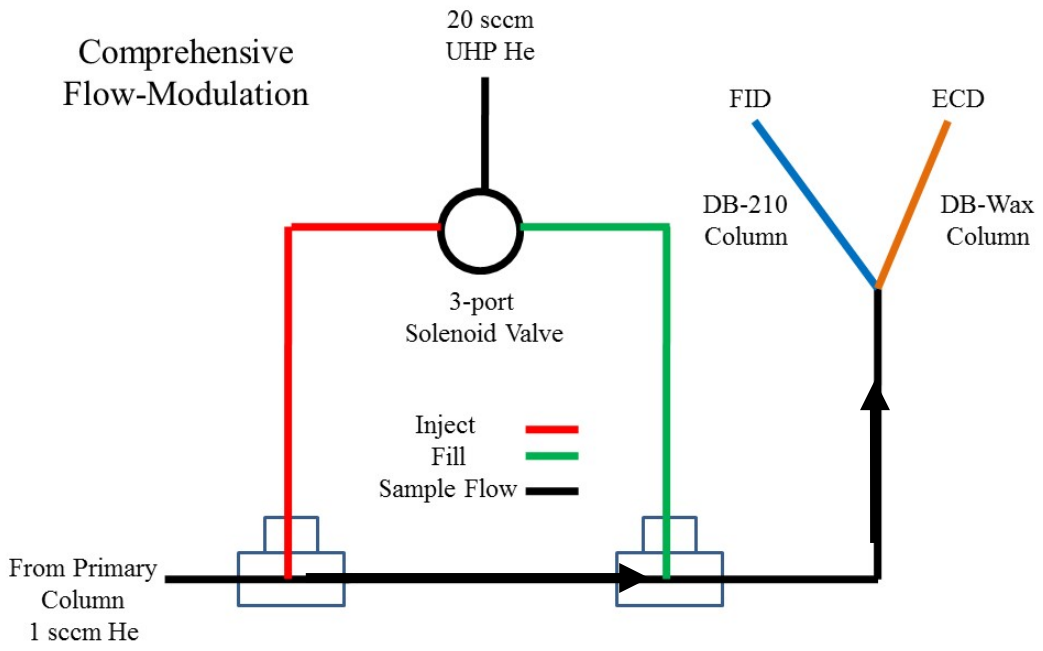

Figure 3.11 Schematic of comprehensive flow modulation.

In flow modulation, the eluent from the primary column fills a small reservoir (a length of fused silica tubing that has ~0.5 mL of volume for the sample to fill) between two tees. After a modulation period (1.5 seconds for this instrument), the 3 port valve is switched and an excess flow of UHP He is diverted from the second tee to the first tee to flush the reservoir into the secondary columns for 1.5 seconds. The 3 port valve is then switched back and the reservoir is allowed to fill again. The primary column was a RTX-5 (5% diphenyl 95% dimethyl polysiloxane) while two semi-polar secondary columns where used for two different detectors. To separate and identify nitrooxy containing compounds, a 5 m strand of a DB-Wax (polyethylene glycol) column was used in conjunction with an electron-capture detector (ECD). To separate all other BVOCs, a 5 m DB-210 (50%

trifluoropropyl 50% methylpolysiloxane) column was used as the secondary column and was used in conjunction with a flame-ionization detector (FID).

3.2.4 Sampling Line

For sampling during SOAS, a ~6 m length of 3/8 inch OD stainless steel, coated with Silcosteel (Restek Inc. Bellefonte, PA), was used to sample in 1.5 LPM of air. To keep rain from entering the sample line, it was bent towards the ground. No filters were used to separate the particulate phase from the gas phase because the presence of Teflon from the filter holders created large artifact peaks in blank measurements. From the 1.5 LPM of air, 100 sccm was sampled through the single trap. At a tee at the beginning of the sampling line, a flow of 7.2 sccm of 1044 ppm NO in N_2 was added to the sample flow to scrub O_3 (Holdren et al., 1979), yielding a concentration of 0.3 ppm NO in the sample air. This works by converting O_3 to O_2 by reaction 3.1. We calculated that 99.99% of all O_3 was removed.

$$NO + O_3 \longrightarrow NO_2 + O_2 \qquad \text{Reaction 3.1}$$

O_3 is removed during sampling because it reacts with analytes (particularly alkenes) adsorbed to the sorbent materials (Helmig, 1997) and therefore leads to artificially low measurements.

3.2.5 Sampling Locations

Configuration 1 of the sampling system was tested at the University of Michigan Biological Station in Pellston, MI. A description of the site can be found elsewhere (Carroll et al., 2001). Configuration 2 was tested during smog chamber experiments

performed at Purdue University and during the 2013 Southern Oxidant and Aerosol Study (SOAS) campaign. Configuration 3 was tested during SOAS in Brent, AL. The SOAS study occurred between June 1st and July 15th, 2013. The site was located outside of the Omugele Division of the Talladega National Forest which is shown in Figure 3.12. This site was chosen because average temperatures at this site have not risen over the past three decades (Portmann et al., 2009) and a hypothesis that the climate anomaly may be due to radiative effects of aerosols derived from BVOCs has been proposed (Goldstein et al., 2009).

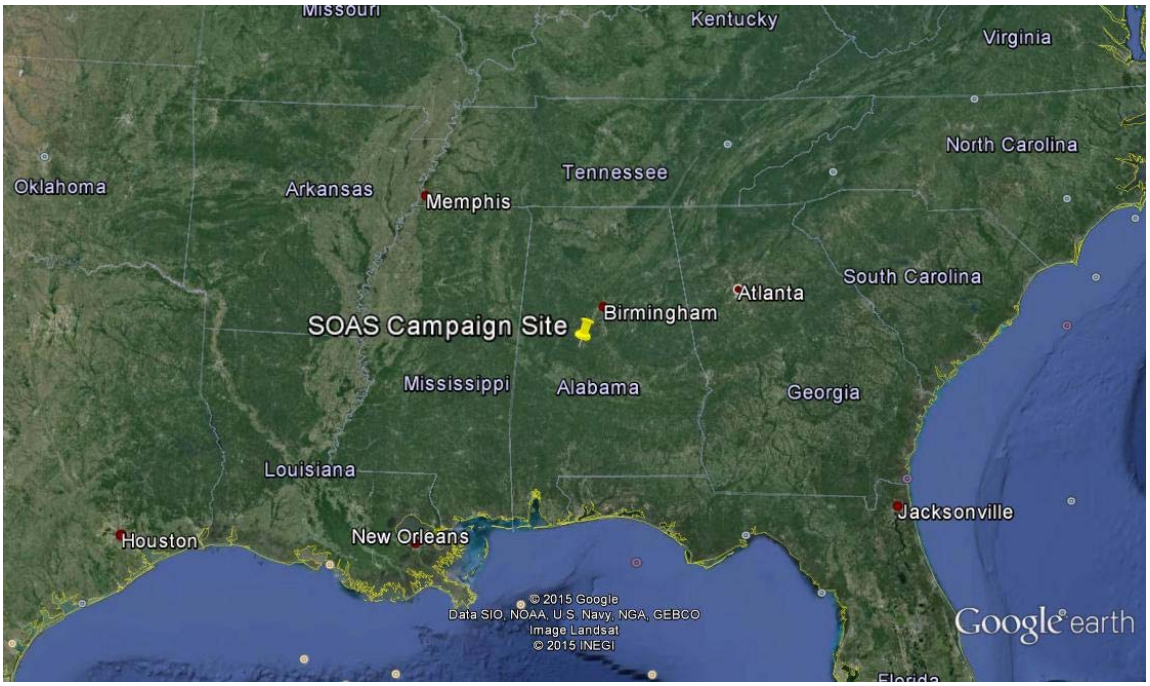

Figure 3.12 Site of the SOAS campaign in relation to the southeastern United States.

3.3 Results and Discussion

3.3.1 Calibration System

Figure 3.13 shows the mass loss rates of the standards from the calibration system for the three different time periods. As shown in the figures, the mass loss rates are linear, the shape of which yields an accurate calibration source.

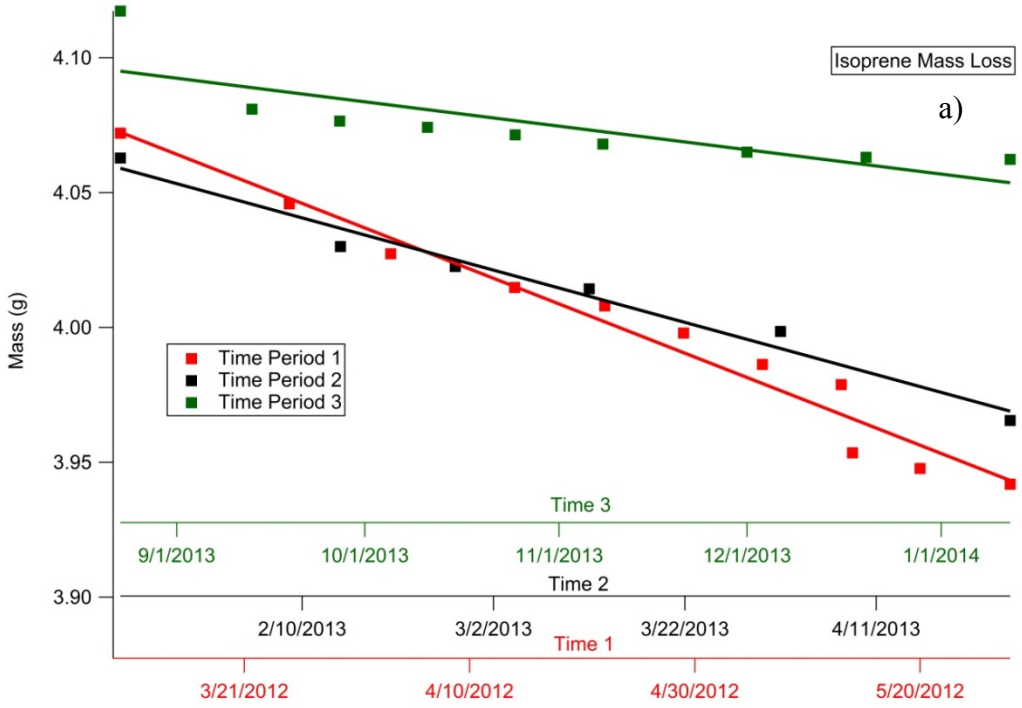

Figure 3.13 Mass loss measurements of the seven standards during the 3 measurement periods for isoprene (a), trans-caryophyllene (b), toluene (c), isobutyl-nitrate (d), decane (e), 2-ethyl hexyl nitrate (f), and α-pinene (g).

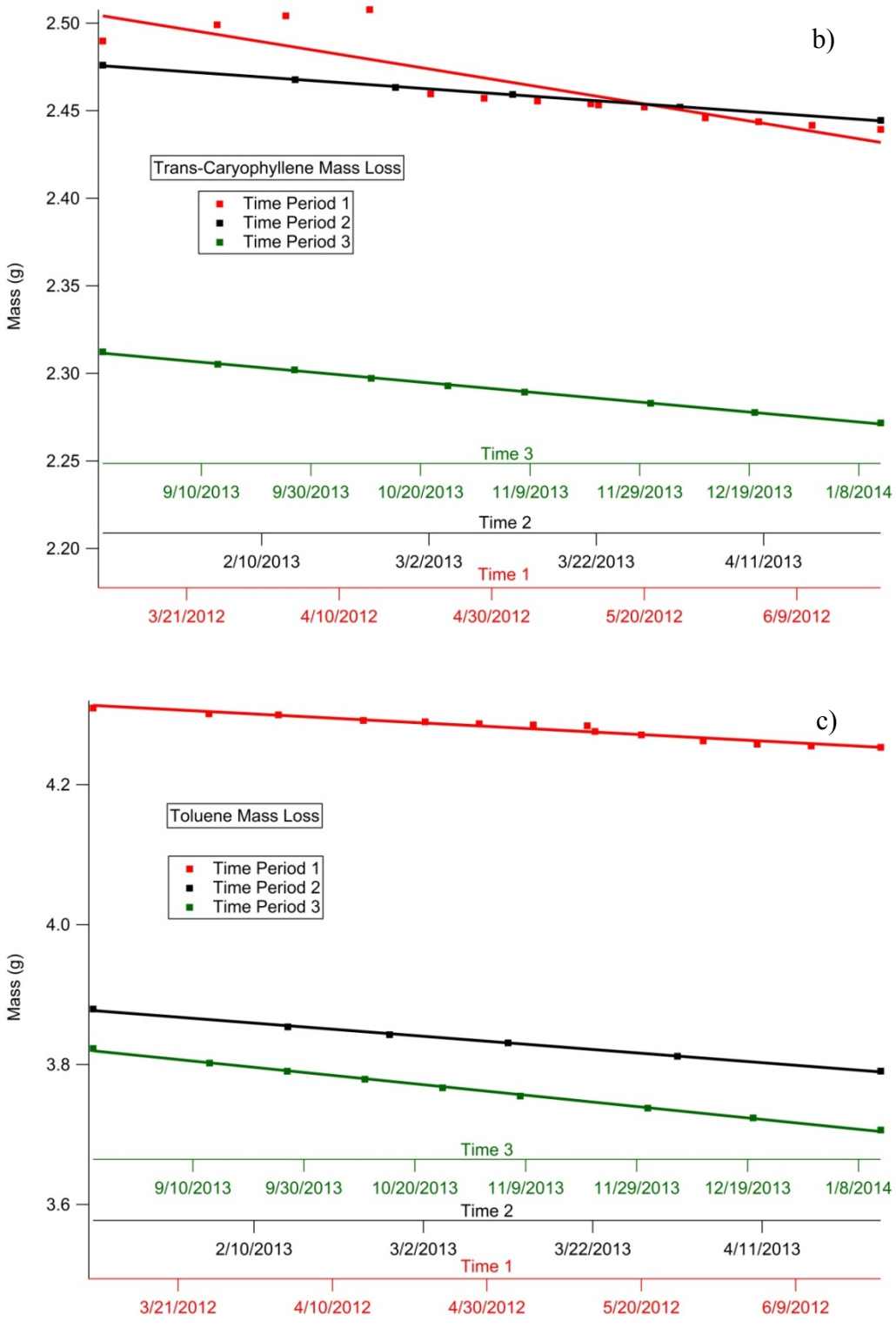

Figure 3.13 continued.

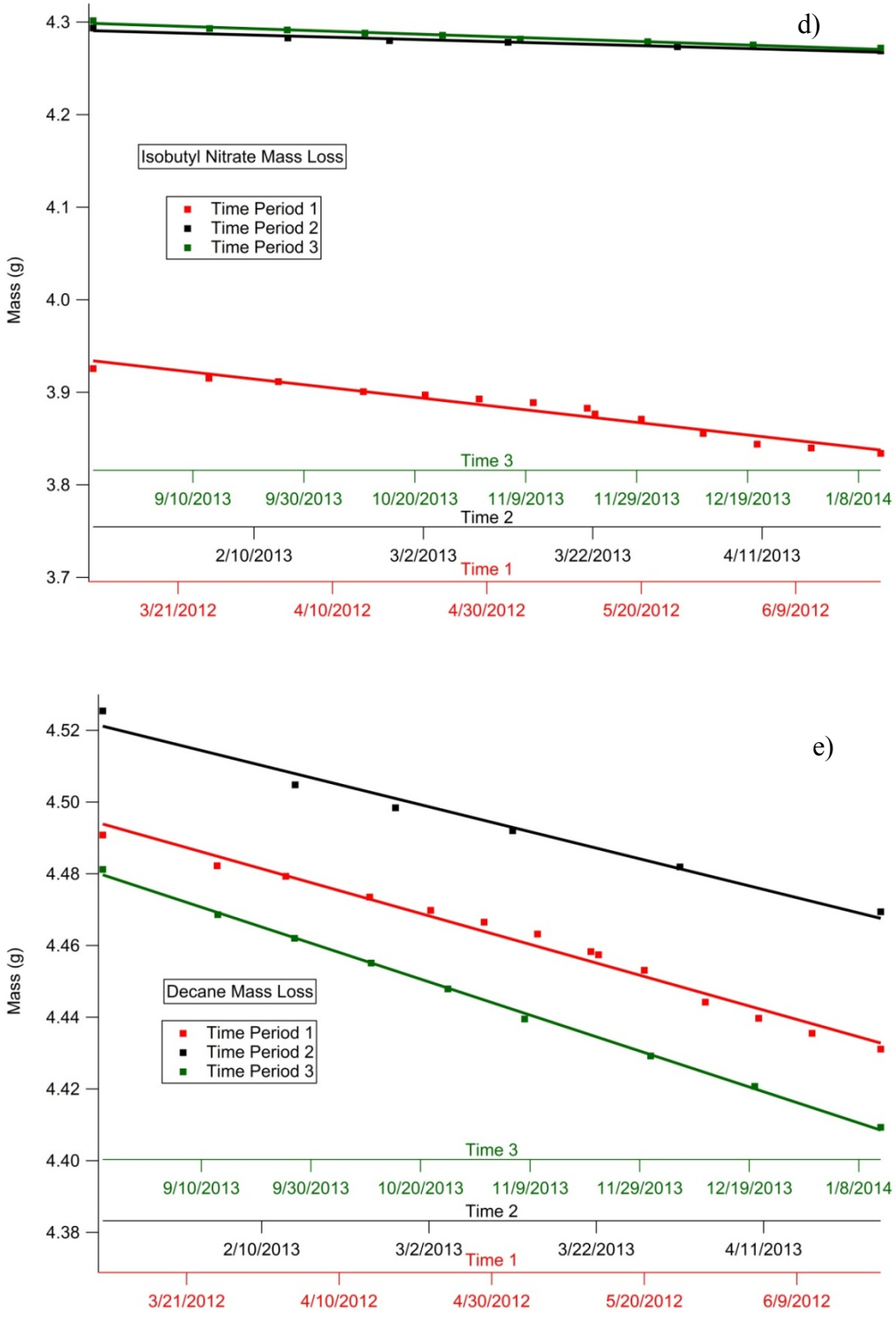

Figure 3.13 continued.

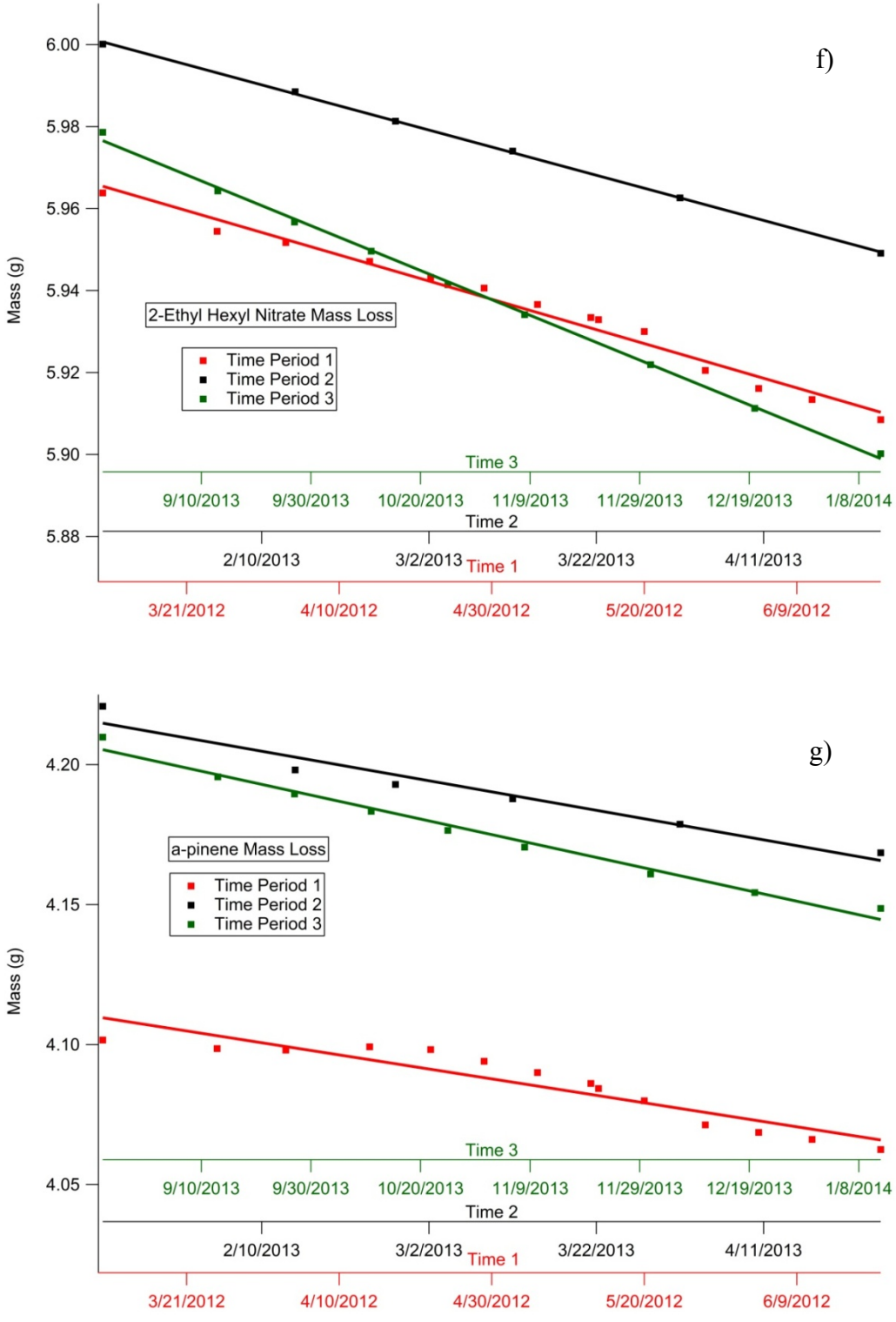

Figure 3.13 continued

The first time period was from March 10th, 2012 to June 20th, 2012, the second time period was from January 22, 2013 to April 25th, 2013, and the third from August 23rd, 2013 to January 12th, 2014. The second and third time periods represent the mass loss rates of the standards before and after the SOAS field campaign, respectively. Data from all three experiments were used to compare the relative error in the calibrations made during the SOAS campaign. The first design included a large Teflon block which showed a large outgas of contaminants in blank runs. The trans-caryophyllene in the first mass loss period slowly changed from clear to a yellow color, indicating some form of chemical change that would change the vapor pressure. This problem is manifested in the poor linearity of the slope for trans-caryophyllene in Figure 3.13b. An oxygen impurity is unlikely since the block was leak checked daily to insure the integrity of the seals.

Table 3.2 shows the comparison of the mass loss rates of the seven compounds for the three measuring periods. Larger relative error in the measurements for the first time period are most likely due to over sampling. The vials in the first configuration were weighed each week, compared to two weeks for the second and third configuration. The poorer precision during the first mass loss period is most likely a result of dust contamination, chipped glassware, scale drift, and evaporative loss from handling the diffusion tubes (Helmig et al., 2003).

Table 3.2 Mass loss rates and average loss rate for the 3 configurations. Loss rates are all measured in ng/s.

Compound	Loss Rate 1	Loss Rate 2	Loss Rate 3	Average	Std Dev	Relative Error (%)
Isoprene	16.8±5	11.1±5	2.23±0.9	10	7.3	73
trans-caryophyllene	3.85±2	3.91±0.4	3.31±0.4	3.69	0.3	9
toluene	4.03±2	10.8±1	9.55±1	8.13	3.6	44
isobutyl-nitrate	7.63±2	2.92±1	2.42±1	4.32	3	66
decane	5.96±1	6.74±2	5.89±0.7	6.2	0.5	8
2-ethyl-hexylnitrate	5.48±1	6.37±0.4	6.37±0.7	6.07	0.5	8
α-pinene	6.78±3	6.17±3	5.57±1	6.17	0.6	10

3.3.2 Ambient Air Sampling

The third configuration was built and used at SOAS after the failure of the second configuration. While we determined the retention times of α-pinene, β-pinene, camphene, limonene, γ-terpinene, terpinolene, myrcene, and the monoterpenoid p-cymene, the only observable species at the site were the first four. Mycrene could not be distinguished in the 2D plots as its primary and secondary retention times were indistinguishable of those for β-pinene. Figure 3.10 shows a 2D chromatogram taken during the campaign.

The third configuration enabled separations of monoterpenes and other species with a similar vapor pressures, yet still suffered from poor resolution. While the first configuration was able to produce baseline peak widths of 3 s, the third configuration produced baseline peak widths of 12 s. This resolution problem became an issue when determining the mycrene and limonene concentrations. Due to the wide peak widths, mycrene and β-pinene were completely indistinguishable, while limonene could only occasionally be baseline resolved due to another unknown compound that co-eluted.

These observations illustrate the difficulty and the importance of resolving power in the determination of monoterpenes.

In spite of the limitations, configuration 3 provided useful data, and therefore configuration 3 was used for the SOAS data acquisitions. A large comprehensive data set was collected, and therefore the remaining sections of this chapter will deal with focusing on characterizing the third configuration of the automated GCxGC.

3.3.3 Determination of Retention Times

Commercial samples of α-pinene, β-pinene, camphene, limonene, γ-terpinene, terpinolene, myrcene, and p-cymene were diluted in HPLC grade hexane to concentrations of 0.1% by volume during the SOAS campaign and injected into carefully metered 80 L Teflon bags through a heated glass tee. The liquid phase standard solutions were used to obtain the primary and secondary retention times and used periodically throughout the SOAS campaign to assure that there was no drift in the retention time during the campaign. The results can be seen in Table 3.3 and an ambient chromatogram is shown in Figure 3.14.

Table 3.3 Retention times of monoterpenes as measured during the SOAS campaign.

Compound	Primary Retention Time (s)	Secondary Retention Time (s)
p-cymene	756.0	2.355
α-pinene	669.0	2.170
β-pinene	711.0	2.220
limonene	760.0	2.280
terpinolene	817.5	2.315
myrcene	715.5	2.225
γ-terpinene	750.0	2.265
camphene	681.0	2.180

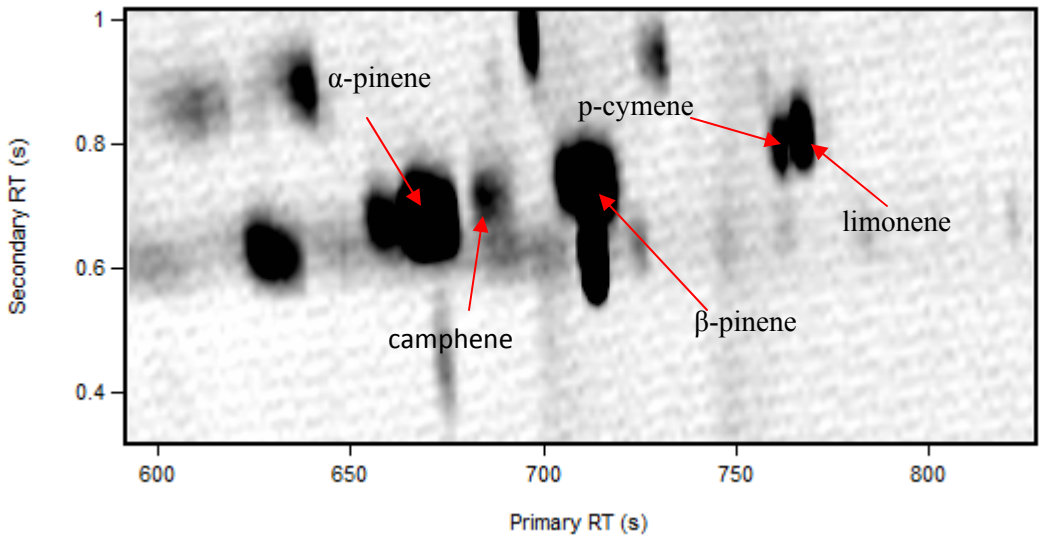

Figure 3.14 Ambient chromatogram of monoterpenes measured during SOAS.

Myrcene's primary and secondary retention times were too similar to that of β-pinene for it to be baseline resolved. Myrcene appeared as a shoulder on β-pinene peaks in the 2D chromatograms. Another problem that arose during the field campaign was the presence of a compound that co-eluted with limonene. This occurred in over half of the chromatograms during the campaign. To distinguish and confidently identify limonene, a Welch's t-test was used to assure the difference separation of the two co-eluting peaks. The t-test was performed and there was no statistical difference between the primary retention time of the first eluting peak and the primary retention time of the limonene standards ($t = 1.65 < 2.78$, the critical t-value at $p=0.05$). It was concluded that the peak that eluted first was limonene.

3.3.4 Calibration

Every day during the SOAS campaign a gas-phase standard bag was made to calibrate the instrument. An 80 L Teflon bag was filled with an accurately known volume of ultra-zero air using a calibrated mass flow controller, and then attached to the diffusion source at the end of the ultra-zero air fill for various time periods to make a gas phase standard. The peak areas for each gas phase standard were divided by the number of liters of air sampled to correct any differences in the volume sampled. The calibration range covered the range of ambient values. The calibration data for each day throughout the field campaign is shown in Figure 3.15. From variability of the blanks, and the slope of the calibration curve, the limit of detection (LOD = 3 x σ/ sensitivity) for α-pinene for was determined to be 0.05 ppt. The standard error of the slope was 2.7 ppb s^{-1}, or 7%.

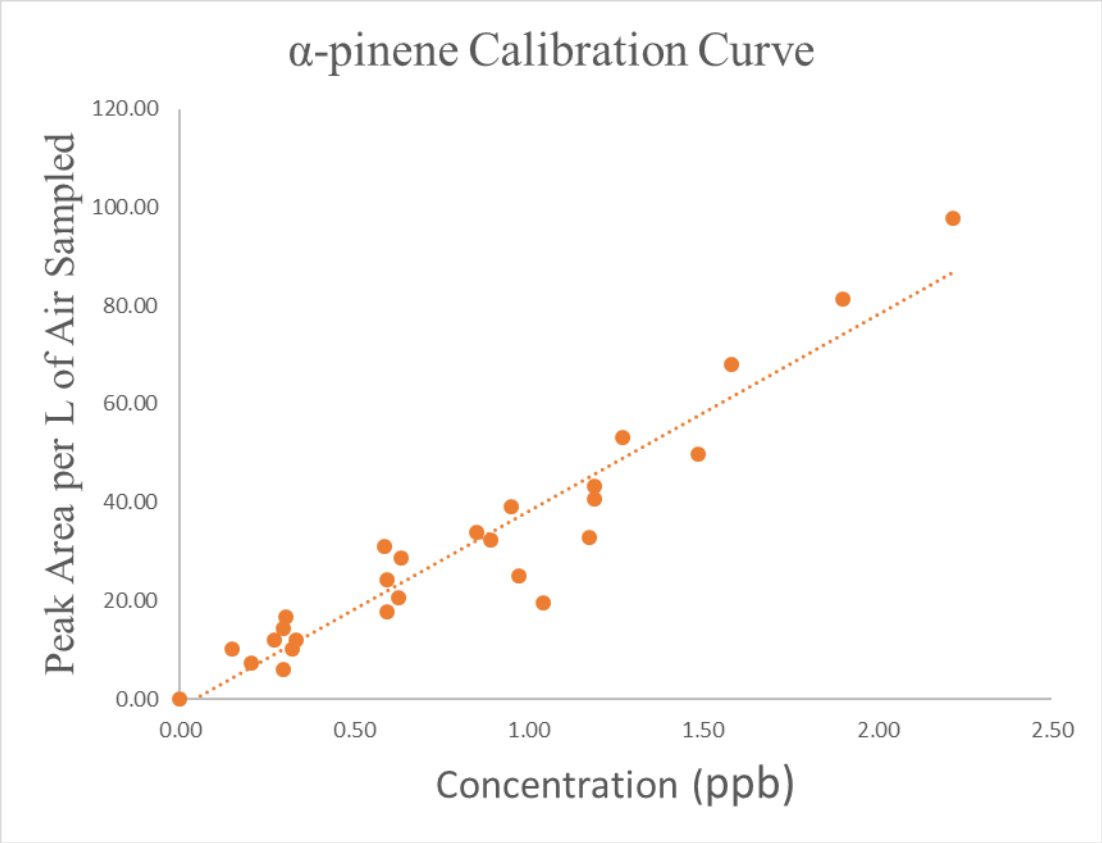

Figure 3.15 Calibration Curve obtained during the SOAS campaign.

3.3.5 Sensitivity Analysis

It was determined that a simple linear regression wasn't applicable to determining the sensitivity of the GCxGC. In a simple linear regression, it is assumed that the uncertainty in data is solely or dominantly in the dependent variable. There is a large uncertainty in the process of making the calibration standard bags at low concentrations (MFC error, stopwatch error, and most importantly the diffusion source calibration system). The dominant uncertainty for our calibrations was not in the dependent variable, but in the independent variable. To account for errors in the regressor and dependent variable, an error-in-variables model was chosen.

A Deming regression is a simple error-in-variables model that was used to determine the slope, y-intercept, and errors in those parameters. A Deming regression is a special case of total least squares in which any number of predictors is allowed. In a simple linear regression the residuals of the least squares analysis are minimized about the y-axis assuming a normal distribution (Figure 3.16). In a Deming regression, the residuals are minimized about the y-axis and x-axis. This allows for the error in the dependent and independent variable to be factored into finding the best fit line within the bounds placed on the measured errors. In this case a simple Deming regression was used. This means that the error terms are constant and the data are not weighted (Martin, 2000).

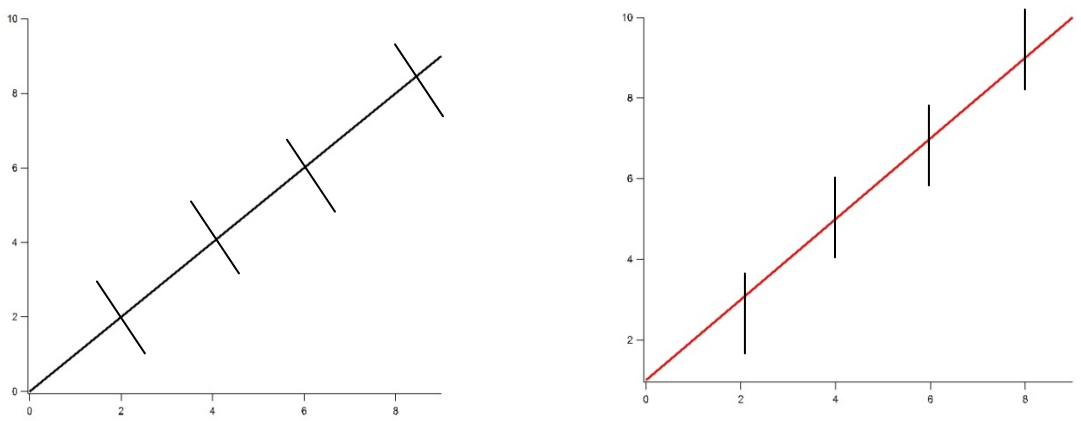

Deming Regression Linear Least Squares Regression

Figure 3.16 Difference between a simple linear regression and Deming regression.

In a Deming regression, the slope of the line is calculated by using Equation 3.6.

$$m = (s_{yy}-\delta s_{xx} + [(s_{yy}-\delta s_{xx})^2+4\delta s^2_{xy}]^{1/2})/2s_{xy} \qquad \text{Equation 3.6}$$

The y-intercept for a Deming regression is calculated using Equation 3.7.

$$b = (\bar{y} - m\bar{x}) \qquad \text{Equation 3.7}$$

For Equations 3.6 and 3.7:

$$s_{xx} = (1/n-1)\sum(x_i-\bar{x})^2 \qquad \text{Equation 3.8}$$

$$s_{yy} = (1/n-1)\sum(y_i - \bar{y})^2 \qquad \text{Equation 3.9}$$

$$s_{xy} = (1/n-1)\sum(x_i-\bar{x})(y_i - \bar{y}) \qquad \text{Equation 3.10}$$

$$\bar{x} = 1/n \sum x_i \qquad \text{Equation 3.11}$$

$$\bar{y} = 1/n \sum y_i \qquad \text{Equation 3.12}$$

$$\delta = \sigma_y/\sigma_x \qquad \text{Equation 3.13}$$

This leads to a new calibration curve equation:

$$y = 43.13x-3.619$$

This is 6% different from the simple linear regression result of y = 40.48x -1.63.

GraphPad Prism, a statistical software, was used to perform a Deming regression on the calibration and it calculated the errors, as shown below. The analysis found that at the 95% confidence interval, the y-intercept includes 0.

Table 3.4 Deming regression analysis of the calibration curve obtained during the SOAS campaign.

GraphPad Results	
Best-fit values	
Slope	43.1 ± 2.3
Y-intercept when X=0.0	-3.6 ± 2.2
X-intercept	0.085
1/slope	0.023
95% Confidence Intervals	
Slope	38.3 to 48.0
Y-intercept when X=0.0	-8.4 to 1
Goodness of Fit	
r^2	
Sy.x	6.396

It should be noted that in a Deming regression an r^2 (coefficient of correlation) is not calculated. In a normal least squares regression, r^2 is the fraction of the variation that is accounted for by the model. No known method for determining the r^2 of a Deming regression is currently exists (Martin, 2000).

3.3.6 Transfer Efficiency Tests

One of the main uncertainties that arose during the SOAS campaign was an incomplete understanding of the transfer efficiency of the sorbent trap. The transfer

efficiency is a measure of the fraction of the amount of analyte that is transferred from the sorbent trap and injected into the column, relative to the amount injected. This quantity assumes 100% collection efficiency and also includes reactive loss on the sorbent trap. It is critical to know so that any corrections to the data could made so that accurate concentration measurements would be reported. Due to the lack of repeat transfer efficiency tests during the SOAS campaign, the sampling system was rebuilt at Purdue. The 2-dimension Agilent 7890 was replaced with a 1-dimensional Varian 450-GC. An Rtx-5 (95% dimethyl polysiloxane, 5% diphenyl) column was used to separate selected monoterpenes, similar to that of the primary column used in the Agilent 7890. All calibration standard bags were directly connected to a heated ¼ inch OD Silcosteel line connected to the back of the sampling system so that the sampling flow was 100 sccm. The temperature lines of the sampling line was maintained at ~100° C, similar to the temperature used during the SOAS campaign. A 1 sccm flow of 1044 ppm NO was injected into the sample flow to replicate the SOAS set-up. A simple configuration is shown in Figure 3.17.

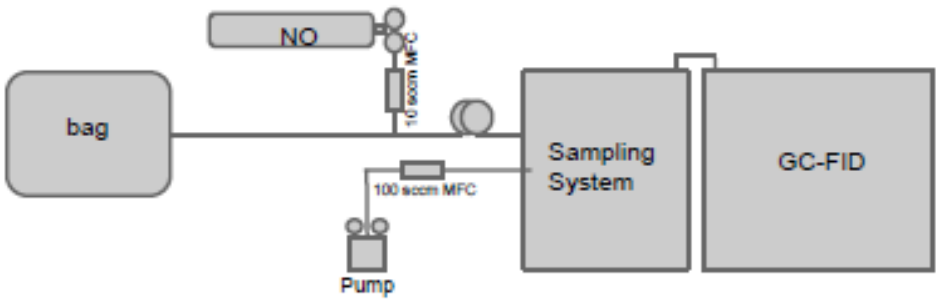

Figure 3.17 Basic setup of transfer efficiency tests.

A liquid sample was made that contained α-pinene, b-pinene, limonene, and camphene, diluted in HPLC grade hexane. The first solution was 0.17% by volume camphene and 0.50% by volume α-pinene, β-pinene, and limonene. This solution was called the "limonene mix". Due to the inability of the 1D-GC column to separate p-cymene and limonene, a second solution containing α-pinene, p-cymene, γ-terpinene, and terpinolene was made to quantify the transfer efficiency for p-cymene. The solution was called the "p-cymene mix".

The limonene mix solution was directly injected 5 times into the GC through a liquid injector with a 1:20 split ratio. The peak areas measured were then divided by the area of the α-pinene peak to give the relative peak areas as seen in Table 3.5. This then quantifies the quantities of each terpene in the sample, relative to α-pinene.

Table 3.5 Relative peak areas for 5 liquid injections.

	Peak Area					Relative Peak Area					Average Relative Peak Area	Relative Standard Deviation
	1	2	3	4	5	1	2	3	4	5		
α-pinene	133.3	210.6	97.8	63.7	43.5	1.00	1.00	1.00	1.00	1.00	**1.00**	
camphene	43.8	70.4	32.8	21.5	15.1	0.328	0.334	0.335	0.337	0.347	**0.336**	**0.021**
β-pinene	122.4	202.2	92.1	60.2	40.7	0.918	0.960	0.942	0.945	0.936	**0.940**	**0.016**
limonene	114.6	190.5	86.0	54.4	39.6	0.860	0.905	0.879	0.854	0.910	**0.881**	**0.025**

The 1 μL aliquot of the limonene mix was then injected into a 28 L bag, and this bag was sampled a total of 4 times. The resulting peak areas and relative peak areas are shown in Table 3.6. A new bag was made and 0.5 μL of the limonene mix was injected

and the results are presented as experiment 5. Since the first 4 experiments were performed from the same calibration bag and there is no significant change in the peak areas observed, it was determined that wall loss was not a major factor in this error analysis.

Table 3.6 Relative peak areas of 5 bag samples.

	Peak Area					Relative Peak Area					Average Relative Peak Area	Relative Standard Deviation
	1	2	3	4	5	1	2	3	4	5		
α-pinene	791.8	789.4	793.6	790.5	435	1.00	1.00	1.00	1.00	1.00	**1.00**	
camphene	268.9	270.6	272.3	269.2	149.6	0.340	0.343	0.343	0.340	0.344	**0.342**	**0.006**
β-pinene	715.6	717.1	718.7	705.1	392.5	0.904	0.908	0.906	0.892	0.902	**0.902**	**0.007**
limonene	332.0	319.3	337.7	335.2	181.6	0.419	0.404	0.425	0.424	0.417	**0.418**	**0.02**

To obtain the transfer efficiency of the compounds, Equation 3.14 was used where the averages for the relative peak areas from the bag samples were divided by the averages for the relative peak areas of the liquid samples. In this equation, the FID response of the individual monoterpenes canceled giving a unitless transfer efficiency value. Errors in the transfer efficiency will be discussed below.

$$\text{transfer efficiency} = \frac{\left(\frac{\text{peak area}_{x}}{\text{peak area}_{\alpha\text{-pinene}}}\right)_{\text{bag injection}}}{\left(\frac{\text{peak area}_{x}}{\text{peak area}_{\alpha\text{-pinene}}}\right)_{\text{liquid injection}}} \qquad \text{Equation 3.14}$$

The resulting transfer efficiencies were:

Table 3.7 Preliminary transfer efficiency results for limonene mix 1.

Compound	Transfer Efficiency (1)
α-pinene	1.00
camphene	1.02
β-pinene	0.960
limonene	0.474

To expand the data set, two more "limonene mix" solutions were made. The first solution contained 0.50% by volume α-pinene, β-pinene, and limonene and 0.16% by volume camphene. The second solution contained 0.25% by volume α-pinene, β-pinene, and limonene and had a concentration of camphene that was 0.13% by volume. The same test described above was performed on the two "limonene mixes." Finally, a gas-phase calibration standard bag was filled with zero air passed through a bubbler to add humidity to the bags, to test for the impact of water on the transfer efficiencies. To assure leaks in the bag were not affecting the transfer efficiency results, new bags were made for each solution and leak checked before use. In total, 11 liquid injections and 11 bag injections, 5 from the first mix, and 3 from each of the subsequent two mixes were used to calculate the relative response of the monoterpenes to α-pinene. The final transfer efficiencies calculated from averaging these 11 liquid and 11 gas phase samples is shown in Table 3.8. The uncertainties in Table 3.8 are described below.

Table 3.8 Transfer Efficiencies for the compounds found in the limonene mix solutions.

Compound	Transfer Efficiency	Uncertainty in Transfer Efficiency
α-pinene	1.00	-
Camphene	1.06	0.02
β-pinene	0.95	0.03
Limonene	0.40	0.05

To calculate the precision of the transfer efficiency, the standard deviation of the relative areas from the liquid and gas phase injections for each solution were propagated to give a final uncertainty for the 3 selected monoterpenes. Uncertainties were calculated using Equation 3.15 where x, y, and z represent the standard deviation and average of limonene mix 1, limonene mix 2, and limonene mix 3, respectively. Random errors of 0.02, 0.03, and 0.05 were calculated for camphene, β-pinene, and limonene, respectively and can be seen in Table 3.8.

$$\sigma_{TT}\sigma_T = \sqrt{\left(\frac{\partial z}{\partial x}\right)^2 + \left(\frac{\partial z}{\partial y}\right)^2 + \left(\frac{\partial z}{\partial z}\right)^2}$$ Equation 3.15

To obtain the transfer efficiency for p-cymene, one solution of p-cymene mix was made that contained 0.5% p-cymene, terpinolene, and γ-terpinene. Only one p-cymene mix was made due to the little variation in transfer efficiencies between the 3 limonene mixes. The same procedure for determining the transfer efficiency was followed as described previously. The transfer efficiencies of the p-cymene mix were combined with the transfer efficiencies of the limonene mix and the results shown in Table 3.9.

Table 3.9 The final transfer efficiencies and errors in transfer efficiencies.

Compound	Transfer Efficiency	Uncertainty in Transfer Efficiency
α-pinene	1.00	0.00
camphene	1.05	0.06
β-pinene	0.95	0.03
limonene	0.41	0.08
p-cymene	0.30	0.02
γ-terpinene	0.21	0.02
terpinolene	0.14	0.02

From Tables 3.3, 3.8, and 3.9, it can be seen that as the retention time of the compound increased, the transfer efficiency decreased. The vapor pressures at 20° C according to Sigma Aldrich of β-pinene, p-cymene, limonene, γ-terpinene, and terpinolene are 2 mm Hg, 1.5 mm Hg, 1 mm Hg, 0.7 mm Hg, and 0.5 mm Hg, respectively. This means that the 200° C heating temperature was probably not efficient at desorbing analytes with lower vapor pressures than β-pinene.

3.3.7 Error Analysis

The mass loss rate of the calibration system was measured on three separate occasions. The results are shown in Table 3.10.

Table 3.10 Uncertainties in the analysis of the diffusion rate from the calibration system

Compound	Loss Rate 1	Loss Rate 2	Loss Rate 3	Average	Std Dev	Relative Error (%)
trans-caryophyllene	3.85±2	3.91±0.4	3.31±0.4	3.69	0.3	9
toluene	4.03±2	10.8±1	9.55±1	8.13	3.6	44
isobutyl-nitrate	7.63±2	2.92±1	2.42±1	4.32	3	66
decane	5.96±1	6.74±2	5.89±0.7	6.2	0.5	8
2-ethyl-hexylnitrate	5.48±1	6.37±0.4	6.37±0.7	6.07	0.5	8
α-pinene	6.78±3	6.17±3	5.57±1	6.17	0.6	10

The transfer efficiency data and the calibration error data were then used to calculate the uncertainty in the concentration measurements for each species. To calculate the uncertainty in the measurements, the concentrations were calculated according to Equation 3.16, and the uncertainties in each term propagated to yield a final uncertainty for the result.

$$[C] = [(pa/V)/b]/T \qquad \text{Equation 3.16}$$

In Equation 3.16, C is the concentration of monoterpene, pa is the peak area, V is the sample volume, b is the sensitivity of the instrument to α-pinene measured as counts per ppb per liter sampled, and T is the transfer efficiency. The uncertainty in the concentration measurements was calculated using Equation 3.17.

$$\text{Uncertainty } (\alpha_A/A) = [(\sigma_{pa}/pa)^2+(\sigma_V/V)^2+(\sigma_b/b)^2+(\sigma_T/T)^2]^{1/2} \qquad \text{Equation 3.17}$$

Since σ_A/A = relative standard deviation (RSD), we assumed A is the true value and therefore the uncertainties will be reported in RSD. In Equation 3.17, the variables are the same as those in Equation 3.16. The uncertainty of the sample volume was determined by

repeatedly measuring the flow rate of the sample mass flow controller, and the precision was found to be 1.2%. The uncertainty in determining the peak area was determined by calculating the area of a standard peak that was measured three times, and the precision was found to be 0.5%. The uncertainty in the sensitivity was determined by using the Graph Pad analysis shown in Table 3.11. The uncertainty in the transfer efficiencies was described above and can be found in Table 3.9. Table 3.11 lists the overall uncertainty for each of the species that, or could be, measured using the GCxGC sampling system.

Table 3.11 Uncertainty of measurement calculated through propagation of errors.

Compound	Uncertainty in Measurement (RSD)
a-pinene	11%
camphene	11%
b-pinene	11%
limonene	12%
p-cymene	13%
y-terpinene	13%
terpinolene	15%

3.3.8 Finalized Data

From the extensive characterization of the instrument and the error analysis performed, the measurements of the 4 monoterpenes and p-cymene during the SOAS campaign data were compiled and are presented in Figure 3.18. The peak areas of all the

chromatograms were calculated using an automated program designed by John Seeley of Oakland University. On average, the uncertainty in peak integration was small, with a relative standard deviation of 0.5%.

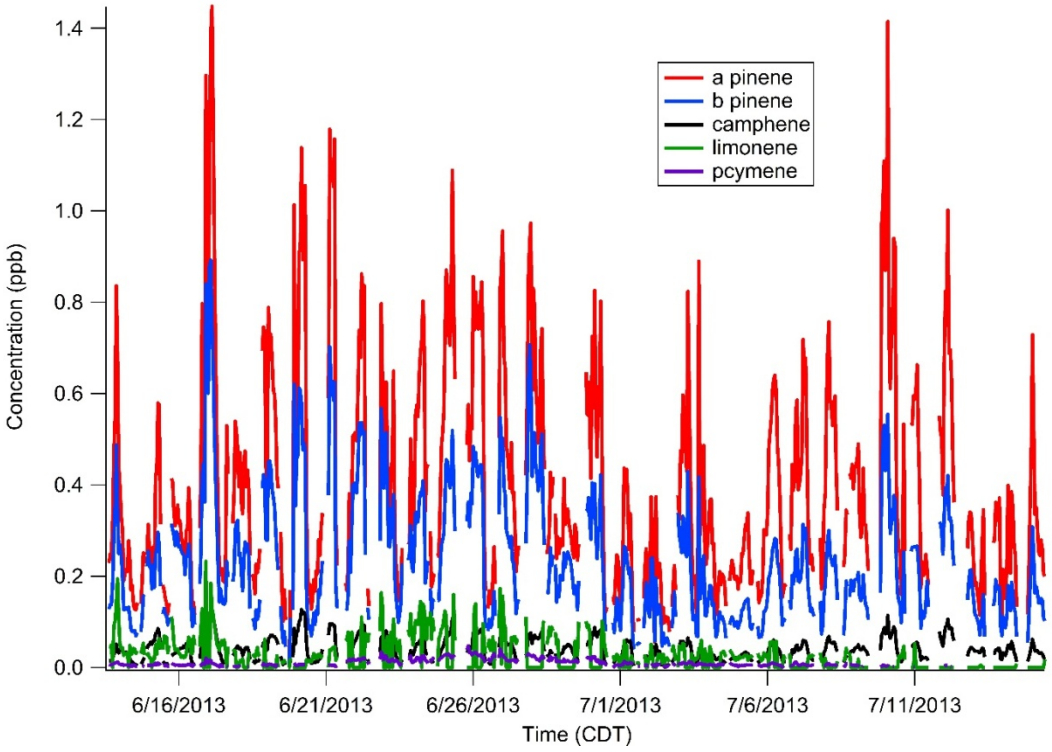

Figure 3.18 Finalized monoterpene and p-cymene data from SOAS 2013.

3.3.9 Comparison to a GC-MS

The measurements obtained at the SOAS field campaign were compared to the measurements conducted at the site by Abigail Koss (National Oceanic and Atmospheric Administration), Joost de Gouw (National Oceanic and Atmospheric Administration), Kevin Olson (University of California Berkeley), and Allen Goldstein (University of California Berkeley), using GC-MS. The GC-MS sampled from atop a 40 m tower while

the GCxGC measured monoterpenes from approximately 4 m above the ground. Locations of sampling site can be seen in Figure 3.19. The GCxGC was located on top of a grassy hill while the GC-MS was located above a forest canopy, and due to the different locations, this comparison is not ideal.

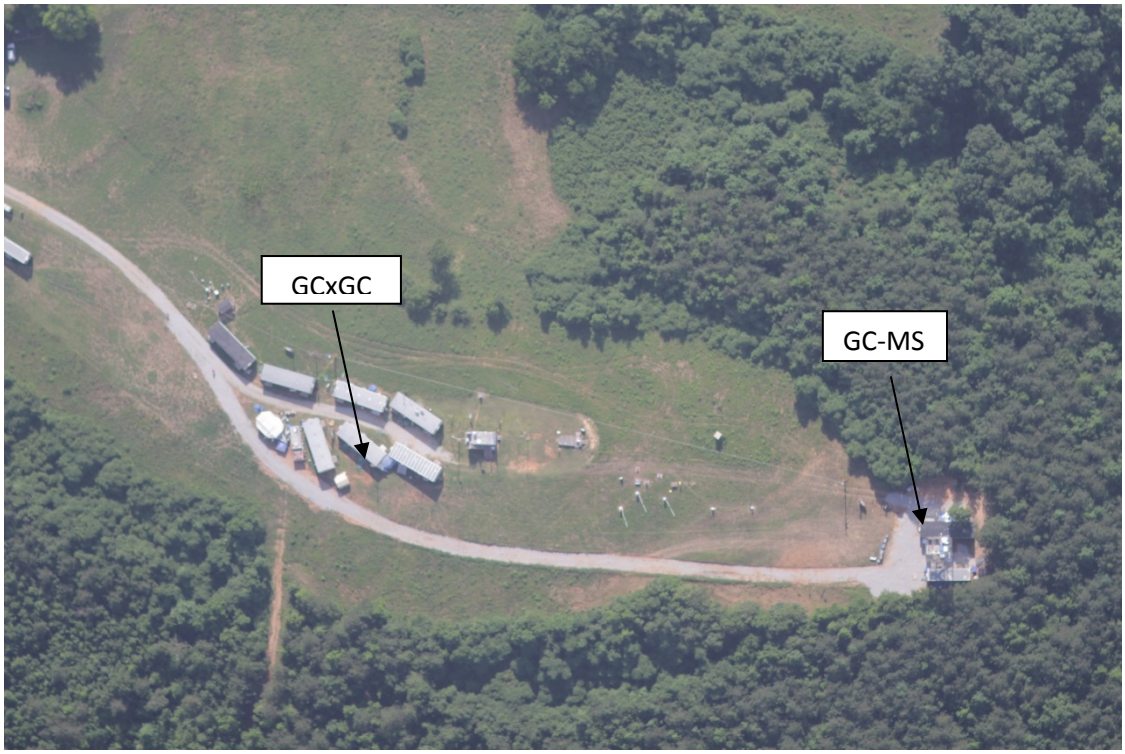

Figure 3.19 Sampling locations of GCxGC and GC-MS.

For a wind speed of 5 m/sec, the BVOCs were transported on the order of 100 meters (in about 20 seconds), much larger than the distance between inlets.

To compare the two data sets, the concentrations of the monoterpenes measured by the GCxGC were compared with the concentrations of the monoterpenes measured by the GC-MS for overlapping samples. The GC-MS operated at 30 minute intervals, at

every hour and half hour mark (i.e. 0100, 0130, 0200, 0230, etc…) while the GCxGC system sampled every hour (0100, 0200, 0300, etc…). This means that when operational, there is a GC-MS data set for every GCxGC data set. The results are seen in Figure 3.20.

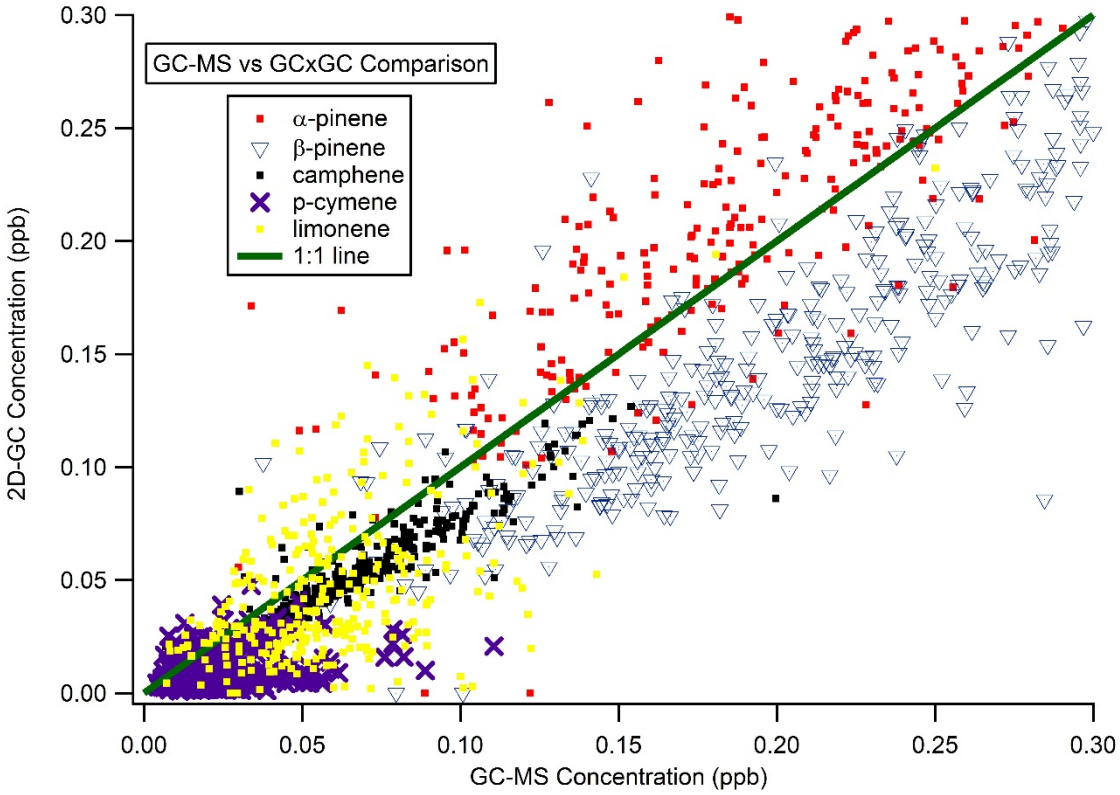

Figure 3.20 Comparison of GC-MS to GCxGC data during SOAS 2013.

There are slight differences between the two measurement methods. The GCxGC tends to detect α-pinene at higher concentrations while β-pinene and camphene tend to be measured at lower concentrations. The limonene and p-cymene data are very scattered and appear to have poor correlation. To determine if there is a linear relationship between the GC-MS data and the GCxGC data, the correlation coefficient was calculated according to Equation 3.18.

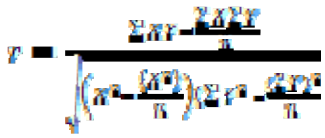

Equation 3.18

In equation 3.18, r is the correlation coefficient, X is a concentration value measured at time t by the GCxGC system, Y is a concentration value measured at time t by the GC-MS, and n is the number of data points compared. The correlation coefficient was calculated to be 0.946 for α-pinene, 0.945 for β-pinene, 0.952 for camphene, 0.581 for limonene, and 0.327 for p-cymene. Using an ANOVA test, it was concluded that at $p<0.05$ for $n>100$, there is a significant relationship between the two data sets. Measurements of p-cymene are consistently at or near the detection limit for both instruments (LOD = ~0.1 ppt for the GC-MS) and may be the reason there is such a poor correlation between the data sets. A reason for the limonene difference may be due to the reactivity of limonene. Hu et al. (2013) found that around 80% of limonene emitted within the forest canopy at a forested site in North Carolina was consumed in ~100 s. Due to limonene's high reactivity towards the OH, O_3, and NO_3, there may be measurably different concentrations at the two measuring sites. The poor correlation between the limonene data sets may be due to the transfer efficiency not being constant throughout the campaign. No long term measurements were made to see if the transfer efficiency of limonene remained constant.

3.4 Conclusions and Future Work

Demonstrated above is a comprehensive flow-modulated GCxGC instrument developed to quantify BVOC concentrations of various carbon number ranges. Three sampling configurations were tested, each with their own advantages and disadvantages.

A large data set of monoterpenes and other unknown compounds was collected at the SOAS field campaign.

However, there is still instrumentation work to be done. One goal that was unachieved by this instrument was the quantification of organic nitrates, specifically the isoprene nitrates. ECD data from the SOAS field campaign was not interpretable. The blank measurements obtained had more analyte peaks then the ambient samples. There is no known reason for this problem currently. Adequate testing of sorbent materials was also not performed. Sorbent materials were chosen using previous literature suggestions on making measurements with the highest trapping efficiency with the lowest contamination potential. An optimal sorbent material would be able to adsorb C4-C20 species with no affinity for water. An added advantage would be the ability to measure the aerosol phase organic species through an online aerosol sampling system utilizing humidification and inertial impaction as described in Williams et al. (2006). Proper sorbent material, along with a better temperature profile, could lead to a possible method for the detection of organic nitrates in the atmosphere.

There is also a need to improve the range of species this instrument can separate and detect. The first and third configurations were successful at quantifying species that were C_{10} and above, but unable to trap high volatility compounds such as isoprene (C_5). While the cryofocuser was successful at trapping high volatility species, it made injection plugs entering the GCxGC system too small for precise quantification. A better trapping, purging, and desorption method is needed to accurately and precisely identify a very broad range of BVOCs in the atmosphere.

CHAPTER 4 THE IMPACT OF ORGANIC NITRATE PRODUCTION ON OZONE PRODUCTION IN A SOUTHEASTERN MIXED FOREST ENVIRONMENT

4.1 Introduction

BVOCs are emitted at a rate of 1150 Tg C yr globally and account for ~90% of total non-methane volatile organic compound emissions (Guenther et al., 1995). BVOC emissions are dominated by isoprene (C_5H_8), monoterpenes ($C_{10}H_{16}$), reactive volatile organic compounds ($C_xH_yO_z$), and non-reactive volatile organic compounds ($C_xH_yO_z$) have atmospheric lifetimes between minutes to days due to the reaction with OH radicals, NO_3 radicals, and O_3 (Atkinson, 2007; Guenther et al., 1995). Understanding the chemistry of BVOCs is essential in understanding the production of ozone (Ridley et al., 1992a), the formation of secondary organic aerosol (Hallquist et al., 2009), and the nitrogen cycle (Costa et al., 2011; Galloway et al., 2008). Details of BVOC chemistry can be found in Chapter 1.

Equation 4.1-4.3 shows the NO_x cycle and equations 4.4 through 4.9 show a simplified oxidation pathway of BVOCs, where R represents BVOCs and R'O is generally an aldehyde or ketone.

$$NO + O_3 \longrightarrow NO_2 + O_2 \quad (4.1)$$

$$NO_2 + h\nu \longrightarrow NO + O(^3P) \quad (4.2)$$

$$O_2 + O(^3P) \longrightarrow O_3 \quad (4.3)$$

$$R + OH \xrightarrow[O_2]{} ROO \quad (4.4)$$

$$ROO + NO \longrightarrow RO + NO_2 \quad (4.5)$$

$$ROO + NO \longrightarrow RONO_2 \quad (4.6)$$

$$RO + O_2 \longrightarrow R'O + HO_2 \quad (4.7)$$

$$HO_2 + NO \longrightarrow NO_2 + OH \quad (4.8)$$

$$OH + NO_2 \longrightarrow HNO_3 \quad (4.9)$$

Reactions 4.1 through 4.3 show that NO and NO_2 interconvert through photolysis and reaction with O_3 to form a null catalytic cycle (Thornton et al., 2002). From reaction 4.6 and 4.8, NO is able to be converted into NO_2 without the destruction of O_3 as is the case for reaction 4.1. While concentrations of RO_2 and HO_2 are typically ~1000 times lower than O_3, the rate constants for reaction 4.6 and 4.8 are typically ~1000 faster than reaction 4.1, providing a mechanism for the production of O_3. Usually, the carbonyl compound formed in 4.7 continues to be oxidized, yielding more than two O_3 molecules per BVOC emitted (Thornton et al., 2002). This production rate is dependent on the assumptions that steady state has been reacted, or that the chemistry described in reactions 4.1-4.9 is complete and there are no new sources or sinks of NO_x into the system (Thornton et al., 2002). Greater detail of the chemistry can be found in Chapter 1.

It can be seen that the production of organic nitrates, defined in this chapter as $RONO_2$ (reaction 4.6), acts as a chain termination step in these cycles and limits the production ozone by preventing peroxy radicals (RO_2) from converting NO into NO_2 without the loss of O_3 (Ridley et al., 1992a; Thornton et al., 2002), and removal of NO_x,

the ozone precursor. Understanding of the branching ratio or the percent of time equation 4.6 occurs over the both RO_2 + NO reactions (4.5 and 4.6) shown as γ in Equation 4.1, is one of the most important parameters in understanding organic nitrate formation.

$$\gamma = \frac{k_{4.6}}{k_{4.5} + k_{4.6}} \qquad \text{Equation 4.1}$$

Yet, measurements of the branching ratio for isoprene vary from 7% (Lockwood et al., 2010) to 14% (Lee et al., 2014b).

Understanding the formation of organic nitrates is critical to understanding tropospheric chemistry. Measurements of total $RONO_2$ have shown that $RONO_2$ is a large portion of NOy (NOy=NO+NO_2+NO_3+HNO_3+all other oxidized nitrogen species) in rural environments (Browne and Cohen, 2012; Murphy et al., 2006). Work by O'Brien et al. (1995) first showed that BVOCs should dominate organic nitrate production. Work by Browne et al. (2013) has shown that the instantaneous production of organic nitrates exceeds the production of HNO_3 over a boreal forest in rural Canada and organic nitrates were on average 22% of total NO_y. However, the reactions and production of organic nitrates remain poorly understood and their effect on the composition of the atmosphere is poorly studied (Mao et al., 2013; Sommariva et al., 2011; Thornberry et al., 2001).

Due to isoprene being the dominant BVOC emission, there has been much research in the area of effect of isoprene nitrates and their effect on local and regional tropospheric chemistry (Ito et al., 2007; Lockwood et al., 2010; Mao et al., 2013; O'Brien et al., 1995; Paulot et al., 2012; von Kuhlmann et al., 2004; Weaver et al., 2009; Wu et al., 2007; Xie et al., 2013). By adjusting the production yield of isoprene nitrates from 4% to 12%, Wu et al. 2007 modeled a 10% decrease in worldwide O_3 concentrations.

There are large uncertainties in isoprene + NO_3 chemistry, as studies have shown that NO_3 oxidation only accounts for 6-7% of isoprene oxidation (Horowitz et al., 2007), but the reaction contributes 30-60% to the formation of isoprene nitrates (Paulot et al., 2012; Perring et al., 2009b; von Kuhlmann et al., 2004). This organic nitrate formation pathway is important as isoprene is a significant sink for NO_3, mainly at night (Brown et al., 2009; Starn et al., 1998).

While there has been considerable research into isoprene nitrates, there have been few studies on the production or impact of monoterpene nitrates and other nitrate species (Browne et al., 2014; Pratt et al., 2012). These organic nitrates could have a large impact on ozone production as Pratt et al. (2012) reported that monoterpene nitrates were simulated to comprise up to 83% of primary organic nitrate production at night and during the early morning (no radiation present). The specific reactions or pathways that lead to organic nitrate production have not been well characterized (Paulot et al., 2009). Understanding these reactions is also critical to understanding secondary organic aerosol production, as organic nitrates are believed to be SOA precursors (Hallquist et al., 2009; Ng et al., 2008). Ng et al. (2008) have shown that the NO_3 + isoprene reaction leads to the formation of dinitrates and aerosol-phase oligomers meaning this reaction removes NO_x from the troposphere. It is critical to understand the impact of individual organic nitrates so that future laboratory studies can focus on measuring and characterizing the most important species that form organic nitrates.

The southeastern United States has not observed the higher temperatures that the rest of the United States has observed in previous decades (Goldstein et al., 2009; Portmann et al., 2009). Goldstein et al. (2009) hypothesized that the large BVOC

emissions from this region react with anthropogenic pollution to form SOA, and result in an overall cooling effect. This emphasizes the need for further investigation of the emissions and chemistry occurring in the region to test this hypothesis. Pye et al. (2010) have shown that including NO_3 radical chemistry, monoterpene and sesquiterpene aerosol doubles and isoprene aerosol is enhanced by 30% to 40% in the Southeast United States. Ng et al. (2007) have shown that monoterpenes and sesquiterpenes exhibit larger yields under high-NO_x conditions as a result of either a higher probability of isomerization of RO_2 radicals (Ehn et al., 2014a) or it could be due to higher organic nitrate yields observed with larger BVOCs (Arey et al., 2001). The Southern Oxidant and Aerosol Study (SOAS) was conducted in Brent, Alabama in the summer of 2013 to identify the unique chemistry and species that are occurring in the southeastern United States.

Due to global climate change, increasing temperatures will cause increases in BVOC emissions (Guenther et al., 1993). Using the best known models, climate warming in the past 30 years has increased BVOC emissions by 10% globally (IPCC, 2007). A predicted 2-3° C increase in mean global temperature could increase BVOC emissions by an additional 30-45% (Penuelas and Llusia, 2003). While NO_x concentrations in the United States and Europe have steadily decreased in the past decade, emissions have increased in Asia. The emissions in Asia offset any reduction in other parts of the world, and overall emissions of NO_x are increasing and these emissions impact air quality (Lamsal et al., 2011). A better understanding of the chemistry occurring between NO_x and BVOCs is needed to understand future air quality. In this study, we have identified the important BVOCs that lead to organic nitrate formation, the pathways in which they

are formed, and the effect organic nitrate formation has on ozone production during the SOAS campaign.

4.2 Experimental

4.2.1 SOAS Site Description

The Southern Oxidant and Aerosol Study (SOAS) was an undertaking to lead to a greater understanding of the chemistry and physical processes occurring in the southern eastern United States atmosphere focusing on the following questions:

1. What are the magnitudes, variations, and controlling processes for biosphere-atmosphere fluxes of oxidants and reactive carbon and nitrogen across spatial scales relevant to air quality and climate?
2. What are the chemical and physical processes that control the oxidation of BVOC? How do anthropogenic emissions alter the distribution of the BVOC oxidation products, and what are the implications for the formation of O_3, reactive nitrogen, and aerosol precursors?
3. To what extent do anthropogenic influences impact biogenic SOA formation?
4. How does aqueous chemistry and cloud processing of BVOCs and related aerosols influence atmospheric SOA?
5. What are the climate-relevant properties of biogenic aerosol (VOC of biogenic origin)?

Figure 4.1 shows the location of the sampling site.

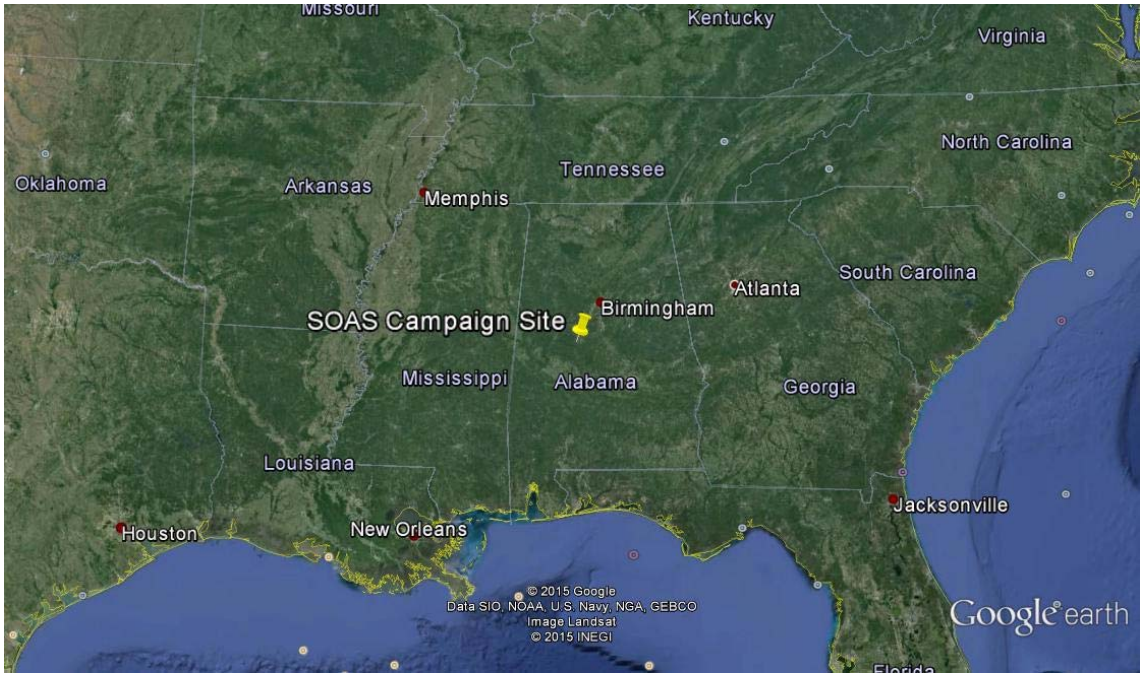

Figure 4.1 Location site of the SOAS campaign in relation to the southeastern United States.

The SOAS campaign occurred during the summer of 2013 outside the Oakmulgee division of the Talladega National Forest in central Alabama (32.94, -87.174722). Full details of the site can be found in Nguyen et al. (2015). A brief description of the site is given here. Measurements of BVOCs were performed on a tower located ~40 m from the surface, while measurements of O_3, NO_x, relative humidity, and radiation were conducted at approximately 10 m from the ground the Atmospheric Research and Analysis trailer located approximately 100 meters from the tower. PAN (peroxyacetic nitric anhydride), PPN (peroxypropionic nitric anhydride), MPAN (peroxymethacrylic nitric anhydride) and isoprene nitrates were measured at a trailer approximately 30 meters from the Atmospheric Research and Analysis trailer, and ~130 meters from the tower-based measurements. Vegetation at this site was dominated by pine and oak trees with a

mixture of sweetgum, hawthorn, dogwood, tulip and maple trees. Mean wind at this site generally came from the southeast.

4.2.2 Instrumentation

Measurements of NO_2, NO, O_3, OH, HO_2, CO, relative humidity, temperature, and a suite of BVOCs were continually measured at the site. Table 4.1 lists the species, detection methods, and uncertainties for each detection method for the SOAS campaign.

Table 4.1 List of species constrained in the model along with measurement technique and uncertainty. Abbreviations are as follows, laser induced fluorescence (LIF) and gas chromatography-mass spectrometry (GC-MS).

Constrained Species	Measurement Technique	Reference	Measurement Uncertainty (%)
OH	LIF	Mao et al. 2012	32
HO2	LIF	Mao et al. 2012	32
NO	Chemilumenescence	Ridley et al. 1990	5.5
NO2	Chemilumenescence	Ridley et al. 1990	15
CO	IR Spectroscopy		7.4
O3	UV Spectroscopy		6.1
isoprene	PTR-MS	De Gouw and Warneke 2007	30-50
MVK+MACR	PTR-MS	DeGouw and Warneke 2007	30-50
a-pinene	GC-MS	Goldan et al. 1995	20
b-pinene	GC-MS	Goldan et al. 1995	20
limonene	GC-MS	Goldan et al. 1995	20
myrcene	GC-MS	Goldan et al. 1995	20
camphene	GC-MS	Goldan et al. 1995	20
ethane	GC-MS	Goldan et al. 1995	20
ethene	GC-MS	Goldan et al. 1995	20
propane	GC-MS	Goldan et al. 1995	20

Table 4.1 continued.

Constrained Species	Measurement Technique	Reference	Measurement Uncertainty
propene	GC-MS	Goldan et al. 1995	20
ethyne	GC-MS	Goldan et al. 1995	20
iso-butane	GC-MS	Goldan et al. 1995	20
butane	GC-MS	Goldan et al. 1995	20
iso-pentane	GC-MS	Goldan et al. 1995	20
pentane	GC-MS	Goldan et al. 1995	20
acetalaldehyde	GC-MS	Goldan et al. 1995	20
methanol	GC-MS	Goldan et al. 1995	20
ethanol	GC-MS	Goldan et al. 1995	20
propanol	GC-MS	Goldan et al. 1995	20
dimethyl sulfide	GC-MS	Goldan et al. 1995	20
acetone	GC-MS	Goldan et al. 1995	20
hexane	GC-MS	Goldan et al. 1995	20
methacrolein	GC-MS	Goldan et al. 1995	20
butanal	GC-MS	Goldan et al. 1995	20
methyl vinyl ketone	GC-MS	Goldan et al. 1995	20
butadione	GC-MS	Goldan et al. 1995	20
methyl ethyl ketone	GC-MS	Goldan et al. 1995	20
toluene	GC-MS	Goldan et al. 1995	20
o-xylene	GC-MS	Goldan et al. 1995	20
decane	GC-MS	Goldan et al. 1995	20
temperature	Resistance Detector		0.1
relative humidity	Hygromer Passive Filament		0.80
boundary layer height	LIDAR		13

OH measurements were made using laser-induced fluorescence (Mao et al., 2012). Isoprene nitrates were measured using chemical ionization mass spectrometry utilizing iodide water clusters as the ionization agent (Lee et al., 2014a). The peroxy acyl nitrates, PAN, PPN, and MPAN were measured using a cooled GC-ECD (Bertman et al., 1993).

4.2.3 0-D Modeling

A 0-D box model was constructed using the Master Chemical Mechanism (MCM) v3.2 (Saunders et al., 2003). A 0-D box model is an atmospheric chemical kinetic model that only looks the chemical processes occurring in the modeled area, in this case, the SOAS ground site. That means it cannot account for the dilution of clean air from aloft due to thermal mixing or advection (Chapter 1.2). FACSIMILE Kinetic Modeling software was used to compile and solve the differential equations found in the MCM. The model was run to simulate June 14th, June 26th, and July 12th. Thirty-four species, which are listed in Table 4.1, were constrained to observed concentrations. Isoprene chemistry was updated using the changes found in Xie et al. (2013), Peeters et al. (2014), and Xiong et al. (2015). All peroxy acyl nitrate formation and degradation rate constants were changed to IUPAC values (Atkinson et al., 2006). Myrcene and camphene chemistry was updated according to Wolfe and Thornton (2011) and their organic nitrate yield from OH chemistry was set as 23% as used in Pratt et al. (2012). In the Wolfe and Thornton (2011) paper, all of the isomers of myrcene nitrates were treated as a single isomer. Photolysis rate values were calculated using the Tropospheric Ultraviolet and Visible Radiation Model v4.4 (Madronich, 1992). This model looks at primary organic nitrates (e.g. isoprene nitrates, α-pinene nitrates) and secondary organic nitrates (e.g. Methacrolein nitrate, pinonaldehyde nitrate) formation for simplicity. Deposition velocities for organic nitrates were set as 2.7 cm s^{-1} as calculated in Zhang et al. (2012) and Farmer and Cohen (2008). All organic nitrates were subject to the same deposition velocity for simplicity and a lack of known speciated deposition velocities. The deposition velocity of all peroxy acyl nitrates was set as 0.5 cm s^{-1} as measured by (Shepson et al., 1992). Deposition

velocities were divided by the boundary layer height to give a depositional loss rate. The depositional loss rate is used to simulate the irreversible loss of the nitrates to absorption or adsorption on ground level surfaces. In other 0-D models, a dilution loss rate from thermal mixing is generally added as an additional loss factor (Jacob et al., 1992). In this model, no dilution loss was added, and the reason will be discussed within.

Initial values of the isoprene nitrates were set as 15 ppt, the diurnal average of isoprene nitrates at midnight during the SOAS campaign. The initial value of PAN was set as 110 ppt for each day, which was the average of PAN at midnight during the SOAS campaign. Initial values cannot be given to any summed values (RO_2, summed isoprene nitrates, total O_3 production) through the FACSIMILE software, and therefore, it is recommended that at least the first data point at midnight for each day run be ignored.

To observe the production rates of organic nitrates, counters were added to the model. Counters are unique variables added to the end of reactions in the MCM, so that when the FACSIMILE software converged on a solution, each time a reaction with a counter occurred, the counter would increase. Counters were added for each type of reaction studied as shown in Figure 4.2.

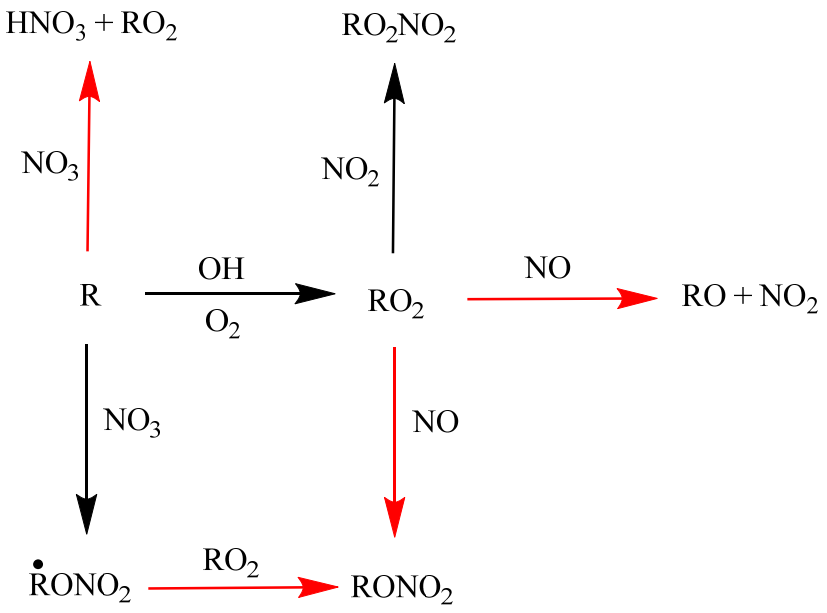

Figure 4.2 Graphical representation of all counters used to identify organic nitrate production. The red arrows represent reactions with counters.

Counters were added to all RO_2 + NO reactions that yielded NO_2, including HO_2 + NO. Counters were added to all RO_2 + NO reactions that yielded an organic nitrate ($RONO_2$). Counters were added to all ($RONO_2$) species formed from NO_3 + BVOC chemistry that reacted with RO_2 (including HO_2) to form a stable organic nitrate.

Three days (June 14th, June 26th, and July 12th, 2013) where chosen to model due to large organic nitrate formation, relatively stable boundary layer (±200 m after full growth past 1200 each day), and a comprehensive data set for those days. To visualize the source and intensity of the prevailing winds for each day measured, wind rose plots for the three days studied are shown in Figure 4.3.

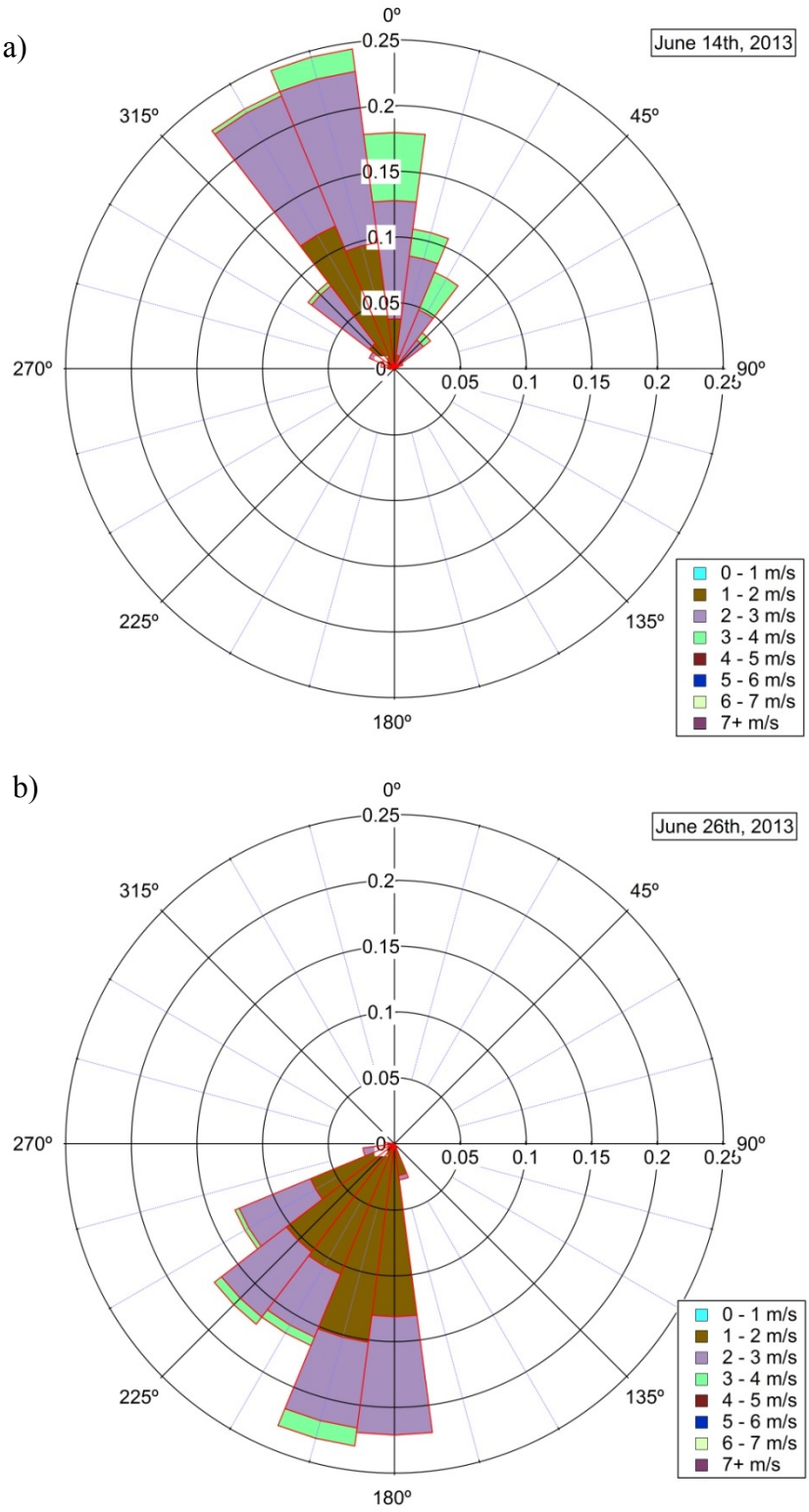

Figure 4.3 Wind rose plots showing wind speed, direction, and frequency of direction for the days of June 14th (a), June 26th (b), and July 12th (c), 2013.

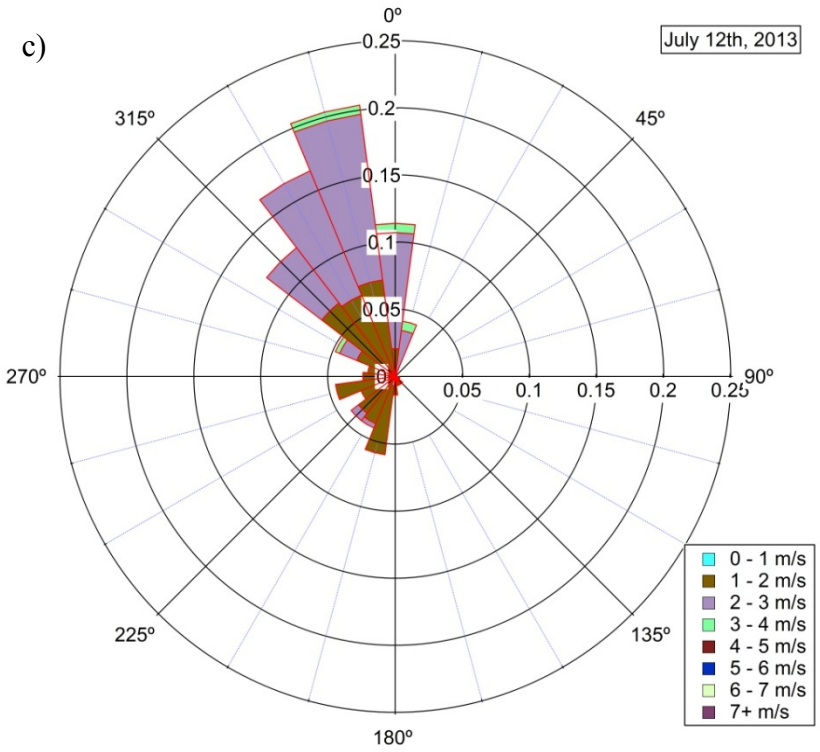

Figure 4.3 continued

In the wind rose plots, the frequency of different wind speeds is plotted as a function of the direction from which they originated. Figure 4.3 shows that the prevailing winds are from the north northwest on June 14th and July 12th and from the southwest on June 26th. The Hybrid Single-Particle Lagrangian Integrated Trajectory (HYSPLIT) model was used to calculate the back trajectories of the air masses arriving at the site. The HYSPLIT model is a model that uses meteorological data to calculate the advection, or trajectory, of air parcels (Draxler and Rolph, 2014b). Twelve hour back trajectories show that the air mass that arrived at the site on June 26th traversed over the Gulf of Mexico and the greater New Orleans area. The 12 hour HYSPLIT back trajectories show that the air

masses that arrived at the site on June 14th and July 12th were influenced by forests in central Tennessee and northern Alabama.

Boundary layer height for the days studied were measured by LIght Detection And Ranging (LIDAR) (Wang et al., 2012) and followed a general pattern. For all days, the boundary layer grew after sunrise and reached a near maximum near 1500 and varied by ~200 m during the afternoon until around 1800. Boundary layer heights for the three days can be seen in Figure 4.4.

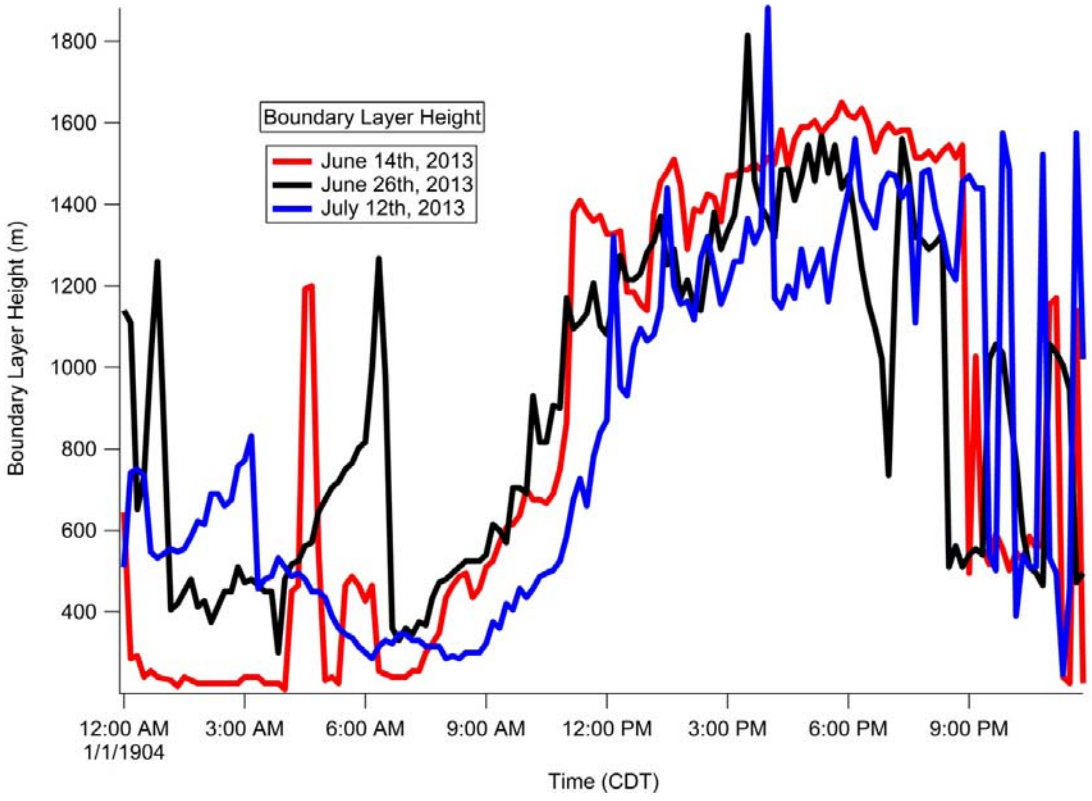

Figure 4.4 Boundary layer height development and growth during June 14th, June 26th, and July 12th, 2013.

4.3 Results and Discussion

4.3.1 Measurements of BVOCs, NO_x, NO_3, OH, and O_3

To begin to assess the chemical conditions that lead to organic nitrate formation, the main components of BVOC chemistry (the BVOCs and oxidants) are plotted in Figure 4.5. BVOC data was observed by a GC-MS run by Kevin Olson and Abigail Koss as part of a collaboration between Allen Goldstein's group at the University of California-Berkeley and Joost de Gouw's group at the National Oceanic and Atmospheric Administration. NO and NO_x data are courtesy of the Karsten Baumann at Atmospheric Research and Analysis, Inc. Due to the very low concentrations of NO_3 at the site, no observed data is available and all NO_3 data here is modeled.

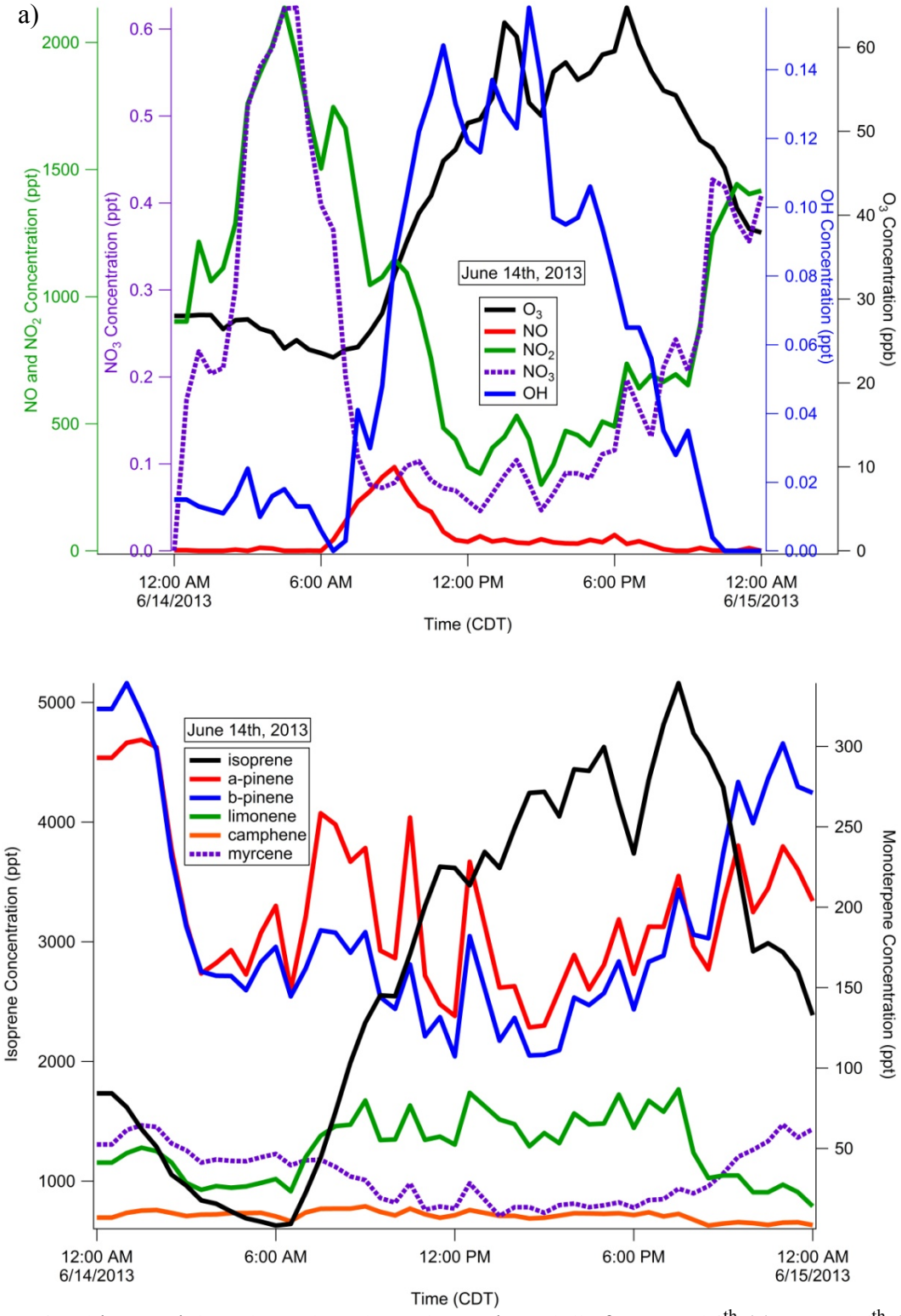

Figure 4.5 Observed OH, O_3, NO, NO_2, NO_3, and BVOCs for June 14th (a), June 26th (b), and July 12th (c) during the SOAS campaign.

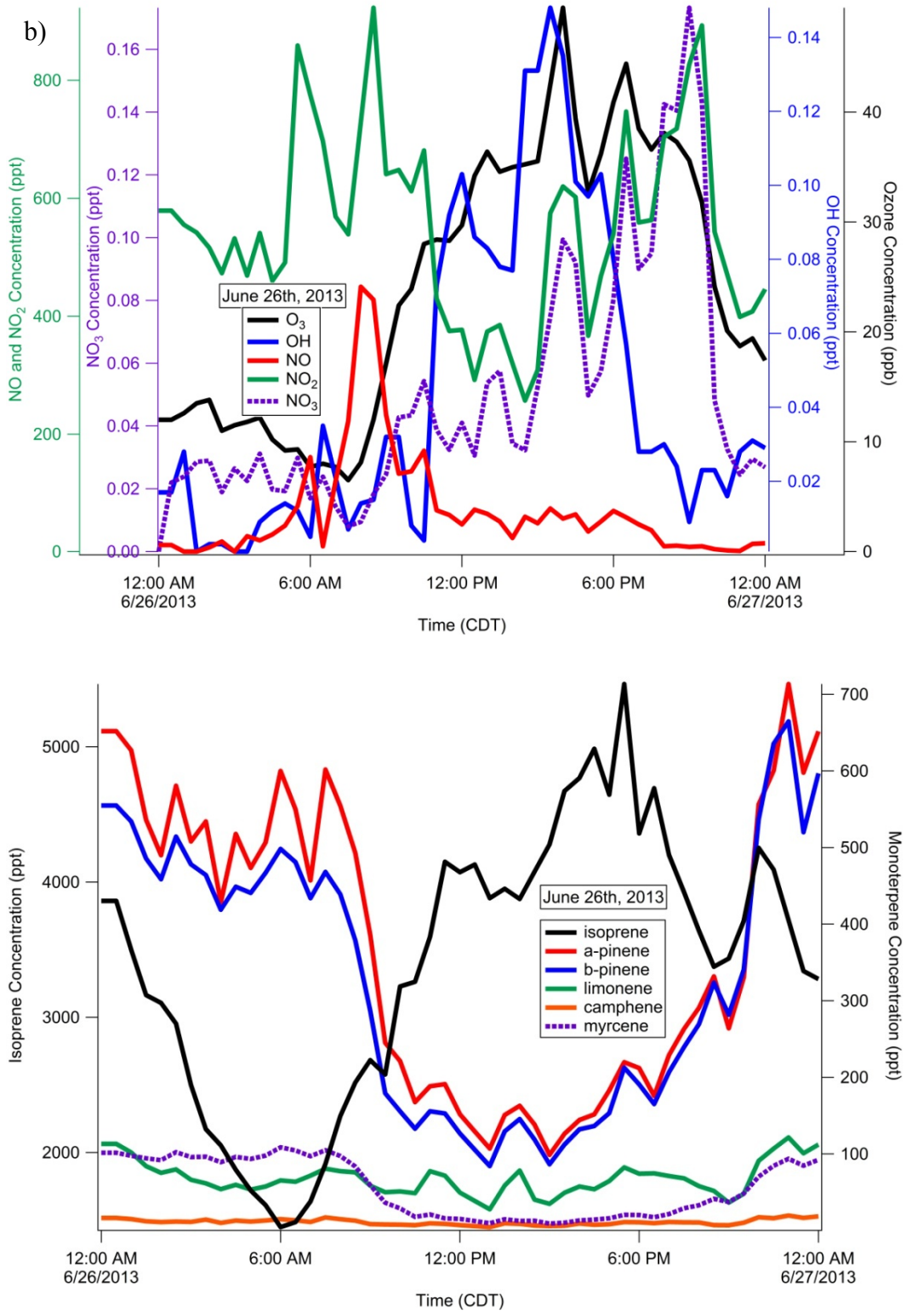

Figure 4.5 continued.

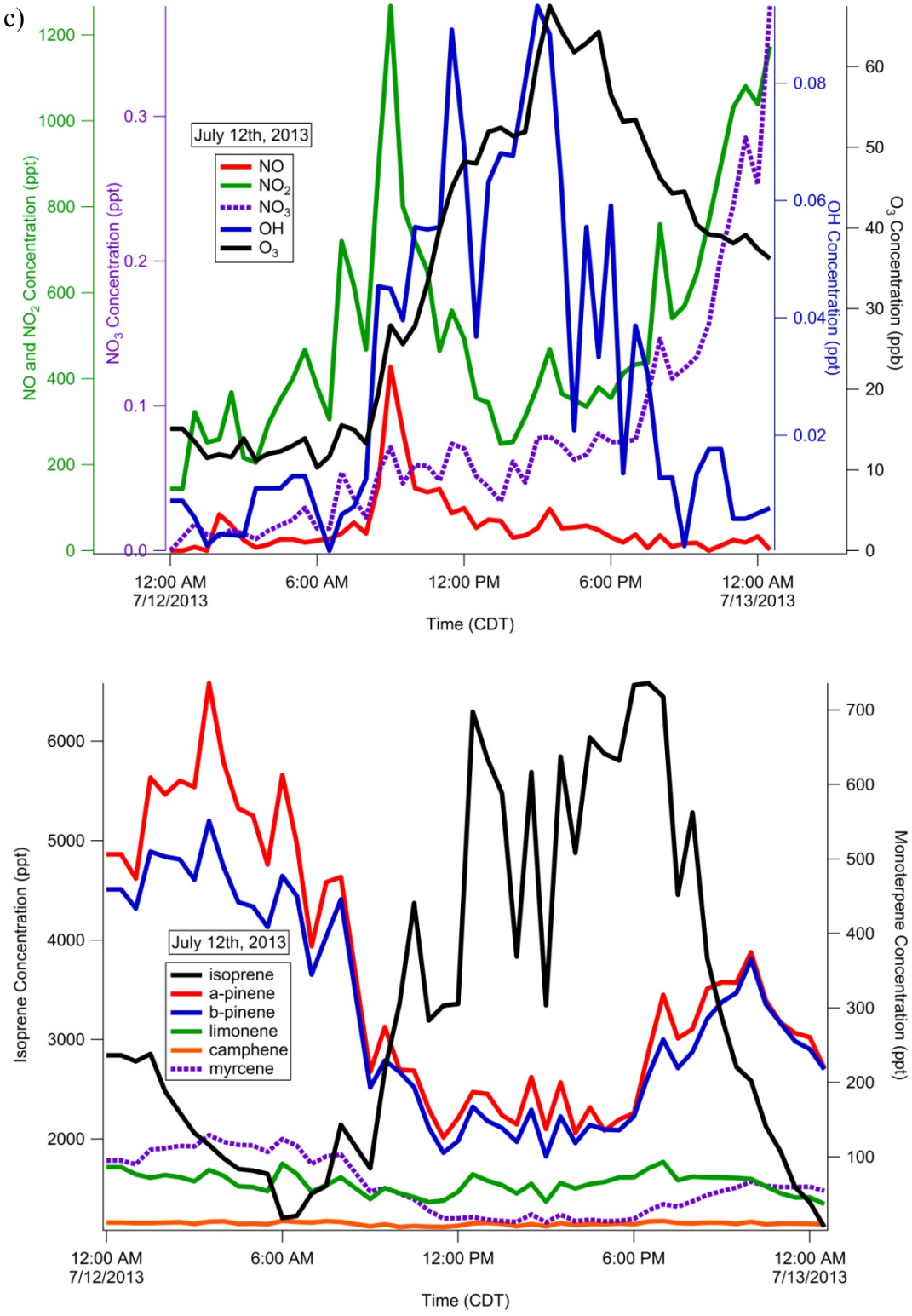

Figure 4.5 continued.

The monoterpenes, a-pinene, b-pinene, limonene, mycrene, and camphene, had maximum concentrations during the early morning and quickly decreased shortly after sunrise for all three days. Even though monoterpene emissions are temperature dependent (Guenther et al., 1993), dilution due to boundary layer growth and photochemical losses exceeded any additional emissions during the daytime. Isoprene had its lowest concentrations during the night since isoprene emissions are not only temperature dependent, but light dependent (Guenther et al., 1993). Isoprene emissions quickly rose after sunrise, peaking in the late afternoon for all three days. OH radical and O_3 concentrations were lowest during the early morning hours, and grew throughout the day, peaking in the afternoon.

As shown in Figure 4.5, NO_3 concentrations were the highest on June 14th with the highest concentrations in the early morning hours before sunrise and after sunset. NO_3 concentrations on June 26th and July 12th were low, and grew throughout the day. The primary means to form NO_3 is from the reaction of NO_2 and O_3 as shown in reaction 4.10.

$$NO_2 + O_3 \longrightarrow NO_3 + O_2 \qquad (4.10)$$

The pattern of NO_3 for June 14th is to be expected as there was a large concentration of NO_2 present in the early morning hours, and the concentrations of O_3 and NO_2 followed that pattern of NO_3. The pattern of NO_3 following NO_2 also follows for June 26th and July 12th at night, as a late evening rise in NO_2 correlated with an increase in NO_3. The gradual increase in NO_3 during the day is currently unexplainable. Concentrations of NO_3 were below the 1 ppt detection limit of a cavity-ring down spectrometer that attempted to

quantify NO_3 at the site, and therefore, we have no observational data to compare modeled NO_3.

4.3.2 Model Evaluation

To evaluate the accuracy of the model, the model was run to simulate June 14th, June 26th, and July 12th 2013 and the concentrations of observed and modeled isoprene nitrates and PAN are shown in Figure 4.6. Figure 4.6 shows that the model generally over predicts isoprene nitrates, but is in agreement with PAN concentrations.

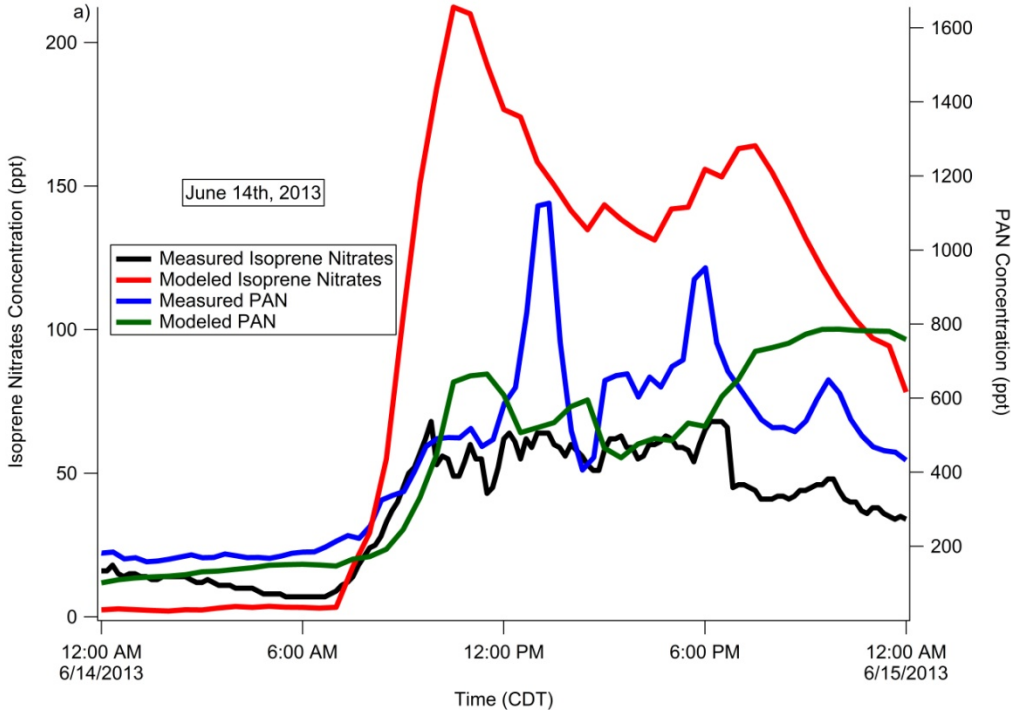

Figure 4.6 Comparison of modeled vs. measured isoprene nitrates and PAN for June 14th (a), June 26th (b), and July 12th, 2013 (c). There is no available measured isoprene nitrate data for July 12th.

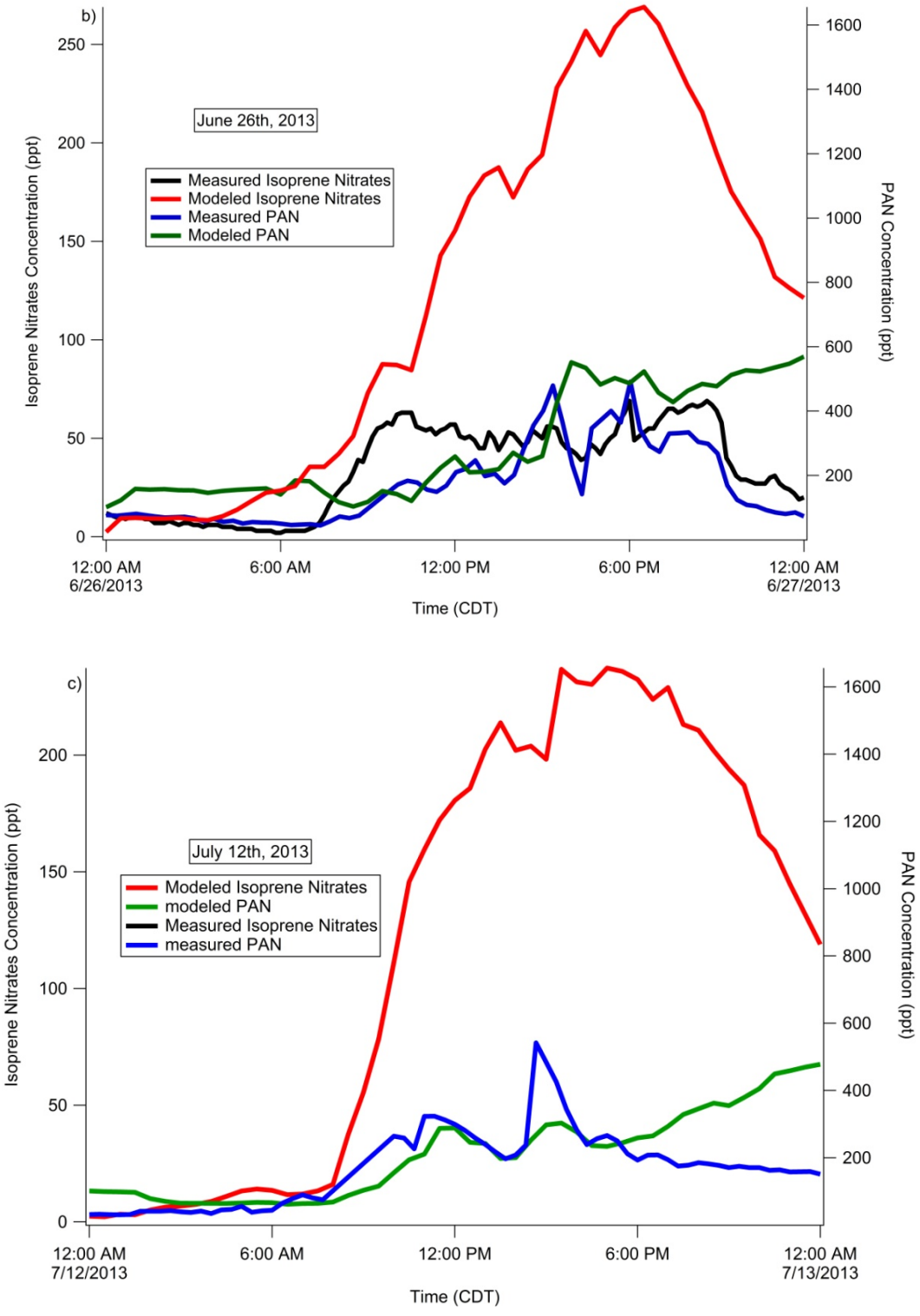

Figure 4.6 continued.

Since the 0-D model cannot account for dilution from thermal mixing, a better means of evaluating the accuracy of the model is by plotting the ratio of the concentrations methyl vinyl ketone (MVK) plus methacrolein (MACR) over the concentration of isoprene nitrates. By plotting the ratio of the two first generation isoprene oxidation products, the dilution factor affecting the ground level concentration of the two species should cancel out. The GC-MS at the site measured MVK and MACR separately, but recent work by Rivera-Rios et al. (2014) has shown that GC-MS systems convert isoprene hydroperoxides (ISOPOOH) into MVK and MACR. This is a problem, as a $CF3O^-$ chemical ionization mass spectrometer run by Tran Nguyen and Alex Teng of Paul Wennberg's group at the California Institute of Technology have reported that ISOPOOH concentrations at the SOAS site are between 20-300 ppt. MVK concentrations measured by the GC-MS averaged 614 ppt while MACR concentrations averaged 396 ppt. This means that a significant unknown fraction of the MVK and MACR measured at the site could be due to ISOPOOH. A better alternative is to use the summed concentrations of MVK and MACR measured by a PTR-MS run by Pawel Misztal (UC Berkeley) (de Gouw and Warneke, 2007). MVK and MACR are summed together because they are structural isomers and indistinguishable in the PTR-MS used at the site. Rivera-Rios et al. (2014) also showed that a fraction of ISOPOOHs are converted to MVK or MACR during the ionization process in PTR-MS instruments. However, sampling tests done by Pawel Misztal have shown the ISOPOOHs are unable to survive the sampling inlet and that upon injecting ISOPOOH standards at the inlet, no increase in concentrations of MVK and MACR were seen with the PTR-MS. This sampling test was

not performed on the GC-MS inlet, and therefore the PTR-MS data will be used for this evaluation.

Figure 4.7 shows the ratio of measured isoprene nitrates over the measured sum of MVK and MACR versus the ratio of modeled isoprene nitrates over the modeled sum of MVK and MACR.

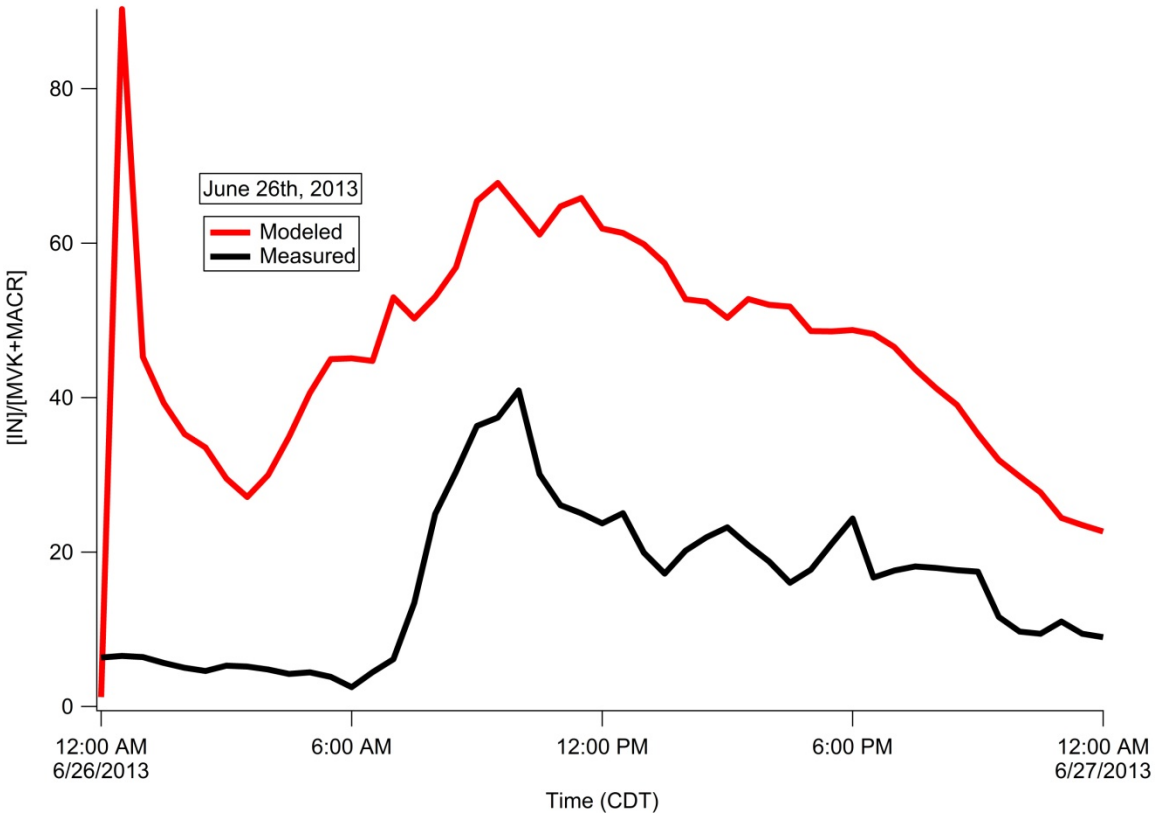

Figure 4.7 Ratio of the concentration of isoprene nitrates over MVK+MACR for the modeled and measured concentrations on June 26th, 2013.

The modeled ratio was four times larger than the measured ratio. It is currently unknown why there is such a large difference in the two ratios. However, Xiong et al. (2015), which uses a variation of this model (only constrains the BVOCs and not the small VOCs

such as propene, acetone, methyl ethyl ketone, etc…) has shown that there are many days in which the modeled and measured ratios are similar. There are no MVK+MACR observed data for June 14th and there are no observed isoprene nitrate data for July 12th.

4.3.3 Species contributing most to O_3 Production

From reactions 4.4 through 4.9 (shown in intro), the oxidation of BVOCs by OH leads to production of peroxy radicals (reaction 4.4) and HO_2 (reaction 4.7), that can then oxidize NO into NO_2 (reactions 4.5 and 4.8, respectively). The photolysis of NO_2 (reaction 4.2) then leads to the production of O_3. Overall, the production of O_3 can be defined by equation 4.1 (Thornton et al., 2002).

$$P_{O3} = k_{NO+HO2}[NO][HO_2] + k_{NO+RO2}[NO][RO_2] \qquad \text{Equation 4.2}$$

The production of O_3 as defined by equation 4.2 along with the speciated production of NO_2 from HO_2 + NO and VOC specific RO_2 + NO reactions was plotted for the three modeled days in Figure 4.8.

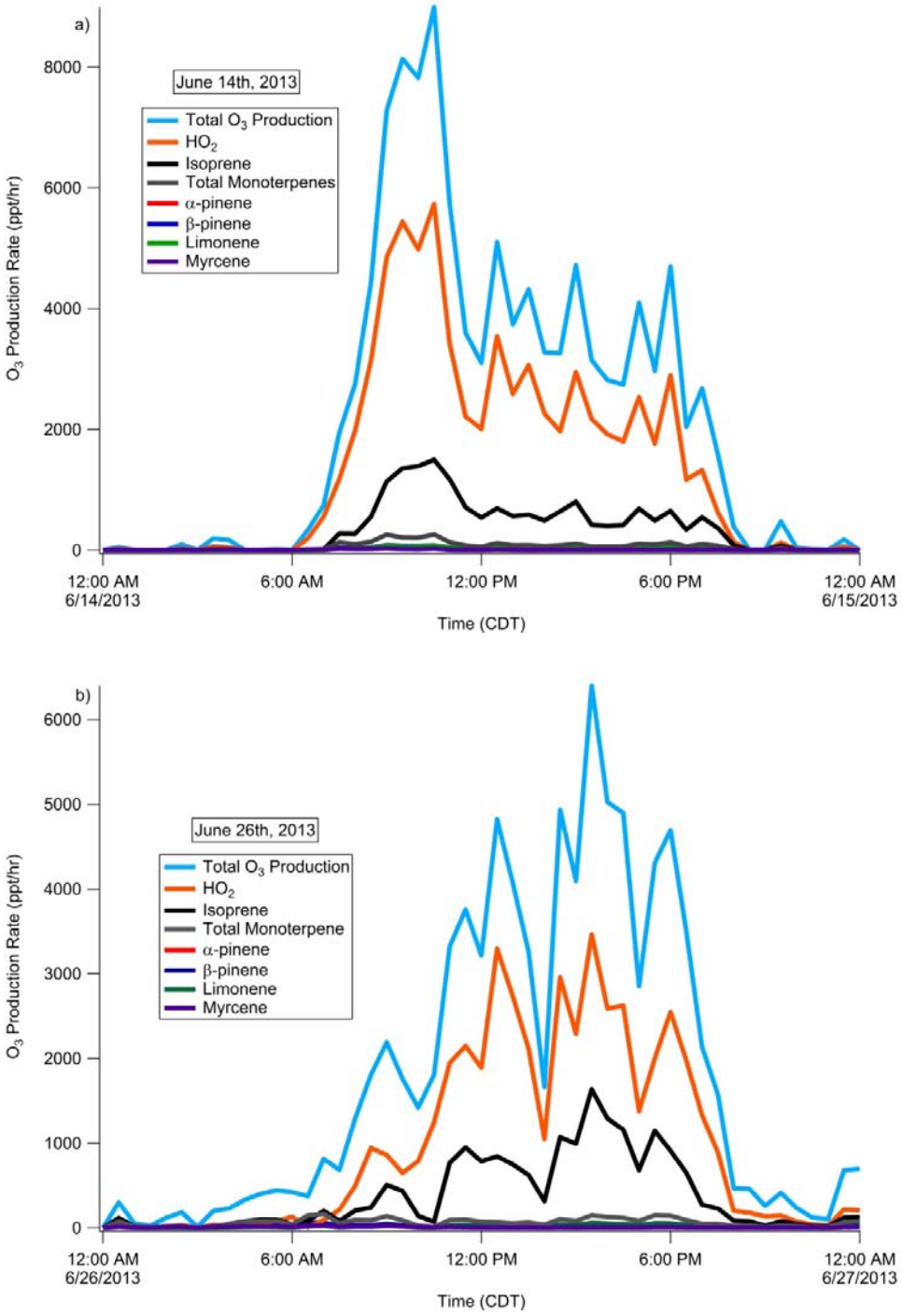

Figure 4.8 Total O_3 production plotted for the three modeled days, June 14th (a), June 26th (b), and July 12th (c), 2013. The individual BVOC derived RO_2s plotted represent the summed peroxy radicals + NO ➔ NO_2 reactions of the parent BVOC indicated.

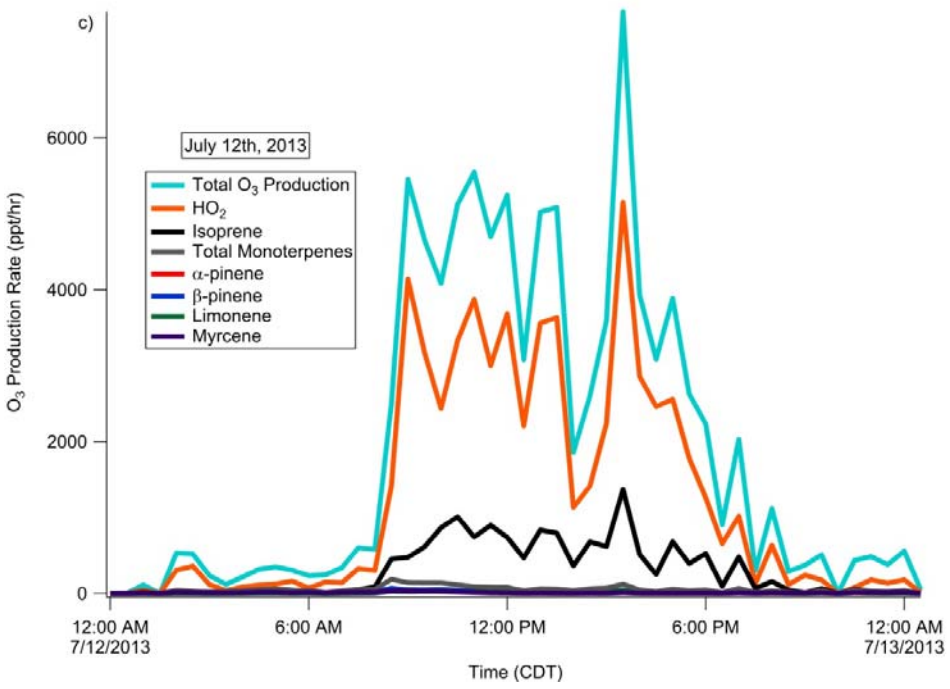

Figure 4.8 Continued.

In the figure, the total production of O_3 is the sum of reactions 4.5 and 4.8 as defined in equation 4.2. Figure 4.8 shows that reaction 4.8 (HO_2 + NO) is the dominant pathway leading to the production of O_3 for all three days. Reaction 4.8 comprised 49%, 39%, and 53% of the total O_3 production for June 14th, 26th, and July 12th, respectively. To identify the dominant BVOC leading to the production of O_3, individual RO_2 + NO ➔ NO_2 reactions were summed for each BVOC (the rate of O_3 production from α-pinene photooxidation shown in Figure 4.8 is the sum of the three peroxy radical isomers reacting with NO to form NO_2). The peroxy radicals formed from the photooxidation of isoprene dominated the production of peroxy radicals at this site for the three days being studied. The formation of NO_2 from the reaction of NO with the peroxy radicals created during isoprene OH oxidation comprised on average 30%, 34%, and 33% of the total O_3

production from all RO_2 + NO reactions for June 14th, 26th, and July 12th, respectively. During the time with large O_3 production (0800-1800), the isoprene derived RO_2 + NO reactions account for 59%, 52%, and 51% of the total RO_2 + NO reactions that produce O_3. The oxidation of monoterpenes contributed to 10%, 13%, and 12% of the total O_3 production. Each day, ~50% of the total O_3 production was due to the oxidation of second and further generation products (e.g. MVK and MACR) and other smaller volatile organic compounds such as ethyne.

4.3.4 NO_x Limited vs NO_x Saturated Production of O_3

From reactions 4.1 through 4.9, the rate-determining step among the propagation reactions is usually the reaction between NO and HO_2 (reaction 4.6) or RO_2 (reaction 4.8) (Thornton et al., 2002). When NO_x concentrations are low and peroxy radical concentrations (HO_2 + RO_2) are high, the primary chain terminating step of the HO_x catalytic cycle are the HO_x + HO_x reactions shown in reactions 4.10 through 4.12 (Sillman et al., 1990).

$$OH + HO_2 \longrightarrow H_2O + O_2 \quad (4.10)$$

$$HO_2 + HO_2 \longrightarrow H_2O_2 + O_2 \quad (4.11)$$

$$HO_2 + RO_2 \longrightarrow ROOH + O_2 \quad (4.12)$$

O_3 production in low NO_x conditions is called NO_x-limited and the O_3 production rate increases approximately linearly with increases in the concentration of NO_x. When NO_x concentrations are high, radical termination can occur from the reaction of OH with NO_2 (reaction 4.9) and through production of organic nitrates (reaction 4.6). At 150 ppt (Xie et al. 2013) of NO, reactions 4.6 and 4.9 become faster than the HOx-HOx reactions (4.11

and 4.12) and the O_3 production begins to slow. This region is called either NO_x-saturated or BVOC limited (Thornton et al. 2002). Thus in this condition, increasing VOC concentrations does not increase the rate of O_3 production. This is critical to understanding the future of global ground level background O_3 concentrations. Increases in global temperature will cause increases in BVOC emissions by ~30-45% (Penuelas and Llusia, 2003) and overall global anthropogenic NO_x emissions are increasing, mainly due to economic growth in Asia (Lamsal et al., 2011). Knowing which geographical regions are NO_x limited and NO_x saturated will help better predict future regional climate change.

The southeastern United States represents a unique photochemical environment as BVOC emissions in the region rival those of tropical forests (Geron et al., 1994; Guenther et al., 2000). Tropical forests such as those in the Amazon have been determined to be NO_x limited regimes, and future warming will not dramatically increase O_3 production due to the very limited NO_x concentrations present in remote rainforests (Bela et al., 2015). The southeastern United States is rare in that there are significant anthropogenic sources of NO_x that react with the BVOC derived RO_2 radicals (Goldstein et al., 2009). To determine if the SOAS site was NO_x limited or NO_x saturated, the production rate of O_3 as defined by Equation 4.2 was plotted against the concentration of NO, as shown in Figure 4.9.

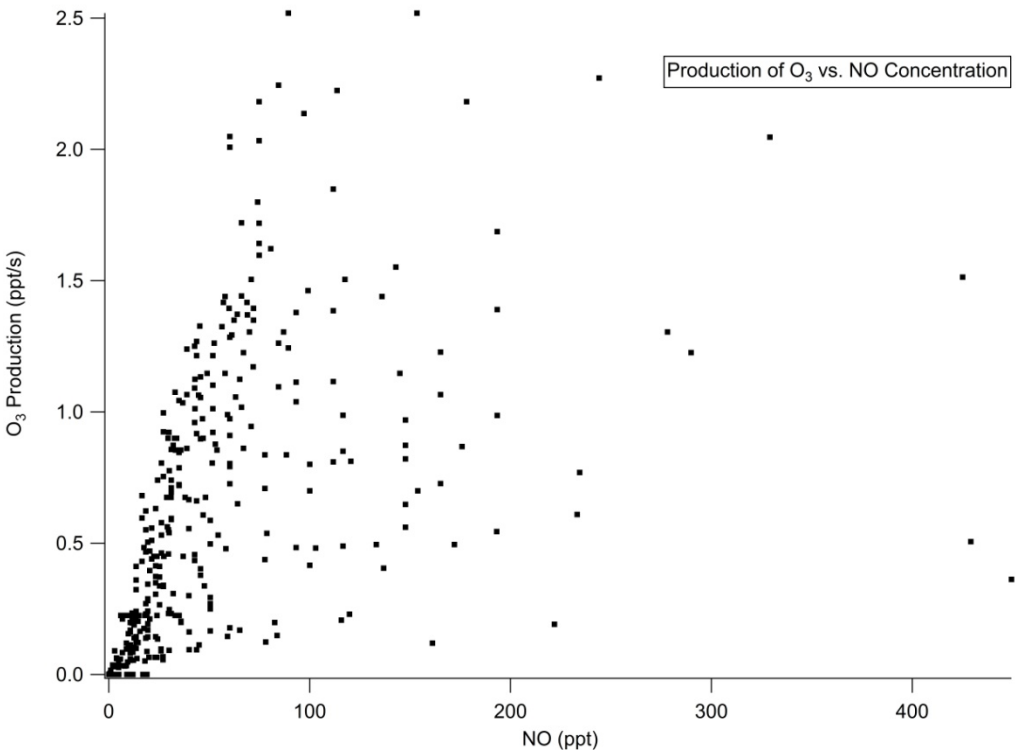

Figure 4.9 Production of O_3 (ppt/s) plotted against concentration of NO (ppt).

It is difficult to determine the region in which NO concentrations transfer from NO_x-limited to NO_x-saturated due to a limited number of NO observations above 200 ppt. The average concentration of NO during the campaign was 100 ppt and the standard deviation was also 100 ppt. This means there is limited spread of the data and that 95% of the time during the campaign, the concentration of NO was below 300 ppt. Figure 4.9 shows that most NO concentrations were between 0-200 ppt. Xie et al. (2013) found that in the southeastern United States, the NO_x limited to NO_x saturated regime was ~150 ppt. The data presented in Figure 4.9 are mostly indicative of a NO_x limited regime.

4.3.5 Speciated Organic Nitrates vs Total Organic Nitrates

To determine the extent to which organic nitrate production effects O_3 production, the 0-D chemical model was used to determine the instantaneous $RONO_2$ production rate for all BVOCs shown in Table 4.1. While much of the research on organic nitrates has focused on isoprene nitrates, there has been very little research into the impact of other organic nitrates, including monoterpene nitrates and nitrates formed from the oxidation of second generation oxidation products of isoprene (Browne et al., 2014; Paulot et al., 2009; Pratt et al., 2012). To simplify the output for organic nitrate production, the isomeric nitrates produced from each BVOC were summed. The individual isomers and which category, along with common descriptions, either in literature or the MCM model, are shown in Figure 4.10.

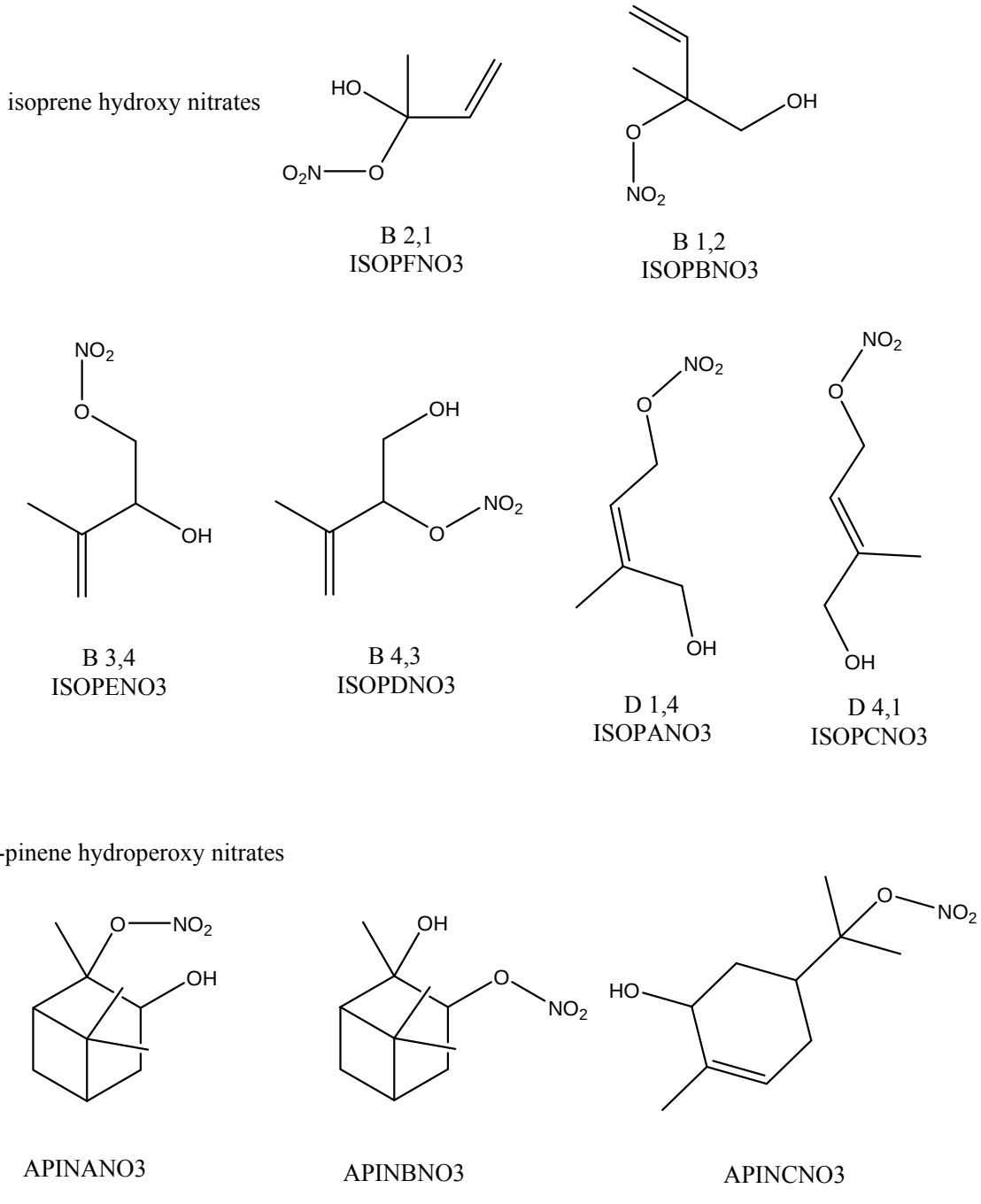

Figure 4.10 Skeletal structure of organic nitrates and the category into which they were summed.

b-pinene hydroxy nitrates

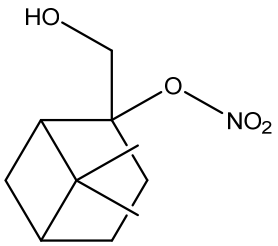

BPINANO3

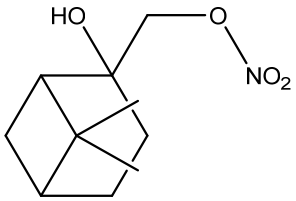

BPINBNO3

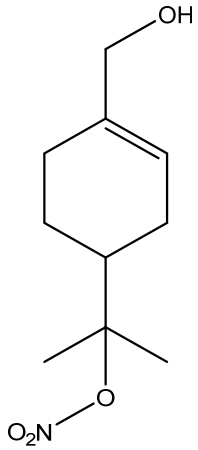

BPINCNO3

limonene hydroxy nitrates

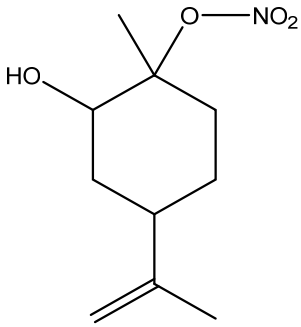

LIMANO3

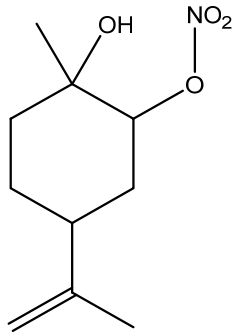

LIMBNO3

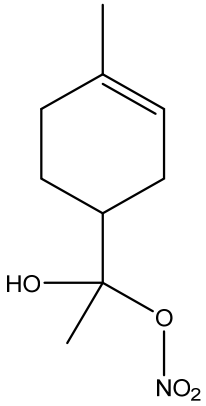

LIMCNO3

camphene nitrate

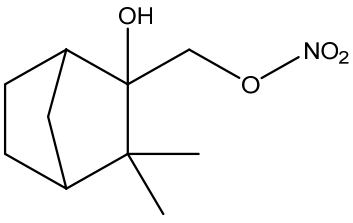

MTO2NO3

myrcene nitrate

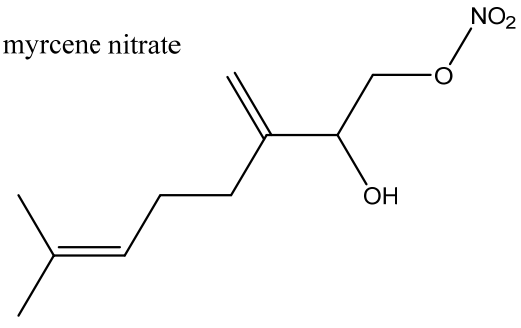

MTO1NO3

Figure 4.10 continued.

Isoprene hydroperoxide nitrates

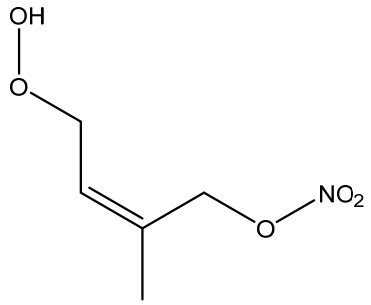

NISOPOOH

Isoprene carbonyl nitrates

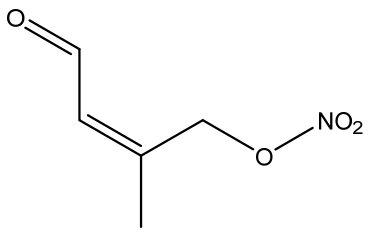

NC4CHO

Monoterpene hydroperoxide nitrates

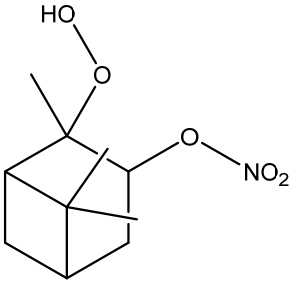

NAPINAOOH

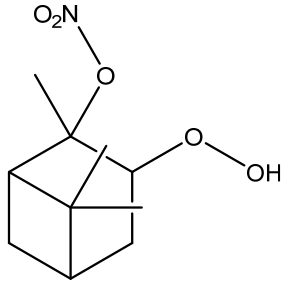

NAPINBOOH

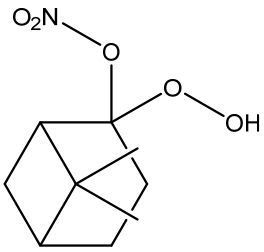

NBPINAOOH

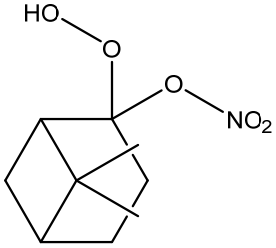

NBPINBOOH

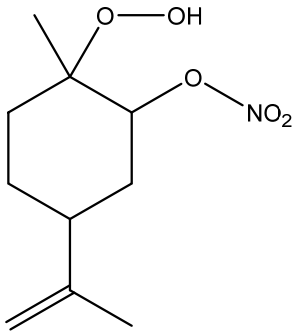

NLIMOOH

Figure 4.10 continued.

Second Generation Isoprene Oxidation Product Nitrates

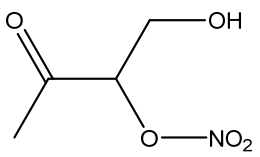

MVKNO3

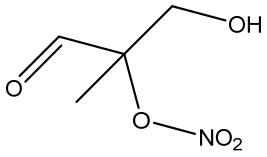

MACRNO3

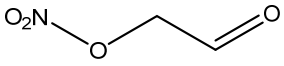

ETHLN

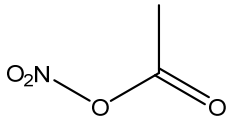

PROPNN

Second Generation Monoterpene Oxidation Product Nitrates

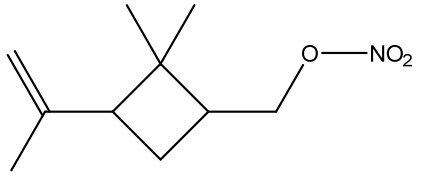

C96NO3

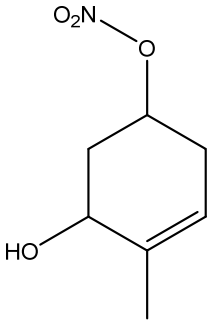

C720NO3

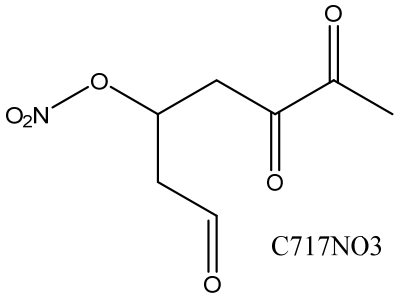

C717NO3

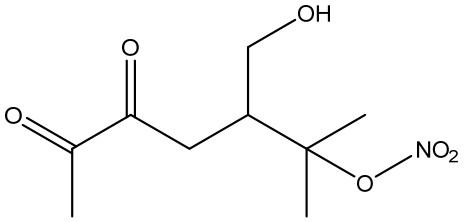

C98NO3

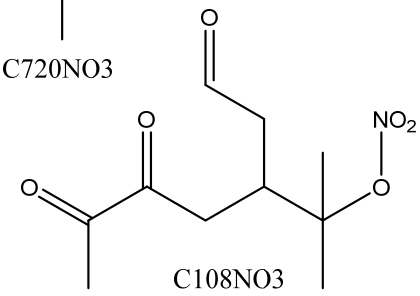

C108NO3

Figure 4.10 continued.

To identify which BVOCs produce the most organic nitrates, the production rate of the isomers of each BVOC species were summed (e.g. isoprene nitrate is the summation of the eight isoprene nitrate ($C_5H_{10}NO_4$) isomers) and are shown in Figure 4.11. The production rates shown in Figure 4.11 are a combination of the organic nitrates formed from photochemistry and NO_3 chemistry, as both act a means to removing NO_x from the troposphere.

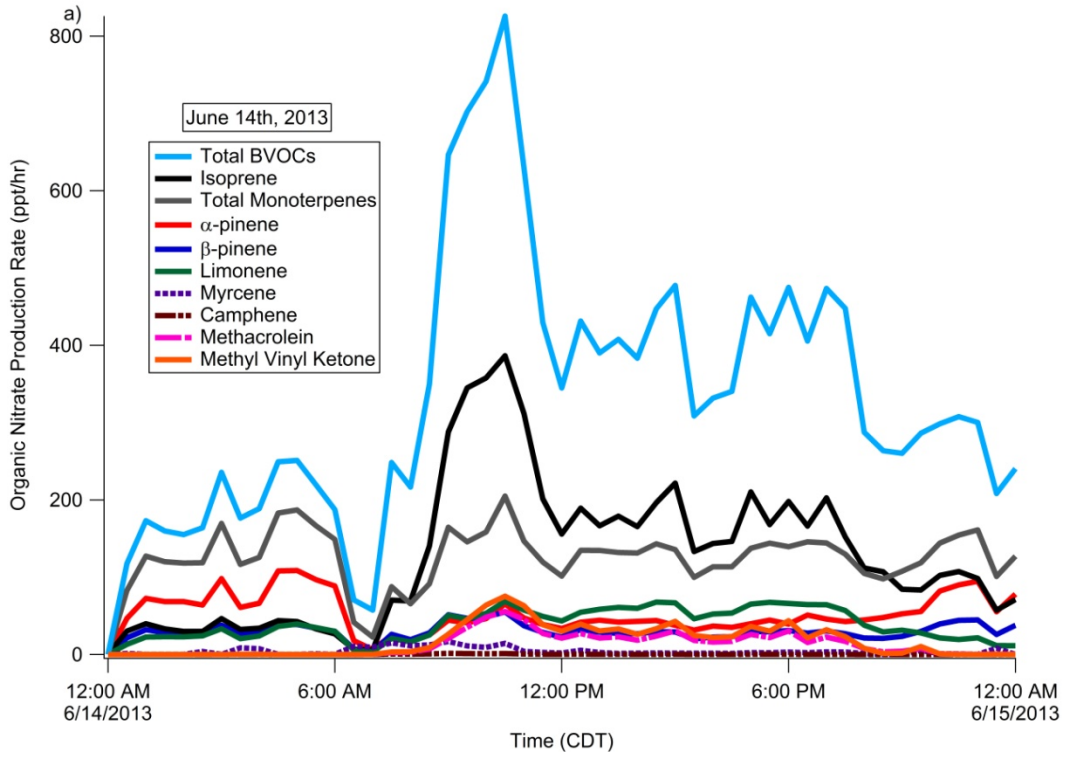

Figure 4.11 Plot of total organic nitrate production rate along with which BVOCs contribute most to the total production for June 14th (a), June 26th (b), and July 12th (c).

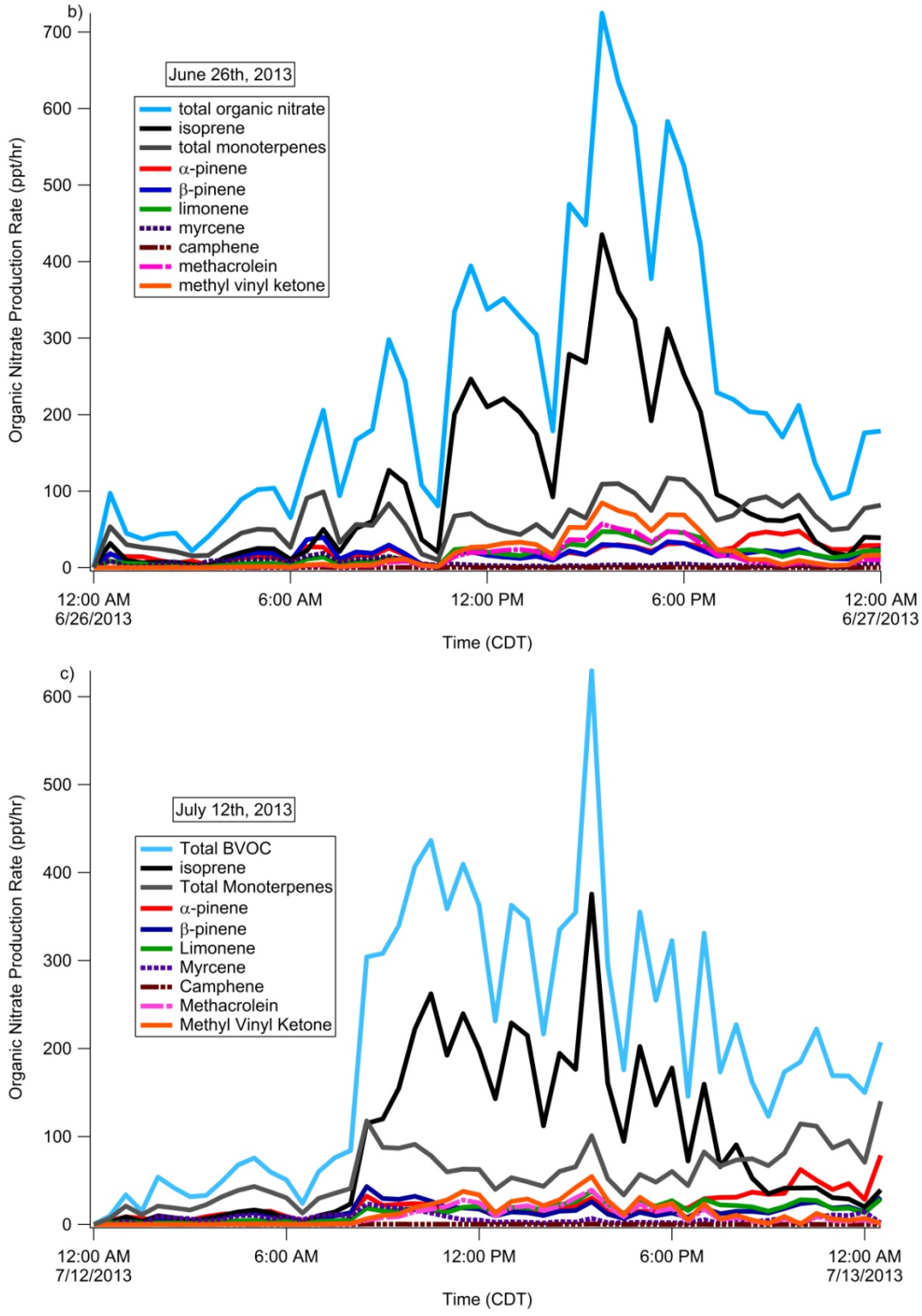

Figure 4.11 continued.

Figure 4.11 shows that for the three days studied, the production of the summed monoterpene nitrates dominated the production of total organic nitrates during the late evening and early morning hours (~2100-1000). Isoprene emissions, which are dependent on radiation and temperature (Guenther et al., 1993) began to rise in the early morning hours. Isoprene nitrate production dominated during the day, peaking in the early morning for June 14th, and in the late afternoon for June 26th and July 12th.

To better understand the impact of second generation organic nitrates, the individual and summed second generation organic nitrate production rate was plotted and is shown in Figure 4.12. Second generation organic nitrates are produced from two different sources. The first is from the BVOC+OH+NO oxidation when the BVOC is the product of the primary BVOC (e.g. isoprene, α-pinene, and limonene) + OH chemistry. The other source of secondary organic nitrates is from the oxidation of primary organic nitrates (e.g. isoprene nitrates, α-pinene nitrates, limonene nitrates).

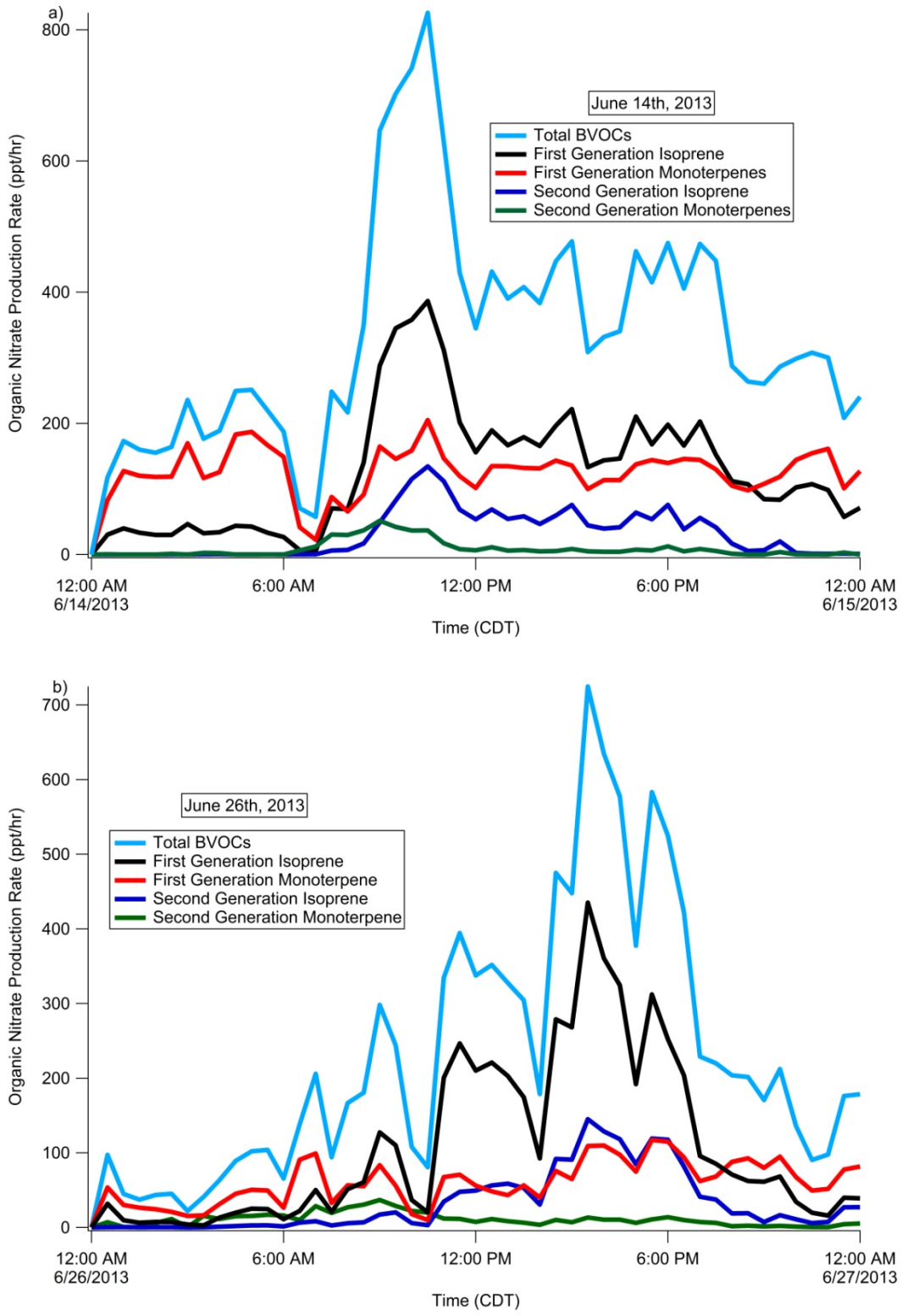

Figure 4.12 Comparison of the production of first and second generation organic nitrates for June 14th (a), June 26th (b), and July 12th (c).

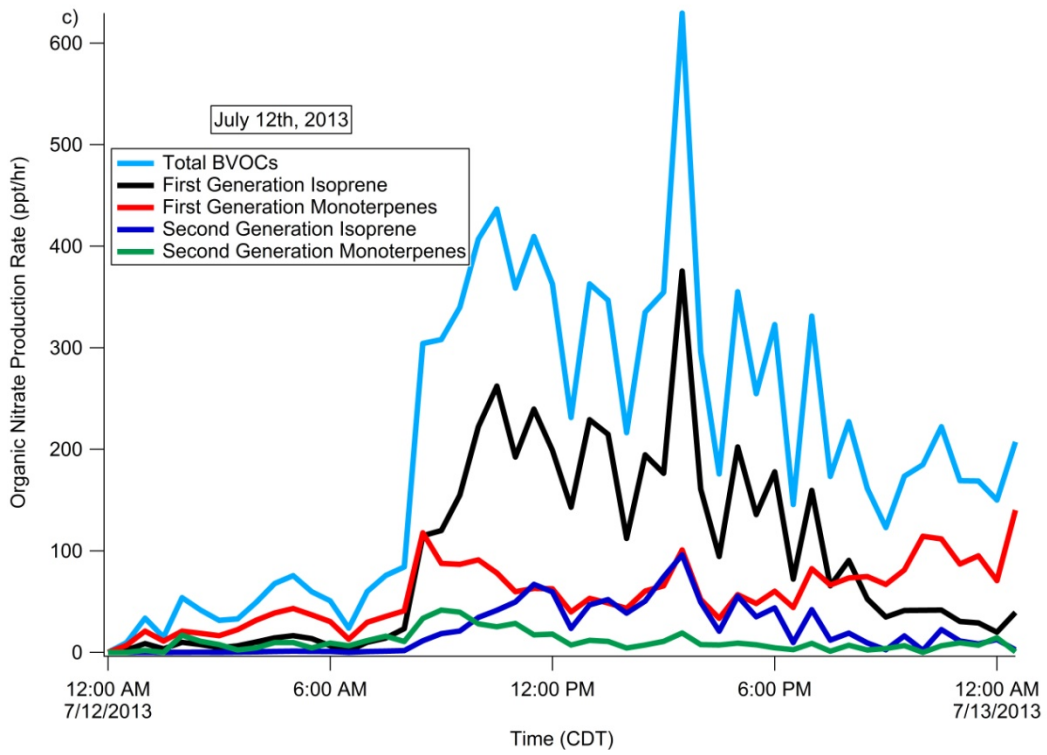

Figure 4.12 continued.

Figure 4.12 shows that while there is a significant primary monoterpene nitrate production, the production of second generation organic nitrates from isoprene rival primary monoterpene nitrate production during the afternoon for all three days. On average, for the three days, the production of organic nitrates from second generation isoprene products contributed to 8% of the total organic nitrate production. Second generation organic nitrates from monoterpenes are low during the day, and significant during the early morning (0000-0600) hours. On average, for the three days, the production of second generation organic nitrates from monoterpenes contributes to 6% of the total organic nitrate production.

Monoterpene nitrate formation has become a recent area of study due to the better understanding of isoprene chemistry (Browne et al. 2014). The presence of monoterpene nitrates over areas where monoterpene emissions are dominant, such as a boreal forest in Canada (Browne et al. 2013) or the forests over the western United States (MacKenzie et al. 2011), has been shown. Even in a forest that is a large isoprene emitter, monoterpene nitrates have been shown to have an effect on the oxidizing capacity of the atmosphere. The dominance of monoterpene nitrates in a forest in the early morning has been observed before in Pratt et al. (2012), who stated monoterpene nitrate production in the early morning hours accounts for ~80% of the total organic nitrate production. In this study we find that on average, 61% of early morning hour organic nitrate production is from monoterpene nitrate production for the three days studied. After sunset (~1900), isoprene nitrate production steeply declined for June 26th and July 12th, but remained high for June 14th, and monoterpene nitrates began to exhibit larger production rates towards the end of the day.

From Figure 4.11 and 4.12, on average 61% of the total organic nitrate production budget for the 3 days studied here comes from the production of monoterpene nitrates during the morning (midnight to just before sunrise for each day). During the afternoon and after sunset, monoterpene nitrates still contributed on average to 24% and 51% of the total organic nitrate budget, respectively. Figure 4.8 shows that the photo-oxidation of monoterpenes only contributes to on average, 7% of the total O_3 production total. Figure 4.13 shows the speciated monoterpene organic nitrate production in greater detail.

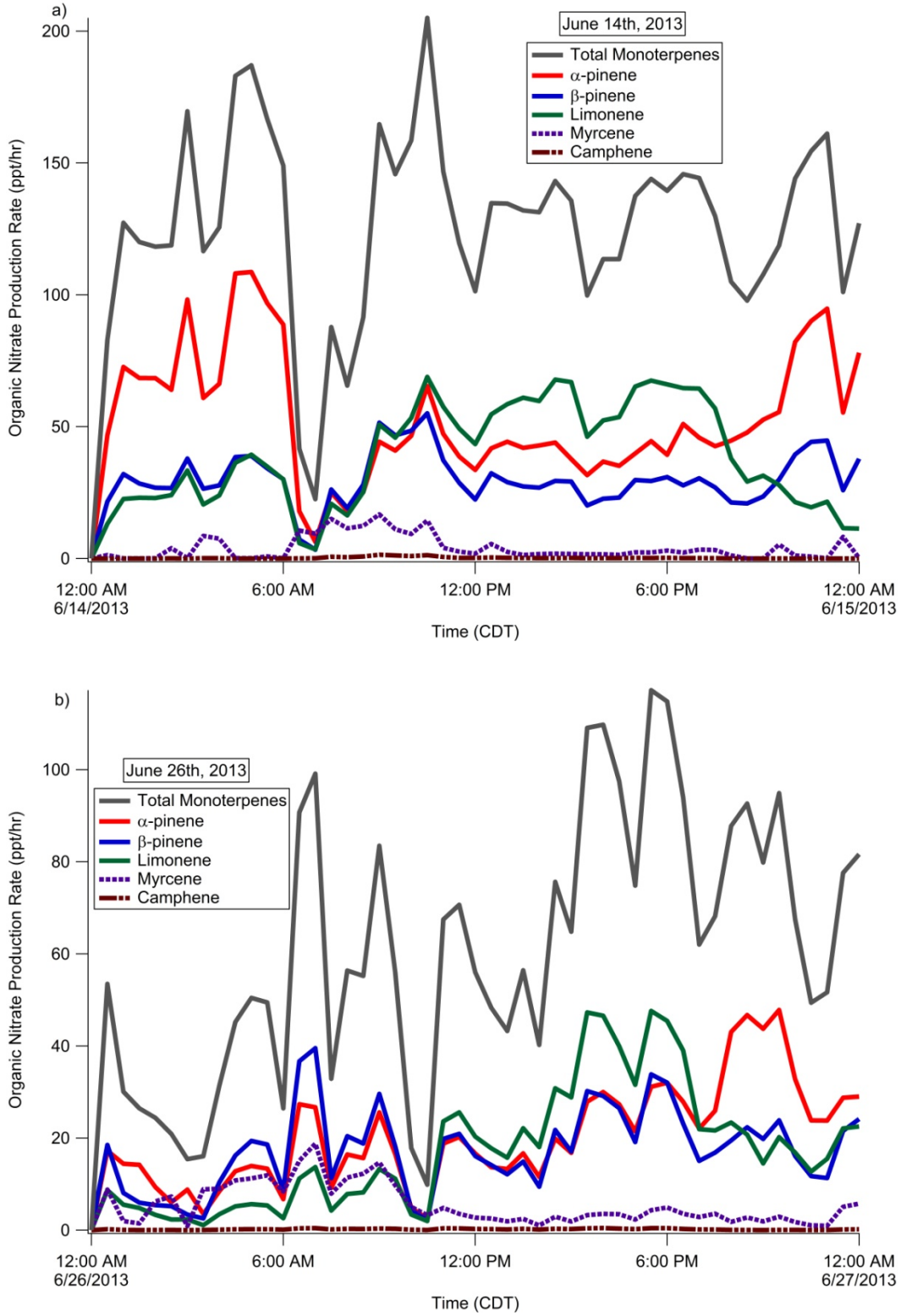

Figure 4.13 Total monoterpene nitrate production as compared to individual monoterpene nitrate production for June 14th (a), June 26th (b), and July 12th (c).

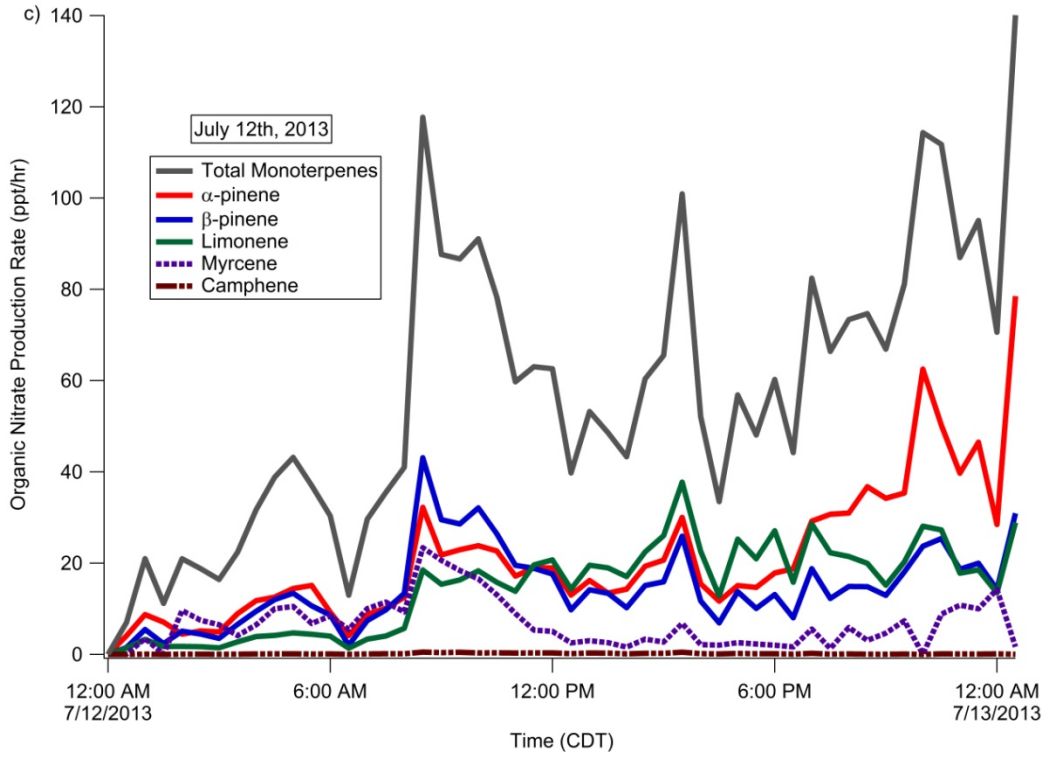

Figure 4.13 continued.

Figure 4.13 shows that even though α-pinene and β-pinene are the dominant organic nitrate precursors among monoterpenes found at this site, the production of limonene nitrates is comparable during periods with no radiation, and greater than α-pinene and β-pinene on June 14th and June 26th, and very similar to α-pinene on July 12th. Limonene is found at concentrations 2-3 times lower than α-pinene, however the OH + limonene rate constant is 3 times greater than the α-pinene + OH and the NO_3 + limonene rate constant is 2 times greater than the α-pinene + NO_3 rate constant. The camphene + NO_3 rate constant is 11 times larger than α-pinene + NO_3 and the reaction with OH has similar rate constants (5.33 x 10^{-11} and 5.31 x 10^{-11} for camphene and α-pinene, respectively) (Atkinson et al. 2003). Since camphene concentrations were ~97% lower than α-pinene

or β-pinene emissions, their contribution to total organic nitrate production was minimal as shown in Figure 4.13. Future studies of monoterpene nitrates should focus not only on the fates of α-pinene nitrates and β-pinene nitrates, but on limonene nitrates.

4.3.6 Photochemically Produced Nitrates vs. NO_3 Produced Nitrates

The impact of organic nitrates not only depends on the photochemistry, but on NO_3 chemistry, which occurs during night times, but also during the day. NO_3 chemistry also plays an important role in influencing daytime photochemistry (Brown and Stutz, 2012). Penkett et al. (1993) have shown that NO_3 more efficiently removes unsaturated hydrocarbons from the troposphere than OH on regional scales. NO_3 chemistry effects the NO_x cycle, as Stutz et al. (2010) have shown that up to 50% of emitted NO_x throughout a 24 hour period in urban areas can be removed through nocturnal processing. In order to understand the importance of NO_3 chemistry, the organic nitrates formed from NO_3 chemistry were separated from those formed during OH initiated oxidation.

To show the importance of second generation nitrates from isoprene and monoterpene nitrates, the production of the two classes of nitrates was separated into NO_3 produced organic nitrate and photochemically produced nitrate and is shown in Figure 4.14.

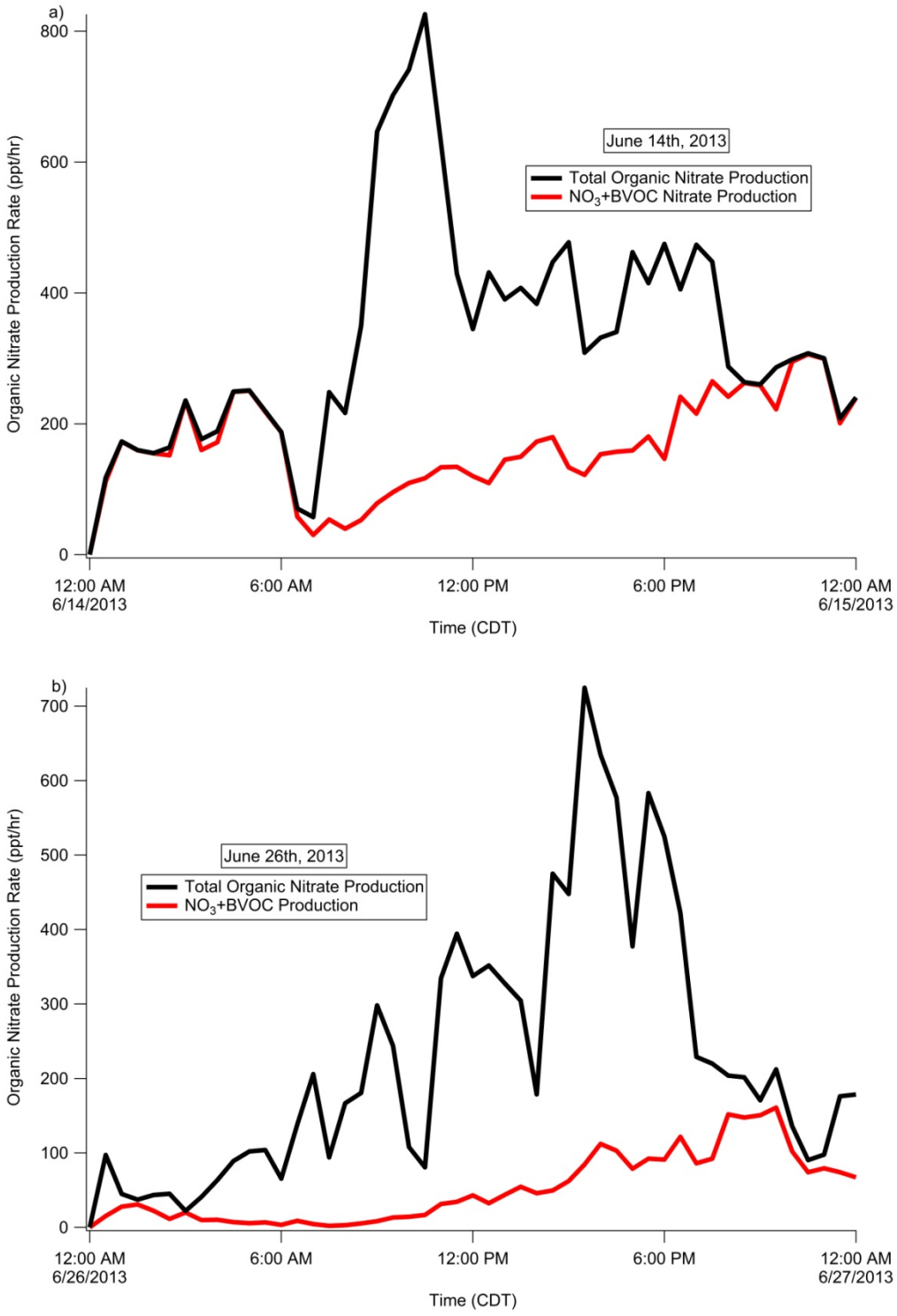

Figure 4.14 Comparison of total organic nitrate production and the fraction of organic nitrate formed from BVOC + NO_3 chemistry for June 14th (a), June 26th (b), and July 12th (c).

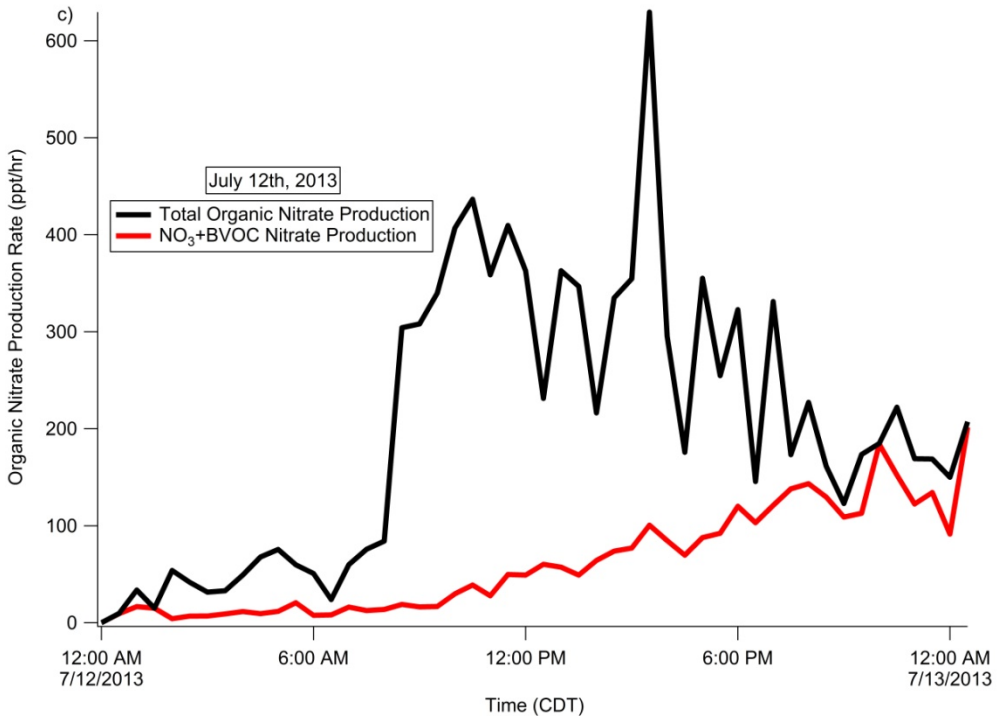

Figure 4.14 continued.

Figure 4.14 shows that for June 14th, 96% of the total organic nitrate produced is formed from NO_3 chemistry in the early morning hours (before sunset), 26% during the day (when radiation was present), and near 87% during the late evening (between sunset and midnight). The rate of organic nitrate production from BVOC + NO_3 chemistry is much lower on June 26th and July 12th, with 11% and 14% of organic nitrate production from NO_3 + BVOC chemistry. This is most likely due to the lower NO_3 values on these two days, as shown in Figure 4.5.

It has been shown in Pratt et al. (2012) that even during the day ~8% of organic nitrate production was from isoprene + NO_3 chemistry. NO_3 + monoterpene chemistry has received attention because monoterpenes emissions are usually only temperature

dependent, and are therefore emitted at night (Fry et al., 2014; Guenther et al., 1993). The large production of organic nitrate from NO_3 chemistry, even during the day, is explained by the large organic nitrate yield from BVOC + NO_3 chemistry. While the organic nitrate yield for isoprene photochemistry in the presence of NO_x has a yield between 4% (Horowitz et al., 2007) and 14% (Lee et al., 2014b), studies have shown that isoprene + NO_3 has an ~80% product yield of organic nitrates (Perring et al., 2009b). This very large yield difference between the two pathways is not always seen in monoterpene chemistry, where a-pinene + OH + NO produces between 18%-26% organic nitrates (Rindelaub et al., 2015) and a-pinene + NO_3 chemistry produces 20% organic nitrate (Spittler et al. 2006). However, β-pinene + OH produces 23% organic nitrate while β-pinene + NO_3 chemistry produces 43% organic nitrate (Fry et al. 2009). This shows that NO_3 chemistry may have a large influence on ozone production, as ~50% of nocturnal NO_x can be sequestered through this reaction, assuming there is no NO_x recycling from further oxidation (Stutz et al., 2010). This assumption is made on the fact that the dominant monoterpene nitrates observed (α-pinene and β-pinene nitrate) are unable to undergo ozonolysis, NO_3, or OH reaction, due to the lack of an available double bond. Ozonolysis is a high energy oxidation, and the most likely means to removing NO_x from an organic nitrate.

One large uncertainty of the model that is not well understood is a parameter called the NO_x recycling efficiency. The NO_x recycling efficiency of an organic nitrate is the amount of NO_2 released when oxidation by OH, O_3, or NO_3 occurs. Figure 4.15 shows an example of this problem.

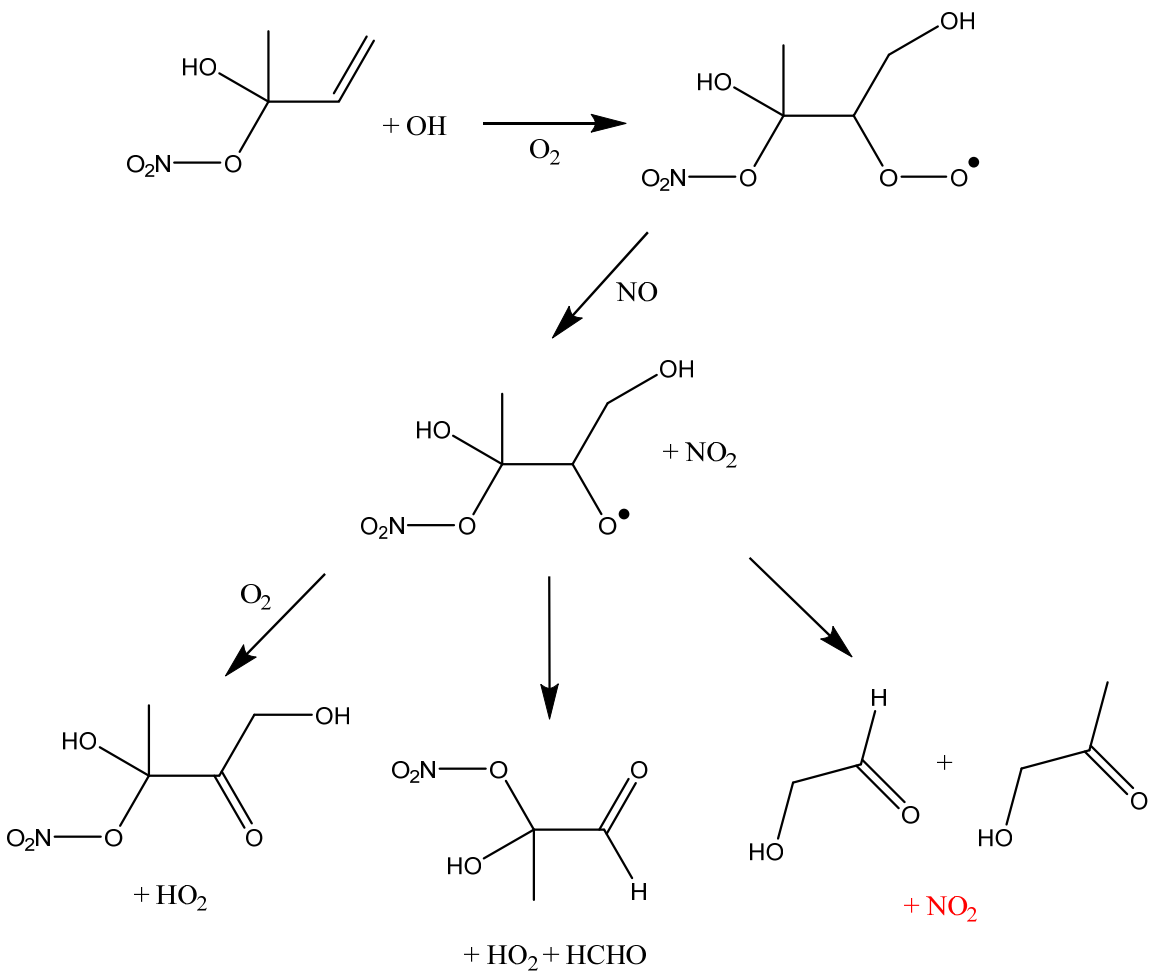

Figure 4.15 Example of NO_x being released during the OH oxidation of an isoprene nitrate.

In the model, the NO_x recycling efficiency of isoprene nitrates is set at 50% as described in (Paulot et al., 2009). The NO_x recycling efficiency of the monoterpene and second generation organic nitrates is set at 0%. The problem with these numbers is that it they have not been experimentally measured. This measurement is critical to understanding the impact of organic nitrates on ozone production, as it determines which organic nitrates are permanent reservoirs of NO_x (whose ultimate fate is deposition to surfaces), or temporary reservoirs of NO_x (nitrates that release NO_x upon further oxidation). This

problem is currently being addressed experimentally in the Shepson Lab and through models of the SOAS data by Ron Cohen's group at the University of California Berkeley.

4.3.7 Effect of Organic Nitrate Production on Ozone Production

From Figure 4.11, isoprene is the dominant BVOC contributing to organic nitrate formation during the daytime (during maximum O_3 production as shown in figure 4.8) and monoterpene nitrates, specifically a-pinene, b-pinene, and limonene nitrates, are the dominant nitrate formed when radiation was not present. To understand the effect of organic nitrate formation on the traditional ozone production definition (Equation 4.1), we eliminated all organic nitrate production to observe the difference in ozone production. From this analysis, the production of organic nitrates reduced ozone production by 4.2% for June 14th, 6.9% for June 26th, and 4.4% for July 12th. This gives an average of 5.2 ± 1.5%. Wu et al. (2007) found that by increasing the yield of isoprene nitrates from 4% to 12% would result in a 10% decrease in the concentration of O_3 worldwide. The updated 0-D model used in this study has the isoprene nitrate yield at 11% (Xiong et al., 2015). By removing the 11% isoprene nitrate yield, along with the production of all the other nitrates, we could not get numbers similar to the Wu et al. (2007). This means a further study into the fate of NO_x at the SOAS site is needed. This study is currently being done by Paul Rommer of Ron Cohen's group at the University of California Berkeley.

4.4 Conclusions

This work shows illustrates the effect of organic nitrate formation on the production of O_3. Isoprene is the most important BVOC precursor for organic nitrate production and is responsible for on average 44% of the total organic nitrate budget per day. The sum of the production of monoterpene nitrates rivals the production of isoprene nitrates. The production of monoterpene nitrates contributing to, on average, 31% of the total organic nitrate budget, with a-pinene (12%), b-pinene (7.9%), and limonene (8.8%) being the dominant $RONO_2$ precursors among the monoterpenes. While the photochemical production of organic nitrates dominates the production of organic nitrates, there is a significant fraction of organic nitrates formed from NO_3 + BVOC chemistry, and future work on organic nitrate production should include a better understanding of branching ratio differences along with determining the fate of organic nitrates and their role in the NO_x cycle.

CHAPTRER 5 CONCLUSIONS AND FUTURE WORK

5.1 Conclusions

The research presented in this dissertation has provided new insights into the location, magnitude, and effect of tropospheric NO_x chemistry at two rural forested sites. The first and second configurations of the comprehensive two-dimensional gas chromatography (GCxGC) system offers a clear advantage over traditional one-dimensional gas chromatography in separation power and demonstrated in this thesis is the ability to sample and analyze atmospheric samples in field conditions. Configuration three had poor injections into the GCxGC system and made the characteristics of the system (e.g. resolution, limit of detection, peak capacity) comparable to a GC-MS. There is still work needed to better understand NO_x-BVOC chemistry, including better measurement techniques, the synthesis of known standards, and more sampling locations.

Presented in this research are the results of two field campaigns. The first demonstrated that early morning spikes in the concentrations of NO_x appear to be due to the break-up of the nocturnal boundary layer, and that the downward transport of polluted air from aloft towards the forest canopy plays a role in the early morning NO_x peaks. It was also shown that there is significantly different chemistry occurring below and above the canopy during the night. There was a significantly higher concentration of NO_x above the canopy compared to observations in-canopy and below the canopy during times when

turbulence was low. No biogenic volatile organic compound (BVOC) measurements were made below and above the canopy, and therefore, the chemistry of the difference between the two sampling sites is unknown. There could be significant NO_3+BVOC reactions (Chapter 1.5.3) occurring within and below the canopy, however, no NO_3 or BVOC measurements were made at any height during our field campaign.

A sampling system for a comprehensive flow modulated two-dimensional gas chromatography instrument was developed. The use of a two-trap system was able to concentrate semi-volatile species (species with a carbon number greater than 10 including monoterpenes and sesquiterpenes) into the GCxGC system. The use of a cryofocuser was able to effectively trap highly volatile species (species with a carbon number of 4 and greater), but was not ideal for long term ambient monitoring. Water vapor damaged most of the cooling elements during field deployments and a redesign of the cryofocuser, or entire trap system, is needed to minimize water damage. A field modified single trap system was used to obtain monoterpene measurements during the 2013 Southern Oxidant and Aerosol Study.

Modeled concentrations of organic nitrates, important NO_x reservoirs, were made for the Southern Oxidant and Aerosol Study. The impact of these species on ozone production was determined and agree with previous measurements and models of the southeastern United States. It was found that limonene nitrates are more prevalent than α-pinene and β-pinene nitrates during the daytime, and this is due to limonene reacting faster with NO_3 and OH radicals. It was also found that the organic nitrates from the second generation isoprene oxidation products methyl vinyl ketone (MVK) and methacrolein (MACR) were produced at a similar rate as monoterpene nitrates during

peak O_3 production times. These two findings cannot be compared to observations at SOAS. This is because there are no known analytical standards for methyl vinyl ketone nitrates or methacrolein nitrates. The speciation of monoterpene nitrates has not been performed in the field or in a laboratory environment. Recently, this lab has synthesized an α-pinene nitrate (Rindelaub et al., 2015), but standards of β-pinene nitrates and limonene nitrates are not currently available. There is also no current method for the separation and detection of monoterpene nitrates.

5.2 Future Instrumentation Work

There have been considerable improvements in the field of analytical instrumentation for the study the effect of NO_x on tropospheric chemistry in the past 60 years. New techniques have been invented to measure the total mixing ratio of peroxy acyl nitrates and organic nitrates (Day et al., 2002). Advancements in GCxGC and OH measurements have increased our knowledge of the vast number of BVOCs and their oxidation pathways (Hamilton, 2010b; Mao et al., 2012). Most of the field of analytical atmospheric chemistry is heavily set on expanding the potential of chemical ionization mass spectrometry (CIMS) to identify new oxidation products of tropospheric BVOC chemistry (Beaver et al., 2012; Ehn et al., 2014b; Huey, 2007; Lee et al., 2014a; Paulot et al., 2009). This field will continue as new atmospherically relevant species are identified, and the chemical pathways in which BVOCs proceed are identified including organic nitrates and their speciation (Lee et al., 2014b; Nguyen et al., 2011). Riveria-Rios et al. (2014) have recently shown that isoprene hydroperoxide compounds decompose into MVK and MACR inside GC and proton-transfer mass spectrometry (PTR-MS)

instruments. As shown at SOAS, the concentration of isoprene hydroperoxides are between 20-300 ppt, which is a significant fraction of the total MVK and MACR concentrations, which averaged 614 and 396 ppt, respectively. This means the main oxidation products of isoprene, MVK and MACR, may not be as dominant a pathway as previously believed.

One area of research that is needed is the rapid quantification of isomers in the field to obtain flux measurements. GCxGC is an excellent technique for the separation of small chain alkanes, alkenes, alkynes, and mono-oxygenated BVOCs, but similar to one-dimensional gas chromatography systems, suffers from drastic loss of multi-functional and liable species, such as hydroperoxides (Hallquist et al., 2009) and a does not have the time resolution needed for flux measurements. However, there is room for improvement in the field of GCxGC. Identified compounds from traditional chromatography and mass spectrometry have only accounted for less than an estimated 20% of the total organics in aerosols (Williams et al., 2006). To address the problem of sample loss during analysis, different sampling methods are needed to address these issues. The ideal sampling system would need to have the analyte have minimal surface contact during quantification to reduce depositional losses, have a detection system with a limit-of-detection that requires no pre-concentration, and have the ability to quantify any species found in the atmosphere, which encompasses a currently unknown large volatility and polarity range.

Future work in the field of atmospheric GCxGC should focus on method development for difficult to detect compounds. Traditional GC-ECD measurements for peroxy acyl nitrates species requires the use cold (~15º C) ovens (Bertman et al., 1993). Organic nitrates ($RONO_2$) have been shown to thermally degrade at ~150º C (Hiskey et

al., 1991). Using our temperature and transfer time (200º C and a transfer time of 10 minutes for trap to trap, trap to cryofocuser, and/or trap to GCxGC), 79% of nitrate ester bonds are thermally degraded inside the trap (Hiskey et al., 1991). Future work into GCxGC instrumentation should focus on testing sorbent materials (PDMA, carboxen, etc..) with synthesized standards of organic nitrates (Lee et al., 2014b; Lockwood et al., 2010) at low temperatures (<150º C) to find a possible means of concentrating and focusing ambient samples for injection into a GCxGC system.

The main difficulty in this method development is finding a suitable pre-concentration technique. The use of cryofocusers, such as the one described in Goldan et al. (1995), require large amounts of cryogens. A sorbent material that can effectively trap BVOCs with a wide range volatilities and polarities and subsequently release them with a low amount of heat has not been developed. The ideal trap should consist of multiple sorbent materials. The first sorbent material should be polydimethylsiloxane (PDMS). PDMS is an inert material that does not retain water, but thermally degrades and causes large artifact peaks (Baltussen et al., 1999). It is also subject to loss of high volatility compounds (Dettmer and Engewald, 2002). Therefore, a second higher adsorbent strength should be used in series with the PDMS. The second sorbent material used for the trap should be made of multiple graphitized black carbon (GBC) sorbent materials, such as Carbopack B described in Chapter 3.2.2 or Carbopack X. Graphitized black carbon has a very low affinity for water and has been shown to be able to pre-concentrate C3 to greater than C20 compounds (Dettmer and Engewald, 2002). However, these sorbents have a low affinity for compounds with a high polarity, but produce no known artifact signals (Dettmer and Engewald, 2002). The high polarity compounds should be

adsorbed to the PDMS before entering the GCB sorbent material. The combination of PDMS and GCB should offer a pre-concentration system that has limited water interference, limited artifact signal, a high affinity for both low and high polarity compounds, and a high affinity for compounds with either a high or low vapor pressure.

5.3 Future Field Work

This thesis has shown that night time measurements of NO_x below and above the canopy are vastly different, and that the chemistry occurring below a forest canopy in northern Michigan is highly uncertain. Vertical profile measurements of NO_x show that there is a measureable difference between above canopy and below canopy NO_x concentrations. There have been a many field campaigns that have measured the flux of NO_x (Farmer et al., 2006; Kitzler et al., 2006; Farmer et al., 2008; Filippia et al., 2009; Min et al., 2014). Flux measurements of NO_x in the Amazonian rain forest by Rummel et al. (2002) found that soil emissions of NO are significantly larger at night than during the day. Flux measurements below and above the canopy performed by Min et al. (2014) found that the NO_x canopy reduction factor (Chapter 2.1 and 2.3.6) for the Blodgett forest in Northern California was ~50%.

However, there are still significant gaps in our understanding of NO_x sources and sinks, as these studies only represent a fraction of the total biosphere. One of the main challenges in understanding NO_x chemistry is the lack of direct measurements, both temporally and spatially (Geddes and Murphy, 2014). Most direct NO_x measurements are taken over a short time period (~1 to 2 months) at specific sites that may or may not represent the region in which they are located. There is also a large uncertainty in the

NO_x compensation point, the point at which trees become NO_x sinks or NO_x sources (Conrad, 1996; Raivonen et al., 2009). This value been measured to be between 0.2 and 3 ppb in forest environments, which encompasses the typical range of rural NO_x concentrations (Lerdau et al., 2000). There is a great need for not only accurate flux measurements of NO_x within canopies, but a need for the parameters which govern the biological functions of trees (e.g. fixed nitrogen availability, rainfall).

One of the largest uncertainties in NO_x chemistry is the lack of understanding the vertical concentration gradients of NO_x and other BVOCs from below the canopy to the top of the boundary layer. Recent work by Min et al. (2014) found significant in-canopy NO_x chemistry that was responsible for sequestering NO_x before it reached a canopy height of 8 m. Work by Goldstein et al. (2004), Hu et al. (2013), and Wolfe et al. (2011) have all shown that in-canopy chemical processes have a significant effect on the composition of the troposphere. This chemistry may be significantly different, as the proposed BVOCs that exist with-in the canopy and not outside of the canopy are thought to be sesquiterpenes and very reactive monoterpenes, such as ocimene (Wolfe et al., 2013; Min et al., 2014). These compounds, including their oxidation product speciation and yields, are not as well studied as those of isoprene and the monoterpenes α-pinene and β-pinene. Understanding the chemistry and processes that occur within the canopy is the next step in understanding discrepancies between modeled vs measured O_3 (Wu et al., 2007) and SOA (Goldstein and Galbally, 2007; Hallquist et al., 2009) concentrations.

To better understand in-canopy chemical and physical processes, future field campaigns need to focus on simultaneous flux measurements of NO_x, O_3, and BVOCs below, within, and above the canopy. As shown in this work, measurements of within and

above canopy measurements need to be taken in time periods under the canopy transport time of near 100 s (Min et al., 2014). The ideal field campaign to study NO_x-BVOC chemistry would require multiple instruments, including multiple GCxGCs, OH-LIF instruments, O_3 monitors, chemiluminescent NO_x instruments, and cavity ring down spectrometers (for measuring NO_3). This study would address the question, what compounds are causing NO_x removal below the canopy, and how are these compounds removing NO_x from below the canopy. Multiple GCxGCs could identify the specific BVOCs that exist above and below the canopy. Pratt et al. (2012) found that the monoterpenes ocimene and γ-terpinene should be large organic nitrate precursors based on leaf-level emissions. However, there are very few quantitative measurements of ocimene above the forest canopy. There would have to be multiple instruments simultaneously measuring above and below the canopy to fully understand the knowledge gap between in-canopy and above-canopy chemistry.

5.4 Future Laboratory Studies

One of the major limitations in understanding NO_x and BVOC chemistry is the lack of analytical grade (greater than 95% purity) standards. From Chapter 4, limonene nitrates are modeled to be an important fraction of the total monoterpene nitrates. There is currently a reaction to create α-pinene nitrates as described in Rindelaub et al. (2015). Limonene nitrates could be synthesized in a similar fashion as shown in reaction 5.1.

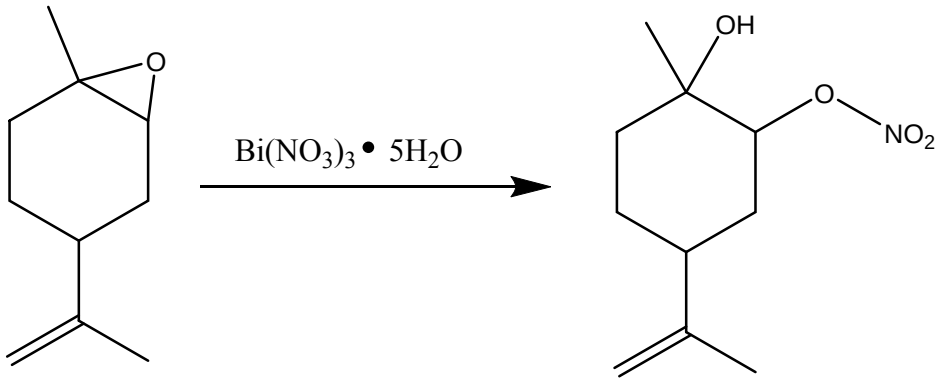

Figure 5.1 Proposed synthetic pathway for limonene nitrates.

Other possible reagents that can be used to open the epoxide ring could include HNO_3 or $TlNO_3$ (Mincione and Lanciano, 1980). With synthesized standards of new atmospherically relevant compounds (e.g. organic nitrates, hydroperoxides, alcohols), actual rate constants, product yields, and product analysis can be performed. This would be helpful, and would help replace the large amount of rate constants and product speciated predicted by structure activity relationships that are used in the Master Chemical Mechanism.

LIST OF REFERENCES

LIST OF REFERENCES

Adahchour, M., Beens, J., Vreuls, R.J., Brinkman, U.A., Recent developments in comprehensive two-dimensional gas chromatography (GCxGC): I. Introduction and instrumental set-up, *TrAC Trends in Analytical Chemistry* **25**(2006), pp. 438-454.

Alaghmand, M. *et al.*, The morning NO_x maximum in the forest atmosphere boundary layer, *Atmos. Chem. Phys. Discuss.* **11**(2011), pp. 29251-29282.

Altshuller, A.P., Cohen, I.R., Application of diffusion cells to the production of known concentrations of gaseous hydrocarbons, *Analytical Chemistry* **32**(1960), pp. 802-810.

Anderson, S.M., Zahniser, M.S., Open-path tunable diode laser absorption for eddy correlation flux measurements of atmospheric trace gases, *Meas. Atmos. Gases* **1433**(1991), pp. 167-178.

Arey, J., Aschmann, S.M., Kwok, E.S.C., Atkinson, R., Alkyl nitrate, hydroxyalkyl nitrate, and hydroxycarbonyl formation from the NO_x -air photooxidations of C_5-C_8 n-alkanes, *J. Phys. Chem. A* **105**(2001), pp. 1020-1027.

Arnts, R.R., Evaluation of adsorbent sampling tube materials and Tenax-TA for analysis of volatile biogenic organic compounds, *Atmospheric Environment* **44**(2010), pp. 1579-1584.

Aschmann, S.M., Arey, J., Atkinson, R., OH radical formation from the gas-phase reactions of O_3 with a series of terpenes, *Atmos. Environ.* **36**(2002), pp. 4347-4355.

Aschmann, S.M., Atkinson, R., Rate constants for the reactions of Cl atoms with a series of C_6-C_{10} cycloalkanes and cycloketones at 297 +/- 2K, *Int. J. Chem. Kinetics.* **45**(2013), pp. 52-58.

Atkinson, R., Gas-phase tropospheric chemistry of organic compounds: a review *Atmospher. Environ.* **24A**(2007), pp. 1-41.

Atkinson, R., Arey, J., Gas-phase tropospheric chemistry of biogenic volatile organic compounds: a review, *Atmospheric Environment* **37**(2003), pp. S197-S219.

Atkinson, R. *et al.*, IUPAC Subcommittee for Gas Kinetic Data Evaluation, *Atmos. Chem. Phys.* **6**(2006), pp. 3625-4055.

Aumont, B., Szopa, S., Madronich, S., Modelling the evolution of organic carbon during its gas-phase tropospheric oxidation: development of an explicit model based on a self generating approach., **5**(2005), pp. 2497-2517.

Ball, B.A., Folinsbee, L.J., Peden, D.B., Kehrl, H.R., Allergen bronchoprovocation of patients with mild allergic asthma after ozone exposure, *J Allergy Clim Immunol* **104**(1999), pp. 1198-1204.

Barr, A.G. *et al.*, Use of change-point detection for friction-velocity threshold evaluation in eddy-covariance studies, *Agricultural and Forest Meterology* **171-172**(2013), pp. 31-45.

Baltussen, E., David, F., Sandra, P., Cramers, C., On the performance and inertness of different materials used for the enrichment of sulfur compounds from air and gaseous samples, *J. Chrom. A.*, **864**(1999), pp. 345-350.

Beaver, M.R. *et al.*, Importance of biogenic precursors to the budget of organic nitrates: observations of multifunctional organic nitrates by CIMS and TD-LIF during BEARPEX 2009, *Atmos. Chem. Phys.* **12**(2012), pp. 5773-5785.

Behnke, W., George, C., Scheer, V., Zetzsch, C., Production and decay of $ClNO_2$, from the reaction of gaseous N_2O_5 with NaCL solution, *J. Geophys. Res.-Atmos.*(1997).

Bela, M.M. *et al.*, Ozone production and transport over the Amazon Basin during the dry-to-wet and wet-to-dry transition seasons, *Atmos. Chem. Phys.* **15**(2015), pp. 757-782.

Bertman, S.B., Buhr, M.P., Roberts, J.M., Automated cryogenic trapping technique for capillary GC analysis of atmospheric trace compounds requiring no expendable cryogens: Application to the measurement of organic nitrates, *Analytical Chemistry* **65**(1993), pp. 2944-2946.

Bollinger, M.J., Sievers, R.E., Fahey, D.W., Fehsenfeld, F.C., Conversion of nitrogen dioxide, nitric acid, and n-propyl nitrate to nitric oxide by gold-catalyzed reduction with carbon monoxide, *Anal. Chem.* **55**(1983), pp. 1980-1986.

Breuninger, C., Oswald, R., Kesselmeier, J., Meixner, F.X., The dynamic chamber method: trace gas exchange fluxes (NO, NO_2, O_3) between plants and the atmosphere in the laboratory and the field, *Atmos. Meas. Tech.* **5**(2012), pp. 955-989.

Brown, S.S. *et al.*, Nocturnal isoprene oxidation over the Northeast United States in summer and its impact on reactive nitrogen partitioning and secondary organic aerosol, *Atmos. Chem. Phys.* **9**(2009), pp. 3027-3042.

Brown, S.S., Stutz, J., Nighttime radical observations and chemistry, *Chem. Soc. Rev.* **41**(2012), pp. 6405-6447.

Browne, E.C., Cohen, R.C., Effects of biogenic nitrate chemistry on the NOx lifetime in remote continental regions, *Atmos. Chem. Phys.* **12**(2012), pp. 11917-11932.

Browne, E.C. *et al.*, Observations of total $RONO_2$ over the boreal forest: NO_x sinks and HNO_3 sources, *Atmos. Chem. Phys.* **13**(2013), pp. 4543-4562.

Browne, E.C., Wooldridge, P.J., Min, K.E., Cohen, R.C., On the role of monoterpene chemistry in the remote continental boundary layer, *Atmos. Chem. Phys.* **14**(2014), pp. 1225-1238.

Bruner, F., Crescentini, G., Mangani, F., Graphitized carbon black: A unique adsorbent for gas chromatography and related techniques, *Chromaotgraphia Vol.* **30**(1990), pp. 565-572.

Bryan, A.M. *et al.*, In-canopy gas-phase chemistry during CABINEX 2009: sensitivity of a 1-D canopy model to vertical mixing and isoprene chemistry, *Atmos. Chem. Phys.* **12**(2012), pp. 8829-8849.

Bueno, P.A., Seeley, J.V., Flow-switching device for comprehensive two-dimensional gas chromatography, *Journal of Chromatography A* **1027**(2004), pp. 3-10.

Buhr, M.P., Solid-state light source photolytic nitrogen dioxide converter. in: Patent, U.S. (Ed.), United States (2007).

Carroll, M.A., Shepson, P.B., Bertman, S.B., Overview of the program for research on oxidants: PHototchemistry Emissions, and Transport (PROPHET) summer 1998 measurments intensive, *J. Geophys. Res.* **106**(2001), pp. 24275-24288.

Chapparo-Suarez, I.G., Meixner, F.X., Kesselmeier, J., Nitrogen dioxide (NO_2) uptake by vegetation controlled by atmospheric concentrations and plant stomatal aperature, *Atmos. Environ.* **45**(2011), pp. 5742-5750.

Conrad, R., Soil microorganisms as controllers of atmospheric trace gases (H_2, CO, CH_4, OCS, N_2O, and NO), *Microbiol. Rev.* **60**(1996), pp. 609-640.

Costa, A.W., Michalski, G.W., Alexander, B., Shepson, P.B., Analysis of atmospheric inputs of nitrate to a temperate forest ecosystem from delta^{17}O isotope ratio measurements, *Geophys. Res. Lett.* **38**(2011).

Council, N.R., Rethinking the Ozone Problem in Urban and Regional Air Pollution. National Academy Press, Washington, DC (1991), p. 489.

Crounse, J.D., McKinney, K.A., Kwan, A.J., Wennberg, P.O., Measurement of gas-phase hydroperoxides by chemical ionization mass spectrometry, *Anal. Chem.* **78**(2006), pp. 6726-6732.

Davidson, C.I., Phalen, R.F., Solomon, P.A., Airborne particulate matter and human health: A review, *Aerosol Sci. Technol.* **39**(2005), pp. 737-749.

Davidson, E.A., Kingerlee, W., A global inventory of nitric oxide emissions from soils, *Nutrient Cycling in Agroecosystems* **48**(1997), pp. 37-50.

Day, D.A., Wooldridge, P.J., Dillon, M.B., Thornton, J.A., Cohen, R.C., A thermal dissociation laser-induced fluorescence instrument for in situ detection of NO_2, peroxy nitrates, alkyl nitrates, and HNO_3, *J. Geophys. Res.* **107**(2002).

de Gouw, J., Warneke, C., Measurements of volatile organic compounds in the earth's atmosphere using proton-transfer-reaction mass spectrometry, *Mass Spec. Rev.* **26**(2007), pp. 223-257.

de Vries, W., Dobbertin, M.H., Solberg, S., van Dobben, H.F., Schaub, M., Impacts of acid deposition, ozone exposure and weather conditions on forest ecosystems in Europe: an overview, *Plant Soil.* **380**(2014), pp. 1-45.

deGouw, J., Warneke, C., Measurements of volatile organic compounds in the earth's atmosphere using proton-transfer-reaction mass spectrometry, *Mass Spec. Reviews* **26**(2007), pp. 223-257.

Dentener, F.J., Crutzen, P.J., A 3-dimensional model of the global ammonia cycle, *Atmos. chem.* **19**(1994), pp. 331-369.

Dettmer, K., Engewald, W., Adsorbent materials commonly used in air analysis for adsorptive enrichment and thermal desorption of volatile organic compounds, *Anal. Bioanal. Chem.* **373**(2002), pp. 490-500.

Dockery, D.W. *et al.*, Health effects of acid aerosols on North American children: respiratory symptoms, *Environ Health Perspect* **104**(1996), pp. 500-505.

Dodge, M.C., Combined use of modeling techniques and smog chamber data to derive ozone-precursor relationships. in: EPA (Ed.), Environmental Sciences Research Laboratory, Research Triangle Park, NC (1977), pp. 881-889.

Draxler, R.R., Rolph, G.D., HYSPLIT (HYbrid Single-Particle Lagrangian Integrated Trajectory) Model access via NOAA ARL READY website (http://ready.arl.noaa.gov/HYSPLIT.php). NOAA Air Resources Laboratory, Silver Spring, MD (2014a).

Draxler, R.R., Rolph, G.G., HYSPLIT (HYbrid Single-Particle Lagrangian Integrated Trajectory) Model access via NOAA ARL READY website (http://ready.arl.noaa.gov/HYSPLIT.php). NOAA Air Resources Laboratory, Silver Spring, MD (2014b).

Edwards, S.J. *et al.*, A compact comprehensive two-dimensional gas chromatography (GCxGC) approach for the analysis of biogenic VOCs, *Analytical Methods* **5**(2013), pp. 141-150.

Ehn, M. *et al.*, A large source of low-volatility secondary organic aerosol, *Nature* **506**(2014a), pp. 476-479.

Elshorbany, Y.F. *et al.*, Oxidation capacity of the city air of Santiago, Chile, *Atmos. Chem. Phys.* **9**(2009), pp. 2257-2273.

Erickson, D.J., Seuzaret, C., Keene, W.C., Gong, S.L.A., A general circulation model based calculation of HCl and $ClNO_2$ production from sea salt dechlorination: Reactive chlorine emissions inventory, *J. Geophys. Res.-Atmos.* **104**(1999), pp. 8347-8372.

Fang, S.X., Mu, Y.J., Air/surface exchange of nitric oxide between two typical vegetable lands and the atmosphere in the Yangze delta, China, *Atmos. Environ.* **40**(2006), pp. 6329-6337.

Farmer, D.K., Cohen, R.C., Observations of HNO_3, AN, PN, and NO_2 fluxes: Evidence for rapid HO_x chemistry within a pine forest canopy, *Atmos. Chem. Phys.* **8**(2008), pp. 3899-3917.

Farmer, D.K., Jimenez, J.L., Real-time atmospheric chemistry field instrumentation, *Anal. Chem.* **82**(2010), pp. 7879-7884.

Farmer, D.K., Wooldridge, P.J., Cohen, R.C., Application of thermal-dissocation laser induced fluorescence (TD-LIF) to measurement of HNO_3, ANs, PNs, and NO_2 fluxes using eddy covariance, *Atmos. Chem. Phys.* **6**(2006), pp. 3471-3486.

Faxon, C.B., Allen, D.T., Chlorine chemistry in urban atmospheres: a review, *Environ. Chem.* **10**(2013), pp. 221-233.

Fehsenfeld, F. *et al.*, Emissions of volatile organic compounds from vegetation and the implications for atmospheric chemistry, *Global Biogeochemical Cycles* **6**(1992), pp. 389-430.

Filippia, G., *et al.*, Winter and summer nitrous oxide and nitrogen oxides fluxes from a seasonally snow-covered subalpine meadow at Niwot Ridge, Colorado, *Biogeochemisty* **95**(2009), pp. 131-149.

Finlayson-Pitts, B.J., Pitts, J.N., *Chemistry of the Upper and Lower Atmosphere*. Academic Press, San Diego, CA (2000) 969 pp.

Fishtine, S.H., Reliable Latent Heats of Vaporization, *Industrial and Engineering Chemistry* **55**(1963), pp. 47-56.

Fontijn, A., Sabadell, A.J., Richard, R.J., Homogeneous Chemiluminescent Measurement of Nitric Oxide with Ozone, *Anal. Chem.* **42**(1970), pp. 575-579.

Forkel, R. *et al.*, Trace gas exchange and gas phase chemistry in a Norway spruce forest: A study with a coupled 1-dimensional canopy atmospheric chemistry emission model, *Atmos. Environ.* **40**(2006), pp. 28-42.

Fry, J. *et al.*, Secondary organic aerosol formation and organic nitrate yield from NO_3 oxidation of biogenic hydrocarbons, *Environ. Sci. Technol.* **48**(2014), pp. 11944-11953.

Fry, J.L. *et al.*, Observations of gas- and aerosol-phase organic nitrates at BEACHON-RomBAS 2011, *Atmos. Chem. Phys.* **13**(2013), pp. 8585-8605.

Fuchs, H. *et al.*, Experimental evidence for efficient hydroxyl radical regeneration in isoprene oxidation, *Nature Geoscience* **6**(2013), pp. 1023-1026.

Galloway, J.N. *et al.*, Transformation of the Nitrogen cycle: Recent trends, questions, and potential solutions, *Science* **320**(2008), pp. 889-892.

Ganzeveld, L., Valverde-Canossa, J., Moortgat, G., Steinbrecher, R., Evaluation of peroxide exchanges over a coniferous forest in a single-column chemistry-climate model, *Atmos. Environ.* **40**(2006), pp. 68-80.

Ganzeveld, L.N. *et al.*, Global soil-biogenic NO_x emissions and the role of canopy processes, *J. Geophys. Res.* **107**(2002).

Gao, W., Wesley, M., Doskey, P., Numerical modeling of the turbulent-diffusion and chemistry of NO_x, O_3, isoprene and other reactive trace gases in and above a forest canopy, *J. Geophys. Res.-Atmos.* **96**(1993), pp. 18761-18769.

Gauderman, W.J. *et al.*, Association between air pollution and lung function growth in southern California children, *Am J Respir Crit Care Med* **162**(2000), pp. 1383-1390.

Gautrois, M., Koppmann, R., Diffusion technique for the production of gas standards for atmospheric measurements, *J. Chromat. A* **848**(1999), pp. 239-249.

Geddes, J.A., Murphy, J.G., Observations of reactive nitrogen oxide fluxes by eddy covariance above two mid-latitude North American mixed hardwood forests, *Atmos. Chem. Phys.* **14**(2014), pp. 2939-2957.

Gerboles, M., Lagler, F., Rembges, D., Brun, C., Assessment of uncertainty of NO_2 measurements by the chemiluminescence method and discussion of the quality objective of the NO_2 European Directive, *J. Environ. Monit.* **5**(2003), pp. 529-540.

Geron, C.D., Guenther, A.B., Pierce, T.E., An improved model for estimating emissions of volatile organic compounds from forests in the eastern United States, *J. Geophys. Res. Atmos.* **99**(1994), pp. 12773-12791.

Ghosh, A., Bates, C.T., Seeley, S.K., Seeley, J.V., High speed Deans switch for low duty cycle comprehensive two-dimensional gas chromatography, *J. Chromatogr. A* **1291**(2013), pp. 146-154.

Giacopelli, P., Ford, K., Espada, C., Shepson, P.B., Comparison of the measured and simulated isoprene nitrate distributions above a forest canopy, *J. Geophys. Res.* **110**(2005), p. D01304.

Goldan, P.D., Kuster, W.C., Fehsenfeld, F.C., Montzka, S.A., Hydrocarbon measurements in the southeastern United States: The Rural Oxidants in the Southern Enviornment (ROSE) Program 1990, *J. Geophys. Res.* **100**(1995), pp. 25945-25963.

Goldstein, A.H., Galbally, I.E., Known and unexplored organic constituents in the Earth's atmosphere, *Environmental Science and Technology* **41**(2007), pp. 1514-1521.

Goldstein, A.H., Koven, C.D., Heald, C.L., Fung, I.Y., Biogenic carbon and anthropogenic pollutants combine to form a cooling haze over the southeastern United States, **106**(2009), pp. 8835-8840.

Goldstein, A.H. *et al.*, Forest thinning experiment confirms ozone deposition to forest canopy is dominated by reaction with biogenic VOCs, *Geophys. Res. Letters* **31**(2004).

Goldstein, A.H. *et al.*, Thermal desorption comprehensive two-dimensional gas chromatography for in-situ measurements of organic aerosols, *Journal of Chromatography A* **1186**(2007), pp. 340-347.

Gossard, E.E., Gaynor, J.E., Zamora, R.J., Neff, W.D., Fine structure of elevated stable layers observed by sounder and in situ tower measurements, *J. Atmos. Sci.* **42**(1985), pp. 2156-2159.

Gough, C.M., Vogel, C.S., Harrold, K.H., George, K., Curtis, P.S., The legacy of harvest and fire on ecosystem carbon storage in a north temperate forest, *Glob. Change Biol.* **13**(2007), pp. 1935-1949.

Grain, C.F., *Vapor Pressure. Chapter 14*. American Chemical Society (1990) 960 pp.

Grosjean, D., Harrison, J., Peroxyacetyl Nitrate: Comparison of alkaline hydrolysis and chemiluminescence methods, *Environ. Sci. Technol.* **19**(1985), pp. 749-752.

Guenther, A., The contribution of reactive carbon emissions from vegetation to the carbon balance of terrestrial ecosystems, *Chemosphere* **49**(2002), pp. 837-844.

Guenther, A. *et al.*, Natural emissions of non-methane volatile organic compounds, cabon monoxide, and oxides of nitrogen from North America, *Atmos. Environ.* **24**(2000), pp. 2205-2230.

Guenther, A. *et al.*, A global model of natural volatile organic compound emissions, *Journal of Geophysical Research* **100**(1995), pp. 8873-8892.

Guenther, A.B., Zimmerman, P.R., Harley, P.C., Monson, R.K., Fall, R., Isoprene and monoterpene emission rate variability: Model evaluations and sensitivity analyses, *J. Geophys. Res. Atmos.* **98**(1993), pp. 12609-12617.

Gupta, S. *et al.*, Nocturnal wind structure and plume growth rates due to inertial osciallations, *J. Applied. Meterolo.* **36**(1997), pp. 1050-1063.

Haagen-Smit, A.J., Chemistry and physiology of Los Angeles Smog, *Ind. Eng. Chem.* **44**(1952), pp. 1342-1346.

Hallquist, M. *et al.*, The formation, properties and impact of secondary organic aerosol: current and emerging issues, *Atmos. Chem. Phys.* **9**(2009), pp. 5155-5236.

Hamilton, J.F., *Journal of Chromatographic Science* **48**(2010a), pp. 274-282.

Hamilton, J.F., Using comprehensive two-dimensional gas chromatography to study the atmosphere, *Journal of Chromatographic Science* **48**(2010b), pp. 274-282.

Harrison, R.M., Yin, J., Particulate matter in the atmosphere: which particle properties are important for its effects on health?, *Sci. Total Environ.* **249**(2000), pp. 85-101.

Heald, C.L. *et al.*, Predicted change in global secondary organic aerosol concentrations in response to future climate, emissions, and land use change, *J. Geophys. Res. Atmos.* **113**(2008), pp. D1-D16.

Heard, D.E. *et al.*, High levels of the hydroxyl radical in the winter urban troposphere, *Geophys. Res. Lett.* **31**(2004), p. L18112.

Helmig, D., Ozone removal techniques in the sampling of atmospheric volatile organic trace gases, *Atmos. Environ.* **31**(1997), pp. 3635-3651.

Helmig, D. *et al.*, Calibration system and analytical considerations for quantitative sesquiterpene measurements in air, *Journal of Chromatography A* **1002**(2003), pp. 193-211.

Hewitt, C.N., Street, R.A., A qualitative assessment of the emission of non-methane hydrocarbon compounds from the biosphere to the atmosphere in the U.K.: Present knowledge and uncertainties, *Atmospheric Environment* **26**(1992), pp. 3069-3077.

Hiskey, M.A., Brower, K.R., Oxley, J.C., Thermal decomposition of nitrate esters, *J. Phys. Chem.* **95**(1991), pp. 3955-3960.

Holdren, M.W., Westberg, H.H., Zimmerman, P.R., Analysis of monoterpene hydrocarbons in rural atmospheres, *J. Goephys. Res.* **84**(1979), pp. 5083-5088.

Horii, C.V. *et al.*, Fluxes of nitrogen oxides over a temperate deciduous forest, *J. Geophys. Res.-Atmos.* **109**(2004), p. DO8305.

Horowitz, L.W. *et al.*, Observational constraints on the chemistry of isoprene nitrates over the eastern United States, *J. Geophys. Res.* **112**(2007).

Horri, C.V. *et al.*, Fluxes of nitrogen oxides over a temperate deciduous forest, *J. Geophys. Res.-Atmos.* **109**(2004), p. DO8305.

Hu, X., Fuentes, J.D., Toohey, D., Wang, D., Chemical processing within and above a loblolly pine forest in North Carolina, USA, *J Atmos Chem* **DOI:10.1007/s10874-013-9276-3**(2013).

Huey, G.L., Measurement of trace atmospheric speices by chemical ionization mass spectrometry: speciation of reactive nitrogen and future directions, *Mass Spec. Rev.* **26**(2007), pp. 166-184.

Hurst, J.M. *et al.*, Investigation of the nighttime decay of isoprene, *J. Geophys. Res.-Atmos.* **106**(2001), pp. 24335-24346.

IPCC, *Intergovernmental Panel on Climate Change (IPCC): Climate Change 2007*. Cambridge University Press, Cambridge, UK (2007).

Isaacman, G. *et al.*, Improved resolution of hydrocarbon structures and consititutional isomers in complex mixtures using gas chromatography-vacuum ultraviolet-mass spectrometry, *Anal. Chem.* **84**(2012), pp. 2335-2342.

Isaacman, G. *et al.*, Understanding evolution of product composition and volatility distribution through in-situ GCxGC analysis: a case study of longifolene ozonolysis, *Atmos. Chem. Phys.* **11**(2011), pp. 5335-5346.

Isaksen, I.S.A. *et al.*, Atmospheric composition change: Climate-Chemistry interactions, *Atmos. Environ.* **43**(2009), pp. 5138-5192.

Ito, A., Sillman, S., Penner, J.E., Effects of additional nonmethane volatile organic compounds, organic nitrates, and direct emissions of oxygenated organic species on global tropospheric chemistry, *J. Geophys. Res.* **112**(2007).

Jacob, D.J., Wofsy, S.C., Budgets of reactive nitrogen, hydrocarbons, and ozone over the Amazon-forest during the wet season, *J. Geophys. Res.-Atmos.* **95**(1990), pp. 16737-16754.

Jacob, D.J. *et al.*, Summertime photochemistry of the troposphere at high northern latitudes, *J. Geophys. Res. Atmos.* **97**(1992), pp. 16421-16431.

Jobson, B.T. *et al.*, Measurements of C_2-C_6 hydrocarbons during the Polar Sunrise 1992 Experiment: Evidence for Cl atom and Br atom chemistry, *J. Geophys. Res. Atmos.* **99**(1994), pp. 25355-25368.

Johnston, H.S., Davis, H.F., Lee, Y.T., NO_3 photolysis product channels: Quantum yields from observed energy thresholds, *J. Phys. Chem.* **100**(1996), pp. 4713-4723.

Joseph, D.W., Spicer, C.W., Chemiluminescence methods for atmospheric monitoring of nitric acid and nitrogen oxides, *Anal. Chem.* **50**(1978), pp. 1400-1403.

Kim, S. *et al.*, Emissions and ambient distributions of Biogenic Volatile Organic Compounds (BVOC) in a ponderosa pine ecosystem: interpretation of PTR-MS mass spectra, *Atmos. Chem. Phys.* **10**(2010), pp. 1759-1771.

Kim, S. *et al.*, Evaluation of HO_x sources and cycling using measurment-constrained model calculations in a 2-methyl-3-butene-2-ol (MBO) and monoterpene (MT) dominated ecosystem, *Atmos. Chem. Phys.* **13**(2013), pp. 2031-2044.

Kitzler, B. *et al.*, Controls over N_2O, NO_x and CO_2 fluxes in a calcareous mountain forest soil, *Biogeosciences* **3**(2006), pp. 383-395.

Koren, H.S. *et al.*, Ozone-induced inflammation in the lower airways of human subjects, *Am Rev Respir Dis* **54**(1989), pp. 1061-1069.

Kreuger, P.M., McCloskey, J.A., Porous stainless steel as a carrier gas separator interface material for gas chromatography-mass spectrometry, *Anal. Chem.* **41**(1969), pp. 1930-1935.

Kroll, J.H., Ng, N.L., Murphy, S.M., Flagan, R.C., Seinfeld, J.H., Secondary organic aerosol formation from isoprene photooxidation, *Environ. Sci. Technol.* **40**(2006), pp. 1869-1877.

Kroll, J.H., Seinfeld, J.H., Chemistry of secondary organic aerosol: Formation and evolution of low-volatility organics in the atmosphere, *Atmos. Environ.* **42**(2008), pp. 3593-3624.

Lamsal, L.N. *et al.*, Application of satellite observations for timely updates to global anthropogenic NO_x emission inventories, *Geophys. Res. Lett.* **38**(2011).

Lee, A. *et al.*, Gas-phase products and secondary aerosol yields from the ozonolysis of ten different terpenes, *Journal of Geophysical Research* **111**(2006a).

Lee, A. *et al.*, Gas-phase products and secondary aerosol yields from the photooxidation of 16 different terpenes, *J. Geophys. Res.* **111**(2006b).

Lee, A., Schade, G.W., Holzinger, R., Goldstein, A.H., A comparison of new measuremetns of total monoterpene flux with improved measurements of speciated monoterpene flux, *Atmos. Chem. Phys.* **5**(2005), pp. 505-513.

Lee, B.H. *et al.*, An iodide-adduct high-resolution time-of-flight chemical-ionization mass spectrometer: Application to atmospheric inorganic and organic compounds, *Environ. Sci. Technol.* **48**(2014a), pp. 6309-6317.

Lee, E.P.F. *et al.*, Spectroscopy of the simplest Criegee Intermediate CH2OO: Simulation of the first bands in its electronic and photoelectron spectra, *Chemistry-A. Euro. Journ.* **18**(2012), pp. 12411-12423.

Lee, L., Teng, A.P., Wennberg, P.O., Crounse, J.D., Cohen, R.C., On rates and mechanisms of OH and O_3 reactions with isoprene-derived hydroxy nitrates, *J. Phys. Chem. A* **118**(2014b), pp. 1622-1637.

Lerdau, M.T., Munger, J.W., Jacob, D.J., The NO_2 Flux Conundrum, *Science* **289**(2000), pp. 2291-2293.

Lewis, A.C., Bartle, K.D., Rattner, L., High-speed isothermal analysis of atmospheric isoprene and DMS using on-line two-dimensional gas chromatography, *Environmental Science and Technology* **31**(1997), pp. 3209-3217.

Lewis, A.C. *et al.*, A larger pool of ozone-forming carbon compounds in urban atmospheres, *Nature* **405**(2000), pp. 778-781.

Liao, J. *et al.*, High levels of molecular chlorine in the Arctic atmosphere, *Nature Geoscience* **7**(2014), pp. 91-94.

Lin, X., Trainer, M., Liu, S.C., On the nonlinearity of the tropospheric ozone, *J. Geophys. Res.* **93**(1988), pp. 15879-15888.

Lindinger, W., Jordan, A., Proton-transfer-reaction mass spectrometry (PTR-MS): on-line monitoring of volatile organic compounds at pptv levels, *Chem. Soc. Rev.* **27**(1998), pp. 347-375.

Lindsay, R.W., Richardson, J.L., Chamedies, W.L., Ozone trends in Atlanta, Georgia: Have emission controls been effective?, *JAPCA*(1989), pp. 40-43.

Liu, Z., Phillips, J.B., Comprehensive two-dimensional gas chromatography using an on-column thermal modulator interface, *J. Chromatogr. Sci.* **29**(1991), pp. 227-231.

Lockwood, A.L., Filley, T.R., Rhodes, D., Shepson, P.B., Foliar uptake of atmospheric organic nitrates, *Geophys. Res. Lett.* **35**(2008).

Lockwood, A.L., Shepson, P.B., Fiddler, M.N., Alaghmand, M., Isoprene nitrates: preparations, separation, identification, yields, and atmospheric chemistry, *Atmos. Chem. Phys.* **10**(2010), pp. 6169-6178.

Lovelock, J.E., Ionization methods for the analysis of gases and vapors, *Anal. Chem.* **33**(1961).

MacKenzie, A.R. *et al.*, The atmospheric chemistry of trace gases and particulate matter emitted by different land uses in Borneo, *Phil. Trans. R. Soc. B* **366**(2011), pp. 3177-3195.

Madronich, S., Implications of recent total atmospheric ozone measurements for biologically active ultraviolet radiation reaching the Earth's surface, *Geophys. Res. Lett.* **19**(1992), pp. 37-40.

Magnani, F. *et al.*, The human footprint in the carbon cycle of temperate and boreal forests, *Nature* **447**(2007), pp. 848-852.

Mao, J. *et al.*, Ozone and organic nitrates over the eastern United States: Sensitivity to isoprene chemistry, *J. Geophys. Res. Atmos.* **118**(2013), pp. 11256-11268.

Mao, J. *et al.*, Insights into hydroxyl measurements and atmospheric oxidation in a California forest, *Atmos. Chem. Phys.* **12**(2012), pp. 8009-8020.

Martin, R.F., General Deming regression for estimation systematic bias and its confidence interval in method-comparison studies, *Clinical Chemistry* **46**(2000), pp. 100-104.

McNair, H.M., Miller, J.M., *Basic Gas Chromatography*. John Wiley and Sons, New York, NY (1998).

Meehl, G.A. *et al.*, Global Climate Projections. *IPCC, 2007: Climate Change 2007: the physical science basis*, Cambridge University Press, Cambridge, UK/New York, NY USA (2007), pp. 746-846.

Mielke, L.H., Furgeson, A., Osthoff, H.D., Observations of $ClNO_2$ in a mid-continental urban environment, *Environ. Sci. Technol.* **45**(2011), pp. 8889-8896.

Mielke, L.H. *et al.*, Quantitative determination of biogenic volatile organic compounds in the atmosphere using proton-transfer reaction linear ion trap mass spectrometry, *Anal. Chem.* **82**(2010), pp. 7952-7957.

Min, K. *et al.*, Observations of atmosphere-biosphere exchange of total and speciated peroxynitrates: Nitrogen fluxes and biogenic sources of peroxynitrates, *Atmos. Chem. Phys.* **12**(2012), pp. 9763-9773.

Min, K.E. *et al.*, Eddy covariance fluxes and vertical concentration gradient measurements of NO and NO_2 over a ponderosa pine ecosystem: Observational evidence for within-canopy chemical removal of NO_x. *Atmos. Chem. Phys.* (2014), pp. 5495-5512.

Minarro, M.D. *et al.*, Study of the uncertainty in NO_2 chemiluminescence measurements due to the NO-O_3 reaction in sampling lines, **18**(2011), pp. 436-445.

Mincione, E., Lanciano, F., Thallium nitrate as a reagent for the conversion of epoxides into a-hydroxynitrate esters and for the cleavage of aliphatic ethers, *Tetrahedron Lett.* **21**(1980), pp. 1149-1150.

Murphy, J.G., Day, D.A., Cleary, P.A., Wooldridge, P.J., Cohen, R.C., Observations of the diurnal and seasonal trends in nitrogen oxides in the western Sierra Nevada, *Atmos. Chem. Phys.* **6**(2006), pp. 5321-5338.

Navas, M.J., Jimenez, A.M., Galan, G., Air analysis: determination of nitrogen compounds by chemiluminescence, *Atmos. Environ.* **31**(1997), pp. 3603-3608.

Ng, N.L. *et al.*, Effect of NO_x level on secondary organic aerosol (SOA) formation from the photooxidation of terpenes, *Atmos. Chem. Phys.* **7**(2007), pp. 5159-5174.

Ng, N.L. *et al.*, Secondary organic aerosol (SOA) formation from reaction of isoprene with nitrate radicals (NO_3), *Atmos. Chem. Phys.* **8**(2008), pp. 4117-4140.

Nguyen, M.T., Nguyen, T.L., Ngan, V.T., Nguyen, H.M., Heats of formation of the Criegee formaldehyde oxide and dioxirane, *Chem. Phys. Letts.* **448**(2007), pp. 183-188.

Nguyen, T.B. *et al.*, Rapid deposition of oxidized biogenic compounds to a temperate forest, *PNAS*(2015).

Nguyen, T.B., Laskin, J., Laskin, A., Nizkorodov, S.A., Nitrogen-containing organic compounds and oligomers in secondary organic aerosol formed by photooxidation of isoprene, *Environ. Sci. Technol.* **45**(2011), pp. 6908-6918.

Nightingale, J.A., Rogers, D.F., Barnes, P.J., Effect of inhaled ozone on exhaled nitric oxide, pulmonary function, and induced sputum in normal and asthmatic subjects, *Thorax* **54**(1999), pp. 1061-1069.

O'Brien, J.M. *et al.*, Measurements of alkyl and multifunctional organic nitrates at a rural site in Ontario, *J. Geophys. Res.* **100**(1995), pp. 22795-22804.

O'Neal, H.E., Blumstein, C., A new mechanism for gas phase ozone-olefin reactions, *Int. J. Chem. Kinetics.* **5**(2004), pp. 397-413.

Oliver, J.G.J. *et al.*, Description of EDGAR Version 2.0: A set of global emission inventories of greenhouse gases and ozone depleting substances for all anthropocentric and most natural sources on a per-county basis on a 1'1 degree grid. *RIVM Report 771060 002/TNO-MEP Report*, National Institute for Public Health and the Environment, Bilthoven, Netherlands (1996).

Ollinger, S.V., Aber, J.D., Reich, R.B., Freuder, R.J., Interactive effects of nitrogen deposition, tropospheric ozone, elevated CO_2 and land use history on the carbon dynamics of northern hardwood forests, *Global Change Biol.* **8**(2002), pp. 545-562.

Pankow, J.F. *et al.*, Volatilizable biogenic organic compounds (VBOCs) with two dimensional gas chromatography-time of flight mass spectrometry (GC x GC-TOFMS): sampling methods, VBOC complexity, and chromatographic retention data, *Atmos. Meas. Tech.* **5**(2012), pp. 345-361.

Parrish, D.D. *et al.*, The total reactive oxidized nitrogen levels and the partitioning between the individual species at six rural sites in eastern North America, *J. Geophys. Res.-Atmos.* **98**(1993), pp. 2927-2939.

Paulot, F. *et al.*, Isoprene photooxidation: new insights into the production of acids and organic nitrates, *Atmos. Chem. Phys.* **9**(2009), pp. 1479-1501.

Paulot, F., Henze, D.K., Wennberg, P.O., Impact of the isoprene photochemical cascade on tropical ozone, *Atmos. Chem. Phys.* **12**(2012), pp. 1307-1325.

Peeters, J., Boullart, W., Pultau, V., Vandenberk, S., Vereecken, L., Structure-activity relationships for the addition of OH to (poly)alkenes: Site-specific and total rate constants, *J. Phys. Chem. A* **111**(2007), pp. 1618-1631.

Peeters, J., Muller, J., Stavrakou, T., Nguyen, V.S., Hydroxyl radical recycling in isoprene oxidation driven by hydrogen bonding and hydrogen tunneling: The upgraded LIM1 mechanism, *J. Phys. Chem. A* **118**(2014), pp. 8625-8643.

Peeters, J., Vandenberk, S., Piessens, E., Pultau, V., H-atom abstraction in reactions of cyclic polyalkenes with OH, *Chemosphere* **38**(1999), pp. 1189-1195.

Penkett, S.A. *et al.*, The seasonal variation of nonmethane hydrocarbons in the free troposphere over the North Atlantic Ocean: Possible evidence for extensive reaction of hydrocarbons with the nitrate radical, *J. Geophys. Res.* **98**(1993), pp. 2865-2885.

Penuelas, J., Llusia, J., BVOCs: plant defense against climate warming?, *Trends Plant Sci.* **8**(2003), pp. 105-109.

Perring, A.E. *et al.*, Airborne observations of total $RONO_2$: new constraints on the yield and lifetime of isoprene nitrates, *Atmos. Chem. Phys.* **9**(2009a), pp. 1451-1463.

Perring, A.E., Pusede, S.E., Cohen, R.C., An observational perspective on the atmospheric impacts on alkyl and multifunctional nitrates on ozone and secondary organic aerosol, *Chemical Reviews* **113**(2013), pp. 5848-5870.

Perring, A.E. *et al.*, A product study of the isoprene+NO_3 reaction, *Atmos. Chem. Phys.* **9**(2009b), pp. 4945-4956.

Phillips, J.B., Beens, J., Comprehensive two-dimensional gas chromatography: a hyphenated method with strong coupling between the two dimensions, *J. Chromatog. A* **856**(1999), pp. 331-347.

Platt, U.F., Winer, A.M., Biermann, H.W., Atkinson, R., Pitts, J.N., Measurement of Nitrate Radical Concentrations in Continental Air, *Environ. Sci. Technol.* **18**(1984), pp. 365-369.

Pope III, C.A., Dockery, D.W., Health effects of fine particulate air pollution: Lines that connect, *J. Air Waste Manage.* **56**(2006), pp. 709-742.

Portmann, R.W., Solomon, S., Hegerl, G.C., Spatial and seasonal patterns in climate change, temperatures, and precipitation across the United States, *PNAS* **106**(2009), pp. 8835-8840.

Pratt, K.A. *et al.*, Contributions of individual reactive biogenic volatile organic compounds to organic nitrates above a mixed forest, *Atmospheric Chemistry and Physics* **12**(2012), pp. 10125-10143.

Presto, A.A., Huff Hartz, K.E., Donahue, N.M., Secondary organic aerosol production from terpene ozonolysis. 2. Effect of NO_x concentration, *Environ. Sci. Technol.* **39**(2005), pp. 7046-7054.

Pye, H.O.T., Chan, A.W.H., Barkley, M.P., Seinfeld, J.H., Global modeling of organic aerosol: the importance of reactive nitrogen (NO_x and NO_3), *Atmos. Chem. Phys.* **10**(2010), pp. 11261-11276.

Raivonen, M. *et al.*, Compensation point of NO_x exchange: Net result of NO_x consumption and production, *Agr. Forest Meteorol.* **149**(2009), pp. 1073-1081.

Raizenne, M. *et al.*, Health effects of acid aerosols on North American children: pulmonary function, *Environ Health Perspect* **104**(1996), pp. 506-514.

Raupach, M.R., Finnigan, J.J., Brunei, Y., Coherent eddies and turbulence in vegetation canopies: The mixing-layer analyogy, *Bound. Lay. Meteor.* **78**(1996), pp. 351-382.

Ridley, B.A., Grahek, F.E., A small, low flow, high-sensitivity reaction vessel for NO chemiluminescence detectors, *J. Atmos. and Ocean. Technol.* **7**(1990), pp. 307-311.

Ridley, B.A. *et al.*, Measurements and model simulations of the photostationary state during the Mauna Loa observatory photochemistry experiment: Implications for radical concentrations and ozone production and loss rates, *J. Geophys. Res.* **97**(1992a), pp. 10375-10388.

Ridley, B.A. *et al.*, Measurements and model simulations of the photostationary state during the Mauna Loa observatory photochemistry experiment: Implications for radical concentrations and ozone production and loss rates, *J. Geophys. Res.* **97**(1992b), pp. 10375-10388.

Rindelaub, J.D., McAvey, K.M., Shepson, P.B., The photochemical production of organic nitrates from α-pinene and loss via acid-dependent particle phase hydrolysis, **100**(2015), pp. 193–201.

Rindelaub, J.D. *et al*., Measurements of the hydrolysis of α-pinene nitrates and their products study, (2015), **in preparation**.

Rinsland, C.P., Zander, R., Farmer, B., Norton, R.H., Russell III, J.M., Concentrations of ethane (C2H6) in the lower stratosphere and upper troposphere and acetylene (C2H2) in the upper troposphere deduced from atmospheric trace molecule spectroscopy/space lab 3 spectra, *Journal Geophysical Research* **92**(1987), pp. 11951-11964.

Rivera-Rios, J.C. *et al.*, Conversion of hydroperoxides to carbonyls in field and laboratory instrumentation: Observational bias in diagnosing pristine versus anthropogenically controlled atmospheric chemistry, *Geophys. Res. Lett.* **41**(2014), pp. 8645-8651.

Rollins, A.W., Smith, J.D., Wilson, K.R., Cohen, R.C., Real time in situ detection of organic nitrates in atmospheric aerosols, *Environ. Sci. Technol.* **44**(2010), pp. 5540-5545.

Rolph, G.D., Real-time Environmental Applications and Display sYstem (READY) website (http://ready.arl.noaa.gov). NOAA Air Resources Laboratory, Silver Spring, MD (2014).

Rummel, U., Ammann, C., Gut, A., Meixner, F.X., Andreae, M.O., Eddy covariance measurements of nitric oxide flux within an Amazonian rain forest, *J. Geophys. Res. Atmos*. **107**(2002), pp. LBA 17-1-LBA 17-9.

Russell, A.R., Valin, L.C., Cohen, R.C., Trends in OMI NO_2 observations over the United States: effects of emission control technology and the economic recession, *Atmos. Chem. Phys.* **12**(2012), pp. 12197-12209.

Sadanaga, Y. *et al.*, Development of a selective light-emitting diode photolytic NO_2 converter for continusously measuring NO_2 in the atmosphere, *Anal. Chem.* **82**(2010), pp. 9234-9239.

Saunders, S.M., Jenkin, M.E., Derwent, R.G., Pilling, M.J., Protocol for the development of the Master Chemical Mechanism, MCM v3 (Part A): tropospheric degradation of non-aromatic volatile organic compounds, *Atmos. Chem. Phys.* **3**(2003), pp. 161-180.

Saylor, R.D., The Atmospheric Chemistry and Canopy Exchange Simulation System (ACCESS): model description and application to a temperate deciduous forest canopy, *Atmos. Chem. Phys.* **13**(2013), pp. 693-715.

Schmid, H.P., Su, H.B., Vogel, C.S., Curtis, P.S., Ecosystem-atmosphere exchange of carbon dioxide over a mixed hardwood forest in northern lower Michigan, *J. Geophys. Res.-Atmos.* **108**(2003), pp. 4417-4436.

Schoenbein, C.F., Recherche sur la nature de I'odeur qui se manifeste dans certaines actions chimiques, *Comptes Rendus des Seances Paris* **10**(1840), pp. 706-710.

Seco, R., Penuelas, J., Filella, I., Short-chain oxygenated VOCs: Emission and uptake by plants and atmospheric sources, sinks, and concentrations, *Atmospheric Environment* **41**(2007), pp. 2477-2499.

Seok, B., Helmig, D., Ganzeveld, L., Williams, M.W., Vogel, C.S., Dynamics of nitrogen oxides and ozone above and within a mixed hardwood forest in northern Michigan, *Atmos. Chem. Phys.* **13**(2013), pp. 7301-7320.

Shen, Y., Lee, M.L., General equation for peak capacity in column chromatography, *Anal. Chem.* **70**(1998), pp. 3853-3856.

Shepson, P.B., Bottenheim, J.W., Hastie, D.R., Venkatram, A., Determination of the relative ozone and PAN deposition velocities at night, *Geophys. Res. Lett.* **19**(1992), pp. 1121-1124.

Sillman, S., Logan, J.A., Wofsy, S.C., The sensitivity of ozone to nitrogen oxides and hydrocarbons in regional ozone episodes, *J. Geophys. Res. Atmos.* **95**(1990), pp. 1837-1851.

Smith, N., Plane, J.M.C., Nien, C.-F., Solomon, P.A., Nighttime radical chemistry in the San Joaquin Valley, *Atmospheric Environ.* **29**(1995), pp. 2887-2897.

Sommariva, R. *et al.*, Modelled and measured concentrations of peroxy radicals and nitrate radical in the U.S. Gulf Coast region during TexAQS 2006, *J. Atmos. Chem.* **68**(2011), pp. 331-362.

Sparks, J.P., Monson, R.K., Sparks, K.L., Lerdau, M., Leaf uptake of nitrogen dioxide (NO_2) in a tropical wet forest: Implications for tropospheric chemistry, *Oecologia* **127**(2001), pp. 214-221.

Spicer, C.W. *et al.*, Unexpectedly high concentrations of molecular chlorine in coastal air, *Nature* **394**(1998), pp. 353-356.

Stark, H. *et al.*, Influence of nitrate radical on the oxidation of dimethyl sulfide in a polluted marine environment, **112**(2007).

Starn, T.K. *et al.*, Observations of isoprene chemistry and its role in ozone production at a semirural site during the 1995 Southern Oxidants Study, *J. Geophys. Res.* **103**(1998), pp. 22425-22435.

Stull, R.B., *An Introduction to Boundary Layer Meterology*. Kluwer Academic Publishers, Dordrecht, Netherlands (1988) 670 pp.

Stutz, J. *et al.*, Nocturanl NO_3 radical chemistry in Houston, TX, *Atmospheric Environment* **44**(2010), pp. 4099-4106.

Su, Y., Liu, W., Liao, W., Chiang, S., Wang, J., Full-range analysis of ambient volatile organic compounds by a new trapping method and gas chromatography/mass spectrometry, *J. Chromato. A* **1218**(2011), pp. 5733-5742.

Surratt, J.D. *et al.*, Reactive intermediates revealed in secondary organic aerosol formation from isoprene, *PNAS* **107**(2010), pp. 6640-6645.

Taatjes, C.A., Shallcross, D.E., Percival, C.J., Research frontiers in the chemistry of Criegee intermediates and tropospheric onzonolysis, *Phys. Chem. Chem. Phys.* **16**(2014), pp. 1704-1718.

Takekawa, H., Minoura, H., Yamazaki, S., Temperature dependence of secondary organic aerosol formation by photo-oxidation of hydrocarbons, *Atmos. Environ.* **37**(2003), pp. 3413-3424.

Tang, H., Takigawa, M., Liu, G., Zhu, J., Kobayashi, K., A projection of ozone-induced wheat production loss in China and India for the years 2000 and 2020 with exposure-based and flux-based approaches, *Global Change Biolo.* **19**(2013), pp. 2739-2752.

Taraborrelli, D. *et al.*, Hydroxyl radical buffered by isoprene oxidation over tropical forests, *Nature Geosciences* **5**(2012), pp. 190-193.

Thompson, A.M., The oxidizing capacity of the Earth's atmosphere-Probable past and future changes, *Science* **256**(1992), pp. 1157-1165.

Thomson, G.W., *Techniques of Organic Chemistry*, 3rd ed, New York (1959).

Thornberry, T. *et al.*, Observations of reactive oxidized nitrogen and speciation of NO_y during the PROPHET summer 1998 intensive, *J. Geophys. Res.* **106**(2001), pp. 24359-24386.

Thornton, J.A. *et al.*, A large atomic chlorine source inferred from mid-continental reactive nitrogen chemistry, *Nature* **464**(2010), pp. 271-274.

Thornton, J.A., Wooldridge, P.J., Cohen, R.C., Atmospheric NO_2: In situ laser-induced fluorescence detection at parts per trillion mixing ratios, *Anal. Chem.* **72**(2000), pp. 528-539.

Thornton, J.A. *et al.*, Ozone production rates as a function of NO_x abundances and HO_x production rates in the Nashville urban plume., *J. Geophys. Res.* **107**(2002), pp. 4146-4162.

Tranchida, P.Q. *et al.*, A direct sensitivity comparison between flow-modulated comprehensive 2D and 1D GC in untargeted and targeted MS-based experiments, *J. Separation Sci.* **36**(2013), pp. 2746-2752.

Tucker, W.A., Nelken, L.H., Diffusion Coefficients in Air and Water. in: Lyman, W.J., Reehl, W.F., Rosenblatt, D.H. (Eds.), *Handbook of Chemical Property Estimation Methods*, American Chemical Society, Washington, DC (1990), pp. 1-25.

Turnipseed, A.A. *et al.*, Eddy covariance fluxes of peroxyacetyl nitrates (PANs) and NO_y to a coniferous forest, *J. Geophys. Res.-Atmos.* **111**(2006).

Venkatramani, C.J., Phillips, J.B., Comprehensive two-dimensional gas chromatography applied to the analysis of complex mixtures, *J. Microcolumn Separations* **5**(1993), pp. 511-516.

Vereecken, L., Francisco, J.S., Theoretical studies of atmospheric reaction mechanisms in the troposphere, *Chem. Soc. Rev.* **41**(2012), pp. 6259-6293.

Volz, A., Kley, D., Evaluation of the montsouris series of ozone measurements made int he 19th-century, *Nature* **332**(1988), pp. 240-242.

von Kuhlmann, R., Lawrence, M.G., Poschl, U., Crutzen, P.J., Sensitivities in global scale modeling of isoprene, *Atmos. Chem. Phys.* **4**(2004), pp. 1-17.

Walega, J.G., Dye, J.E., Grahek, F.E., Ridley, B.A., A compact measurement system for the simultaneous determination of NO, NO_2, NO_y, and O_3 using a small aircraft, *Measure. Atmos. Gases* **1433**(1991), pp. 232-241.

Wang, Y.P., Leuning, R., A two-leaf model for canopy conductance, photosynthesis, and partitioning of available energy I: Model description and comparison with a multi-layered model, *Agr. Forest Meterol.* **91**(1998), pp. 89-111.

Wang, Z. *et al.*, Lidar measurement of planetary boundary layer height and comparison with microwave profiling radiometer observation, *Atmos. Meas. Tech.* **5**(2012), pp. 1965-1972.

Weaver, C.P. *et al.*, A preliminary synthesis of modeled climate change impacts on U.S. regional ozone concentrations, *Am. Meteorol. Soc.* **90**(2009), pp. 1843-1863.

Williams, B.J., Goldstein, A.H., Kreisberg, N.M., Hering, S.V., An In-situ instrument for speciated organic composition of atmospheric aerosols: Thermal Desorption Aerosol GC/MS-FID (TAG), *Aerosol Science and Technology* **40**(2006), pp. 627-638.

Williams, J. *et al.*, Regional ozone from biogenic hydrocarbons deduced from airborne measurements of PAN, PPN, and MPAN, *Geophys. Res. Lett.* **24**(1997), pp. 1099-1102.

Winer, A.M., Peters, J.W., Smith, J.P., Pitts, J.N., Response of commerical chemiluminescent NO-NO_2 analyzers to other nitrogen-containing compounds, *Environ. Sci. Technol.* **8**(1974).

Wolfe, G.M. *et al.*, Missing peroxy radical sources within a rural forest canopy, *Atmos. Chem. Phys.* **14**(2013), pp. 4715-4732.

Wolfe, G.M., Thornton, J.A., The Chemistry of Atmosphere-Forest Exchange (CAFE) Moodel- Part 1: Model description and characterization, *Atmos. Chem. Phys.* **11**(2011), pp. 77-101.

Wolfe, G.M., Thornton, J.A., McKay, M., Goldstein, A.H., Forest-atmosphere exchange of ozone: sensitivity to very reactive biogenic VOC emissions and implications for in-canopy photochemistry, *Atmos. Chem. Phys.* **11**(2011), pp. 7895-7891.

Wolfe, G.M. *et al.*, Eddy covariance fluxes of acyl peroxy nitrates (PAN, PPN, and MPAN) above a ponderosa pine forest, *Atmos. Chem. Phys.* **9**(2009), pp. 615-634.

Wu, S. *et al.*, Why are there large differences between models in global budgets of tropospheric ozone, *J. Geophys. Res.* **112**(2007).

Xu., X. *et al.*, Comprehensive two-dimensional gas chromatography (GCxGC) measurements of volatile organic compounds in the atmosphere, *Atmos. Chem. Phys.* **3**(2003), pp. 665-682.

Xie, Y. *et al.*, Understanding the impact of recent advances in isoprene photooxidation on simulations of regional air quality, *Atmos. Chem. Phys.* **13**(2013), pp. 8439-8455.

Xiong, F., Pratt, K., Rivera, C., Shepson, P.B., Observations and insights into isoprene nitrate chemisty, *Atmos. Chem. Phys.* **in prep**(2015).

Xu, L., Kollman, M.S., Song, C., Shilling, J.E., Ng, N.L., Effects of NO_x on the volatility of secondary organic aerosol from isoprene photooxidation, *Environ. Sci. Technol.* **48**(2014), pp. 2253-2262.

Yan, X., Ohara, T., Akimoto, H., Statistical modeling of global soil NO_x emissions, *Global Biogeochem. Cycles* **19**(2005).

Yienger, J.J., Levy, H., Empirical-model of global soil-biogenic NO_x emissions, *J. Geophys. Res.-Atmos.* **100**(1995), pp. 11447-11464.

Zhang, L. *et al.*, Nitrogen deposition to the United States: distribution, sources, and processes, *Atmos. Chem. Phys.* **12**(2012), pp. 4539-4554.

Zhang, R., Xuexi, T., Bond, D., Impacts of anthropogenic and natural NO_x sources over the U.S. on tropospheric chemistry, *PNAS* **100**(2003), pp. 1505-1509.

VITA

VITA

Kevin McAvey was born in San Antonio, TX in 1987 to Kathleen and Timothy McAvey. He is the youngest in the family, with two brothers, James and Christopher. He moved from San Antonio, TX to Westfield, NY, then to Binlock, Germany, Manheim, Germany, West Point, NY, Fort Polk, LA, Leesville, LA, Baton Rouge, LA, New Orleans, LA, and then to West Lafayette, IN.

Kevin attended Leesville High School and graduated with honors. He then attended the University of New Orleans on a Chancellor's Scholarship majoring in Chemistry. He worked at the University of New Orleans's Office of Admissions and in the laboratory of Dr. Richard Cole while obtaining his Bachelor's Degree. Upon graduating Cum Laude from the University of New Orleans, he choose to attend Purdue University to pursue a PhD in analytical chemistry.

PUBLICATION

PUBLICATION

(To be submitted for publication)

The Morning NO_x Maximum in the Forest Atmosphere Boundary Layer

M. Alaghmand[1], K.McAvey[2], J. Geddes[3], J. Murphy[3], P. B. Shepson[2,4,5], T. K. Starn[6], B. T. Jobson[7], W. Wallace[7], M. A. Carroll[8], S. B. Bertman[9], B. Lamb[7], S. Edburg[7], X. Zhou[10], E. Apel[11], D. Riemer[12], P. Stevens[13], and F. Keutsch[14]

1. University of Maryland, Department of Chemistry, College Park, MD, USA

2. Purdue University, Department of Chemistry, West Lafayette, IN, USA

3. University of Toronto, Department of Chemistry, Toronto, ON, CA,

4. Purdue University, Department of Earth, Atmospheric, and Planetary Sciences, West Lafayette, IN , USA

5. Purdue University, Purdue Climate Change Research Center, West Lafayette, IN, USA

6. West Chester University, Department of Chemistry, West Chester, PA, USA

7. Washington State University, Department of Civil and Environmental Engineering, Pullman, WA, USA

8. University of Michigan, Dept. of Atmospheric, Oceanic, and Space Sciences, Ann Arbor, MI, USA

9. Western Michigan University , Department of Chemistry, Kalamazoo, MI, USA

10. Wadsworth Center, SUNY-Albany, NY, USA

11. National Center for Atmospheric Research, Boulder, CO, USA

12. RSMAS, University of Miami, FL, USA

13. Indiana University, School of Public and Environmental Affairs, Bloomington, IN, USA

14. University of Wisconsin, Madison, Dept. of Chemistry, Madison, WI, USA

Abstract

During the 1998, 2000, 2001, 2008, 2009, and 2012 summer intensives of the Program Research on Oxidants: PHotochemistry, Emissions and Transport (PROPHET), ambient measurements of nitrogen oxides ($NO + NO_2 = NO_x$) were conducted. NO and NO_xmole fractions displayed a diurnal pattern with NO_x frequently highest in the early morning. This pattern has often been observed in other rural areas. In this paper, we discussthe potential sources of the frequently observed morning pulse of NO and NO_x, and the potential role of various contributing factors, (i.e. downward mixing, soil and canopy emissions, local pollution, and long range transport) through multiple height measurements, flux measurements, and measurements of other trace gases including CO and volatile organic compounds. We find that the behavior of the NO_x in the early morning hours represents multiple phenomena related to the thermodynamic stability in the nocturnal boundary layer (NBL). We find that the downward transport of NO_x significantly contributes to rises in early morning NO_x mole ratios.

Introduction

A wide variety of environmental and health impacts result from the emission of NO_x ($NO + NO_2$) into the atmosphere, including acidic deposition (Galloway et al. 2008),

stimulation of forest growth (Ollinger et al. 2002, Magnani et al. 2007, Lockwood et al. 2008, Costa et al. 2011) including a potentially strong impact on the atmospheric CO_2 "fertilization effect" (Norby et al. 2010), production of ozone, and altering (indirectly and directly) atmospheric aerosol concentrations(Hallquist et al. 2009). Continental atmospheric boundary layer environments typically have NO_x concentrations of 1-3 ppb (Parrish et al. 1993, Thornberry et al. 2001), while clean, remote locations have very low NO_x concentrations ranging between 4 and 50 ppt(Kondo et al. 1996). NO_xregulates photochemical production of tropospheric ozone, and hydroxyl and peroxy radical concentrations directly and indirectly (Lin, Trainer, and Liu 1988, Thompson 1992, Ridley et al. 1992, Thornton et al. 2002). When nitric oxide (NO) is converted to nitrogen dioxide (NO_2) by oxidants other than ozone, such as hydroperoxyl radicals (HO_2) or organic peroxy radicals (RO_2), a net photochemical production of ozone results (Ridley et al. 1992, Thornton et al. 2002). NO_x chemistry, in the presence of other species such as biogenic volatile organic compounds (BVOCs)(Rollins et al. 2010), NH_3(Dentener and Crutzen 1994), and humidity produces nitric acid and aerosol. Thus, through connection to ozone and aerosol production, and through impacts on the carbon cycle, nitrogen chemistry is linked to changes in climate. Understanding the sources and fate of NO_x and the distribution of odd nitrogen species is important for quantifying human impacts on both atmospheric composition and climate.

There is still a large uncertainty in the determination of the sources, sinks, and chemistry of NO_x due to the complex chemistry and dynamics of the sources and sinks and a lack of direct observations (Geddes and Murphy 2014). Due to the differences between observed NO_x concentrations below the canopy and O_3 concentrations above the

canopy, many large scale models impose an ad-hoc canopy reduction factor which has been seen in field studies(Jacob and Wofsy 1990, Yienger and Levy 1995, Wang and Leuning 1998, Fang and Mu 2006). Alternatively, studies have shown that leaf surfaces can either act as a NO_x source or sink, depending on whether ambient concentrations of NO_x reach a compensation point (Conrad 1996). Compensation points have been shown to range between 0.1-3 ppb (Sparks et al. 2001, Raivonen et al. 2009, Breuninger et al. 2012, Chapparo-Suarez, Meixner, and Kesselmeier 2011). Along with the limited understanding of the biogeochemical process which produce or consume NO_x, much uncertainty remains in the chemical processing of NO_x, including the formation and fate of organic nitrates in the boundary layer (Paulot et al. 2009, Lockwood et al. 2010, Mao et al. 2013).To better understand the chemistry, biological, and meteorological phenomena controlling NO_x concentrations, methods such as measurements at multiple heights (discussed within), flux measurements of NO_y ($NO + NO_2 + NO_3 + HONO + HNO_3$ + all other oxidized nitrogen species) (Turnipseed et al. 2006, Wolfe et al. 2009, Min et al. 2012), and development and use of instrumentation for NO_x flux measurements (Farmer, Wooldridge, and Cohen 2006, Min et al. 2014) have been recently developed.

Since 1997 we have been conducting measurements of NO_x, O_3, VOCs, and radicals as part of the Program for Research on Oxidants: PHotochemistry, Emissions and Transport (PROPHET)) at the University of Michigan Biological Station (UMBS), situated near the tip of the Michigan lower peninsula in a mixed deciduous/coniferous forest site(Carroll, Shepson, and Bertman 2001). At this site, a morning NO_x peak at the sampling location above the forest canopy is routinely observed as shown in Figure 1. A morning NO_x peak has been observed at other surface sites that are removed from

anthropogenic sources(Martin et al. 1991, Parrish et al. 1993, Thornberry et al. 2001). Parrish et al. (1993) reported that the [NO]/[NO_y] peaked in the early morning when NO_2photo-dissociated rapidly. Thornberry et al. (2001) hypothesized that during the breakup of the nocturnal boundary layer (NBL) in the morning, air aloft is mixed down to the surface, resulting in an increase of NO_x at the surface for sites such as PROPHET, where local emissions are small. Day et al. (2009) observed and explained a morning NO_x peak as resulting from the break-up of the NBL and downward mixing of air from the residual layer. However, this hypothesis does not always explain the PROPHET observations, since the morning NO_x peak often starts before sunrise. (i.e. well before the NBL breakup). In addition, there are some cases during which turbulence data do not support interpretation of the morning NO_x peak via downward mixing of polluted air to the surface. There are a number of possible contributors to the observed morning NO_x peak, including: photolysis of highly photo-labile substance that have deposited onto the canopy during nighttime (Zhou et al. 2011); downward mixing of polluted air from the residual layer to the surface when the NBL breaks up(Day et al. 2009), local scale combustion, long-range transport of polluted air, and soil NO_x emissions(Conrad 1996, Ganzeveld et al. 2006). Here, we set out to evaluate these possibilities to identify the underlying cause of this phenomenon and discuss the supporting data and implications. This study leverages a range of observations from the UMBS PROPHET tower site (Carroll, Shepson, and Bertman 2001)situated near the tip of the Michigan lower peninsula in a mixed deciduous/coniferous forest site.

Experimental

Field studies with relevant and supporting data were conducted in the summers of 1998, 2000, 2001, 2008, 2009, and 2012 at the PROPHET measurement site (Carroll, Shepson, and Bertman 2001). This site consists of a 31.5 m tall scaffolding tower located in a rural mixed deciduous/coniferous forested area near the northern tip of the lower peninsula of Michigan (45.559°N, 84.715°W). The typical canopy height is ~22m and is dominated by aspen, with some maple, oak, birch, beech and a successional undergrowth of white pine (Gough et al. 2007). A range of measurements of NO_x, NO_y, PAN, O_3, aerosol, CO, VOCs, radiation, temperature and wind speed/direction are available to aid in the pursuit of this issue. Most instrumentation was located in the PROPHET laboratory building at the base of the tower. For most instruments air was sampled from a port on the lowest segment of the common 5 cm ID Pyrex manifold that drew air from a height of 35 m into the laboratory building at the base of the tower with a residence time of < 2 s (Carroll, Shepson, and Bertman 2001).

In 2008 and 2012, NO_x was measured using a custom built NO chemiluminescence analyzer, constructed as described by Ridley and Grahek (1990). For that instrument, chemiluminescence photons were detected using a Burle Industries 8852 photomultiplier tube. The instrument incorporates a blue light LED NO_2 photolytic converter. Artifact tests were conducted to assess the background from chemiluminescence generated by ozone reaction with other atmospheric compounds other than NO. In 2008, artifact test were done before each ambient air sample measurement. In 2012, artifact tests were performed every 30 minutes. The NO_2

converter, which has two blue light photodiodes on either end of the converter, photolyzes NO_2 to NO. The 395 nm wavelength output of the photodiodes makes the converter very selective for NO_2 because interferences (HONO and NO_3) poorly absorb energy in the photodiode output wavelength range. The average NO_2 conversion efficiency for a flow rate of 1.2 slpm was determined to be 28.6±0.9% in 2008. In 2012, a new photolytic converter from Air Quality Designs (Wheat Ridge, CO) was used with a converter efficiency of 56±6%. The instrument was calibrated daily by dilution of 5.0 ppm NO in nitrogen standard (Praxair) with ultra-zero air. An independent calibration using a separate NO standard (5 ppm; Praxair) was used to evaluate the accuracy of the standards. These two standards differed by 2%. The 3σ, 1 minute average detection limit for the 2008 study for NO and NO_2 was 7 ppt. In 2012, two equal length 100 ft Teflon sampling lines were connected to a Hamilton 4 port valve to allow for the measurement of NO_x at two different heights. In 2001, NO_x and NO_y were measured via a similar instrument, as described by Thornberry et al. (2001).

In 2009 NO and NO_2 were measured simultaneously by a 2-channel chemiluminescence instrument (Air Quality Design) with a blue light LED converter for NO_2. Sensitivity calibrations were performed daily using standard addition of 10 sccm NO calibration gas 101.4 ppmv±1 % NIST traceable from Scott-Marrin, Inc. The blue light NO_2 converter was calibrated by gas phase titration of the NO calibration gas to NO2 using ozone, and the average conversion efficiency was ~60%. The average sensitivity was ~4 counts per pptv and 5 counts per pptv on the NO and NO2 channels, respectively. The background counts were 1300 for the NO channel and 1500 for the NO2 channel. The minimum detection limits defined as 3 time the standard deviation of a

50 second zero air measuremtn were 25 pptv for NO and 33 pptv for NO_2. Sampling was done from 3 separate PFA Teflon inlets to measure the vertical gradients through the canopy. The sampling heights were 6m, 20m, and 34 m. The diameters of the PFA tubes were ½" for the 6-m and 20-m tubes and 5/8" for the 34 m tube. The flow rates were approximately 80 slpm for the ½" tubes and 130 slpm for the 5/8" tube. An automated valve system cycled a 10 min sampling duration sequentially from each inlet for approximately 3 weeks.

In 2012, a two-channel chemiluminescence flux instrument (Air Quality Design, Inc.) was used to measure the flux of NO, NO_2, and NO_y at 34 m. Details of this instrument and measurements can be found in Geddes and Murphy (2014). A single 50 m line was connected to an inlet containing a molybdenum and flux rate photolytic converter (Air Quality Design, Inc.). NO was measured with one channel while the other inlet was switched between the Mo and photolytic converter. Flux measurements and calculations are described in detail in Geddes and Murphy (2014).

Benzene and toluene were measured by GC/MS, as described by Apel et al. (2002). Aerosol size distributions were measured using a Scanning Mobility Particle Sizer (SMPS), deployed on the tower at a height of 26 m., 4 m above the average canopy height. The sampling inlet consisting of 7 m of ¼″ outer diameter (0.028" wall) Tygon tubing. A GAST pump was used to create a fast flow rate, while the SMPS sampled from a tee connected to the tubing that led to the pump. The flow rate of the pump was set to 1.5 L/min using a needle valve. Size distribution data were collected every 5 minutes, continuously, except during periods of vertical profiling within the forest canopy.

A TECO 49C Ozone monitor was employed to determine ozone, with a precision of ~1 ppb. CO concentrations in 2001 were determined using a TECO 48C. PAN was determined using a GC-ECD instrument, as described in (Pippin et al. 2001).

Results and discussion

Figure 1 presents the diurnal average (hourly) NO_x and radiation observed at the PROPHET site during summer 2008. Figure 1S (see supplementary information) shows some example observations at PROPHET 2008. As shown in Figure 1 there is, on average, an increase of ~1 ppb of NO_x at the tower sampling inlet (i.e. 34m, ~12m above canopy height) with a maximum around 7 am local time. Significantly, we observe the average NO_x, and as shown in individual cases below, to begin to increase before sunrise (as NO_2). A plot of the frequency of the time of day for the maximum in NO_x is shown in Figure 2. While the peak in Figure 2 occurs at 0730 (EST), there are significant numbers of events that occur with earlier maxima, when the atmosphere is still quite stable. The timing of the peak in NO_x is at or near the end of the time of day prior to breakup of the NBL due to solar heating. For the time period 0400-0800, the distribution of NO_x observations is very broad, with a peak at 600-800 ppt, but extending out to ~3000 ppt; in contrast, the midday distribution is rather sharp, with a peak in the 500-900 ppt range, with essentially no observations for $[NO_x]$>2000 ppt (data not shown).

The increase in NO in the morning can be readily explained by photolysis of NO_2, and the photostationary state relationship (reactions 1-3) and Equation I.

$$NO_2 + h\nu \longrightarrow NO + O(^3P) \quad (1)$$

$$O(^3P) + O_2 \longrightarrow O_3 \quad (2)$$

$$O_3 + NO \longrightarrow NO_2 + O_2 \quad (3)$$

$$[NO]_{pss} = J_{NO2}[NO_2]/k_3[O_3] \quad I$$

As an example, in Figure 3a we show the observed [NO], along with the calculated $[NO]_{pss}$ from Equation I, for July 1st, 2008. Figure 3b shows the calculated J_{NO2}, and observed O_3 mole fraction for that day. As shown in Figure 3a, $[NO]_{pss}$ has the same shape and comparable magnitude as the observed [NO] in the morning, and thus photolysis of NO_2 can explain the morning NO peak. While NO_2 photolysis can explain the NO peak, it does not explain the morning NO_x peak. The NO_x peak often begins before sunrise. Below we discuss each of the potential mechanisms that could explain a morning NO_x peak.

HONO production and photolysis

As discussed by many in the past, HONO is produced on a variety of surfaces (Sakamaki, Hatakeyama, and Akimoto 1983, Finlayson-Pitts et al. 2003, Zhou et al. 2002, Zhou et al. 2011), e.g. as shown in reaction 4. If sufficient HONO were produced on forest canopy surfaces and released to the stable boundary layer, photolysis upon sunrise (reaction 5) could account for some of the NO_x.

$$2NO_2 + H_2O \longrightarrow HNO_3 + HONO \quad (4)$$

$$HONO + h\nu \longrightarrow NO + OH \quad (5)$$

To test this, we calculated the total possible production of NO_x from HONO photolysis for the average data, using the HONO observations for July 23, 2008; J_{HONO}[HONO] was integrated over the period 3:35 am to 7:10 am, during which [HONO] was 20-25 ppt, and during which NO_x increased by 611 ppt, from about 1100 ppt. Integrated HONO photolysis over this period yielded a total NO_x production of ~84 ppt, only 14% of the observed 611 pptv increase in NOx., We note that we used clear sky J_{HONO} values for this calculation, so our NO_x production from HONOphotoxidation is a maximum. Interestingly, [HONO] increases through the morning with radiation at this site, and thus photo-induced HONO production is much more important than the dark production. Thus while HONO production and photolysis is significant, (especially as an OH source) it appears to represent only a minor source of NO_x production at the surface at this site.

It should be noted that it has been shown that HONO can react with oxygen radicals, hydrogen radicals (Tsang and Herron 1991, Hsu, Lin, and Mebel 1997), NO_3(Wallington and Japar 1989), and OH radical (Atkinson et al. 2004) to form NO_2. These reactions could lead to the possible release of NO_x from HONO stored on leaf surfaces. However, many of these compounds are found in small abundance at the site, and the rate constants of these reactions are relatively small and where not looked at in further detail.

Anthropogenic sources

A possible source of the early morning $NO_x$is long range transport of aged polluted air from anthropogenic sources, e.g., for UMBS, from Detroit or Chicago. A good marker for anthropogenic pollution is toluene, a significant mobile source pollutant.

In Figure 4 we show an example case for Aug. 8, 1998. As shown in the figure, there is an increase in NO_x during the time that O_3 is decreasing in the NBL due to dry deposition. As shown, toluene increases with NO_x, in support of this hypothesis. In Figure 5a, we show the 24hr. isentropic back trajectory (HYSPLIT) showing that the air sampled likely transported at or very near the surface through the night, with an origin in the Detroit metropolitan area. This 24 hour back trajectory is highly conservative, as the lifetime of the conversion of NO_x to organic nitrates or HNO_3 is on the range of 3-10 hours (Min et al. 2014). This hypothesis is only supported if all early morning NO_x plumes have back trajectories that pass through polluted urban regions. We find this not to be the case. Figure 5b shows the 12 hour back trajectory for the morning of August 13th, 2012, and shows the air mass that was sampled passed over Lake Michigan. Back trajectories for other mornings show air masses that traversed over Lake Superior, rural Canada, and rural parts of Wisconsin (data not shown). None of those locations are a known significant source of anthropogenic NO_x, and mean the likely source of the early morning NO_x is not from long range transport.

Upward mixing from surface sources

Apossible source of the early morning NO_x plume is ground or canopy based sources of NO that slowly diffuse upward past the inlet, in the relatively stable night air, and passes the inlet at semi-random times, but are enhanced by sunrise-mediated turbulence. NO flux data obtained by Carleton and Carroll [unpublished data, 2003] indicates a soil flux in this forest of, on average, ~180 nmoles/m^2-hr. If that NO_x mixes into a 40m layer (i.e. up to roughly the tower inlet height) over a 6 hour period (i.e. from

sunset to the typical time of observation of the NO_x increase), this is the equivalent of ~0.7 ppb, within the range of observations. Of course it is more likely that the NO_x emitted would be more stratified and thus the peak concentrations observed as the NO_x-enriched air moves upward past the tower inlet could be greater than this. This then implies that soil emissions followed by upward mixing is one significant possibility. However, recent measurements by Min et al. (2014) show significant in-canopy NO_x chemistry that reduces the amount of NO_x soil emissions that reach sampling inlets located above the canopy.

In the summer of 2009, we conducted vertical profile measurements of NO_x in the below-canopy environment. In Figure 6 we show average of NO_x data at the surface (6-m), at mid-canopy level (20-m), and above the canopy (at 34-m). This plot shows that on average, there is more NO_x at the 34-m height than below. Such an average plot can, however, be impacted by transport events carrying large concentrations just above the canopy, as discussed below. In Figure 7 we show a histogram of the gradients in NO_x for 2009 observations, defined here as $[NO_x]_{20m} - [NO_x]_{6m}$. As shown in Figure 5, while the mode of the distribution represents the no-gradient case, ~41% of the time there is a gradient that would lead to an upward flux of NO_x from the surface.

This trend was not seen in the summer of 2012. Vertical profiles of NO_x measured during the summer of 2009 and as described in Seok et al. (2013) both lacked the time resolution to accurately identify NO_x sources. Typical in-canopy mixing times are ~100 s(Kim et al. 2013, Min et al. 2014) well below the sampling time of the 2009 vertical profile measurements and measurements described in Seok et al. (2013) (10 min

sampling period and 5 min sampling period, respectively). In the summer of 2012, NO_x measurements were made at a height of 31.5 m constantly while another chemiluminescent NO_x instrument switched measurements between 1.5 m and 18 m. In this method, the NO_x gradient profile could be observed on a smaller timescale, with observations within a minute of each other. NO_x mole ratios from August 8th, 2012, August 13th, 2012, and August 14th, 2012are shown in Figure 8a, 8b, and 8c. This day shows a clear increase in the concentration of NO_x above the canopy (31.5 m) before any increase can be seen within the canopy (18 m) or near the forest floor (1.5 m).This suggests that the increase in the concentration of early morning NO_x is due from a source above the canopy, and not from soil emissions. During the mornings observed in the summer of 2012, the concentration of NO_x at 1.5 m wasconsistently lower than the concentration of NO_x measured at 34 m during a morning. Figure 9 shows the ratio of NO_x measured at 31.5 m over 18 m and 1.5 m as a function of time. It can clearly be seen that there is a clear increase in the concentration of NO_x above the forest canopy that cannot be seen below the forest canopy. This leads to the belief that the source of the early morning NO_x is downward mixing of polluted air from the residual layer during the breakup of the NBL.

Downward mixing of polluted air

As discussed by Hastie et al. (1993) and others, the NBL is statically stable, with a positive lapse rate that can be as much as 0.04K/m (see Figure 10, for July 23/24, 2008; this was a typical clear sky night, with a large NO_x peak before sunrise, see Fig. 11).

This isolates the air near the surface from that aloft, resulting in exponential decay in concentrations of various pollutants at the surface, due to dry depositional loss. Downward mixing of polluted (i.e. high NO_x) air from aloft, e.g. from within the residual layer, or from nocturnal jets (Singh, McNider, and Lin 1993), may result in an increase in [NO_x] (or other species that are relatively surface-depleted) at the surface. If this were the case, we can lay out the following scenario: within the polluted layer aloft would be excess CO (if the source is combustion) as well as excess PAN and O_3, relative to the surface layer (i.e. tower height) concentrations, due to dry depositional loss of PAN and O_3 from the surface layer during the time prior to the occurrence of the peak (Hastie et al. 1993). A viable hypothesis is that downward mixing of air not subject to dry depositional losses, or of transported more polluted air, would cause an increase of these species observed at the surface. In Figure 12 we present the diurnal average of CO, NO_x and radiation observed for the summer of 2001. As shown in the figure at the time of the NO_x maximum, CO is flat, and typically less variable than during daytime, inconsistent with downward mixing of polluted air. It is noteworthy that beginning at ~8:00 am, i.e. a time typically associated with the start of the NBL breakup, NO_x actually decreases, likely from dilution with cleaner air from aloft (see also Fig. 1). Figures 11 and 13 present radiation, [NO], [NO_x], and [CO] obtained on July 24thand 20th, 2001, respectively, each of which shows the NO_x peak beginning in the 4-5 am time frame. If combustion were the source of the NO_x in these cases, there would have been a simultaneous increase in CO of ~30-90 ppb, given the typical value for the CO emission factor of $\Delta CO/\Delta NO_x$ ~8 from mobile sources (McGaughey et al. 2004), and ~25 in stationary source combustion plumes (Neuman et al. 2009, Nicks Jr et al. 2003), and the

relatively longer lifetime for CO. However, if the source of the NO_x were mobile sources, the variability in the CO data is such that we cannot rule that out, on the basis of the CO data.

Along with CO, a number of "markers" of combustion exist that are useful; among them is aerosol. In the summer of 2008, we conducted aerosol measurements using an SMPS, mounted ~10 m above the canopy on the PROPHET tower. In Figure 14 we present radiation, fine particle number density (15-40nm diameter range), [NO_x], and ozone observed on July 1, 2008. As shown in this figure, NO_x begins increasing at ~4:00 am, while O_3 is decreasing, presumably a result of dry deposition within the stable boundary layer. At the time of the NO_x peak at ~7am, there is no significant change in small particle number density, i.e. no sign of an impact of downward mixing of polluted air mass or of local combustion related NO_x.

In Figure 15 we present observations of radiation, calculated friction velocity (a measure of turbulent mixing), NO_x, PAN and ozone concentration data for July 20, 2001and August 13th, 2012. As shown in this figure, while there is a ~3 ppb increase in NO_x starting in the 4-5am time frame, neither PAN nor O_3 increase, as would be expected if the source were downward mixing (Hastie et al. 1993). As shown in Figure 15 and as discussed by Hastie et al.(1993), PAN and O_3 do increase later in the morning as the mixed layer rises, and PAN and O_3 mix downward. The friction velocity is flat through the morning NO_x peak. Thus, there is evidence in this case against turbulent mixing playing a role. Indeed, clearly the morning NO_x peak can often occur in very stable conditions.

An insight into the source of the early morning NO_x peak can be found not during sunrise, but in the early morning hours before sunrise. As shown in Figures 8b and 8c, there is a dramatic increase in the concentration of NO_x around 3:00 am that is measured above the canopy that cannot be seen below the canopy. A possible source of this peak may be from atmospheric stratification of the NBL, also called fanning (Gossard et al. 1985). If a stratified parcel of air had a larger concentration of NO_x, sporadic turbulent events or low-level nocturnal jets that form in the early morning could mix NO_x down towards the forest floor and cause the rise in NO_x in the early morning. As shown in Figure 16, on August 9th there is a clear increase in the friction velocity observed at the Ameriflux tower around 3:00 am, however, no increase of NO_x can be seen above the canopy. Instead it is one of the only times that NO_x mixing ratios below the canopy are higher than above the canopy. The opposite of this is seen in Figure 15b. During the early morning of August 13th, 2012, a large spike in [NO_x] is seen above the canopy and due to a small friction velocity, the increase in concentration is not seen within or below the canopy. When friction velocity is less than 0.35, there is not enough turbulence to mix in-canopy and above canopy air masses (Barr et al. 2013). This provides more evidence that the mixing between in-canopy air masses and the boundary layer above the canopy is not well understood, and may indicate that turbulent motion during the night may induce downward mixing of polluted air from the residual layer or a stratified parcel into the canopy

In the summer of 2012, NO_x flux measurements were made as described in further detail by Geddes and Murphy (2014). Due to the limited precision of the instrument, most flux measurements made during the field campaign had uncertainties between 50%

to >100% and therefore the flux measurements of NO_x should not be used to make a conclusive statement. Geddes and Murphy (2014) found no observable mornings in which the NO_x flux was large enough to make a conclusive determination on the direction and magnitude of the flux.

Conclusions

While the NO morning peak is clearly explained by photolysis of NO_2, photochemistry cannot explain the morning peak in NO_x. We showed that this peak is inconsistent with downward mixing from the residual layer when assuming the residual layer is highly polluted, nor can it be caused by photolysis of nitrogen species on the canopy surface, as it often occurs before sunrise. From this work, a picture emerges of a regional surface-bound air mass that "wallows" in the direction of the mean surface wind, while accumulating NO_x from the variety of surface sources, both anthropogenic (point and distributed) and natural (likely widely distributed soil and canopy emissions), culminating in a peak in [NO_x] just before the NBL breakup with associated downward mixing from the residual layer. Such processes can have a large impact on the composition of the atmosphere prior to and at the time of sunrise, leading to relatively NO_x-rich conditions at an otherwise relatively clean-air site. That can have impacts on the early morning nighttime chemistry involving the NO_3 radical (reactions 6-9 below), conversion of

$NO_2 + O_3 \longrightarrow NO_3 + O_2$ 6

$NO_3 + NO_2 \longleftrightarrow N_2O_5$ 7

$N_2O_5 + \text{aerosols} \longrightarrow \text{aerosol nitrate}$ 8

$NO_3 + \text{BVOCs} \longrightarrow RONO_2$ 9

NO_x to HNO_3 and organic nitrates (Perring et al. 2009). There can also be significant impacts on the morning photochemistry, since the enhanced [NO_2] and relatively large relative humidities present at that time can promote HONO production, and thus larger OH production rates at sunrise. As chemical transport at night has been little studied, such processes should be investigated further, as part of organized field campaigns. Much light could be shed on this through vertical profile NO_x measurements at night across a sufficient scale (e.g. the Michigan lower peninsula), and through the full boundary layer, which could be pursued via a series of aircraft low-approach profiles above small airports that have little if any night time activity. There is also a greater need for high precision instrumentation to accurately measure the flux of NO_x from soil and forest canopies.

Figures

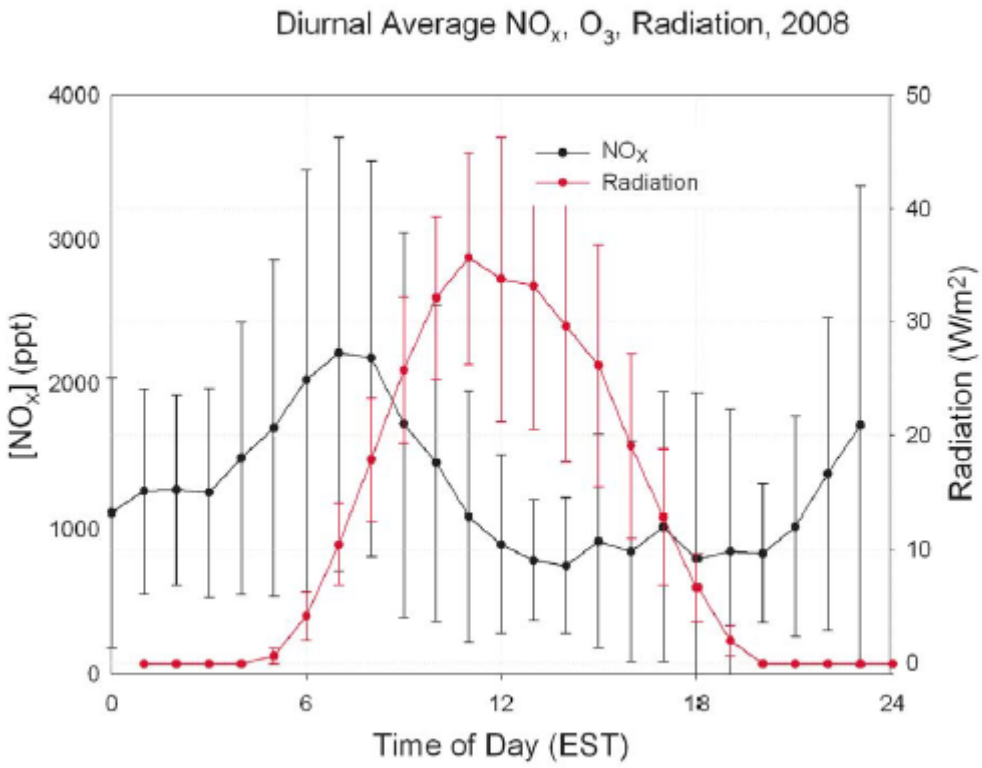

Figure 1: Diurnal variation of NO_x from June 24ththrough July 26th, 2008 at the PROPHET site and the morning NO_x peak observation.

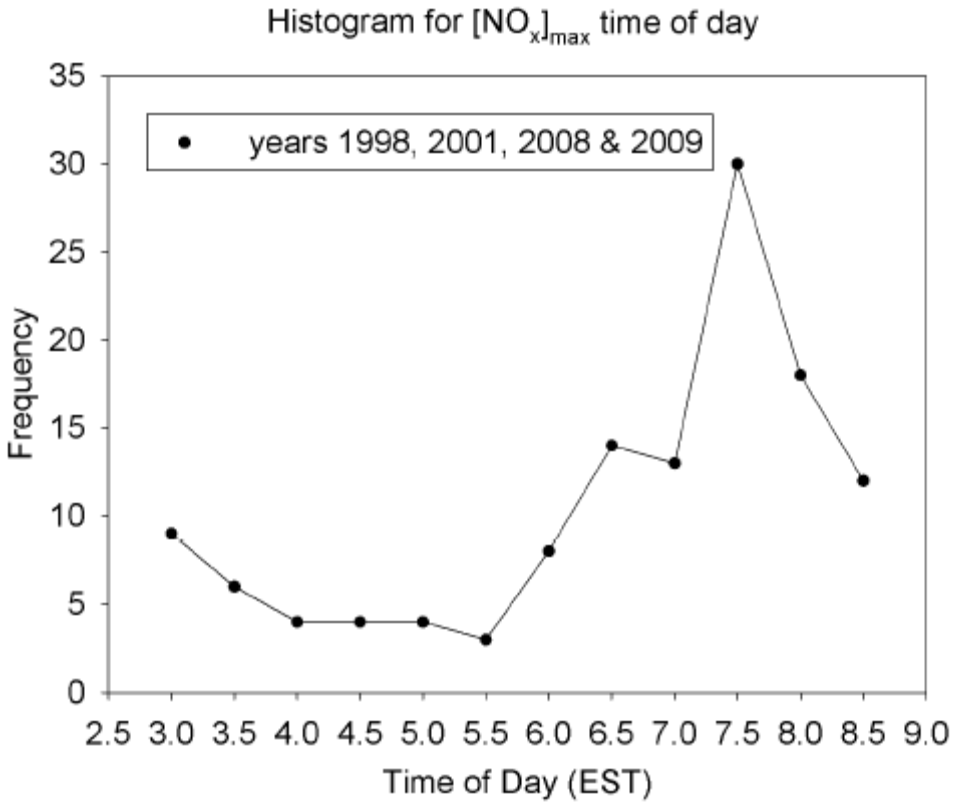

Figure 2: Histogram of the frequency of time of day for maximum NO_x.

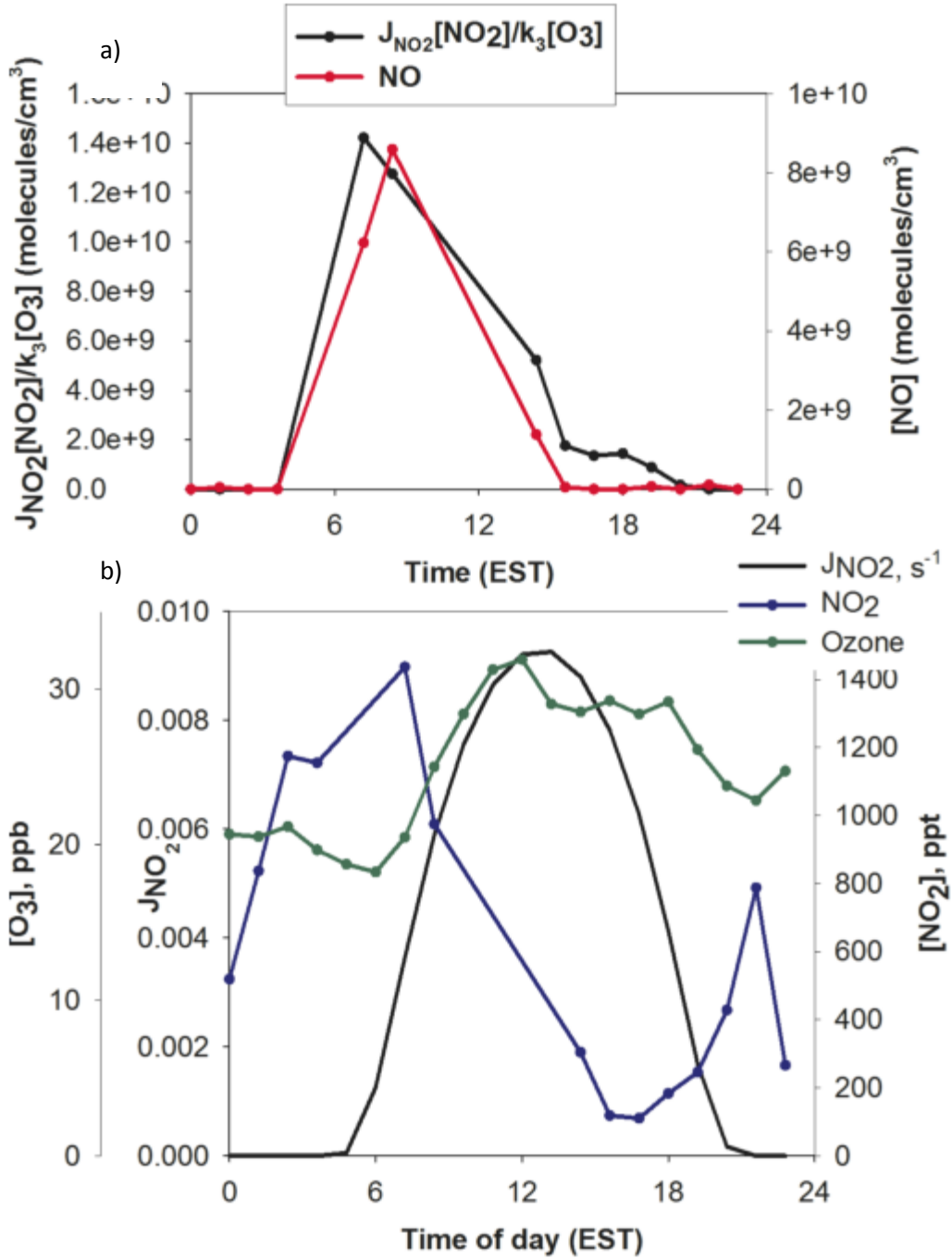

Figure 3. Observed NO, NO_2, O_3, and calculated steady-state NO, for July 2nd, 2008.

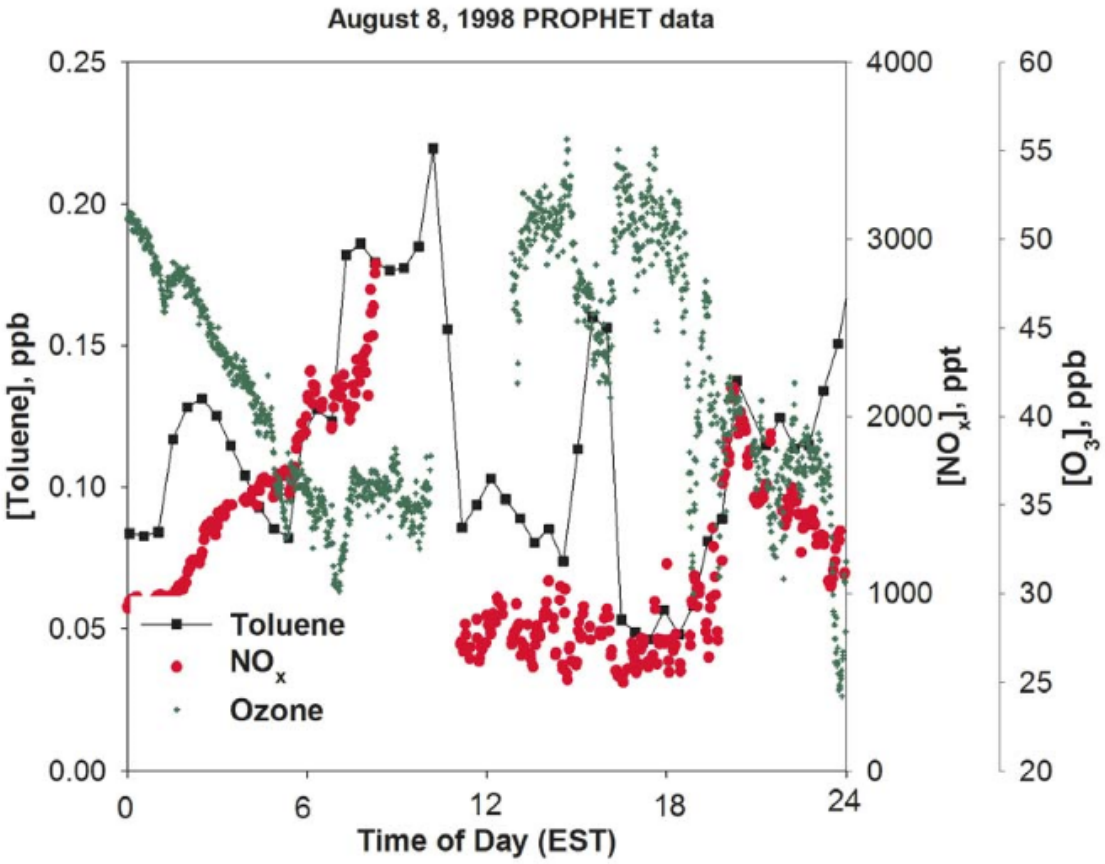

Figure 4: Toluene, NO_x, and O_3 observed on August 8th, 1998.

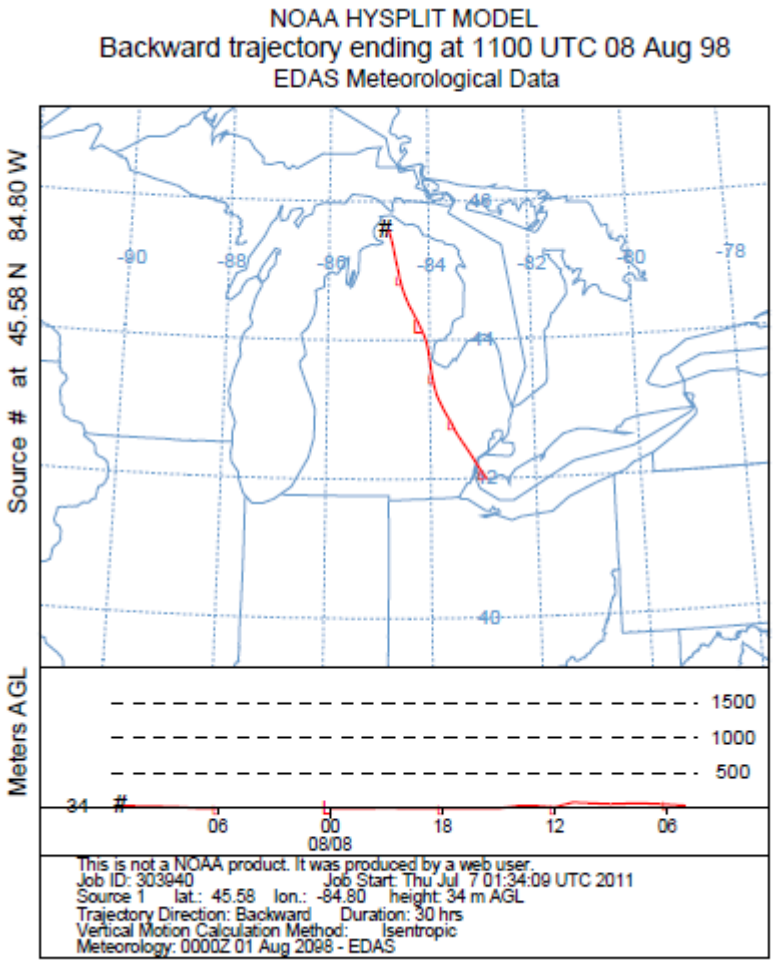
NOAA HYSPLIT MODEL
Backward trajectory ending at 1100 UTC 08 Aug 98
EDAS Meteorological Data
Source # at 45.58 N 84.80 W
Meters AGL
1500
1000
500
34
06
00
18
12
06
08/08
This is not a NOAA product. It was produced by a web user.
Job ID: 303940 Job Start: Thu Jul 7 01:34:09 UTC 2011
Source 1 lat.: 45.58 lon.: -84.80 height: 34 m AGL
Trajectory Direction: Backward Duration: 30 hrs
Vertical Motion Calculation Method: Isentropic
Meteorology: 0000Z 01 Aug 2098 - EDAS

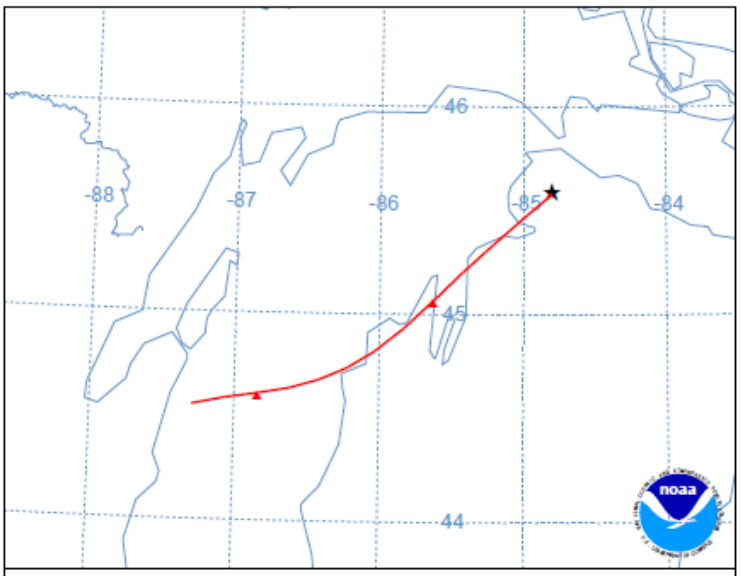
noaa

Figure 5: 24 hour back trajectory for the early morning of August 8th, 1998 and 12 hour back trajectory for August 13th, 2012.

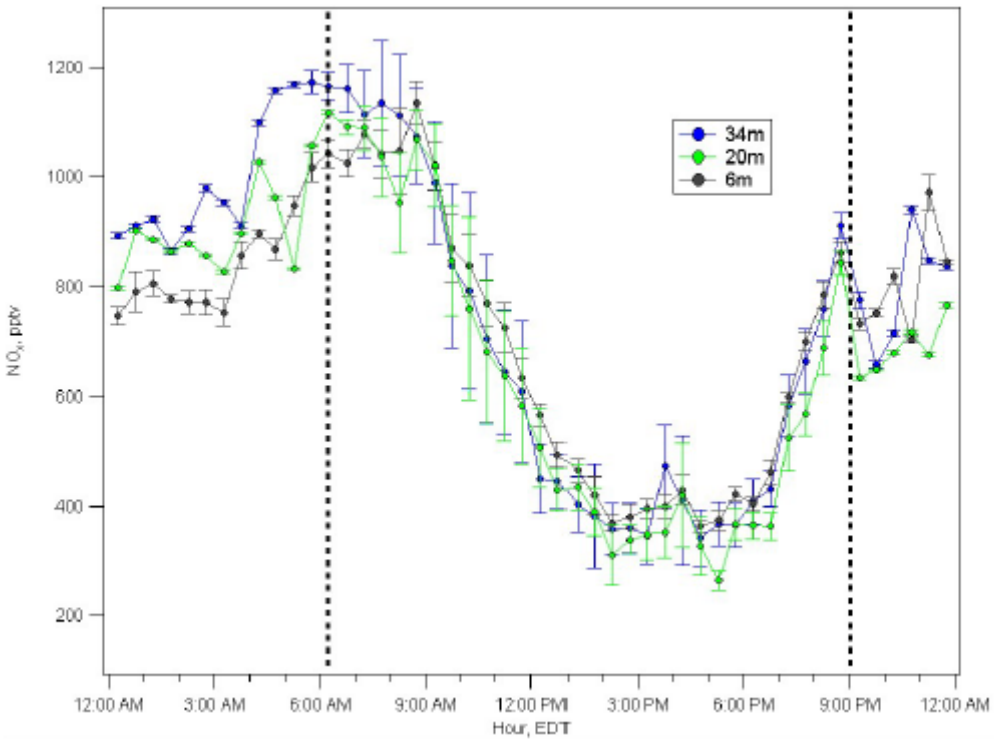

Figure 6: Diurnal variation of NO_x concentration at three levels (above and below the canopy) observed in summer 2009 at the PROPHET site.

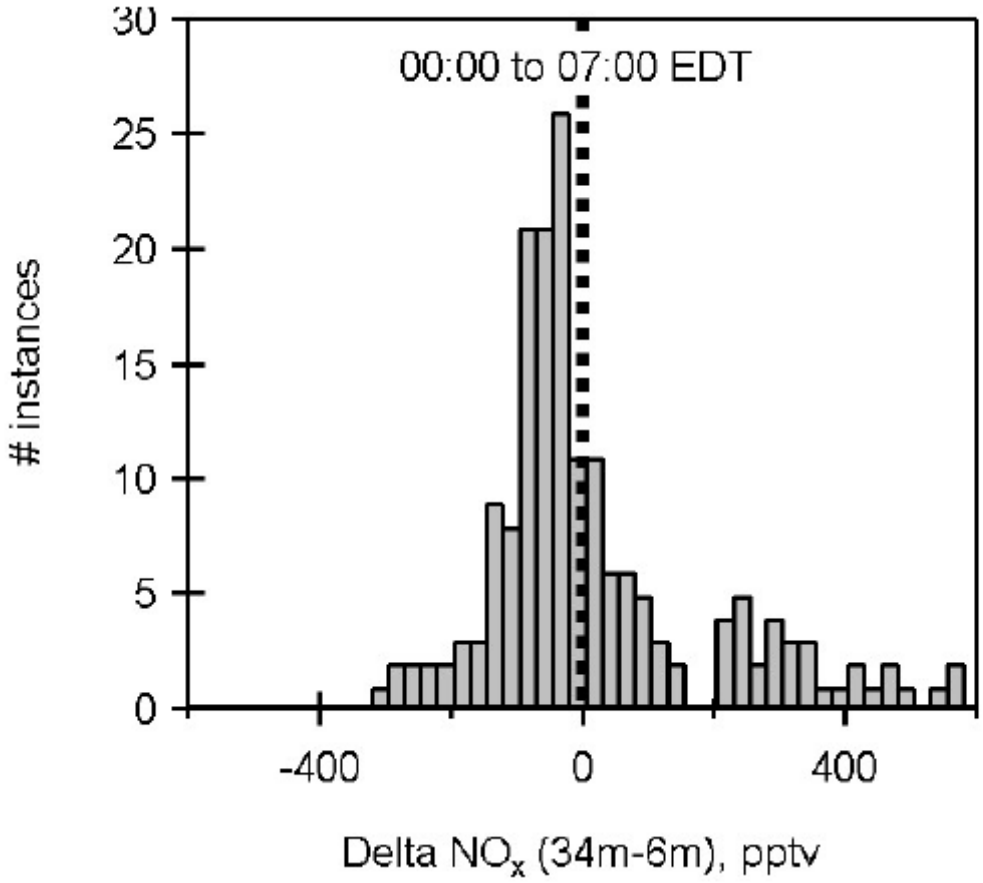

Figure 7: Histogram for the frequency of the magnitude of the NO_x concentration gradient between 34 m and 6 m above ground level, during early morning hours, summer 2009.

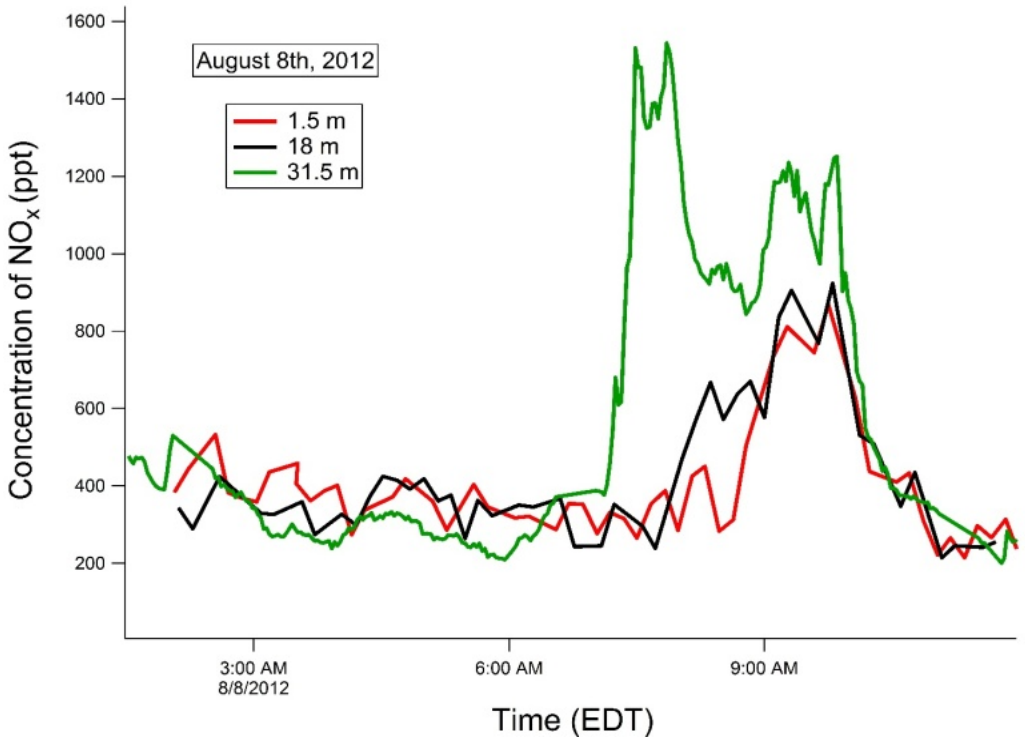
August 8th, 2012
1.5 m
18 m
31.5 m
Concentration of NO_x (ppt)
1600
1400
1200
1000
800
600
400
200
3:00 AM
8/8/2012
6:00 AM
9:00 AM
Time (EDT)

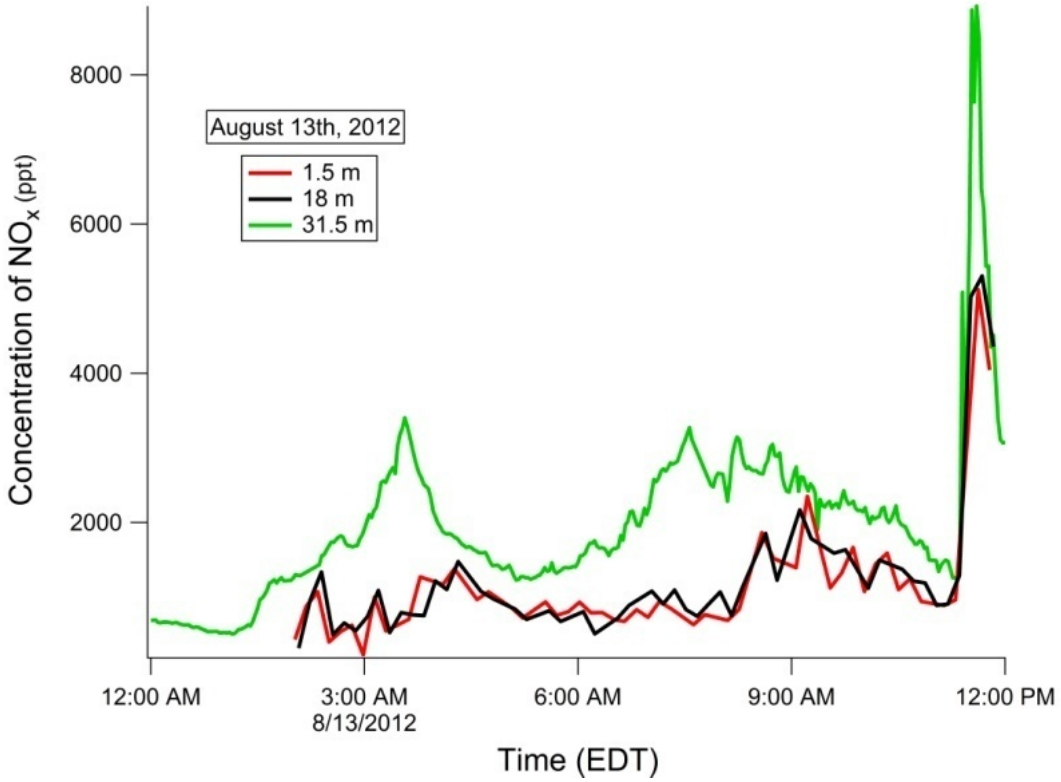
August 13th, 2012
1.5 m
18 m
31.5 m
Concentration of NO_x (ppt)
8000
6000
4000
2000
12:00 AM
3:00 AM
8/13/2012
6:00 AM
9:00 AM
12:00 PM
Time (EDT)

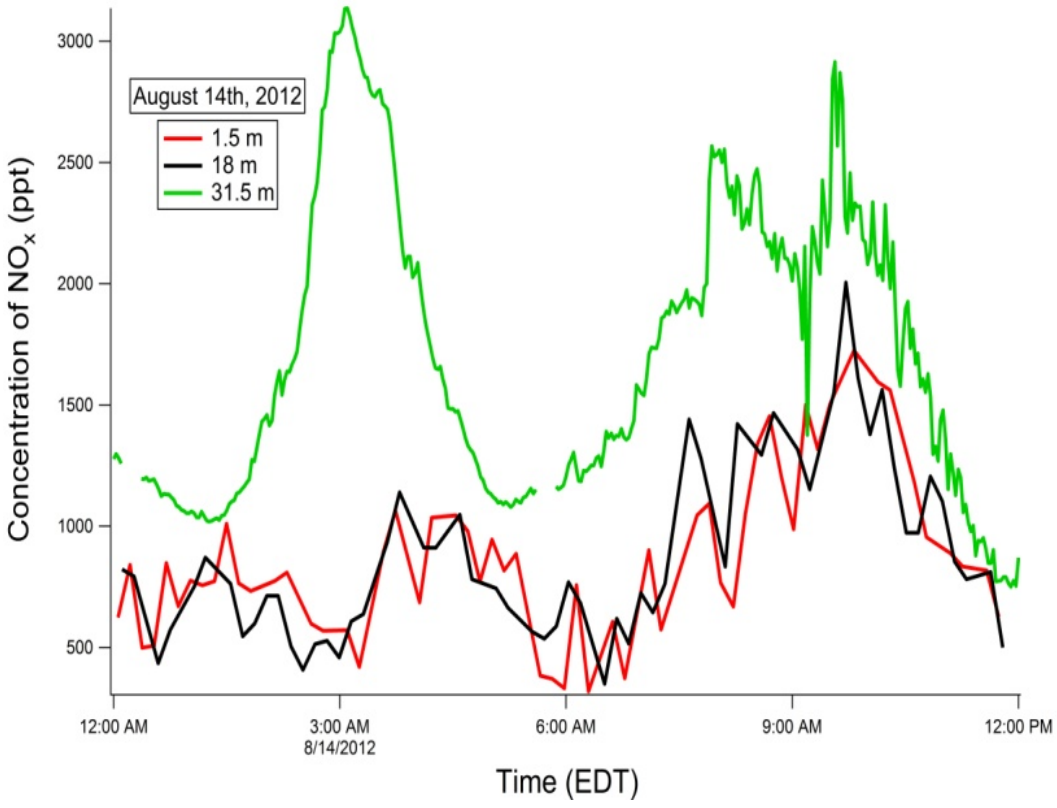

Figure 8: NO_x measurements at 1.5, 18, and 31.5 m during the morning of August 8th, 2012 (a),August 13th, 2012 (b), and August 14th, 2012 (c).

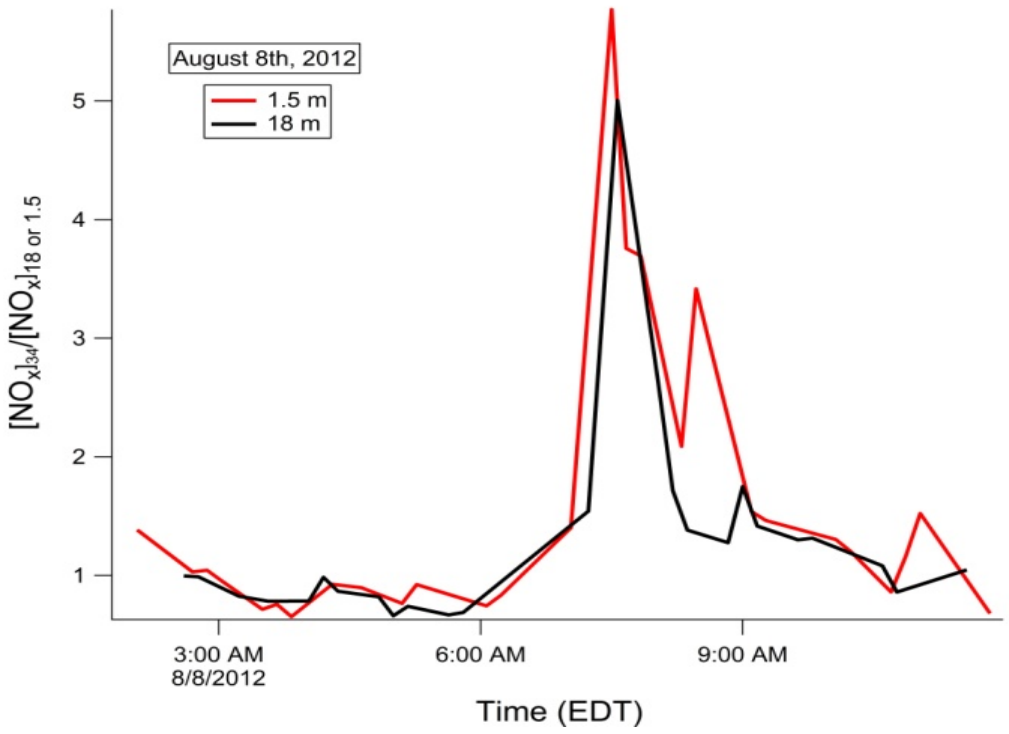
August 8th, 2012
1.5 m
18 m
[NOx]34/[NOx]18 or 1.5
5
4
3
2
1
3:00 AM
8/8/2012
6:00 AM
9:00 AM
Time (EDT)

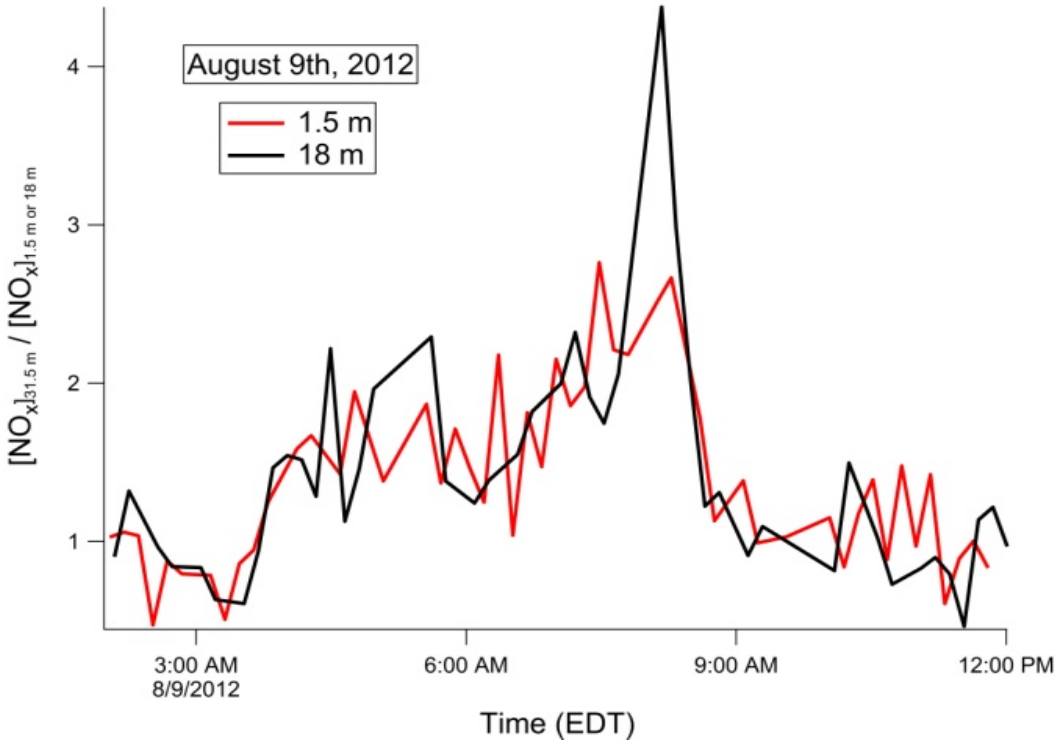
August 9th, 2012
1.5 m
18 m
[NOx]31.5 m / [NOx]1.5 m or 18 m
4
3
2
1
3:00 AM
8/9/2012
6:00 AM
9:00 AM
12:00 PM
Time (EDT)

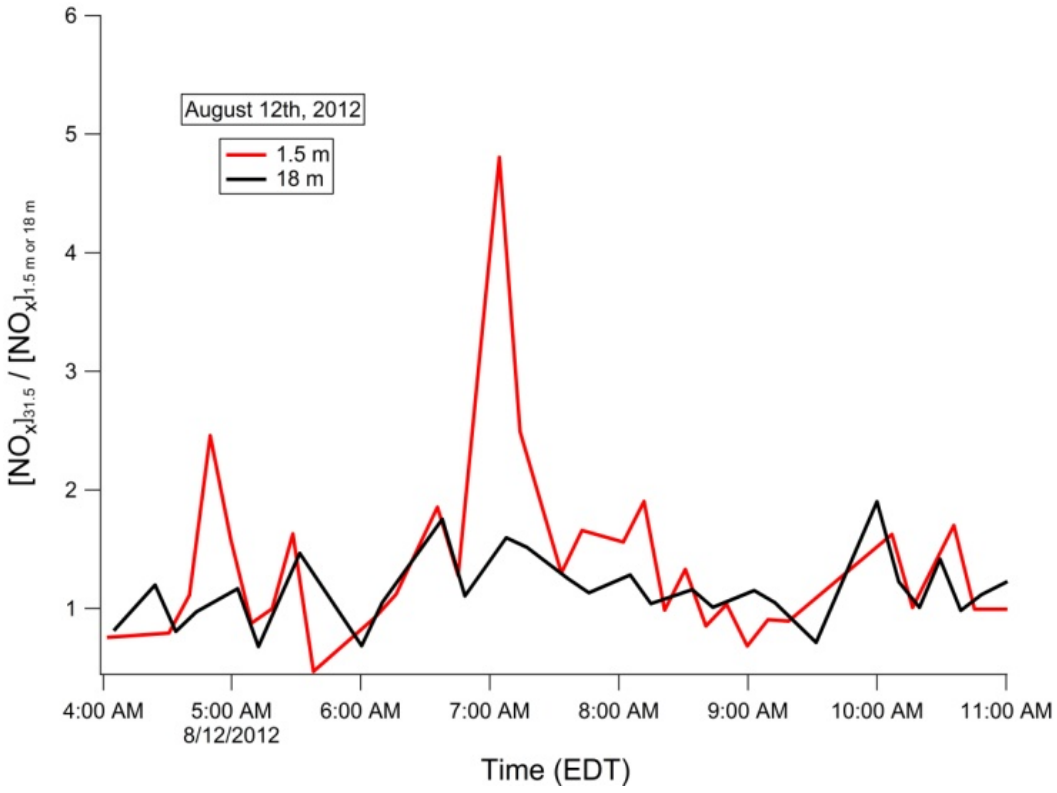
August 12th, 2012
1.5 m
18 m
[NOx]31.5 / [NOx]1.5 m or 18 m
6
5
4
3
2
1
4:00 AM
5:00 AM
8/12/2012
6:00 AM
7:00 AM
8:00 AM
9:00 AM
10:00 AM
11:00 AM
Time (EDT)

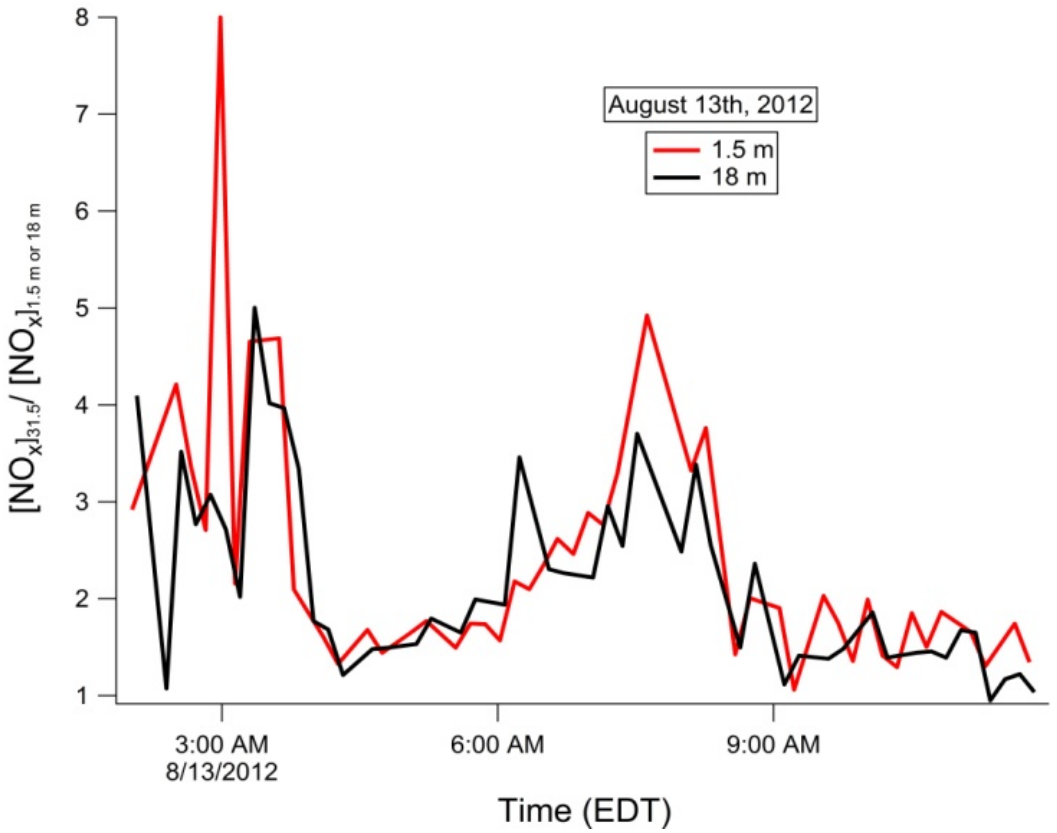
August 13th, 2012
1.5 m
18 m
[NOx]31.5/ [NOx]1.5 m or 18 m
8
7
6
5
4
3
2
1
3:00 AM
8/13/2012
6:00 AM
9:00 AM
Time (EDT)

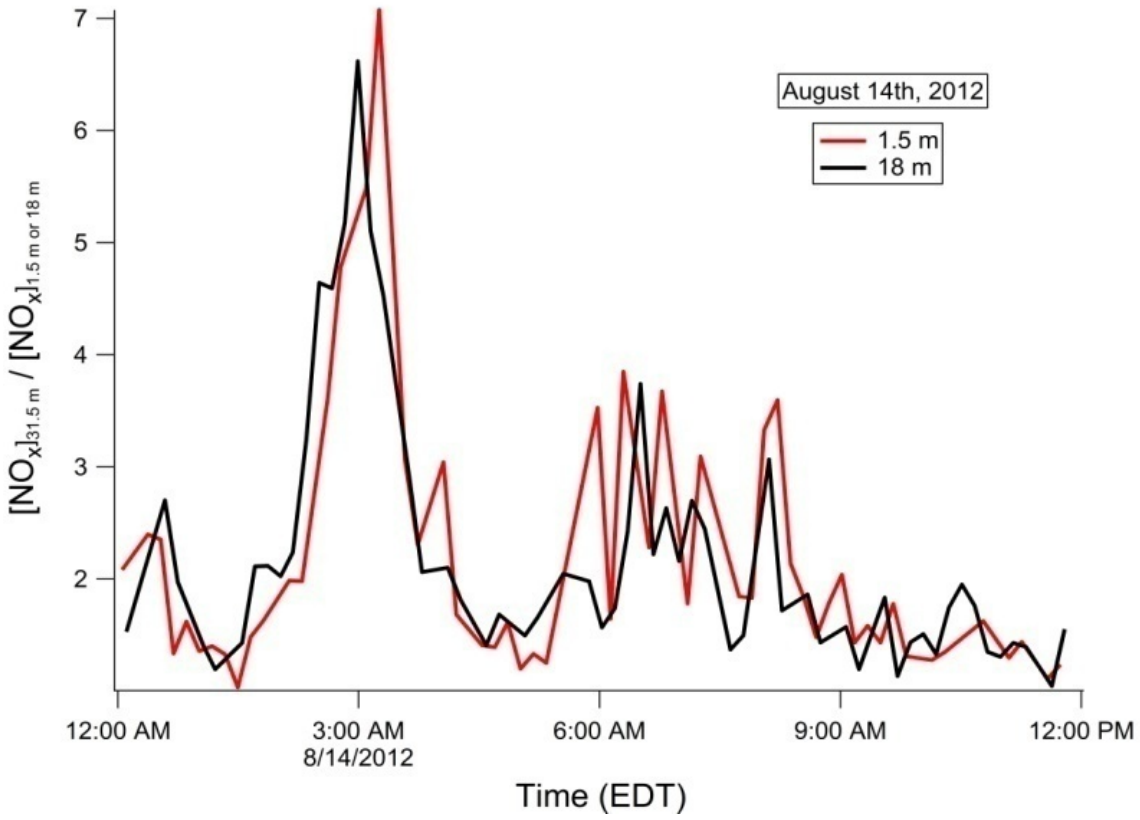

Figure 9: Ratio of $[NO_x]_{31.5}$ over $[NO_x]_{1.5}$and $[NO]_{18}$ for the mornings of August 8th, 9th, 12th, 13th, 14thin the summer of 2012.

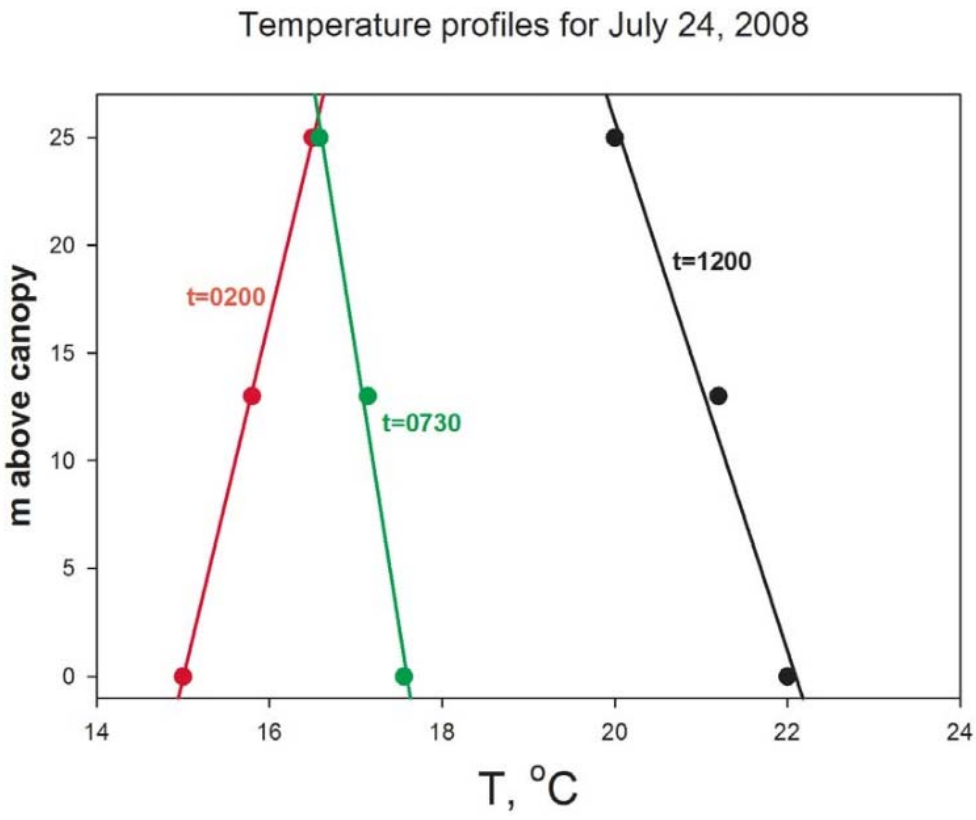

Figure 10: Temperature vertical profiles above the canopy for July 24th, 2008.

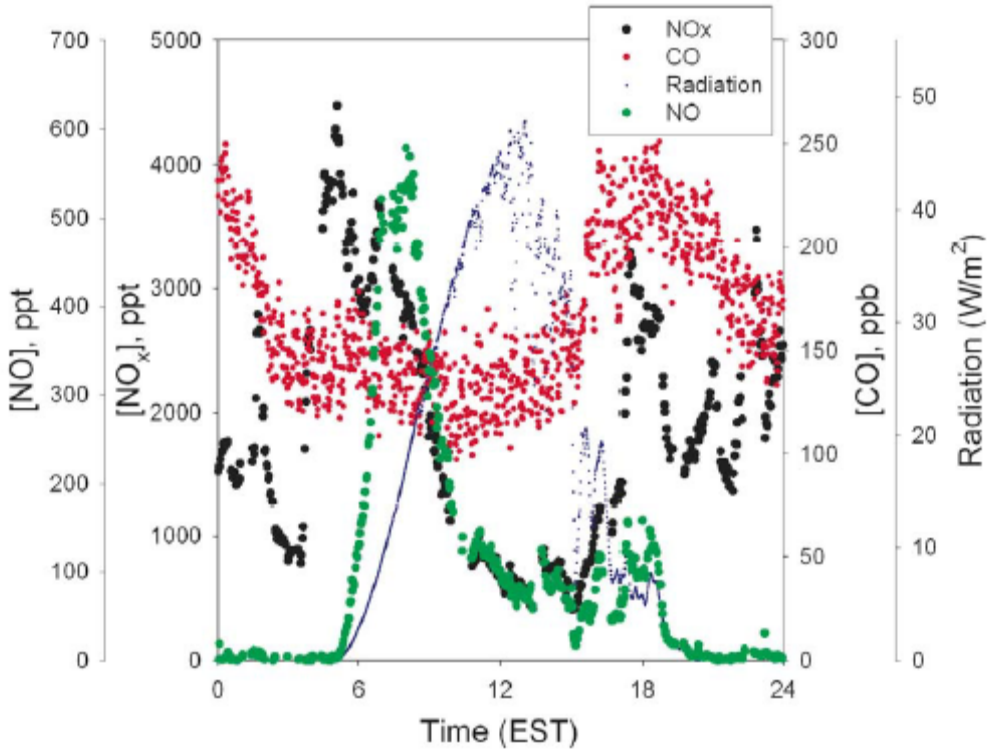

Figure 11: Time series of radiation, NO, NO_x, and CO for July 24th, 2001.

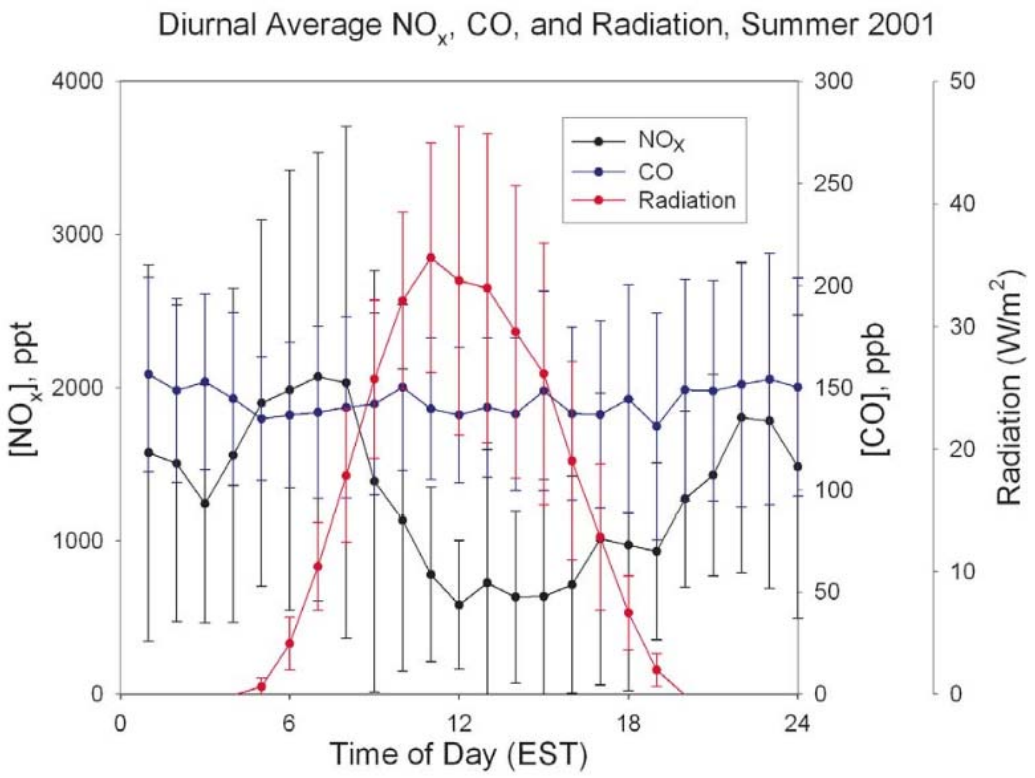

Figure 12: Diurnal variation of CO, NO_x, and radiation observed in the summer of 2001 at the PROPHET site.

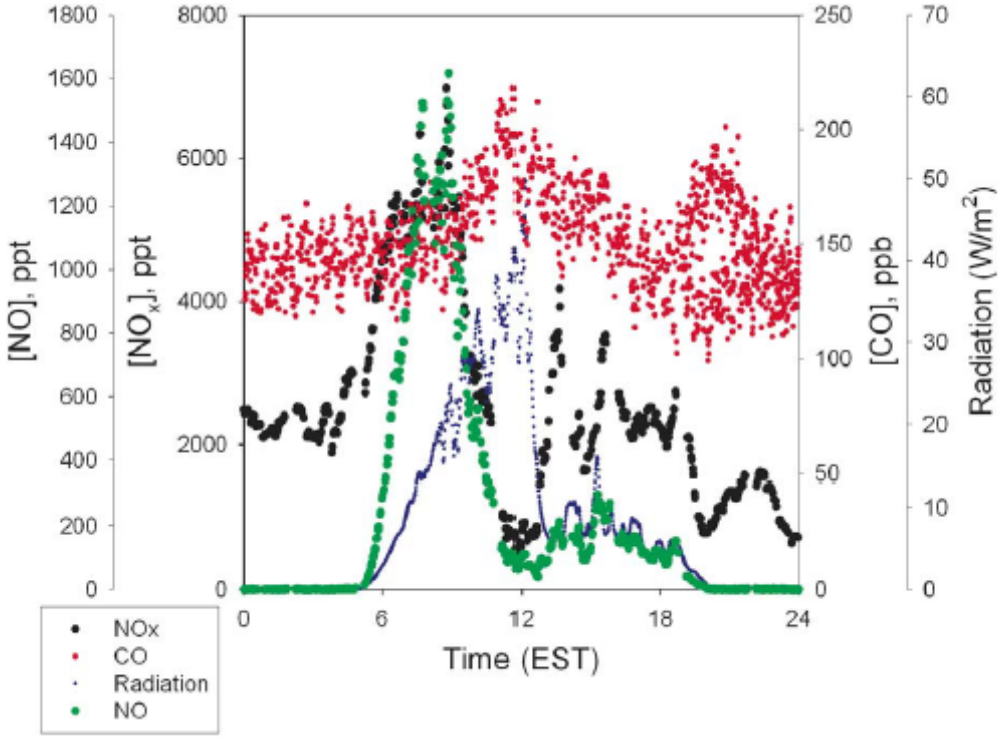

Figure 13: Time series of radiation, NO, NO_x, and CO for July 20th, 2001.

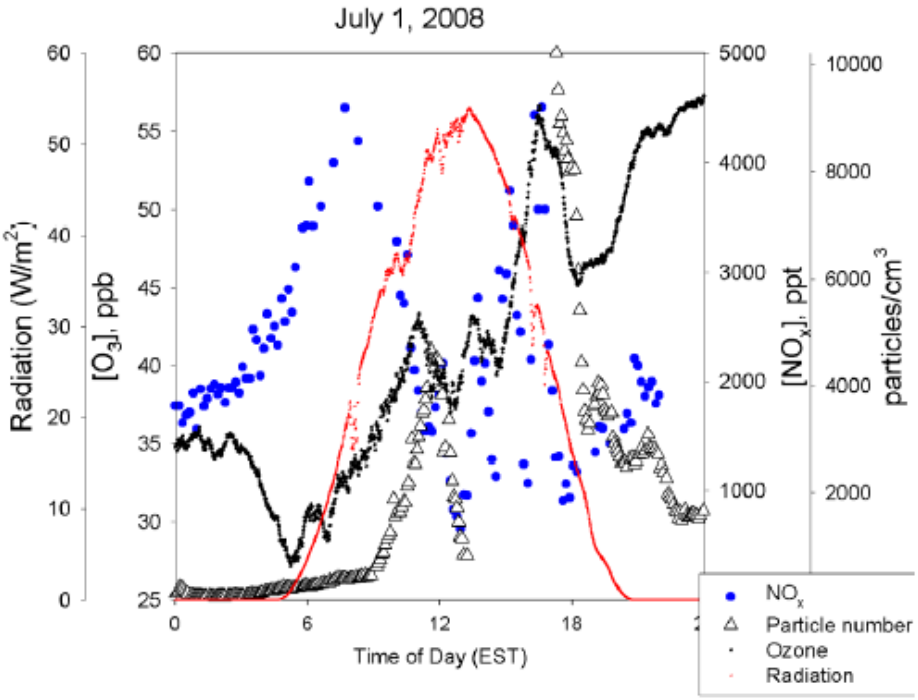

Figure 14: Radiation, particle number density, NO_x, and O_3 observed on July 1st, 2008.

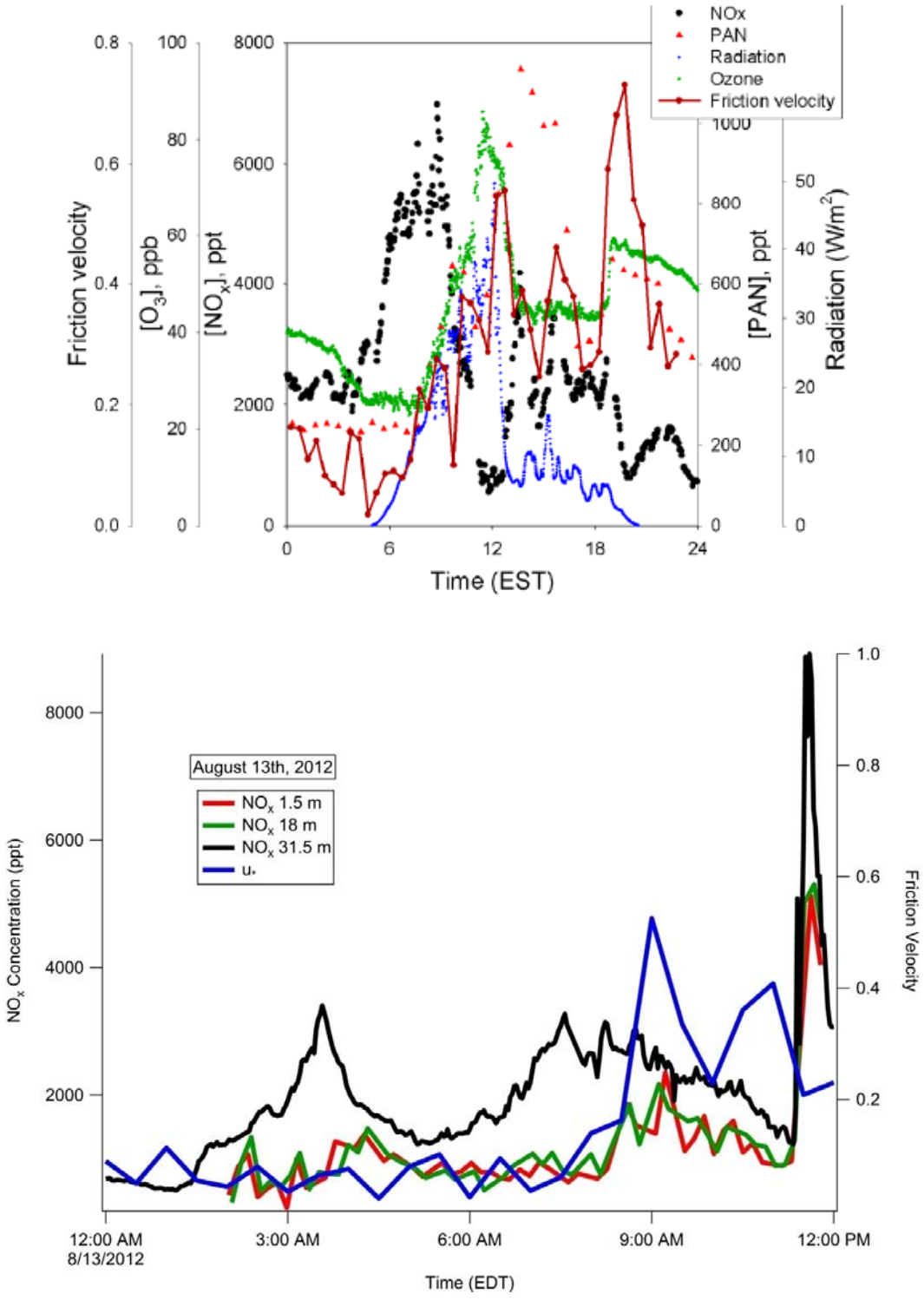

Figure 15: Observed radiation, friction velocity, NO_x, PAN, and O_3 for July 20th, 2001 (a) and friction velocity, NO_x, O_3, and radiation for August 13th, 2012 (b).

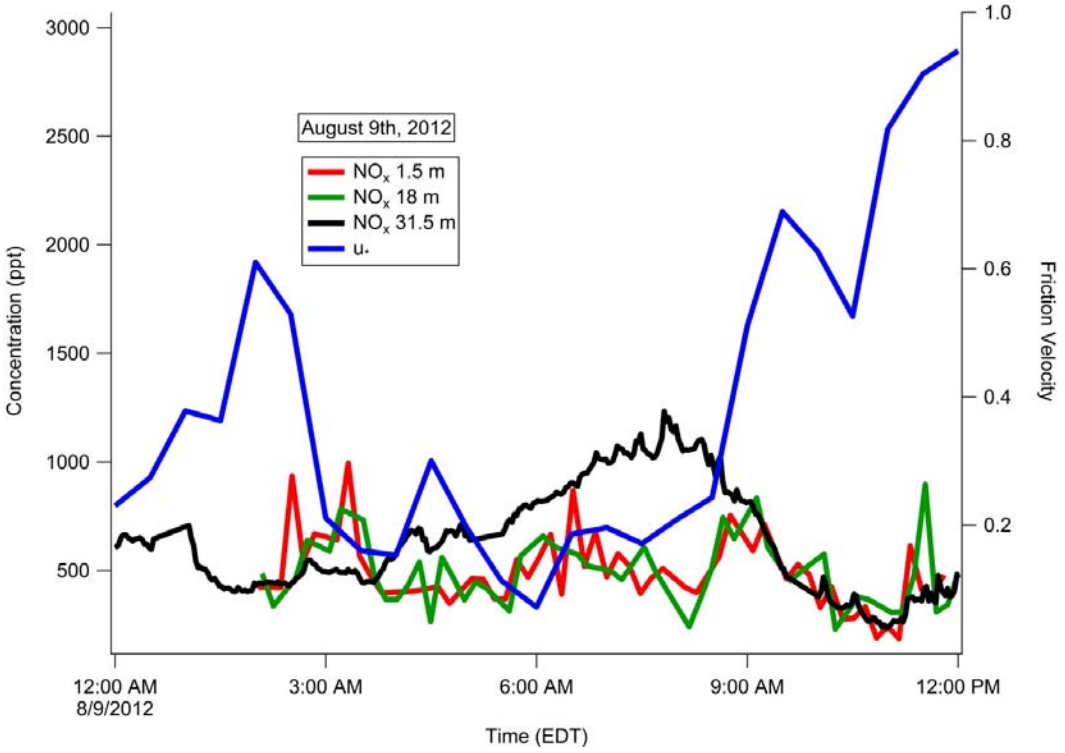

Figure 16: Observed [NO_x] measured at 1.5, 18, and 31.5 m and friction velocity (u*) during the morning of August 9th, 2012.

References

Apel, E.C., D.D. Riemer, A. Hills, W. Baugh, J. Orlando, I. Faloona, D. Tan, W.H. Brune, B. Lamb, H. Westberg, M.A. Carroll, T. Thornberry, and G.D. Geron. 2002. "Measurement and interpretation of isoprene fluxes and isoprene, methacrolein, and methyl vinyl ketone mixing ratios at the PROPHET site during the 1998 intensive." *J. Geophys. Res.* 107 (D3):ACH 7-1-ACH 7-15. doi: 10.1029/2000JD000225.

Atkinson, R., D. L. Baulch, R. A. Cox, J. N. Crowley, R. F. Hampson, R. G. Hynes, M. E. Jenkin, M. J. Rossi, and J. Troe. 2004. "Evaluated kinetic and photochemical data for atmospheric chemistry: Volume I - gas phase reactions of O_x, HO_x, NO_x and SO_x species." *Atmos. Chem. Phys.* 4:1461-1738. doi: 10.5194/acp-4-1461-2004.

Barr, A.G., A.D. Richardson, D.Y. Hollinger, D. Papale, M.A. Arain, T.A. Black, G. Bohrer, D. Dragoni, M.L. Fischer, L. Gu, B.E. Law, H.A. Margolis, J.H. McCaughey, J.W. Munger, W. Oechel, and K. Schaeffer. 2013. "Use of change-point detection for friction-velocity threshold evaluation in eddy-covariance studies." *Agricultural and Forest Meterology* 171-172:31-45. doi: 10.1016/j.agrformet.2012.11.023.

Breuninger, C, R Oswald, J Kesselmeier, and F X Meixner. 2012. "The dynamic chamber method: trace gas exchange fluxes (NO, NO_2, O_3) between plants and the atmosphere in the laboratory and the field." *Atmos. Meas. Tech.* 5:955-989.

Carroll, M A, P B Shepson, and S B Bertman. 2001. "Overview of the program for research on oxidants: PHototchemistry Emissions, and Transport (PROPHET) summer 1998 measurments intensive." *J. Geophys. Res.* 106:24275-24288.

Chapparo-Suarez, I G, F X Meixner, and J Kesselmeier. 2011. "Nitrogen dioxide (NO_2) uptake by vegetation controlled by atmospheric concentrations and plant stomatal aperature." *Atmos. Environ.* 45:5742-5750.

Conrad, R. 1996. "Soil microorganisms as controllers of atmospheric trace gases (H_2, CO, CH_4, OCS, N_2O, and NO)." *Microbiol. Rev.* 60:609-640.

Costa, A W, G W Michalski, B Alexander, and P B Shepson. 2011. "Analysis of atmospheric inputs of nitrate to a temperate forest ecosystem from delta^{17}O isotope ratio measurements." *Geophys. Res. Lett.* 38. doi: 10.1029/2011GL047539.

Day, D.A., D.K. Farmer, A.H. Goldstein, P.J. Wooldridge, C. Minejima, and R.C. Cohen. 2009. "Observations of NO_x, PNs, ANs, and HNO_3 at a rural site in California Sierra Nevada mountains: summertime diurnal cycles." *Atmos. Chem. Phys.* 9:4879-4896.

Dentener, F J, and P J Crutzen. 1994. "A 3-dimensional model of the global ammonia cycle." *Atmos. chem.* 19:331-369.

Fang, S X, and Y J Mu. 2006. "Air/surface exchange of nitric oxide between two typical vegetable lands and the atmosphere in the Yangze delta, China." *Atmos. Environ.* 40:6329-6337.

Farmer, D K, P J Wooldridge, and R C Cohen. 2006. "Application of thermal-dissocation laser induced fluorescence (TD-LIF) to measurement of HNO_3, ANs, PNs, and NO_2 fluxes using eddy covariance." *Atmos. Chem. Phys.* 6:3471-3486.

Finlayson-Pitts, B.J., L.M. Wingen, A.L. Sumner, D. Syomin, and K.A. Ramazan. 2003. "The heterogeneous hydrolysis of NO_2 in laboratory systems and in outdoor and indoor atmospheres: An integrated mechanism." *Phys. Chem. Chem. Phys.* 320:889-892.

Galloway, J N, A R Townsend, J W Erisman, M Bekunda, Z Cai, J R Freney, LA Martinelli, S P Seitzinger, and M A Sutton. 2008. "Transformation of the Nitrogen cycle: Recent trends, questions, and potential solutions." *Science* 320 (doi:10.1126/science.1136674):889-892.

Ganzeveld, L., J. Valverde-Canossa, G. Moortgat, and R. Steinbrecher. 2006. "Evaluation of peroxide exchanges over a coniferous forest in a single-column chemistry-climate model." *Atmos. Environ.* 40:68-80. doi: 10.1016/j.atmosenv.2006.01.062.

Geddes, J A, and J G Murphy. 2014. "Observations of reactive nitrogen oxide fluxes by eddy covariance above two mid-latitude North American mixed hardwood forests." *Atmos. Chem. Phys.* 14:2939-2957.

Gossard, E.E., J.E. Gaynor, R.J. Zamora, and W.D. Neff. 1985. "Fine structure of elevated stable layers observed by sounder and in situ tower measurements." *J. Atmos. Sci.* 42:2156-2159.

Gough, C M, C S Vogel, K H Harrold, K George, and P S Curtis. 2007. "The legacy of harvest and fire on ecosystem carbon storage in a north temperate forest." *Glob. Change Biol.* 13:1935-1949.

Hallquist, M, J C Wenger, U Baltensperger, Y Rudich, D Simpson, M Claeys, J Dommen, N M Donahue, C George, A H Goldstein, J F Hamilton, H Herrmann, T Hoffman, Y Iinuma, M Jang, M E Jenkin, J L Jimenez, A Kiendler-Scharr, W Maenhaut, G McFiggans, T F Mentel, A Monod, A S H Prevot, J H Seinfeld, J D Surratt, R Szmigielski, and J Wildt. 2009. "The formation, properties and impact of secondary organic aerosol: current and emerging issues." *Atmos. Chem. Phys.* 9:5155-5236.

Hastie, D.R., P.B. Shepson, R. Berman, and S. Sharma. 1993. "The influence of the nocturnal boundary layer on the concentration of secondary trace species at Dorset, Ontario." *Atmos. Environ.* 27:533-541.

Hsu, C. C., M. C. Lin, and A. M. Mebel. 1997. "Ab Initio study of the H + HONO reaction: Direct abstraction versus indirect exchange processes." *J. Phys. Chem. A* 101 (1):60-66. doi: 10.1021/jp962286t.

Jacob, D J, and S C Wofsy. 1990. "Budgets of reactive nitrogen, hydrocarbons, and ozone over the Amazon-forest during the wet season." *J. Geophys. Res.-Atmos.* 95:16737-16754.

Kim, S, G M Wolfe, L Mauldin, C Cantrell, A Guenther, T Karl, A Turnipseed, J Greenberg, S R Hall, K Ullmann, E Apel, R Hornbrook, Y Kajii, Y Nakashima, F N Keutsch, J P DiGangi, S B Henry, L Kaser, R Schnitzhofer, M Graus, A Hansel, W Zheng, and F F Flocke. 2013. "Evaluation of HO_x sources and cycling using measurment-constrained model calculations in a 2-methyl-3-butene-2-ol (MBO) and monoterpene (MT) dominated ecosystem." *Atmos. Chem. Phys.* 13:2031-2044.

Kondo, Y., H. Ziereis, M. Koike, S. Kawakami, G.L. Gregory, G.W. Sachse, H.B. Singh, D.D. Davis, and J.T. Merrill. 1996. "Reactive nitrogen over the Pacific Ocean during PEM-West A." *J. Geophys. Res.* 101:1809-1828.

Lin, X, M Trainer, and S C Liu. 1988. "On the nonlinearity of the tropospheric ozone." *J. Geophys. Res.* 93:15879-15888.

Lockwood, A L, T R Filley, D Rhodes, and P B Shepson. 2008. "Foliar uptake of atmospheric organic nitrates." *Geophys. Res. Lett.* 35 (15). doi: 10.1029/2008GL034714.

Lockwood, A L, P B Shepson, M N Fiddler, and M Alaghmand. 2010. "Isoprene nitrates: preparations, separation, identification, yields, and atmospheric chemistry." *Atmos. Chem. Phys.* 10:6169-6178.

Magnani, F, M Mencuccini, M Borghetti, P Berbigier, F Berninger, S Delzon, A Grelle, P Hari, P G Jarvis, P Kolari, A S Kowalski, H Lankreijer, B E Law, A Lindroth, D Loustau, G Manca, J B Moncrieff, M Rayment, V Tedeschi, R Valentini, and J Grace. 2007. "The human footprint in the carbon cycle of temperate and boreal forests." *Nature* 447:848-852.

Mao, Jingqiu, Fabien Paulot, Daniel J Jacob, Ronald C Cohen, John D Crounse, Paul O Wennberg, Chritoph A Keller, Rynda C Hudman, Michael P Barkley, and Larry W Horowitz. 2013. "Ozone and organic nitrates over the eastern United States: Sensitivity to isoprene chemistry." *J. Geophys. Res. Atmos.* 118 (19):11256-11268.

Martin, R.S., H. Westberg, E. Allwine, L. Ashman, J.C. Farmer, and B. Lamb. 1991. "Measurement of isoprene and its atmospheric oxidation products in a central Pennsylvania deciduous forest." *J. Atmos. Chem.* 13:1-32.

McGaughey, G.R., N.R. Desai, D.T. Allen, R.L. Seila, W.A. Lonneman, M.P. Fraser, R.A. Harley, A.K. Pollack, J.M. Ivy, and J.H. Price. 2004. "Analysis of motor

vehicle emissions in a Houston tunnel during the Texas Air Quality Study 2000." *Atmos. Environ.* 38:3363-3372.

Min, K E, S E Pusede, E C Browne, B W LaFranchi, P J Wooldridge, and R C Cohen. 2014. "Eddy covariance fluxes and vertical concentration gradient measurements of NO and NO_2 over a ponderosa pine ecosystem: Observational evidence for within-canopy chemical removal of NO_x." In *Atmos. Chem. Phys.*

Min, K, S E Pusede, E C Browne, B W LaFranchi, P J Wooldridge, G M Wolfe, S A Harrold, J A Thornton, and R C Cohen. 2012. "Observations of atmosphere-biosphere exchange of total and speciated peroxynitrates: Nitrogen fluxes and biogenic sources of peroxynitrates." *Atmos. Chem. Phys.* 12:9763-9773.

Neuman, J.A., J.B. Nowak, W. Zheng, F. Flocke, T.B. Ryerson, M. Trainer, J.S. Holloway, D.D. Parrish, G.J. Frost, J. Peischl, E.L. Atlas, R. Bahreini, A.G. Wollny, and F.C. Fehsenfeld. 2009. "Relationship between photochemical ozone production and NO_x oxidation in Houston, Texas." *J. Geophys. Res.* 114. doi: 10.1029/2008JD011688.

Nicks Jr, D.K., J.S. Holloway, T.B. Ryerson, R.W. Dissly, D.D. Parrish, G.J. Frost, M. Trainer, S.G. Donnelly, S. Schauffler, E.L. Atlas, G. Hubler, D.T. Sueper, and F.C. Fehsenfeld. 2003. "Fossil-fueled power plants as a source of atmospheric carbon monoxide." *J. Environ. Monit.* 5:35-39.

Norby, R J, J M Warren, C M Iversen, B E Medlyn, and R E McMurtrie. 2010. "CO_2 enhancement of forest productivity constrained by limited nitrogen availability." *PNAS* 107 (45):19368-19373.

Ollinger, S V, J D Aber, R B Reich, and R J Freuder. 2002. "Interactive effects of nitrogen deposition, tropospheric ozone, elevated CO_2 and land use history on the carbon dynamics of northern hardwood forests." *Global Change Biol.* 8:545-562.

Parrish, D D, M P Buhr, M Trainer, R B Norton, J P Shimshock, F C Fehsenfeld, K G Anlauf, Bottenheim J W, Y Z Tang, H A Wiebe, J M Roberts, R L Tanner, L Newman, B C Bowersox, J Olszyna, E M Bailey, M O Rodgers, T Wang, H Berresheim, U K Roychowdhury, and K L Demerjianai. 1993. "The total reactive oxidized nitrogen levels and the partitioning between the individual species at six rural sites in eastern North America." *J. Geophys. Res.-Atmos.* 98 (D2):2927-2939.

Paulot, F, J D Crounse, H G Kjaergaard, J H Kroll, J H Seinfeld, and P O Wennberg. 2009. "Isoprene photooxidation: new insights into the production of acids and organic nitrates." *Atmos. Chem. Phys.* 9:1479-1501.

Perring, A. E., T. H. Bertram, P. J. Wooldridge, A. Fried, B. G. Heikes, J. Dibb, J.D. Crounse, P.O. Wennberg, N. J. Blake, D. R. Blake, W. H. Brune, H. B. Singh, and R. C. Cohen. 2009. "Airborne observations of total $RONO_2$: new constraints on the yield and lifetime of isoprene nitrates." *Atmos. Chem. Phys.* 9:1451-1463.

Pippin, M.R., S.B. Bertman, T.D. Thornberry, M.S. Town, M.A. Carroll, and S. Sillman. 2001. "Seasonal variations of PAN, PPN, and O_3 at the upper midwest PROPHET site." *J. Geophys. Res.* 106:24451-24465.

Raivonen, M, T Vesala, L Pirjola, N Altimir, P Keronen, M Kulmala, and P Hari. 2009. "Compensation point of NO_x exchange: Net result of NO_x consumption and production." *Agr. Forest Meteorol.* 149:1073-1081.

Ridley, B A, and F E Grahek. 1990. "A small, low flow, high-sensitivity reaction vessel for NO chemiluminescence detectors." *J. Atmos. and Ocean. Technol.* 7:307-311.

Ridley, B A, S Madronic, R B Chatfield, J G Walega, R E Shetter, M A Carroll, and D D Montzka. 1992. "Measurements and model simulations of the photostationary state during the Mauna Loa observatory photochemistry experiment: Implications for radical concentrations and ozone production and loss rates." *J. Geophys. Res.* 97:10375-10388.

Rollins, A W, J D Smith, K R Wilson, and R C Cohen. 2010. "Real time in situ detection of organic nitrates in atmospheric aerosols." *Environ. Sci. Technol.* 44:5540-5545.

Sakamaki, F., S. Hatakeyama, and H. Akimoto. 1983. "Formation of nitrous-acid and nitric-oxide in the heterogeneous dark reaction of nitrogen-dioxide and water-vapor in a smog chamber." *Int. J. Chem. Kinet.* 15:1013-1029.

Seok, B, D Helmig, L Ganzeveld, M W Williams, and C S Vogel. 2013. "Dynamics of nitrogen oxides and ozone above and within a mixed hardwood forest in northern Michigan." *Atmos. Chem. Phys.* 13:7301-7320.

Singh, M.P., R.T. McNider, and J.T. Lin. 1993. "An analytical study of diurnal wind-structure variations in the boundary-layer and the low-level nocturnal jet." *Boundary Layer Meteorol.* 63:397-423.

Sparks, J P, R K Monson, K L Sparks, and M Lerdau. 2001. "Leaf uptake of nitrogen dioxide (NO_2) in a tropical wet forest: Implications for tropospheric chemistry." *Oecologia* 127:214-221.

Thompson, A M. 1992. "The oxidizing capacity of the Earth's atmosphere-Probable past and future changes." *Science* 256:1157-1165.

Thornberry, Troy, Mary Anne Carroll, Gerald J Keeler, Sanford Sillman, Steven B Bertman, Margaret R Pippin, Kristi Ostling, John W Grossenbacher, Paul B Shepson, Owen R Cooper, Jennie L Moody, and William R Stockwell. 2001. "Observations of reactive oxidized nitrogen and speciation of NO_y during the PROPHET summer 1998 intensive." *J. Geophys. Res.* 106 (D20):24359-24386.

Thornton, J A, P J Wooldridge, R C Cohen, M Martinez, H Harder, W H Brune, E J Williams, J M Roberts, F C Fehsenfeld, S R Hall, R E Shetter, B P Wert, and A Fried. 2002. "Ozone production rates as a function of NO_x abundances and HO_x